RNA methyltransferases influence noncoding RNA biogenesis and function through catalytic-independent activities

Jennifer Porat

A DISSERTATION SUBMITTED TO THE FACULTY OF GRADUATE STUDIES
IN PARTIAL FULFILLMENT OF THE REQUIREMENTS FOR THE DEGREE OF

DOCTOR OF PHILOSOPHY

GRADUATE PROGRAM IN BIOLOGY
YORK UNIVERSITY
TORONTO, ONTARIO

May 2023

Abstract

Continued advances in the high throughput detection of post-transcriptional RNA modifications have enabled large scale, mechanistic studies into the importance of RNA modifications in regulating the structure, function, and stability of coding and noncoding RNAs. While modifications themselves have a major role in influencing the fate of an RNA, recent evidence from bacteria suggests that RNA modification enzymes can possess non-catalytic functions that nevertheless contribute to RNA functionality. This dissertation aims to expand this idea to eukaryotic RNA modification enzymes, with a focus on uncovering the catalytic-independent functions of the fission yeast RNA methyltransferases Bmc1 and Trm1. Bmc1 is a homolog of the human methyl phosphate capping enzyme (MePCE), which has been well studied for its role in catalyzing the addition of a 5′ γ-monomethyl phosphate cap on select RNA Polymerase III transcripts such as the 7SK snRNA. In answer to the long-standing question as to the function of an MePCE homolog in fission yeast, an organism with no known 7SK, this work revealed that Bmc1 assumes a non-catalytic role in the fission yeast telomerase enzyme by promoting holoenzyme assembly and telomerase RNA stability. Further analysis demonstrated that Bmc1 also interacts with the U6 snRNA to direct 2′-O-methylation and influence formation of a U6-containing snRNP, and that neither of these activities requires Bmc1 catalytic activity. Finally, this work shows that the fission yeast tRNA methyltransferase Trm1 promotes tRNA functionality and structural stability even in the absence of catalysis, suggesting its function as a tRNA chaperone. Collectively, these studies provide evidence supporting the multi-faceted nature of eukaryotic RNA modification enzymes and underscores their importance in many fundamental biological processes including splicing, protein translation, and maintaining genome integrity.

Acknowledgements

Here's a weird thing about me: I think the acknowledgements section of a thesis is (often) the most interesting part and as such, usually read it first (if you're wondering if I've read your acknowledgements, dear reader, the answer is most likely yes). It should probably then go without saying that I've been mentally composing my own set of acknowledgements, in some form or another, for a good few years now. And with that admission, let's hope these acknowledgements don't disappoint.

To my supervisor, mentor, and the sane voice to my increasingly extravagant or outlandish ideas, Dr. Mark "Darth La" Bayfield. We first met in your second year Biochemistry course when I told you (only somewhat jokingly) that I wanted to study the molecular basis of superpowers and you told me you didn't accept second year students in your lab. This, of course, sparked the mad desire to prove you wrong and luckily such an endeavor also introduced me to the wonder of RNA research. You therefore have my eternal gratitude for taking a chance on that young, over-eager undergraduate with a crazy idea. We've certainly had an interesting (unforgettable?) few years, full of epic nerd debates, Yiddish words, and ALL THE THINGS—imagine that last one with the accompanying meme. Thank you for guiding me down this crazy path of science, for the amazing birthday cheesecakes, and for only mildly freaking out every time I said, "So I have an idea…" But in all seriousness, thank you for supporting and encouraging me through difficult projects and manuscripts, fellowship applications, postdoc interviews, and intermittent freak outs. And most of all, an extra giant thank you for that time you went to battle for me when I decided to skip fourth year and go straight to grad school (if only we'd gotten you the light saber sooner!). When I say you're a truly one-of-a-kind, all-around awesome mentor, I mean it. (But now that the end is upon us, I think the joke has gone on

long enough: the truth is I don't have any strong opinions on comic sans, despite my promises to hand in a progress report or manuscript written entirely in comic sans.)

To my committee members, Dr. Kathi Hudak and Dr. Andy White, for their attention to detail, helpful suggestions, and guidance as I navigated the uncertainty of grad school. Thank you as well to Dr. White for the ever-spiralling "Why?" questions during committee meetings. No, I still don't have an answer for why the universe is the way it is ("Okay, but *why* is there a lagging strand in DNA replication?") but I promise I'll keep striving to figure it out. Thanks to the rest of my examination committee, Dr. Emanuel Rosonina, Dr. Derek Wilson, and Dr. Juan Alfonzo (extra thanks to Juan for his faith in me since we met in front of my very first poster presentation in undergrad!).

To the Bayfield lab past and present, for many memorable moments, including digging through the trash for experiments. In the order I've met them: thanks to Stefano (Don NRE) for that very first crash course in mini prepping and lunchtime bible study; Jyotsna (Empress of IRESs) for constant advice; Ana (Mother of Trm1) for the yeast tips and tricks and sharing your favourite project with me; Farnaz (Slr1 Khaleesi), Kyra (Lady La), Vanessa (Sla Slayer), and Connor (we still need to find you a nickname!) for weathering the never-ending storm of grad school alongside me; all the awesome Bayfield lab undergrads; and honorary lab member Uma (Princess/General La and yes, there is a theme here) for our Harry Potter conversations (some conducted almost entirely in emojis) and general shenanigans, like that time we went around LSB with a handmade fortune teller. Special thanks to the undergrads I've been fortunate enough to work with: Alita, Mahbod, and Taylor, your enthusiasm and excitement has been inspiring and a welcome bright spot to any day in the lab. But I do hope you haven't picked up too many of my questionable lab habits…

To the many people who offered up their time and wisdom on all things academia: Mark Bayfield, Kathi Hudak, and Andy White (again, you're all awesome and formidable people and scientists); Dr. Andrea Berman, whose advice saved me from a potential catastrophic mistake; Dr. Joan Steitz (I'm still in disbelief over this one); Dr. Andrew Kusmierczyk, for the advice on choosing a postdoc and the pizza recommendations; Dr. Richard Maraia, for the tRNA enthusiasm; and Dr. Marc Fabian, for more postdoc advice.

Thanks to those who kindly provided their insight on the following chapters (any mistakes therein are mine and mine alone): Dr. Marc Fabian (Chapter 2), Dr. Raymund Wellinger (Chapter 2), Dr. Dave Brow (Chapter 3), and Dr. Richard Maraia (Chapter 4, Appendix A). And to the many people who helped with data collection and analysis: Moaine El Baidouri and Dr. Jean-Marc Deragon for evolutionary wizardry (Chapter 2), Dr. Jorg Grigull for guiding us into the world of RNA Seq analysis (Chapter 2), Viktor Slat and Dr. Stephen Rader for all things splicing (Chapter 3), and Dr. Ana Vakiloroayaei and Taylor Cargill for all their work unravelling the mystery of Trm1 (Chapter 4).

And most importantly, to my family, for everything. Your love and support (and willingness to listen to me ramble on about experiments) has meant the world to me. I couldn't have asked for better. Special shoutout to my sister Daniella, who spent the last 2 years of my PhD doing homework and studying at my lab bench as I pipetted. You may have complained daily about all the lab smells and annoying people (same), but you made this journey a lot more fun.

Table of Contents

List of Figures

Chapter 1:

Chapter 2:

Chapter 3:

Chapter 4:

Chapter 5:

Appendix A:

List of Abbreviations

α	alpha
β	beta
γ	gamma
Ψ	Pseudouridine
3′ SS	3′ splice site
5′ SS	5′ splice site
ASL	Anticodon stem loop
ATP	Adenosine triphosphate
Bin3	Bicoid-interacting protein 1
Bmc1	Bin3 methyl phosphate capping enzyme 1
CBCA	Cap-binding complex A
DNA	Deoxyribonucleoic acid
EMSA	Electrophoretic mobility shift assay
FRET	Fluorescence resonance energy transfer
hLa	Human La protein
hTR	Human telomerase RNA
ISL	Internal stem loop
LaM	La motif
LARP	La related protein
MePCE	Methyl phosphate capping enzyme
mRNA	Messenger RNA
mtRNA	Mitochondrial RNA
MTS	Mitochondrial targeting sequence
NEXT	Nuclear exosome targeting complex
NMR	Nuclear magnetic resonance
NLS	Nuclear localization sequence
NRE	Nuclear retention element
PARN	Poly(A)-specific ribonuclease
Pus	Pseudouridine synthase
PrA	Protein A
Pre-tRNA	Precursor tRNA
RBP	RNA binding protein
RIP	RNA immunoprecipitation
RNA	Ribonucleic acid
RNAP	RNA Polymerase
RNP	Ribonucleoprotein
RPG	Ribosomal protein gene
RRM	RNA recognition motif
rRNA	Ribosomal RNA
RT	Reverse transcriptase
RTD	Rapid tRNA decay
SBM	Short basic motif
Sla1	*S. pombe* La protein
snoRNA	Small nucleolar RNA
snRNA	Small nuclear RNA

snRNP	Small nuclear ribonucleoprotein
Tan	tRNA acetyltransferase
TER1/TER	Telomerase RNA
TMG	Trimethylguanosine
TMS	tRNA mediated suppression
TRAMP	Trf4/Air2/Mtr4 Polyadenylation
Trm	tRNA methyltransferase
tRNA	Transfer RNA
Trt1	Telomerase reverse transcriptase 1
Tru	tRNA pseudouridine synthase
UTR	Untranslated region
xRRM	Extended RNA recognition motif

Chapter 1: Evolutionarily conserved RNA binding proteins promote noncoding RNA processing and post-transcriptional modifications

Portions of this chapter were previously published (Porat J., Kothe U., and Bayfield M.A., Revisiting tRNA chaperones: New players in an ancient game, *RNA.* **27:** 543-559 (2021)).

Contributions (Porat *et al.,* 2021): J.P. conceived of, wrote, and edited the manuscript and created figures. U.K. created Figure 2B and edited the manuscript. M.A.B. edited the manuscript.

1.1 Noncoding RNA processing and modification is carried out by RNA binding proteins

Following transcription, RNAs, particularly noncoding RNAs, undergo an extensive maturation process that can involve 5′ capping, 3′ end processing or trimming, and critically, the addition of chemical modifications. The past decade has seen a tremendous surge in our collective understanding of the breadth and importance of these post-transcriptional RNA modifications, brought about in large part by the combination of classic RNA biochemistry and high throughput sequencing (1). While the molecular and chemical mechanisms of each processing step vary greatly depending on the nature of the reaction, a unifying facet is the involvement of RNA binding proteins. Over 1000 RNA binding proteins have been identified and validated in humans alone (2), and the number has only continued to climb with recent proteome-wide studies (3).

RNA binding proteins have been traditionally classified by their mode of RNA binding through well-studied, structured domains. Common domains discussed here include the RNA recognition motif (RRM), which contains two alpha helices and a four-stranded beta sheet, the latter of which interacts with single-stranded RNA (4); the extended RNA recognition motif (xRRM), which differs from the RRM in the presence of an α3 and α3x helix lying across the beta sheet (5); and the La motif, which contains a helix-turn-helix fold involved in uridylate binding (6) (Figure 1). More recently, the RNA-binding proteome has expanded to include so-called non-canonical RNA binding proteins, which lack structured RNA binding domains (3). Curiously, many of these non-canonical RNA binding proteins are metabolic enzymes, with RNA binding often serving to modulate enzymatic activity (7). Still, the ever-expanding list of RNA binding proteins begins to hint at the importance of protein-RNA interactions as a function of their prevalence within the proteome.

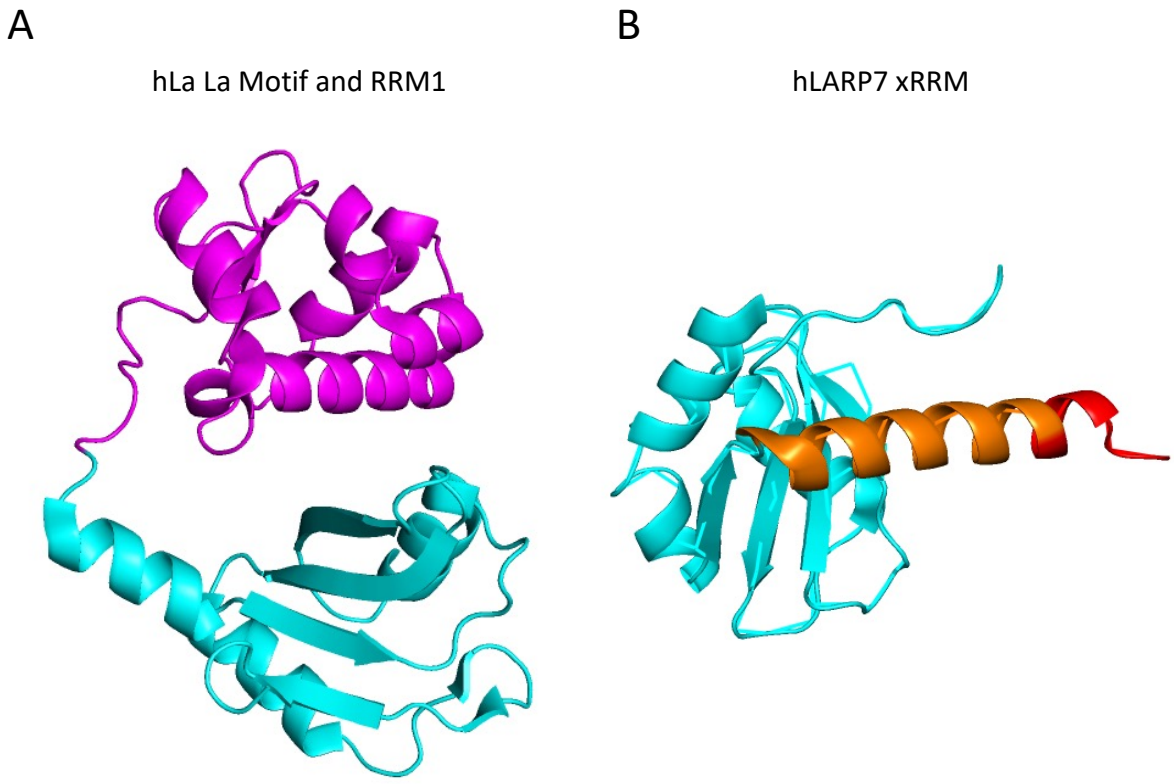

Figure 1: RNA binding domains in human La and La-related proteins
A) Ribbon representation of the La Motif (magenta) and RNA recognition motif 1 (RRM1, cyan) of human La (PDB 2VOO (8)).
B) Ribbon representation of the extended RNA recognition motif (xRRM) of human LARP7 (PDB 6D12 (9)). α3 helix is indicated in orange and α3x helix is indicated in red.

With the limited number of known RNA binding domains and the sequence and structural diversity of RNA substrates, RNA binding proteins can achieve substrate specificity through the use of tandem RNA binding domains within a single protein or several RNA binding proteins that coordinate a single RNA (10). A well-studied example of the former is the eukaryotic La protein (discussed in detail below), which uses its tandem La motif and RRM to form a binding pocket for the 3′ uridylate trailer found in RNA Polymerase III transcripts, including pre-tRNA (6). Telomerase RNA from the fission yeast *Schizosaccharomyces pombe* (discussed in detail below) illustrates the latter, with its 3′ uridylate trailer bound by the Lsm2-8

complex and an internal pseudoknot bound by the xRRM of the La-related protein Pof8 (11–15). Importantly, the involvement of multiple RNA binding domains or RNA binding proteins is also a key determinant for the precise positioning of target RNA bases for post-transcriptional modification.

Post-transcriptional RNA modifications, which are as numerous as they are chemically diverse, occur on coding and noncoding RNAs. To date, more than 170 RNA modifications have been described (16), ranging from chemically simple methylations to the addition of more complex functional groups that require several enzymatic steps for their synthesis (17). RNA modification enzymes often recognize specific sequence or structural motifs on their targets. Well-studied examples of this are the mammalian pseudouridine synthase Pus7, which recognizes a UGUAG motif (the underlined uridine being the target of modification) (18), and the yeast pseudouridine synthase Pus1, which recognizes the target uracil at the 5′ end of a bulged stem loop (19). That these elements can be found in mRNA and tRNA provides an explanation as to how a single modification enzyme can target a diverse array of RNA substrates. In contrast, select RNA modification enzymes only possess catalytic activity and instead rely on RNA-binding protein cofactors to recognize and bind their targets. tRNA and mRNA acetylation is carried out by the acetyltransferase Kre33/Nat10 (nomenclature refers to the yeast and human homologs, respectively) and the non-catalytic cofactor Tan1/THUMPD1, which serves as an adaptor for RNA binding (20). Similarly, m^7G modification on tRNA is catalyzed by the methyltransferase METTL1 and the RNA binding protein WDR4, which acts as a scaffold for METTL1 and the T-arm of the tRNA (21). As RNA binding proteins, including RNA chaperones and RNA modification enzymes, cooperate to ensure RNA structure and functionality, the following sections will explore the mechanistic basis of several post-transcriptional modification

enzymes, with a focus on the interplay between RNA modifications, RNA binding proteins, and noncoding RNA function. Of particular interest is the emerging idea that there are many proteins that do not fit neatly into a single category and instead possess modification and RNA chaperone activities.

1.2 Post-transcriptional modifications influence tRNA stability by promoting base-pairing and tertiary interactions

tRNAs are among the most highly modified RNA species, with an average of 13 post-transcriptional modifications on nuclear-encoded tRNAs (22) (Figure 2). A number of studies have focused on modifications in the anticodon stem-loop (ASL), which primarily affect translational fidelity by maintaining the correct open reading frame and influencing codon-anticodon base-pairing (for review, see (23)), although modifications outside the ASL (henceforth referred to as body modifications) have similarly important functions in influencing tRNA structure. The importance of body modifications can also be inferred from the numerous human diseases characterized by mutations to tRNA modification enzymes (for review, see (24)). Well-studied examples include mutations to the tRNA methyltransferase Trmt1 or the pseudouridine synthase Pus3 that result in intellectual disabilities, as well as the decreased expression of the mitochondrial tRNA methyltransferase Trmt61b associated with Alzheimer's disease (25–28).

Structure of the tRNA D-loop is influenced by the presence of dihydrouridine, which promotes the formation of a hairpin with a stable stem and flexible loop (29). Analogous to D-loop modifications, modification of T-loop nucleotides has also been linked to tRNA stability. The formation of pseudouridine (Ψ) at position 55 results in increased base-stacking ability,

thereby promoting tRNA stabilization (30–34). Another well-characterized T-loop modification is m^1A58, which is catalyzed by the Trm6-Trm61 complex in budding yeast and is required for stability of $tRNA_i$ Met^{CAU}. Importantly, the growth defect observed for Trm6 mutants grown at elevated temperatures can be suppressed by overexpression of $tRNA_i$ Met^{CAU} or the RNA chaperone La, suggesting the lack of modification may result in tRNA misfolding and degradation (discussed in more detail below) (35).

Studies have shown that stability of the juncture between the D-stem and the anticodon stem (also known as the hinge region) is influenced by the presence of $m^2{}_2G26$. Dimethylation of G26 is critical in maintaining the correct balance between hinge flexibility and rigidity by adjusting the angle of the D-stem (36). tRNAs lacking G26 dimethylation show structural rearrangement of the tRNA core due to a lack of base-stacking and the resulting loss of tertiary interactions (37). Further support linking G26 dimethylation to hinge region stability comes from chemical probing experiments demonstrating differences in sensitivity between G26-modified and unmodified tRNA Ser^{UGA}, particularly in the A-U rich anticodon stem and nucleotides in the hinge region (38). *In vivo*, deletion of the *S. pombe* G26 dimethyltransferase Trm1 resulted in impaired function of a suppressor tRNA mutant derived from tRNA Ser^{UGA}. Since suppressor tRNA constructs contain destabilizing mutations that lead to tRNA misfolding, it was suggested that Trm1-catalyzed modification promotes tRNA function by reinforcing the native fold (38, 39).

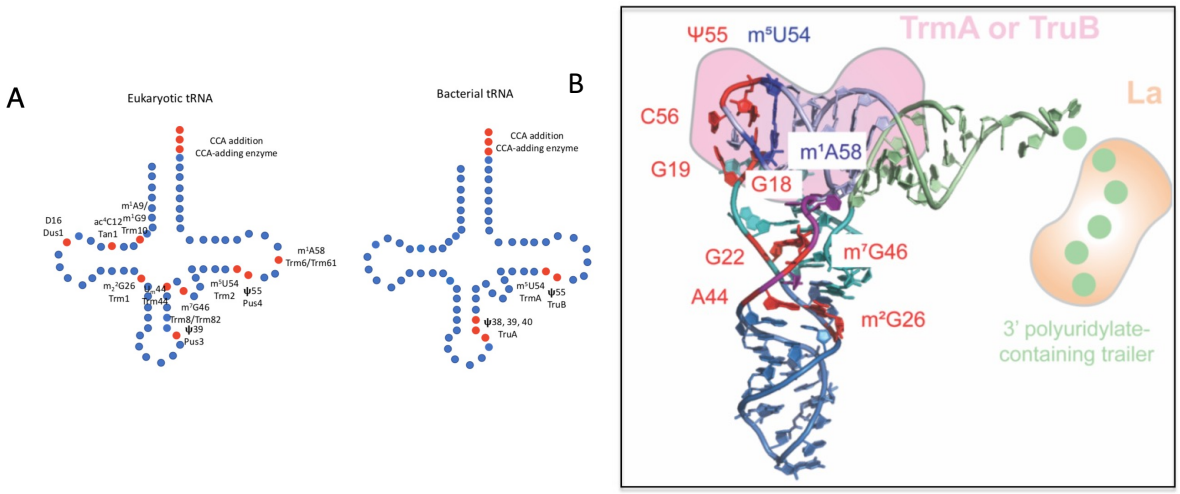

Figure 2: Post-transcriptional tRNA modifications affect secondary and tertiary interactions to promote tRNA folding
A) Schematic of eukaryotic and bacterial tRNA modifications discussed and the respective enzymes responsible for each modification. Modified nucleotides are indicated in red.
B) Three-dimensional tRNA structure highlighting tertiary base pairs and interaction sites of tRNA chaperones. The different tRNA arms are color-coded with the acceptor stem in light green, the D arm in cyan, the anticodon arm in blue, the variable arm in purple, and the T arm in light blue (structure 4TRA from (40)), visualized in PyMOL. Critical tertiary interactions involving modified nucleotides connecting different tRNA arms are highlighted in red: $m^2{}_2$G26-A44 (hinge region), G22-m^7G46, G18-Ψ55, and G19-C56. The tertiary interaction of m^5U54 and m^1A58 in the T-loop is depicted in blue. La (orange) binds the 3′ polyuridylate-containing trailer. TrmA and TruB (pink) both interact with the T arm causing the disruption of tertiary base pairs to the D arm. This figure has previously been published in (41).

1.2.1 Functional links between tRNA modification and quality control pathways

Another indication that post-transcriptional modifications are important structural determinants for tRNA function comes from extensive findings that hypomodified tRNAs are targeted for decay. The nuclear surveillance pathway, best characterized in budding yeast, involves the targeting and degradation of aberrant precursor transcripts, including pre-tRNA (42, 43). Nuclear surveillance is largely mediated by the TRAMP complex (Trf4/Air2/Mtr4), which consists of the poly(A) polymerase Trf4 or the closely related Trf5, the zinc knuckle protein Air2 or its homolog Air1, and the RNA helicase Mtr4 (43). TRAMP facilitates recognition and polyadenylation of aberrant tRNAs, followed by 3′→5′ exoribonucleolytic degradation by the

nuclear exosome (43–45). Initial studies on the structure of $tRNA_i$ Met^{CAU} demonstrated that the loss of m^1A58 modification results in increased susceptibility to nuclear surveillance due to weakened tertiary structure relative to its fully modified counterpart (35). Hypomodified pre-$tRNA_i$ Met^{CAU} was also found to be polyadenylated by the noncanonical poly(A) polymerase Trf4 prior to decay (46). Exosome-mediated decay occurs at an early point in tRNA biogenesis, as polyadenylated substrates still possess a 5′ leader and 3′ trailer. While the mechanism by which hypomodified tRNAs are recognized by TRAMP still remains unclear, the disrupted interaction between nucleotides 54 and 58 resulting from a lack of m^1A modification may lead to an alternate structure recognized as aberrant by the nuclear surveillance machinery (47). Building on the idea that structurally defective pre-tRNAs are targeted for decay by the nuclear surveillance machinery, additional studies in fission yeast revealed that the RNA chaperone La binds to the 3′ end of pre-tRNAs to protect against degradation by the exosome nuclease Rrp6 (48).

The budding yeast rapid tRNA decay (RTD) pathway relies on a different set of exoribonucleases to target structurally unstable mature tRNAs in the cytoplasm. Deletion of Trm8 or Trm82, which form a complex that catalyzes m^7G46 modification, in combination with the deletion of any one of seven nonessential body modification enzymes results in a temperature-sensitive growth defect accompanied by the rapid deacylation and decay of tRNA Val^{AAC} (49). Similar rapid degradation of tRNA $Ser^{CGA/UGA}$ was observed in strains lacking Trm44 and Tan1, which are responsible for Um44 and ac^4C12, respectively (49). RTD involves the exoribonucleases Rat1 and Xrn1, which degrade mature tRNA from the 5′ end, enabling degradation of aminoacylated and deacylated tRNAs (50). The RTD pathway primarily acts on substrates with weakened acceptor and T-stems, which increases accessibility to the 5′ end. It is

therefore likely that hypomodified tRNAs are targeted by the RTD pathway because the lack of modifications including m^7G46, Um44, and ac^4C12 weaken tertiary interactions, thereby increasing accessibility of the acceptor stem for the degradation machinery (50, 51).

The wealth of studies characterizing tRNA quality control pathways suggest a tendency for hypomodified tRNAs to be highly susceptible to decay although it is not necessarily the loss of modification that results in targeting for decay, but rather the structural instability occurring in the absence of modification. The exact mechanism by which aberrant pre-tRNAs are targeted by the nuclear surveillance pathway remains under debate, but several groups have posited that the alternate structures assumed by hypomodified pre-tRNAs lead to slower maturation, aminoacylation, and assembly into ribonucleoprotein (RNP) complexes, resulting in exposure of the 3′ end to polyadenylation and decay (52–54). There is a more straightforward explanation for RTD targeting, where a lack of key modifications destabilizes the acceptor stem to make it more accessible to 5′→3′ exoribonucleases (49–51). Recognition and elimination of hypomodified tRNAs by quality control pathways is of great import since hypomodified tRNAs—but not truncated or improperly end-processed tRNAs—may still be accommodated by the ribosome and therefore able to participate in translation, where their compromised stability can lead to deleterious effects such as impaired translation of certain codons (55).

1.3 Small nuclear RNAs are 3′ processed and post-transcriptionally modified prior to spliceosome assembly

Another class of noncoding RNAs that undergo a complex processing and modification pathway are the uridylate-rich small nuclear RNAs (snRNAs) that assemble into the spliceosome: U1, U2, U4, U5, and U6. snRNAs are transcribed by RNA Polymerase II (RNAP

II), except for U6, which is an RNA Polymerase III (RNAP III) transcript. U6 ends in the characteristic polyuridylate trailer resulting from RNAP III transcription termination and as such, the 3′ polyuridylate trailer of U6 is recognized by the uridylate-binding La protein, which provides protection from exosome-mediated decay or 3′ processing (56). The 3′ end of U6 is subsequently processed into a 2′, 3′-cyclic phosphate in humans and fission yeast (57, 58) or a terminal 3′ phosphate in budding yeast (59). 3′ end processing of U6 serves a dual purpose by providing protection from further exoribonucleolytic processing or decay and decreasing the affinity for U6 by the La protein, thus enabling the handoff of end-matured U6 to the uridylate-binding Lsm2-8 complex (59–61).

Subsequent snRNA processing steps include the installation of post-transcriptional modifications which, much like tRNA, have roles ranging from promoting snRNA stability to modulating their function with respect to splicing. The trimethylguanosine (TMG) cap structure found on RNAP II-transcribed snRNAs—synthesized by hypermethylation of the RNAP II-associated m^7G cap by the evolutionarily conserved methyltransferase Tgs1—is required for proper spliceosome assembly and nuclear localization of U1 (62, 63) (Figure 3). U6 instead acquires a γ-monomethyl phosphate cap on its 5′ end, catalyzed by the methyl phosphate capping enzyme MePCE/BCDIN3/Bin3 (64–67) (Figure 3). The function of the γ-monomethyl phosphate cap on U6 is comparatively understudied relative to the TMG cap, with depletion or deletion of the human and fission yeast MePCE homologs having no effect on steady state levels of U6 (64, 68).

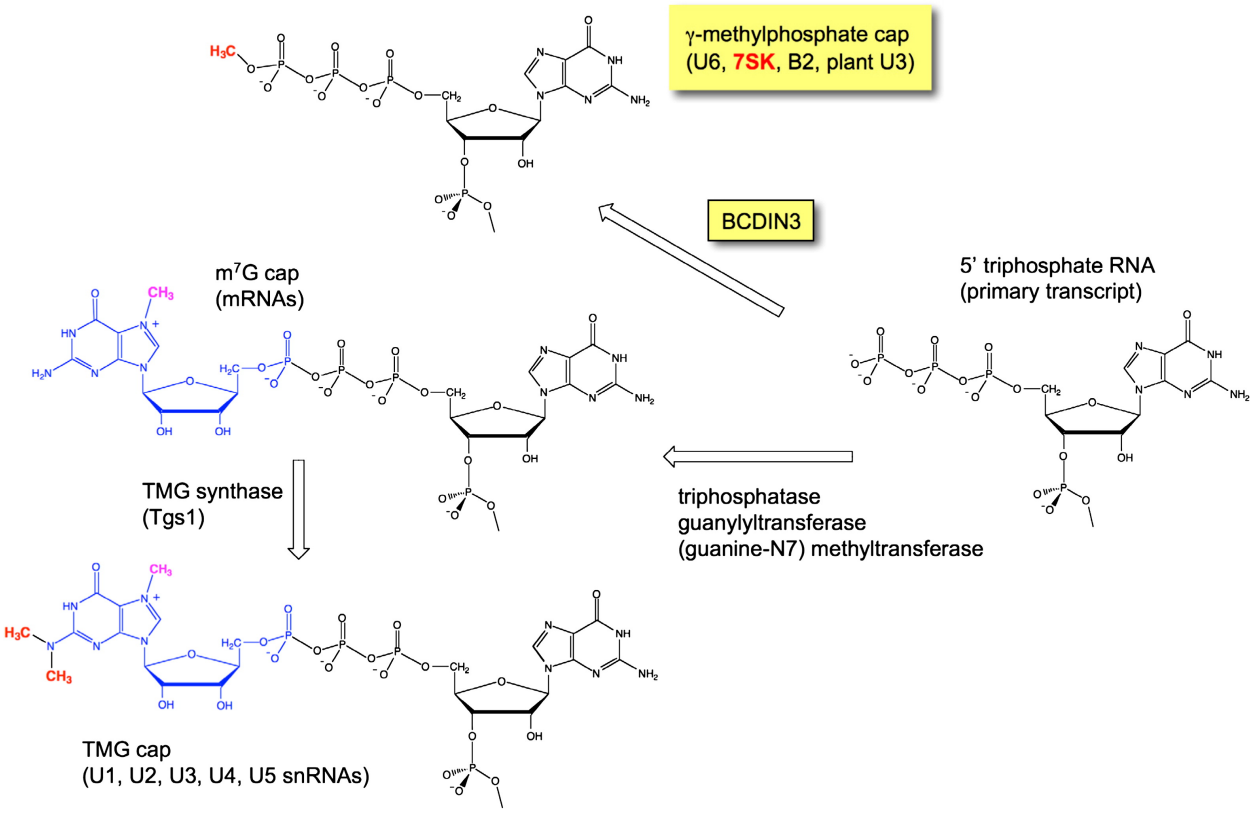

Figure 3: Schematic of 5′ cap structures derived from 5′ triphosphorylated RNA transcripts
The m^{7}G cap found on RNAP II-transcribed messenger RNAs (mRNA) is further methylated to a trimethylguanosine cap (TMG) by the methyltransferase Tgs1 for RNAP II-transcribed snRNAs. Select RNAP III transcripts, including the U6 and 7SK snRNAs are monomethylated on the γ phosphate by the methyl phosphate capping enzyme MePCE/BCDIN3. Figure adapted from (69).

As the catalytic core of the spliceosome (70), much effort has been put into understanding how post-transcriptional modification of U6 shapes spliceosome function. The finding that human U6 contains an m^{6}A at position 43 (Figure 4), located in the conserved ACAGAGA sequence that base-pairs with the 5′ splice site suggested the importance of m^{6}A in modulating splicing (71). U6 methylation by the methyltransferase METTL16 is highly conserved among eukaryotes (72, 73) although a homolog is notably absent in budding yeast. Mechanistic studies in *S. pombe* and *Arabidopsis thaliana* revealed that m^{6}A promotes

cooperation between U5 and U6 for 5′ splice site recognition by enhancing base pairing between U6 and 5′ splice sites that weakly interact with U5 (74, 75). Since the fourth position of the 5′ splice site, which is positioned to interact with m^6A, is enriched for adenosine, m^6A has been demonstrated to enhance base-pairing between U6 and the 5′ splice site (74). Conversely, the fourth position of the 5′ splice site in budding yeast contains an invariant uridine, resulting in Watson-Crick base-pairing between U6 and the 5′ splice site (75).

Several other post-transcriptional modifications on snRNAs are carried out by the coordination of modification enzymes and small nucleolar RNAs (snoRNAs) that base pair with a target RNA to guide modifications at specific sites. snoRNAs are classified into two groups based on sequence and structure motifs and the modifications they guide. Box C/D snoRNAs, which guide 2′-O-methylation of ribosomal RNA (rRNA) and snRNA, share a kink-turn structure and a C box (RUGAUGA) and D box (CUGA) motif (76). Box H/ACA snoRNAs are responsible for directing pseudouridylation on rRNA and snRNA and consist of two hairpins followed by a single-stranded box H (ANANNA) and ACA motif (77). Conserved U6 2′-O-methylating box C/D snoRNAs have been described in humans, fission yeast, and *Xenopus* oocytes (78–80). Since 2′-O-methylations tend to cluster in the region of U6 that base-pairs with U4, disruption of these modifications can manifest as splicing defects (80) (Figure 4). Similarly, snoRNA-guided pseudouridylation of U2 also influences splicing efficiency by promoting spliceosome assembly (63) and altering the structure of the U2 branch site recognition region, which base-pairs with the pre-mRNA branch site (81). Together, these data suggest that post-transcriptional modifications of snRNAs ultimately shape splicing by modulating base-pairing between snRNAs and pre-mRNA, as well as between different snRNAs within the spliceosome.

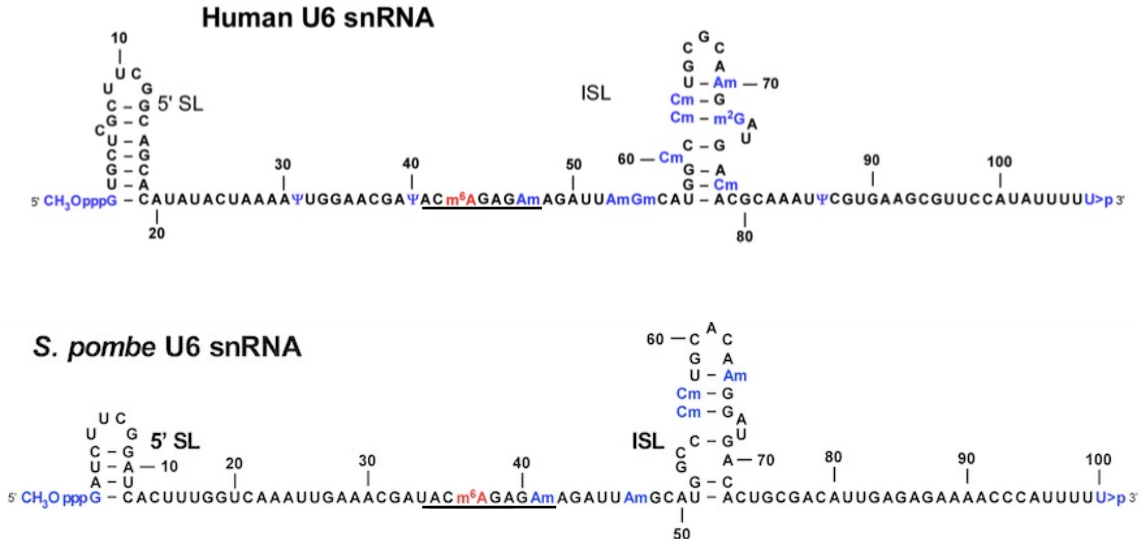

Figure 4: Sites of post-transcriptional modifications in human and *S. pombe* U6 snRNA
CH_3OpppG= γ-monomethyl phosphate cap; Ψ= pseudouridine; m^6A=methyladenosine; Am, Gm, Cm= 2′-O-methylation; m^2G= methylguanosine; U>p= 2′,3′-cyclic phosphate. ISL= internal stem loop. The conserved ACAGAGA sequence that base-pairs with the 5′ splice site is underlined. Figure adapted from (74).

1.4 Divergent RNA processing pathways across evolution: a case study of telomerase RNA

While there are species-specific nuances to processing and post-transcriptional modifications for tRNA and snRNA, many of the processing pathways and modifications themselves are conserved across evolution. In sharp contrast to this idea, the telomerase RNA, which acts as a template for repeat addition to the ends of linear eukaryotic chromosomes, has puzzled biologists for decades as each newly discovered telomerase RNA seemingly breaks prior established rules. In general, telomerase RNA contains a template region for the reverse transcriptase, a pseudoknot for telomerase RNP assembly, and a stem terminus element that stimulates catalytic activity of the enzyme (82). But beyond such broad conservation in organization, telomerase RNA from different species varies greatly in size, structure, constituent RBP partners, and most notably, processing and maturation.

The telomerase RNA was first characterized in the unicellular ciliate *Tetrahymena thermophila* as a component of cell-free extracts capable of adding tandem DNA repeats onto DNA primers without an existing template (83, 84). The *T. thermophila* TER RNA is relatively short at only 159 nucleotides, and is transcribed by RNAP III (84). Transcription by RNAP III is a common feature of all ciliate telomerase RNA (85) and more recently, was also found to be the case for plant (86, 87) and insect telomerase RNA (88). Telomerase RNA in vertebrates and yeast is much longer (450 nucleotides in humans and over 1000 nucleotides in budding and fission yeast) and is transcribed by RNAP II; consistent with this, vertebrate and yeast telomerase RNAs possess a 5′ TMG cap like RNAP II-transcribed snRNAs (89–94). It remains unclear whether transcription by RNAP II or RNAP III produced the ancestral telomerase RNA, although the presence of an RNAP II-transcribed telomerase RNA in Trypanosomes, an early-

branching eukaryote (95), suggests that the evolution of ciliate telomerase RNA from an RNAP II-transcribed ancestor was accompanied by compaction and the switch to RNAP III transcription (96). Even more divergent, the telomerase RNA from the fungus *Ustilago maydis* is processed from the 3′ untranslated region (UTR) of an unannotated protein-coding gene and contains a 5′ monophosphate cap (97).

3′ processing of human telomerase RNA (hTR) involves competition between exosome-mediated degradation and poly(A)-specific ribonuclease- (PARN) mediated maturation. A 3′ extended hTR precursor can either be recognized by the nuclear exosome targeting complex (NEXT) and the cap-binding complex A (CBCA) and subsequently degraded by the exosome, or polyadenylated and processed by PARN into the mature 3′ end (98, 99). hTR also contains an H/ACA motif and although it is bound by the snoRNA-binding proteins NHP2, NOP10, GAR1, and the pseudouridine synthase Dyskerin (100), there is no evidence for hTR acting as a guide RNA to direct pseudouridylation of another target. Rather, Dyskerin uses a catalytic-independent function to bind to the H/ACA box, leading to a conformational change that promotes trimming of the hTR precursor by the exosome, followed by PARN-mediated processing to yield the mature 3′ end (100). In the absence of H/ACA RNP assembly on hTR, the hTR precursor folds into a triple helix that acts as a substrate for exosome-mediated degradation instead of trimming. Taken together, this suggests a model whereby hTR accumulation is limited by H/ACA RNP assembly, which tilts the balance between degradation and 3′ processing (100).

While the fission yeast telomerase RNA, TER1, is also transcribed by RNAP II (92, 93), it undergoes very different processing and maturation steps. The mature 3′ end of TER1 is produced by an incomplete splicing reaction where the intron is removed and the 5′ splice site is released before exon ligation, thus becoming the new 3′ end of the transcript (101). Elements

within the TER1 intron, including a strong branch point and a long distance between the branch point and 3′ splice site, promote a slow transition from the first step of splicing to the second, favoring spliceosome-mediated cleavage rather than a complete splicing reaction. This is achieved largely through full complementarity of the TER1 branch site to the U2 branch site recognition region, which promotes the first transesterification reaction, and a weak polypyrimidine tract that binds U2AF with lower affinity, thereby inhibiting the second transesterification reaction (102). TER1 contains an Sm binding sequence at the spliceosomal cleavage site (94) and recruitment of the Sm complex, which has been well characterized in binding RNAP II-transcribed snRNA (103), promotes splicing and addition of the TMG cap (94). The Sm complex is then replaced by the Lsm2-8 complex, which binds the uridylate-rich sequence at the mature 3′ end of TER1, protects TER1 from exoribonucleolytic degradation and promotes the interaction between TER1 and the reverse transcriptase Trt1 (94). The switch from Sm to Lsm binding correlates with distinct, non-overlapping substrates: TER1 precursors are exclusively bound by Sm, while mature TER1 is only bound by Lsm2-8 (94). The complexity of TER1 maturation, coupled with the sequential assembly of protein complexes on TER1, represents another example of the striking diversification of telomerase RNA among eukaryotic species.

1.5 The RNA chaperones La and LARP7 guide processing and post-transcriptional modification of structured, uridylate-containing noncoding RNAs

Among the many processing steps to yield mature, functional eukaryotic tRNAs, snRNAs, and telomerase RNA, a conserved feature is the involvement of La and La-related proteins (LARPs). La and LARPs have been studied for their roles in the metabolism of coding

and noncoding RNAs and for their roles as RNA chaperones (104–106), a class of proteins that resolve misfolds without external energy input (107, 108). La and LARPs are characterized by the tandem arrangement of the eponymous La motif and an RNA recognition motif (106).

1.5.1 The La protein promotes pre-tRNA processing through 3′ end protection and RNA chaperone activity

Genuine La associates with nascent RNAP III transcripts, including pre-tRNA, through the ubiquitous 3′ polyuridylate-containing trailer (109–111). Numerous structural studies led to insights into the polyuridylate binding mode of La and how it contributes to pre-tRNA binding and maturation. The three terminal uridylates are sequestered in a basic- and aromatic-rich cleft between the La motif and RRM1, with the exposed face of the RRM1 β-sheet available for making additional RNA contacts (Figure 5) (8, 112). In agreement with this additional proposed binding site on the face of the RRM1 β-sheet, it was found that La has a higher affinity for pre-tRNA than end-processed pre-tRNA or a dissociated polyuridylate-containing pre-tRNA trailer, which can be attributed to the additive effects upon pre-tRNA engagement with the polyuridylate binding site and the RRM1 β-sheet binding site (113). The importance of the RRM1 in pre-tRNA binding *in vitro* and *in vivo* has led to a model suggesting that polyuridylate binding by the La motif contributes to binding specificity by directing La to RNAP III transcripts, while the RRM1 further increases pre-tRNA binding affinity through contacts to the pre-tRNA body (113–115).

Consistent with the engagement of different pre-tRNA elements—the polyuridylate trailer and pre-tRNA body—the two separate RNA binding surfaces on the La protein mediate distinct activities in pre-tRNA processing. Mutation of conserved aromatic residues in basic patches in the RRM1 (named RNP1 and RNP2, Figure 5), which project from the β-sheet of

RRM1, had no effect on uridylate binding or 3′ end protection, but were required for tRNA functionality in a tRNA-mediated suppression assay that relies on correctly folded tRNAs for activity (48). This tRNA folding activity was further mapped to include basic residues in loop-3 of the RRM1 (Figure 5), with mutations to loop-3 impairing tRNA-mediated suppression activity and RNA folding in an *in vitro cis*-splicing assay (113). Like other tested RNA chaperones, La is capable of annealing and dissociating RNA duplexes (104, 116), and mutants incapable of strand annealing and dissociation were also inactive in tRNA-mediated suppression, suggesting that La promotes tRNA functionality, at least in part, by using its RNA chaperone activity to assist pre-tRNA folding (104).

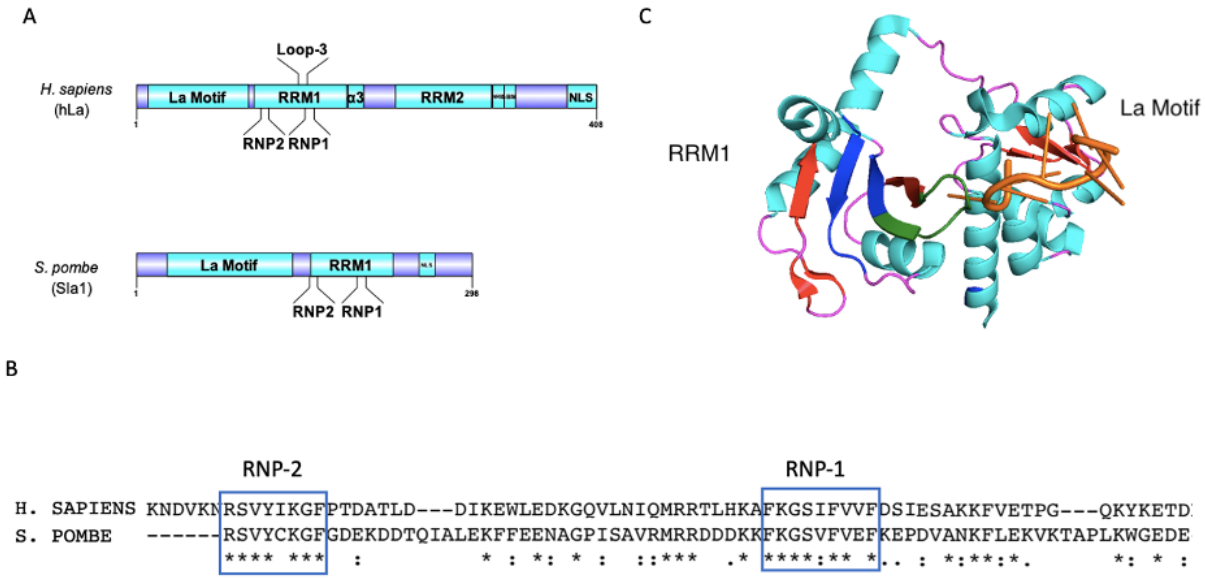

Figure 5: Regions in the RNA recognition motif (RRM1) of the La protein play a role in La's RNA chaperone activity
A) Schematic of the human and fission yeast La proteins. NRE= nuclear retention element, SBM= short basic motif, NLS= nuclear localization sequence.
B) Multiple sequence alignment of the conserved RNP1 and RNP2 sequences in the RRM1 of the human and fission yeast La proteins (113).
C) Ribbon representation of the high-resolution structure of the La motif and RRM1 of the human La protein in complex with a polyuridylate RNA oligomer (orange) (structure 2VOO from (8), visualized in PyMOL). α-helices are pictured in cyan, β-sheets in pink. Regions

important for RNA chaperone activity are highlighted: RNP1 and RNP2 (blue) and loop-3 (green). This figure has previously been published in (41).

A long-outstanding question concerning the La protein and other tRNA chaperones revolves around the mechanism of substrate selection, and whether tRNA chaperones preferentially bind misfolded over natively folded substrates to assist their folding. La and the bacterial modification enzymes TruB and TrmA, which also function as tRNA chaperones, indiscriminately bind folded and misfolded tRNAs, suggesting a general mechanism regarding substrate selection by tRNA chaperones (38, 117, 118). Both studies proposed that chaperones are recruited to tRNA by features relating to their processing state rather than fold. For La, recognition of the polyuridylate-containing trailer on nascent pre-tRNAs enables binding and subsequent chaperone activity. The time between La binding to the pre-tRNA trailer and dissociation following trailer cleavage allows tRNAs to acquire the proper fold through a combination of La-mediated RNA chaperone activity and stabilizing post-transcriptional modifications (Figure 6) (38). Similarly, TruB preferentially binds and modifies unmodified tRNA, which corresponds to a relative early step in tRNA biogenesis and exhibits similar binding affinity for folded and misfolded substrates (117, 119). TrmA also exhibits preferences relating to processing state by binding TruB-modified tRNAs with higher affinity than unmodified tRNAs (119). Together, data from these tRNA chaperones suggest a general model wherein tRNA chaperones can sample all tRNA at a certain point in the maturation pathway. Under conditions where RNA chaperone levels are limiting relative to pre-tRNA substrates (as has been hypothesized for La (48)), this suggests that binding of all tRNAs (misfolded or not) by chaperones may limit chaperone folding efficiency, in which a pool of misfolded tRNAs might not have access to chaperone activity as a result of competition with folded substrates (38). It is not yet known whether this is a common mechanism of all tRNA chaperones, and it is therefore

anticipated that additional structural studies on the binding mechanisms of other known and speculated tRNA chaperones will provide a more comprehensive picture.

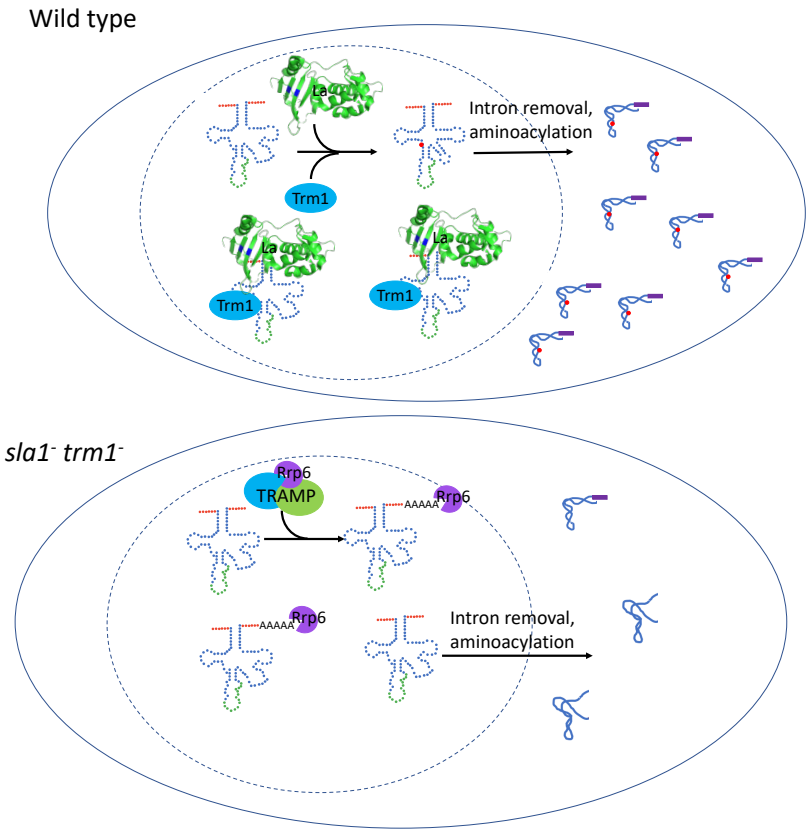

Figure 6: La (Sla1) and the tRNA methyltransferase Trm1 cooperate to promote tRNA folding, accumulation, and functionality in fission yeast
Sla1 is represented by the amino-terminal domain of the human La protein (structure 2VOO from (8)). A combination of La-mediated tRNA chaperone activity and Trm1 modification ensures proper folding such that pre-tRNAs accumulate and undergo aminoacylation (top), while misfolded pre-tRNAs are often degraded by the nuclear surveillance machinery in the absence of La and Trm1 (bottom). Some misfolded or unmodified pre-tRNAs may escape nuclear surveillance and are exported to the cytoplasm, where they may get aminoacylated and function in translation (bottom). This figure has previously been published in (41).

1.5.2 LARP7 associates with diverse RNA Polymerase III transcripts

Like La, LARP7's nuclear localization and tandemly arranged La motif and RRM1 contribute to its propensity to interact with nascent RNAP III transcripts including the U6 and 7SK snRNA and telomerase RNA. Early LARP7 studies focused on the telomerase-associated

protein p65 in *Tetrahymena*. p65, which contains a divergent La motif, an RRM, and a C-terminal xRRM, interacts with the telomerase RNA TER, is required for TER accumulation, and forms a stable component of the telomerase RNP (120, 121). p65 engages TER through the La motif binding the 3′ polyuridylate trail of the RNAP III-transcribed TER, enabling protection from exoribonucleolytic degradation, and the xRRM binding to stem IV to promote its interaction with the reverse transcriptase TERT (122).

More recent work identified a LARP7 homolog in fission yeast, Pof8, that also functions in telomere maintenance (11–13). The putative Pof8 La motif lacks the conserved uridylate binding residues of LARP7 homologs, arguing against a role in uridylate binding and 3′ end protection—a role that is most likely fulfilled by the Lsm2-8 complex (11). Beyond binding to and stabilizing the telomerase RNA TER1, Pof8 also has a role in promoting formation of the telomerase holoenzyme (11). Similar to p65, the xRRM is a major determinant for Pof8-mediated telomere biogenesis, with shorter telomeres, reduced TER1 levels, and a reduced interaction between Pof8 and TER1 in xRRM mutants (12, 13). Further, the xRRM of Pof8 recognizes correctly folded over misfolded TER1 to promote functional telomerase complex assembly in a manner similar to p65 promoting TER folding and assembly with TERT (14). As other fungal Pof8 homologs also possess an xRRM sharing homology with the CTD of LARP7 and p65, it is anticipated that Pof8 may have a conserved role in telomere maintenance beyond fission yeast (12, 13, 123).

To date, there has been no evidence that human LARP7 interacts with hTR or the telomerase holoenzyme. Instead, human LARP7 has been well-characterized for its role in the transcriptional regulatory 7SK snRNP. LARP7 uses its La motif and RRM1 to bind the 3′ polyuridylate trail of the RNAP III-transcribed 7SK snRNA and its xRRM to bind stem loop 4

(SL4) of 7SK (9). Functionally, 7SK acts as a scaffold for LARP7, the 5′ methyltransferase MePCE, and hexamethylene bisacetamide-inducible protein (HEXIM1/2), which in turn bind and sequester positive transcription elongation factor b (P-TEFb) (124–126). When bound to the 7SK snRNP, P-TEFb is unable to phosphorylate the C-terminal domain of the largest subunit of RNAP II, thereby preventing the transition into productive transcription elongation (125, 127, 128). Recent high resolution structures of the 7SK snRNP revealed two distinct conformations of the RNA: a linear 7SK that sequesters P-TEFb and a circular 7SK that leads to P-TEFb release (129). 7SK equilibrium is dynamic, with conformational switching between the two states further regulated in response to cell state. Quiescent cells, which display decreased transcription relative to proliferating cells, are characterized by a greater proportion of 7SK transcripts in the linear, P-TEFb-bound state (130). LARP7 has been proposed to act as an RNA chaperone by promoting conformational switching to the circular state, and as an RNP chaperone by inducing a conformational change in MePCE that results in occlusion of the methyltransferase active site and subsequent catalytic inhibition (129).

Although the U6 snRNA has long been thought to only be part of La's repertoire of RNA targets, studies in humans and mice revealed that LARP7 is also involved in the U6 biogenesis pathway (131, 132). Like La, LARP7 interacts with the 3′ polyuridylate trailer of U6 through the La motif and RRM1 but rather than only providing 3′ end protection, LARP7 also promotes 2′-O-methylation at several positions within U6 (131, 132). Mechanistically, LARP7 facilitates the base-pairing interaction between U6 and 2′-O-methylation guide snoRNAs, the latter of which interacts with LARP7 through the xRRM, providing another example of the importance and versatility of the xRRM in noncoding RNA biogenesis and processing (131). Deletion of LARP7 leads to decreased 2′-O-methylation of U6 and consequent changes in alternative splicing—

including intron retention and exon skipping—that were exacerbated upon heat stress in human cells (131) and in male germ cells in mice (132). While La and LARP7 have mostly non-overlapping targets, their shared propensity for uridylate trailers, RRM-mediated binding of structured RNA, and RNA chaperone activity underscores how nuclear La-related proteins participate in the processing of RNAP III-transcribed non-coding RNAs through the tandem arrangement of shared and distinct RNA binding domains.

1.6 RNA modification enzymes have moonlighting functions as RNA chaperones

Unlike the La protein, tRNA modification enzymes often are not end-binding proteins and as such, would not be expected to offer protection from exoribonucleolytic degradation. Nevertheless, the increase in tRNA degradation observed in yeast and bacteria lacking particular modification enzymes suggests that these enzymes impart structural stability on their substrates, either through the modification itself or an alternate, catalytic-independent function. Initial clues that modification enzymes may have functions beyond their enzymatic activity came from early findings that catalytically inactive mutants of the bacterial tRNA modifying enzymes TruB and TrmA rescue growth defects in the respective bacterial knockout strains (133, 134). A catalytically inactive mutant of Trm2, the eukaryotic homolog of TrmA, partially rescues the temperature-sensitive growth defect caused by a mutant allele of tRNA Ser^{CGA}, suggesting a conserved function in promoting tRNA folding via tRNA chaperone activity (135).

Similar models for RNA modification enzymes acting as RNA chaperones have come from the study of rRNA modification enzymes (136, 137). Depletion of the budding yeast rRNA methyltransferase Dim1 inhibited pre-rRNA cleavage although replacement of the modifiable adenines (A1779 and A1780) with unmodifiable guanosines resulted in normal pre-rRNA

processing (138). Similar findings have been reported for RluD, a bacterial pseudouridine synthase responsible for modifying 3 nucleotides in helix 69 in 23S rRNA. Disruption of the *RluD* gene resulted in a growth defect that could be rescued by expression of a catalytically inactive RluD mutant suggesting that RluD may fold helix 69 independent of modifying it (139, 140).

1.6.1 tRNA modification enzymes can act as tRNA chaperones

Evidence that tRNA modification enzymes also function as genuine RNA chaperones has very recently come to the forefront. Pseudouridine synthases typically use a base-flipping mechanism to access their target nucleotides for modification. Since these enzymes rely on local structural rearrangement, it is tempting to speculate that these enzymes might also act as tRNA chaperones to assist with tRNA folding. For the bacterial pseudouridine synthase TruB, insertion of the histidine imidazole group (H43) into the T-loop forces the target base (U55) to flip out to avoid steric clashes with side chains carboxy-terminal to the inserted histidine. Due to the resulting disrupted tertiary interactions between the T- and D-loops (Figure 2B), the bases of nucleotides 56 and 57 also flip out together with U55, positioning all three bases in the active site of the enzyme (141). It has thus been hypothesized that TruB's ability to disrupt tertiary structure may allow it to act as a tRNA chaperone by giving misfolded substrates another chance to form correct tertiary interactions (141). While the catalytic mechanisms differ between pseudouridine synthases and methyltransferases, bacterial and eukaryotic tRNA methyltransferases also use base-flipping to access target nucleotides. tRNA methylation by the bacterial methyltransferase TrmA, which is responsible for m^5U54 modification, requires rearrangement and refolding of the T-arm to position U54 in the active site of the enzyme (118).

The extensive findings that tRNA modification enzymes often refold their substrates, as well as studies suggesting a fitness advantage conferred by catalytically inactive mutants converge upon a model wherein tRNA modification enzymes have dual functions in catalysis and tRNA folding. Several elegant studies have expanded upon so-called classical RNA chaperones, characterizing prokaryotic tRNA modification enzymes as a novel class of tRNA-specific chaperones. Alternate functions of TruB were explored, revealing that a catalytically inactive TruB mutant is capable of folding tRNA *in vitro* (117). *In vitro* folding activity correlated with the degree of growth rescue in co-culture competition assays; consequently, amino acid substitutions abolishing tRNA binding led to decreased folding activity and bacterial fitness, supporting the idea that binding and chaperone activity, rather than solely modification, are crucial for fitness (117). Rapid-kinetic stopped-flow experiments using tRNA fluorescently labeled at nucleotide 57 revealed that following TruB binding, the tRNA elbow region is quickly and repeatedly unfolded and refolded before pseudouridylation, thereby revealing the molecular mechanism of TruB's tRNA chaperone activity (117, 141). It has been suggested that TruB's slow catalytic rate may have evolved as a mechanism to allow for multiple rounds of unfolding and refolding by TruB to assist tRNA folding into native, functional conformations (117, 142). Underscoring the potential evolutionary conservation of dual function tRNA modification enzymes, many of the residues identified by structural and biochemical studies that are required for tRNA binding (117, 143) are conserved among TruB homologs (Figure 7A).

Additional studies on tRNA methyltransferases raised the possibility that tRNA modification enzymes functioning as tRNA chaperones may be more prevalent than previously thought. Expanding on initial studies demonstrating that the methyltransferase TrmA is essential for viability but its catalytic activity is not (133), phenylalanine and histidine residues (F106 and

H125) were identified as critical for tRNA binding (118). Much like TruB, wild type and catalytically inactive TrmA possess *in vitro* folding activity, with substitutions of H125 and F106 showing reduced to no folding activity, respectively. The implication that an aromatic residue, in particular, is required for tRNA binding and by extension, tRNA chaperone activity, is supported by the high degree of conservation of F106 as an aromatic residue among bacterial and eukaryotic TrmA homologs (Figure 7B). Integrating previous structural data on TrmA, the authors proposed a model in which F106 and H125 act as wedges to disrupt tertiary interactions in the elbow region through steric clashes with G18 at the interface of the D and T arms, thereby providing tRNA with a second chance at forming correct tertiary interactions (Figure 2B) (118, 144). These studies provided a foundation upon which to continue exploring catalytic-independent activities of RNA modification enzymes and signals a paradigm shift regarding the role of these enzymes in tRNA maturation.

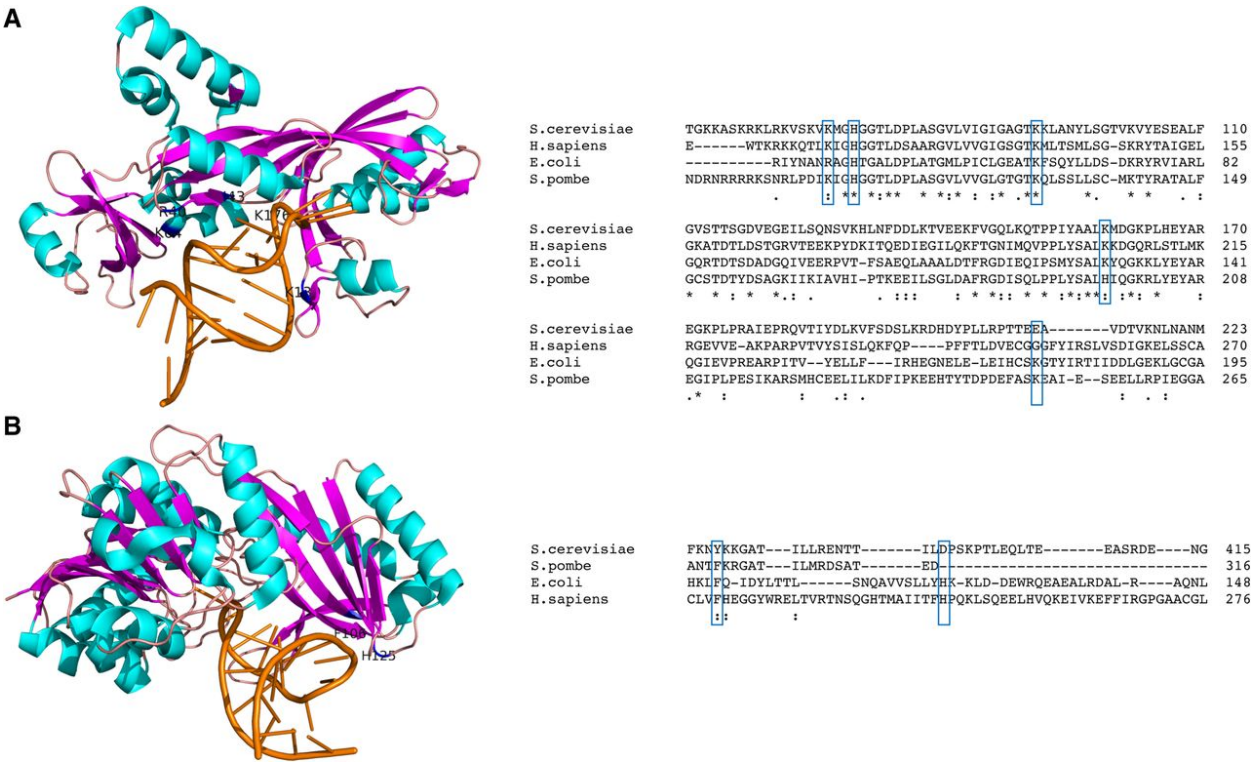

Figure 7: Select tRNA-binding residues are conserved among TruB and TrmA homologs
A) Sequence alignment and ribbon representation of the high-resolution structure of the bacterial pseudouridine synthase TruB in complex with a T stem-loop RNA (orange) (structure 1K8W from (141)), visualized in PyMOL. α-helices are pictured in cyan, β-sheets in pink. Experimentally identified tRNA binding regions (117, 141) are indicated in blue.
B) Sequence alignment and ribbon representation of the high-resolution structure of the bacterial methyltransferase TrmA in complex with a T stem-loop RNA (orange) (structure 3BT7 from (144)), visualized in PyMOL. α-helices are pictured in cyan, β-sheets in pink. Experimentally identified tRNA binding regions (118) are indicated in blue. This figure has previously been published in (41).

1.7 Scope of thesis

While it has long been appreciated that RNA modifications have a variety of roles ranging from promoting RNA structure and stability to modulating interactions with RNA binding proteins, more recent evidence suggests that certain RNA modification enzymes may also possess catalytic-independent functions. Despite the newfound appreciation for these so-called “moonlighting” enzymes, studies characterizing these modification-independent functions have largely been limited to bacterial tRNA modifying enzymes, raising the question of how

extensive this phenomenon might be. **The primary aim of this work was to uncouple catalysis from catalytic-independent activities to determine if eukaryotic RNA modification enzymes also possess alternate activities that do not rely on catalysis.**

Dissertation summary:

1. The human methyl phosphate capping enzyme (MePCE) has been well studied for its role in 5′ capping select RNAP III transcripts such as the 7SK RNA (64). It is therefore puzzling that there is an MePCE homolog in fission yeast, an organism with no known 7SK. To interrogate the function of the fission yeast MePCE homolog Bmc1, I characterized its RNA interactome. **This work revealed that Bmc1 is a component of the fission yeast telomerase holoenzyme and assumes a non-catalytic role in promoting holoenzyme assembly and telomerase RNA stability (Chapter 2).** Further, I demonstrated that Bmc1 interacts with the RNA binding protein LARP7 in the telomerase holoenzyme, much in the same manner as the human Bmc1 and LARP7 homologs interact in the 7SK snRNP, thereby providing a novel link between two very distinct RNPs.

2. Although a γ-monomethyl phosphate cap has been found on the 5′ end of the U6 snRNA in humans and fission yeast (65, 67), the role of MePCE/Bmc1 in U6 biogenesis and stability has not been studied. **This work demonstrated that Bmc1 is important for directing internal 2′-O-methylations in U6 that promote spliceosome assembly to fine-tune splicing, particularly at elevated temperatures (Chapter 3).** Much like the role of Bmc1 in telomerase, catalytic activity is not critical for this function. This work therefore provides additional evidence supporting the idea of catalytic-independent functions for eukaryotic RNA modification enzymes.

3. While previous work has linked the tRNA methyltransferase Trm1 to the La protein for its role in promoting pre-tRNA stability (38, 145), these studies solely focused on the contribution of Trm1-catalyzed methylation to tRNA structure and function. **This work identified and mutated residues critical for catalytic activity to show that Trm1 influences pre-tRNA processing through a combination of methylation and catalytic-independent tRNA chaperone activity (Chapter 4).** This is the first comprehensive characterization of a eukaryotic tRNA modification enzyme that also functions as a tRNA chaperone and as such, suggests that tRNA chaperone activity may be an evolutionarily conserved feature of RNA modification enzymes.

Using the fission yeast RNA methyltransferases Bmc1 and Trm1 as proof-of-principle concepts, this work provides evidence supporting newly described non-catalytic roles for eukaryotic RNA modification enzymes.

Chapter 2: The methyl phosphate capping enzyme Bmc1/Bin3 is a stable component of the fission yeast telomerase holoenzyme

Jennifer Porat[1], Moaine El Baidouri[2, 3], Jorg Grigull[4], Jean-Marc Deragon[2, 3, 5], and Mark A. Bayfield[1*]

1. Department of Biology, York University, Toronto, Canada
2. LGDP-UMR5096, Université de Perpignan Via Domitia, Perpignan, France
3. CNRS LGDP-UMR5096, Perpignan, France
4. Department of Mathematics and Statistics, York University, Toronto, Canada
5. Institut Universitaire de France, Paris, France

*Correspondence: bayfield@yorku.ca (M.A.B.)

This chapter was previously published as Porat J., El Baidouri M., Grigull J. Deragon J-M., and Bayfield M.A. The methyl phosphate capping enzyme Bmc1/Bin3 is a stable component of the fission yeast telomerase holoenzyme. *Nat Commun* **13**, 1277 (2022). https://doi.org/10.1038/s41467-022-28985-3

Contributions: J.P. conceived of the study, designed, performed, and analyzed all experiments, and wrote the first draft of the manuscript with input from all authors. M.E.B. and J.-M.D. performed phylogenetic analyses (Figure 6, supplementary figure 7). J.P. analyzed RNA-Seq data with help from J.G. M.A.B. conceived of the study, designed experiments, supervised the project, and edited the manuscript.

2.1 Abstract

The telomerase holoenzyme is critical for maintaining eukaryotic genome integrity. In addition to a reverse transcriptase and an RNA template, telomerase contains additional proteins that protect the telomerase RNA and promote holoenzyme assembly. Here we report that the methyl phosphate capping enzyme (MePCE) Bmc1/Bin3 is a stable component of the *S. pombe* telomerase holoenzyme. Bmc1 associates with the telomerase holoenzyme and U6 snRNA through an interaction with the recently described LARP7 family member Pof8, and we demonstrate that these two factors are evolutionarily linked in fungi. Our data suggest that the association of Bmc1 with telomerase is independent of its methyltransferase activity, but rather that Bmc1 functions in telomerase holoenzyme assembly by promoting TER1 accumulation and Pof8 recruitment to TER1. Taken together, this work yields new insight into the composition, assembly, and regulation of the telomerase holoenzyme in fission yeast as well as the breadth of its evolutionary conservation.

2.2 Introduction

To ensure complete DNA replication, the termini of eukaryotic chromosomes contain tandem repeats, or telomeres, that can be continually extended as the ends of linear chromosomes are lost through DNA replication(146). Telomeres serve as protection from DNA degradation, end-to-end fusions, chromosomal rearrangements, and chromosome loss (146, 147). With very few exceptions, eukaryotes extend telomeric DNA sequences through the telomerase holoenzyme, a complex containing the telomerase reverse transcriptase (Trt1 in the fission yeast *Schizosaccharomyces pombe*), an RNA template (TER1 in *S. pombe*), and accessory proteins that promote complex assembly and tethering to telomeric DNA (92, 93, 146–148). While the reverse transcriptase/RNA template core of telomerase is generally well-conserved among

eukaryotes, major differences exist, including in the sequence and structure of the RNA template. In contrast to ciliate telomerase RNAs, which are small RNA Polymerase III transcripts (84), yeast and metazoan telomerase RNAs are longer and transcribed by RNA Polymerase II as precursors(89, 149). These precursors then undergo an extensive maturation process to yield the mature form that integrates into the telomerase holoenzyme (89, 92, 93, 149).

In *S. pombe,* the mature form of TER1 is generated from an intron-containing precursor through a spliceosome-catalyzed reaction involving release of the 5′ exon prior to exon ligation (101). TER1 maturation then proceeds with the sequential binding of the Sm and Lsm complexes. Sm proteins, well-characterized for their role in splicing, bind TER1 immediately upstream the 5′ splice site and promote 3′ maturation and the addition of a 5′ trimethylguanosine (TMG) cap by the methyltransferase Tgs1 (94). The Sm complex is then replaced by the Lsm2-8 complex, which serves to protect the mature 3′ end of TER1 from exoribonucleolytic degradation and promotes the interaction between TER1 and Trt1 in the active telomerase holoenzyme. The switch from the Sm to Lsm complexes correlates with distinct, non-overlapping substrates: TER1 precursors are exclusively bound by the Sm complex, while the mature form of TER1, ending in a polyuridylate stretch upstream the spliceosomal cleavage site, is only bound by the Lsm2-8 complex (94).

More recently, a role has been proposed for Pof8, a La-related protein 7 (LARP7) homolog, in telomerase assembly and telomere maintenance in *S. pombe*. Ciliate LARP7 family proteins, including p65 from *Tetrahymena thermophila*, have previously been characterized for their functions in telomerase assembly (120). Binding of p65 to stem IV of the *T. thermophila* telomerase RNA TER results in a conformational change to the RNA and subsequent binding of the reverse transcriptase TERT, suggesting a p65-dependent hierarchical assembly of the

telomerase holoenzyme (150). Pof8 is hypothesized to function similarly in *S. pombe*, with Pof8 binding to TER1 promoting recruitment of the Lsm2-8 complex and enhancing the interaction between TER1 and Trt1. Accordingly, Pof8 deletion strains possess shorter telomeres indicative of a defect in telomerase function (11–13). Pof8 also functions in telomerase RNA quality control through recognition of the correctly folded pseudoknot region and subsequent recruitment of the Lsm2-8 complex to protect the 3′ end from degradation (14). Telomerase-related functions in LARP7 family proteins, particularly Pof8, map to a conserved C-terminal domain characteristic of LARP7 family members, the extended RNA recognition motif (xRRM)(122, 151). The Pof8 xRRM is a major determinant for Pof8-mediated telomerase activity, contributing to TER1 binding and complex assembly (12, 15). As other fungal Pof8 homologs also possess an xRRM, it is anticipated that Pof8 may have a conserved role in telomere maintenance beyond fission yeast (12, 123).

Conversely, LARP7 homologs in higher eukaryotes are best characterized in the transcriptional regulatory 7SK snRNP, which includes the RNA polymerase III transcribed 7SK snRNA, the methyl phosphate capping enzyme (MePCE), and hexamethylene bisacetamide-inducible protein (HEXIM1/2). The 7SK snRNP inhibits transcription by sequestering positive transcription elongation factor (P-TEFb) and preventing it from phosphorylating the C-terminal domain of the largest subunit of RNA Polymerase II, which is associated with the transition into productive transcription elongation (125, 127, 128). The La module and xRRM of LARP7 bind 7SK through its polyuridylate trailer and the 3′ hairpin, respectively, and promote MePCE recruitment to the complex (9, 152). In addition to adding a γ-monomethyl phosphate cap (i.e. CH_3-pppN) to 7SK snRNA as a means of protecting it from 5′ exoribonucleolytic degradation, MePCE remains stably bound to 7SK snRNA to stabilize the complex (152). MePCE, a homolog

of the *Drosophila melanogaster* Bin3/BCDIN3 protein, also catalyzes the addition of this atypical cap structure to U6 snRNA (64). Bin3/MePCE homologs are present in many eukaryotes, but to date little has been studied outside of humans and *Drosophila* (153). More recent work has identified BCIND3D, a related Bin3 family protein overexpressed in breast cancer cells, as the enzyme responsible for methylating the 5′ monophosphate of histidine transfer RNA and pre-miR-145 (154, 155). Despite the many insights into the role of Bin3/MePCE in RNA processing in higher eukaryotes, the function of the *S. pombe* Bin3 homolog has yet to be determined.

In this work, we have explored the RNA targets of the *S. pombe* Bin3 homolog (henceforth referred to as Bmc1; Bin3/MePCE1) in an effort to uncover its function. In addition to an expected association of Bmc1 with U6 snRNA, we present data showing that Bmc1 is a stable component of the *S. pombe* telomerase RNP. Our results also provide evidence for an evolutionarily conserved interaction between Bmc1 and LARP7 homologs. Importantly, we show that the Bmc1-Pof8 interaction is required for the recruitment of Bmc1 to both U6 snRNA and the active telomerase holoenzyme. Additionally, we provide data that Bmc1 does not catalyze the addition of a γ-monomethyl phosphate cap on TER1, suggesting a catalytic independent function. Rather, we present evidence that Bmc1 functions in concert with Pof8 to promote telomerase assembly and TER1 accumulation. Taken together, our results identify Bmc1 as a component of the *S. pombe* telomerase holoenzyme, thus adding a new layer of complexity to telomerase assembly and telomere maintenance.

2.3 Results

2.3.1 *S. pombe* Bmc1 interacts with U6 snRNA and the telomerase RNA TER1

While Bmc1/MePCE is conserved in many eukaryotes, its presence in the fission yeast *S. pombe*, an organism lacking 7SK snRNA (153, 156), is not well understood. Unlike the longer Bmc1/MePCE homologs from higher eukaryotes, *S. pombe* Bmc1 only contains a conserved methyltransferase/SAM-binding domain (Supplementary Figure 1A). Alignment of the methyltransferase domain of *S. pombe* Bmc1 to that of *H. sapiens* MePCE and *D. melanogaster* Bin3 reveals that previously identified residues critical for SAM and SAH binding and nucleotide binding (157) are highly conserved in *S.* pombe (Supplementary Figure 1B, C).

We first sought to determine the RNA substrates of *S. pombe* Bmc1 to better understand its role in the processing of fission yeast non-coding RNA(s). Following integration of a protein A (PrA) tag into the Bmc1 genomic locus, we performed RNA immunoprecipitation coupled to sequencing (RIP-Seq), followed by validation of potential candidate substrates with northern blotting and semi-quantitative RT-PCR (Figure 1, Supplementary Data 1). Consistent with previous reports of MePCE interacting with U6 snRNA (64), U6 emerged as one of the most highly enriched Bmc1-interacting RNA transcripts in our Seq dataset (Figure 1A, Supplementary Data 1). *S. pombe* U6 is an unusual transcript in that it is transcribed by RNA Polymerase III yet contains an mRNA-type intron removed by the spliceosome (158, 159). Alignment of RIP-Seq reads to the *S. pombe* genome suggested that Bmc1 interacts exclusively with the spliced form of U6. We confirmed this with northern blotting, demonstrating robust immunoprecipitation of mature U6 and no immunoprecipitation of the intron-containing precursor (Figure 1B). Chromatin immunoprecipitation studies suggest that 7SK and U6 snRNA may be co-

transcriptionally modified by the human MePCE homolog (160), however our data are consistent with a model wherein *S. pombe* Bmc1 interacts with U6 post-splicing.

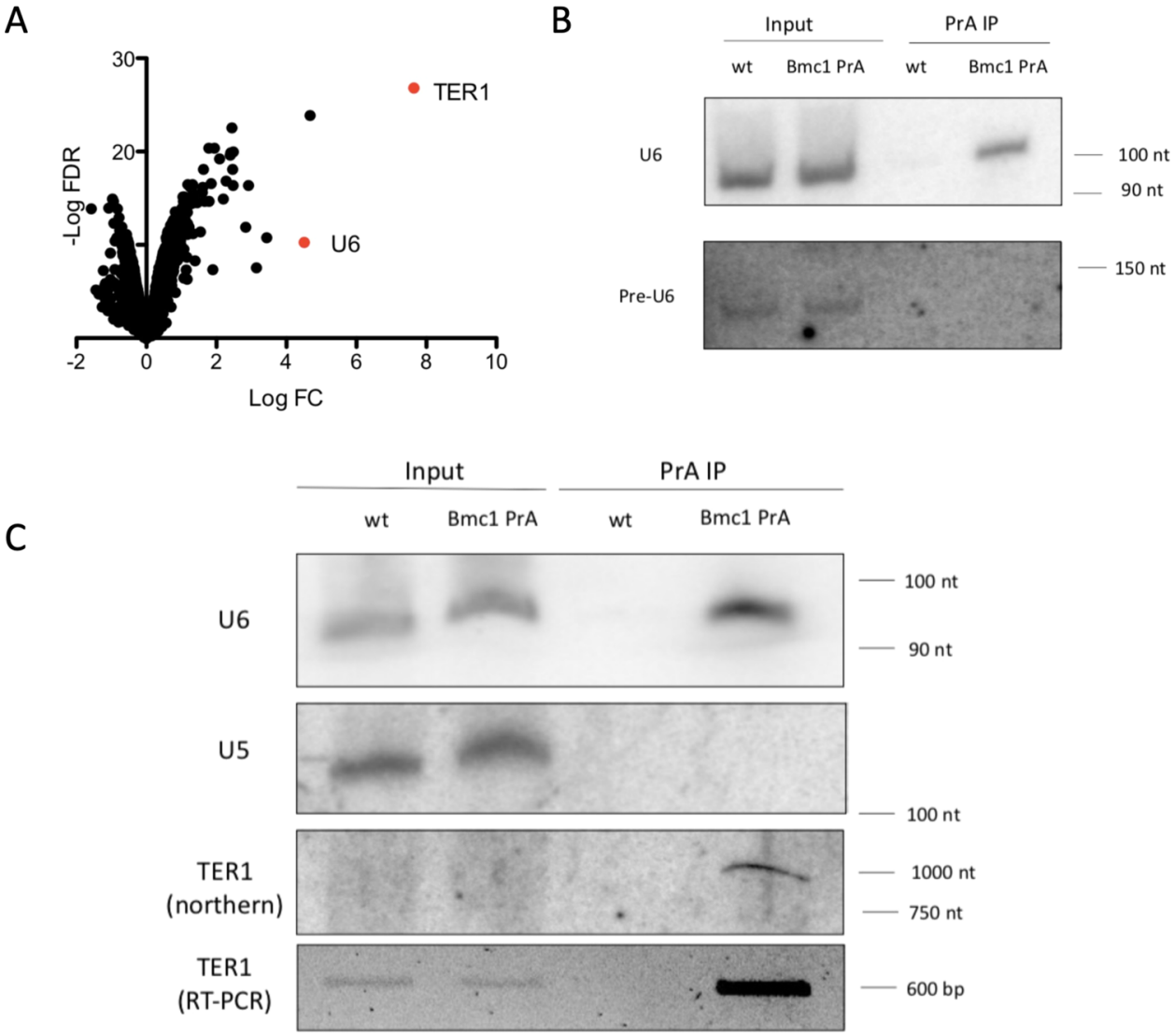

Figure 1: Bmc1 interacts with U6 snRNA and the telomerase RNA TER1
A) Enrichment of Bmc1 PrA immunoprecipitated transcripts compared to an untagged control (biological replicates = 3). Axes represent log2 of fold change (FC) and negative log of false discovery rate (FDR) (Benjamini-Hochberg adjusted p-value ≤0.05).
B) Northern blot analysis of the mature and intron-containing U6 from total RNA and PrA immunoprecipitates from untagged (wild type, wt) and PrA-tagged Bmc1 strains.
C) Northern blot of the telomerase RNA TER1, U6, and U5 from total RNA and PrA immunoprecipitates from untagged and PrA-tagged Bmc1 strains, and semi-quantitative RT-PCR analysis of TER1. Source data are provided as a Source Data file.

Surprisingly, the *S. pombe* telomerase RNA TER1 was the most highly enriched hit in the Bmc1 immunoprecipitates (Figure 1A, C). Given the previously established link between the human Bmc1 homolog MePCE and human LARP7, (125) as well as the established link between the *S. pombe* LARP7 homolog Pof8 and the telomerase holoenzyme (11–13), we considered the possibility that Bmc1 may also be part of the telomerase holoenzyme through an evolutionarily conserved interaction with LARP7 family members.

2.3.2 Bmc1 interacts with the mature form of TER1

Since TER1 processing and maturation involves a spliceosome-catalyzed reaction (101), we next set out to determine the processing state of Bmc1-associated TER1 by sequencing the 5′ and 3′ ends through circularized rapid amplification of cDNA ends (cRACE) (Figure 2A). We also performed cRACE on TER1 immunoprecipitated by Pof8, the telomerase reverse transcriptase Trt1, and Lsm3, all known components of the mature TER1-containing active telomerase holoenzyme (11–13, 92–94). All sequenced candidates had a discrete 5′ end consistent with the reported 5′ end (92, 93) and a similar distribution of 3′ ends ending immediately upstream the 5′ splice site (101), suggesting that Bmc1 interacts with the full-length, 3′ end-matured TER1 associated with the active telomerase holoenzyme. The heterogeneity observed at the 3′ end of all candidates is likely the result of exoribonucleolytic nibbling prior to binding of the Lsm2-8 complex (94). To investigate this further, we subjected TER1 RNA immunoprecipitated by Bmc1, Trt1, Pof8 and Lsm3 to RNase H cleavage to generate shorter 5′ and 3′ fragments and compared fragment size by northern blot (Figure 2B). The sizes of the 5′ and 3′ ends of TER1 were similar across immunoprecipitates, further

substantiating that Bmc1 binds the mature form of TER1, rather than the intron-containing precursor.

Further TER1 processing in *S. pombe* involves the addition of a 5′ trimethylguanosine (TMG) cap by Tgs1 (94). Since Bmc1 homologs are normally associated with the formation of a γ-monomethyl phosphate cap, and to further understand when Bmc1 interacts with TER1 with respect to TER1 processing, we examined the cap structure of Bmc1-associated TER1 by immunoprecipitating RNA associated with Bmc1 and subsequently re-immunoprecipitating this RNA with an anti-TMG antibody. The specificity of the anti-TMG antibody was confirmed by showing that it effectively enriched the TMG cap-containing U5 snRNA over the TMG cap-lacking U6 snRNA or an unrelated tRNA (Figure 2C). While Bmc1-associated U6 snRNA was not immunoprecipitated by the anti-TMG antibody, in agreement with data demonstrating the presence of a γ-monomethyl phosphate cap on U6 *in S. pombe* (65), Bmc1-associated TER1 RNA was effectively enriched by anti-TMG immunoprecipitation (Figure 2D). These data are consistent with previous work demonstrating a TMG cap on TER1 in *S. pombe,* and also with Bmc1 associating with TER1 following spliceosomeal cleavage and 5′ TMG capping, similar to what has been posited for Pof8 (11). This suggests that Bmc1 interacts with the primary cohort of TMG capped TER1 transcripts, and that TER1 is not a substrate for Bmc1-catalyzed γ-monomethyl phosphate capping.

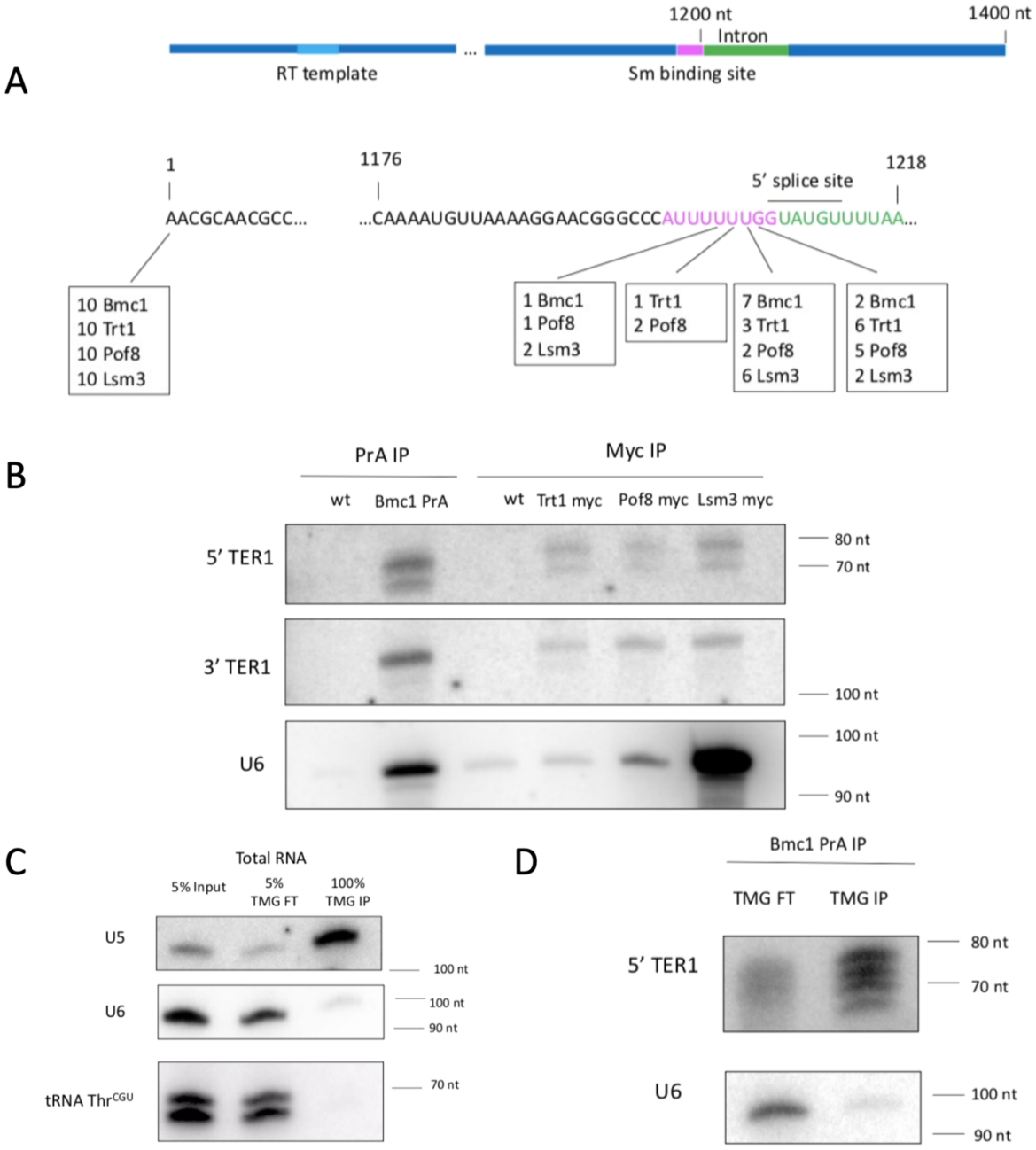

Figure 2: Bmc1 interacts with the same TER1 species as well-established components of the telomerase holoenzyme

A) The 5′ and 3′ ends of Bmc1-, Trt1-, Pof8-, and Lsm3-associated TER1 were identified by cRACE. The results of 10 independent clones per immunoprecipitation are shown below a schematic of the architecture of TER1.

B) RNase H northern blots of RNase H-generated 5′ and 3′ ends of TER1 immunoprecipitated by various telomerase components. The same blot was stripped and reprobed for U6.

C-D) Northern blot of α-TMG flow through (FT) and immunoprecipitated (IP) transcripts from total RNA (C) and Bmc1-associated RNA (D). Source data are provided as a Source Data file.

2.3.3 Bmc1 interacts with components of the mature telomerase holoenzyme

Since our results indicate that Bmc1 interacts with the mature form of TER1, we set out to confirm the presence of Bmc1 in the *S. pombe* telomerase holoenzyme. We immunoprecipitated Bmc1 and identified interacting proteins through mass spectrometry, followed by validation using co-immunoprecipitation (Figure 3). We identified Pof8, the Lsm2-8 complex, and Trt1 in Bmc1 immunoprecipitates, all of which make up the catalytically active core telomerase holoenzyme (11–13, 94, 148, 161, 162) (Supplementary Data 2). We also detected the RNase P and RNase MRP subunit Pop100 in Bmc1 immunoprecipitations. Pop1, Pop6, and Pop7, subunits of RNase P and RNase MRP in budding yeast, have recently been identified as components of the budding yeast telomerase complex (163–165), suggesting that the involvement of RNase P and RNase MRP subunits in telomere maintenance is evolutionarily conserved. The finding that Bmc1 interacts with core components of the telomerase holoenzyme, and not the TMG capping enzyme Tgs1, suggests Bmc1 does indeed associate with the active telomerase holoenzyme rather than a precursor. The involvement of Bmc1 in the telomerase holoenzyme was further substantiated by gene ontology analysis to determine overrepresented biological processes and cellular components among the top 50 Bmc1 interactors. Telomerase holoenzyme complex assembly and telomere maintenance via telomerase emerged as the top overrepresented biological processes (Figure 3A). Similarly, overrepresented cellular components include the Lsm2-8 complex, the telomerase holoenzyme, and spliceosomal snRNPs (Supplementary Table 1). We also repeated immunoprecipitations in the presence of benzonase to determine if these interactions are direct or mediated through a nucleic acid intermediate. With the exception of Pof8, certain members of the Lsm2-8 complex, and an uncharacterized protein (SPCC18B5.09c, recently identified as the telomerase component

Thc1(166)), interactions between Bmc1 and other components of the telomerase holoenzyme were lost, suggestive of an interaction mediated by TER1 (Supplementary Data 2).

We validated the interactions between Bmc1 and Pof8, as well as Bmc1 and Trt1, through co-immunoprecipitation (Figures 3B, 3C, Supplementary Figure 2). We also performed co-immunoprecipitations with benzonase, demonstrating that the interaction between Bmc1 and Pof8 persists with benzonase treatment, while the Bmc1-Trt1 interaction is lost (Figures 3B and 3C). To confirm that the Bmc1-Trt1 interaction is mediated by TER1, we repeated co-immunoprecipitations in a TER1 knockout strain. The direct interaction between Bmc1 and Pof8 remained intact in the absence of TER1, while the Bmc1-Trt1 interaction was completely lost, indicative of Bmc1 assembly in the telomerase holoenzyme nucleated, in large part, by the telomerase RNA itself. The RNA-dependence of the interaction between Bmc1 and Trt1 is reminiscent both of the budding yeast telomerase RNA TLC1, which acts as a scaffold for telomerase holoenzyme assembly (167), as well as the MePCE/Bin3-containing 7SK snRNP (168). The finding that Bmc1 and Pof8 interact directly is in agreement with previous reports demonstrating a protein-protein interaction between MePCE and LARP7 in the context of the vertebrate 7SK snRNP (160, 168), suggesting the direct interaction may be evolutionarily conserved.

A

GO biological process	Fold enrichment	Raw P value	False discovery rate
Telomerase holoenzyme complex assembly	49.39	2.04E-08	5.33E-05
Telomere maintenance via telomerase	31.75	2.54E-04	4.74E-02
RNA-dependent DNA biosynthetic process	31.75	2.54E-04	4.58E-02
Ribonucleoprotein complex assembly	5.47	6.70E-06	2.50E-03
Ribonucleoprotein complex subunit organization	5.29	9.01E-06	2.77E-03
mRNA cis splicing, via spliceosome	5.25	6.76E-05	1.54E-02
mRNA splicing, via spliceosome	4.78	5.48E-05	1.43E-02
RNA splicing, via transesterification reactions with bulged adenosine as nucleophile	4.78	5.48E-05	1.43E-02
RNA splicing, via transesterification reactions	4.72	6.08E-05	1.45E-02
RNA splicing	4.52	8.60E-05	1.80E-02

B

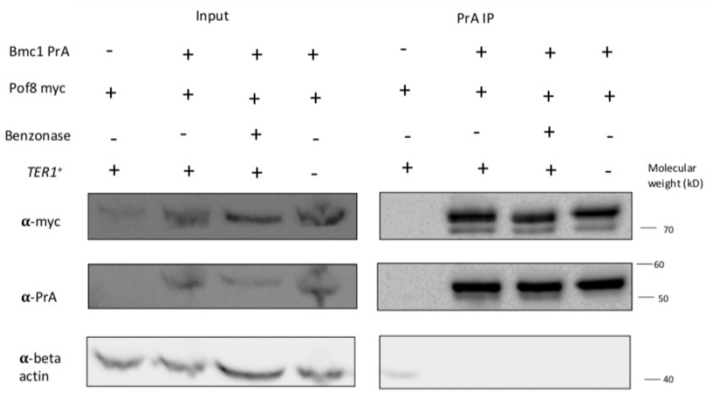

C

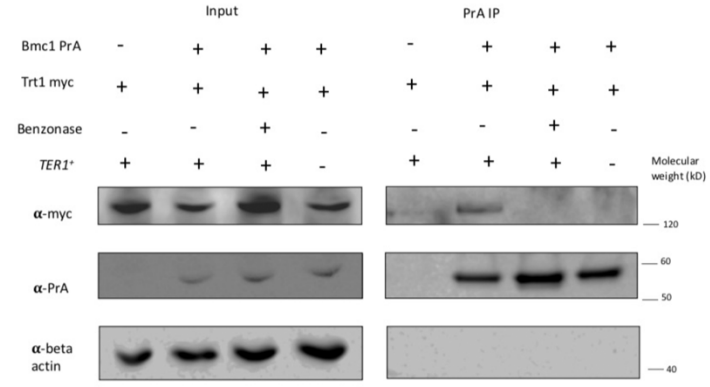

Figure 3: Bmc1 interacts with components of the mature telomerase holoenzyme
A) Gene ontology analysis (biological process) of top 50 Bmc1 protein interactors.
B-C) Examination and nucleic acid-dependence of interactions between Bmc1 and Pof8 (B) and Bmc1 and Trt1 (C) by co-immunoprecipitation and western blotting. Blots were re-probed for beta actin as a loading control. Source data are provided as a Source Data file.

2.3.4 Bmc1 is recruited to the active telomerase holoenzyme through the LARP7 family protein Pof8

We then tested whether Bmc1 was recruited to the telomerase holoenzyme through its interaction with Pof8, much like the human LARP7 homolog promotes MePCE recruitment to 7SK snRNA (152). Immunoprecipitation of Bmc1 in the context of a *pof8*Δ strain resulted in a complete loss of TER1 binding, providing evidence that the interaction between Bmc1 and TER1 is dependent on an interaction between Bmc1 and Pof8 (Figure 4A,B). Unexpectedly, the interaction between Bmc1 and U6 was also lost in the *pof8*Δ strain. Recent findings indicate that mammalian LARP7 binds U6 to guide post-transcriptional modification (131, 132), so it is tempting to speculate that Pof8 may also mediate Bmc1 binding to U6 in fission yeast. To address this, we immunoprecipitated Pof8 alongside Bmc1 and other components of the telomerase holoenzyme and looked for U6 enrichment. We observed slight enrichment of U6 in Pof8-myc immunoprecipitates relative to immunoprecipitation using an untagged strain or the Trt1-myc tagged strain (Figure 4C). We did not see enrichment for the intron-containing precursor, suggesting that like Bmc1, Pof8 interacts with the spliced form of U6. The slight enrichment of U6 with Pof8 immunoprecipitation, compared to the more robust immunoprecipitation seen with Bmc1 and Lsm3, suggests that Pof8 may transiently bind U6, perhaps serving to load Bmc1 on U6. Since LARP7 binding has been reported to disrupt the catalytic activity of MePCE (160), a transient Pof8-U6 interaction may be consistent with U6 receiving a γ-monomethyl phosphate cap, compared to TER1, where stable Pof8 binding may prevent Bmc1 catalytic activity.

To further investigate how the presence of Bmc1 in the TER1-containing telomerase holoenzyme is reliant on Pof8, we fractionated lysates from a wild type and a *pof8*Δ strain on a

glycerol gradient and analyzed the sedimentation patterns of Bmc1, Pof8, and TER1 (Supplementary Figure 3). We found that Bmc1 and Pof8 co-sedimented with TER1 in higher molecular weight fractions in a wild type strain. In contrast, Bmc1 was depleted from higher molecular weight fractions containing TER1 in the absence of Pof8. We also noted a slight shift in TER1 towards lighter fractions in the Pof8 deletion strain, which could be due to a lighter-migrating telomerase holoenzyme lacking Bmc1 and Pof8. These data are also consistent with Bmc1 stably associating with the telomerase holoenzyme in a manner that is dependent on Pof8.

Knowing that Bmc1 interacts with TER1 and components of the telomerase holoenzyme, we next set out to confirm whether Bmc1 is part of the catalytically active telomerase holoenzyme. We performed a previously described *in vitro* telomerase assay that relies on the presence of the TER1- and Trt1-containing telomerase holoenzyme to extend an oligonucleotide resembling telomeric DNA (11) (Figure 4D). Bmc1 immunoprecipitates extended the oligonucleotide in a similar manner previously demonstrated for Pof8 ((11) and see Figure 5D), as well as showed the same loss of activity upon RNase A treatment, supporting the idea that Bmc1, much like Pof8, is a component of the active telomerase holoenzyme (Figure 4D). Consistent with previous results(11, 14), we also observed a loss of activity for Bmc1 immunoprecipitated from a *pof8*Δ strain, which can largely be attributed to the loss of functional, correctly assembled telomerase occurring in the absence of Pof8. Since Trt1 is only recruited to the telomerase holoenzyme following Pof8 and Lsm2-8 binding, coupled with the idea that the assay relies on the presence of a reverse transcriptase, these results are consistent with a model in which Bmc1 is recruited to TER1 through its interaction with Pof8 and remains bound through subsequent holoenzyme assembly and the catalytic cycle (Figure 4E).

To further investigate the link between Bmc1 and Pof8 in telomerase holoenzyme assembly, we tested whether overexpression of Bmc1 could rescue the short telomere phenotype of a *pof8*Δ strain (11–13). Consistent with a model in which Bmc1 requires Pof8 for its assembly into the active telomerase holoenzyme, Bmc1 overexpression in a *pof8*Δ strain was insufficient to rescue telomere shortening, as measured by Southern blot, as well chromosome fusions occurring after telomeres reach a critically short length previously associated with *the pof8*Δ strain (11) (Supplementary Figure 4).

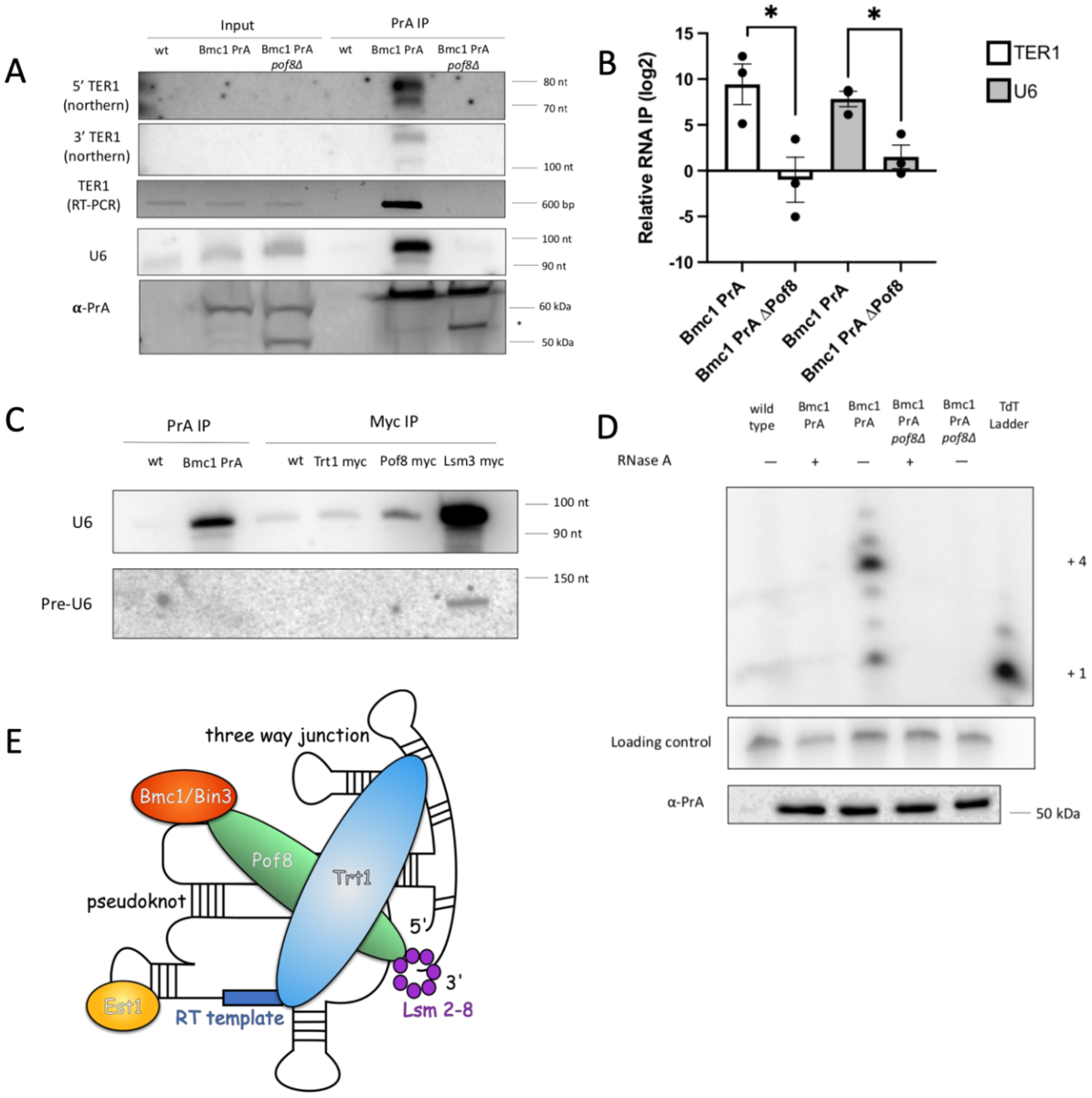

Figure 4: Bmc1 is recruited to the active telomerase holoenzyme by Pof8 (legend on next page)
A) Northern blot and semi-quantitative RT-PCR of TER1 and U6 in PrA immunoprecipitates for an untagged wild type (wt), PrA-tagged (Bmc1 PrA), and PrA-tagged Pof8 knockout strain (Bmc1 PrA Δ*Pof8*). Bmc1 PrA was detected in input and immunoprecipitated samples by western blots probing for PrA (bottom panel). Possible cleavage products are indicated with an asterisk.
B) qRT-PCR of TER1 and U6 in Bmc1 PrA immunoprecipitates from a wild type and *pof8*Δ strain normalized to input RNA. Relative TER1 and U6 IP was calculated by comparing percent immunoprecipitation of TER1 or U6 to immunoprecipitation from an untagged strain (mean ± standard error, two-tailed unpaired *t* test * at $p < 0.05$, ** at $p < 0.01$, *** at $p < 0.001$, and **** at $p<0.0001$) (n=3 biological replicates).
C) Northern blot of mature and intron-containing U6 in PrA- and myc-tagged immunoprecipitated RNA.
D) Telomerase assay of PrA-tagged Bmc1 in a wild type and *pof8*Δ strain. A ^{32}P-labeled 100-mer oligonucleotide was used as a loading control. Telomerase extension products were compared to a terminal transferase ladder, with +1 and +4 extension products indicated. Western blot probing for PrA following PrA immunoprecipitation is shown in the panel below.
E) Proposed model of the fission yeast telomerase holoenzyme. TER1 structure and binding locations are based on models constructed by Hu and colleagues (14) and Mennie and colleagues (12). Source data are provided as a Source Data file.

2.3.5 Bmc1 promotes TER1 accumulation and Pof8 recruitment to telomerase

We then interrogated the functional role of Bmc1 in telomerase by creating a *bmc1* knockout strain where we replaced the *bmc1* open reading frame with a phleomycin resistance cassette which was confirmed by PCR and sequencing, as well as qRT-PCR to confirm a lack of *bmc1* mRNA (Supplementary Figure 5A, B). To address conflicting reports in the literature as to the nature of *bmc1*'s essentiality in *S. pombe*(169, 170), we back-crossed our *bmc1* deletion strain with a wild type strain. Sporulation and tetrad dissections yielded viable haploid colonies possessing phleomycin resistance (Supplementary Figure 5C), confirming that *bmc1* is not essential and enabling us to conduct further mechanistic studies.

Consistent with its strong dependence on Pof8 for recruitment to telomerase, *bmc1* deletion appears to decrease steady-state TER1 levels, much like a *pof8* deletion strain, with no reduction in U6 abundance (Figure 5A). Importantly, re-introduction of plasmid expressed Bmc1

to *bmc1*Δ cells was sufficient to restore wild type levels of TER1 (Supplementary Figure 5D). To understand the mechanism by which Bmc1 appears to promote TER1 accumulation, we combined our *bmc1*Δ strain with deletion of *rrp6*, an exoribonuclease component of the nuclear exosome that has been previously implicated in TER1 degradation (11, 13, 14, 171, 172). We observed a restoration of TER1 levels in the *bmc1*Δ *rrp6*Δ strain (Figure 5A), similar to what has been observed for *pof8*Δ, where *rrp6* deletion rescues decreased TER1 levels(13). From this, we hypothesize that Bmc1 promotes TER1 accumulation by preventing 3′ decay by the exosome to maintain steady state TER1 levels.

In line with decreased TER1 levels, *bmc1* deletion resulted in shorter telomere length compared to a wild type strain, which became more evident when genomic DNA was digested with ApaI to yield shorter telomere fragments (Figure 5B). We continued passaging strains to get to the point of crisis (>100 generations), where telomeres are lost and cells either die or circularize their chromosomes, leading to a loss of an observable telomere signal by Southern blot (173). As expected, a strain lacking TER1 showed a complete loss of telomeric DNA, whereas deletion of *pof8* and *bmc1* only resulted in shorter telomeres, suggesting that while the two proteins are important for telomere maintenance, they are not strictly required like TER1 (Supplementary Figure 6).

To better understand how Bmc1 affects telomere length and TER1 accumulation, we examined how the Pof8-TER1 interaction changes upon *bmc1* deletion. Somewhat surprisingly, considering that Bmc1 completely relies on Pof8 for recruitment to telomerase, we found that *bmc1* deletion also impaired Pof8 binding to TER1 (Figure 5C), much like the cooperative binding of Pof8 and Lsm2-8 to TER1 (14). Similarly, we observed decreased telomerase activity immunoprecipitated by Pof8 in the *bmc1*Δ strain, with normalization of the intensity of the

extension bands to TER1 levels revealing that the compromised activity cannot only be attributed to the loss of TER1 following *bmc1* deletion (Figure 5D, E). Conversely, normalization of telomere extension activity to the amount of TER1 immunoprecipitated by Pof8 revealed that although less Pof8-containing telomerase complexes form in the absence of Bmc1, the ones that do form are not defective (Figure 5D, F). Thus it appears that not only does Bmc1 affect TER1 accumulation but also contributes to Pof8 association with TER1, suggesting a further role for Bmc1 in ensuring holoenzyme functionality.

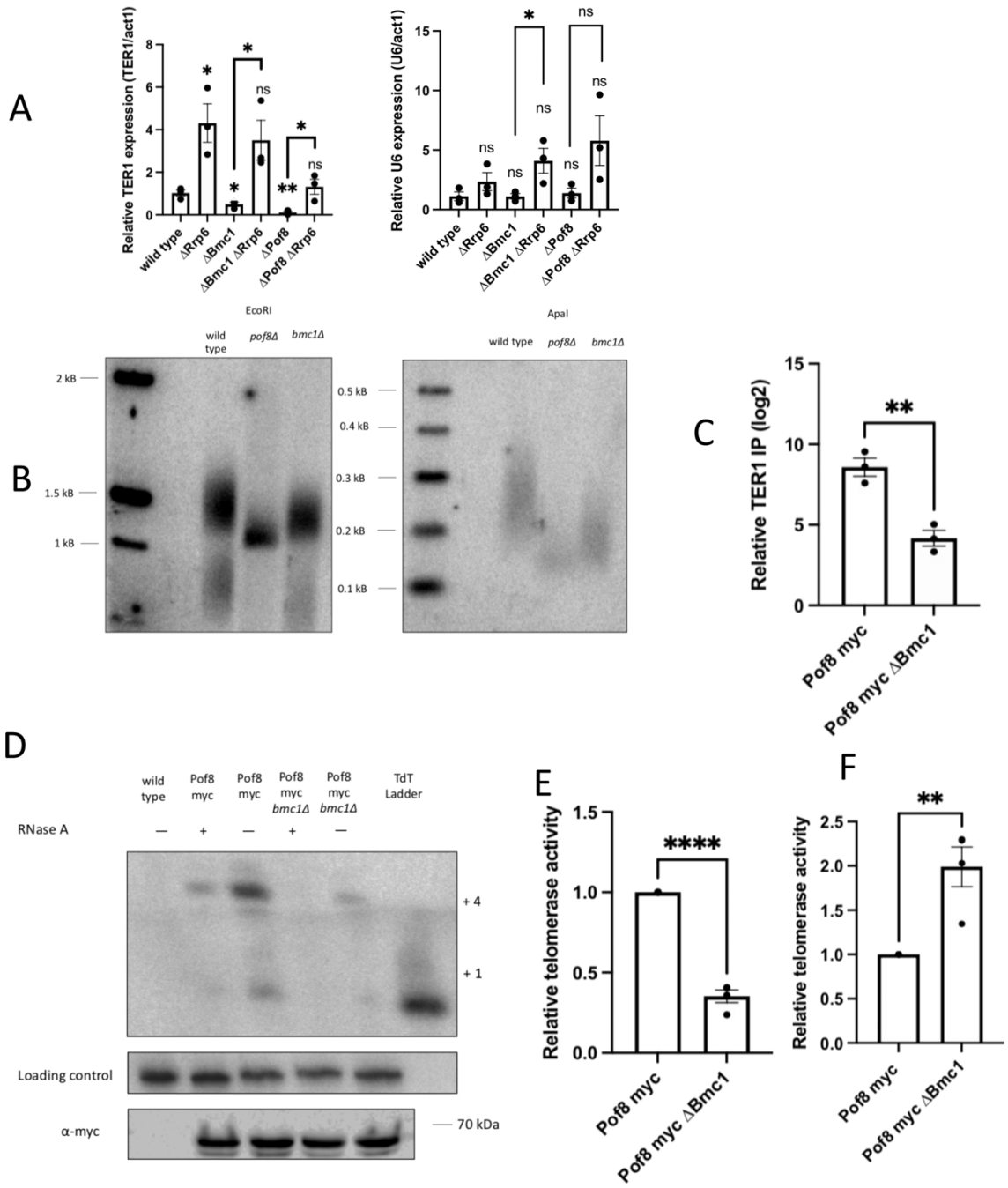

Figure 5: Bmc1 promotes TER1 accumulation and Pof8 recruitment to telomerase
A) Quantitation of TER1 and U6 in total RNA by qRT-PCR, normalized to *act1* mRNA. P-values over bars represent comparison to a wild type strain (mean ± standard error, unpaired *t* test * at $p < 0.05$, ** at $p < 0.01$, *** at $p < 0.001$, and **** at $p<0.0001$) (n=3 biological replicates).
B) Southern blot comparing telomere length in following 3 restreaks on rich media (one restreak= 20-25 generations). Genomic DNA was digested with EcoRI (left) or ApaI (right) to yield different sized telomere restriction fragments.

C) qRT-PCR of TER1 in Pof8 myc immunoprecipitates from a wild type and *bmc1*Δ strain normalized to input RNA. Relative TER1 IP was calculated by comparing percent immunoprecipitation of TER1 to immunoprecipitation from an untagged strain (mean ± standard error, unpaired *t* test * at $p < 0.05$, ** at $p < 0.01$, *** at $p < 0.001$, and **** at $p<0.0001$) (n=3 biological replicates). P-values over each bar represent results of a two-tailed unpaired t-test with Pof8 myc.
D) Telomerase assay of myc-tagged Pof8 in a wild type and *bmc1*Δ strain. A ^{32}P-labeled 100-mer oligonucleotide was used as a loading control. Telomerase extension products were compared to a terminal transferase ladder, with +1 and +4 extension products indicated. Western blot probing for myc following myc immunoprecipitation is shown in the panel below.
E-F) Relative telomerase extension activity for myc-tagged Pof8 immunoprecipitates in a wild type and *bmc1*Δ strain. The intensity of the +4 extension product was normalized to a precipitation loading control, then further normalized to TER1 expression (E) or the amount of TER1 immunoprecipitated with Pof8 (F). P-values over each bar represent results of a two-tailed unpaired t-test with Pof8 myc (n=4 biological replicates, mean ± standard error). Source data are provided as a Source Data file.

2.3.6 Pof8-like proteins are associated with Bin3/Bmc1-like proteins in diverse fungal lineages

The interaction between Bmc1 and Pof8, coupled with the conservation of such an interaction in other examined eukaryotes, led us to wonder at the extent of this interaction on a phylogenetic scale. While Bin3/Bmc1/MePCE (referred to in this section as Bin3 for ease of identifying fungal homologs) and LARP7/Pof8 family members are ubiquitous in higher eukaryotes, their absence or presence is more varied in fungal lineages. We queried hundreds of representative fungal species for the presence of Bin3- and Pof8-like proteins and identified many species with a) both a Bin3 and Pof8 homolog, b) only a Bin3 homolog, or c) neither a Bin3 nor a Pof8 homolog (Figure 6, Supplementary Figure 7). Conversely, only four out of 472 examined species contained a Pof8-like protein but no Bin3-like protein, and in these species the Pof8 homolog was noted to have a shortened N-terminal domain that would lack the La module observed in other LARP7 family members, raising the possibility that members of this rare cohort may not be bona-fide LARP7 family members, at least as these are currently appreciated

(123). Based on the observed distribution, it seems likely that both genes were present in a fungi common ancestor, but Pof8 or both Bin3 and Pof8 were lost in certain lineages. Examination of the distribution of Bin3- and LARP7-family members in basal eukaryotic lineages reveals a similar pattern: Bin3 can be present without LARP7, but there are no instances where a LARP7-family member exists in a lineage lacking a Bin3 homolog (Supplementary Table 2). Similarly, LARP7-family proteins are represented in Alveolates, Stramenopiles, Amoebozoa, Fungi, and Metazoans, while Bin3-family proteins are present in all eukaryotic lineages. Since the presence of Pof8/LARP7 is very highly linked to the presence of a Bin3/Bmc1 homolog, these data suggest that the function of LARP7 family members may be more intimately associated with the function of Bin3/Bmc1/MePCE than has been previously appreciated.

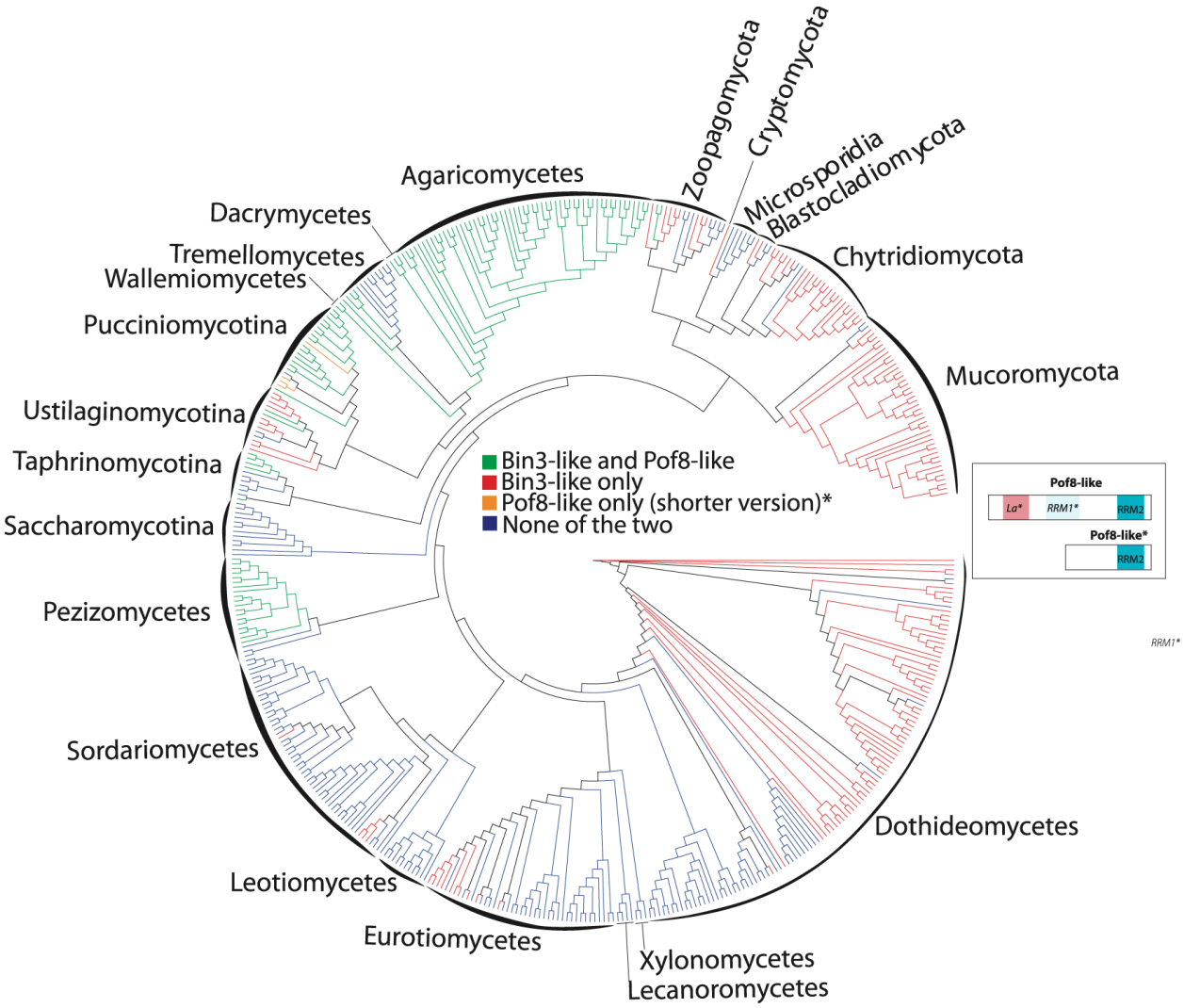

Figure 6: Phylogenic distribution of Bmc1/Bin3 and Pof8 in fungi
Consensus cladogram describing the phylogenic relationships of 472 species representative of fungi phylum and classes and highlighting (using a color code) the distribution of Bin3 and Pof8 in these species. The cladogram is a consensus tree of 5328 distinct protein coding gene trees resulting from a genome-wide, against all, protein comparison (see Materials and Methods). Only posterior probabilities inferior to 1 are shown. The Bin3 and Pof8 distribution is recapitulated in Supplemental Data 3 with corresponding protein sequences. A cartoon presenting structural domains of Pof8 is presented. Pof8 La module and RRM1 are only inferred from secondary structure predictions and are represented by *La** and *RRM1** in the corresponding cartoon. In four species (colored in orange in the cladogram) only an N-terminal truncated version of Pof8 (Pof8*) that cannot accommodate the La module is present. Full cladogram with species names and statistical supports of the different nodes is presented in Supplementary Figure 7.

2.4 Discussion

In this study, we have identified Bmc1 as a component of the *S. pombe* telomerase holoenzyme. In addition to showing an interaction between Bmc1 and U6 snRNA, we demonstrate that Bmc1 interacts with the telomerase RNA TER1 and components of the active telomerase holoenzyme in a manner that is dependent on the presence of the LARP7 family protein Pof8. Together, our results indicating that Bmc1 interacts with the mature, spliced form of TER1 and that Bmc1 immunoprecipitates possess telomerase activity *in vitro* strongly suggest that Bmc1 is a constitutive component of the telomerase holoenzyme containing Trt1, Pof8, Lsm2-8, and Est1 scaffolded on TER1 (Figure 4E). Our results are in agreement with recent findings from the Baumann lab reporting the presence of Bmc1/Bin3 in the telomerase holoenzyme (166). The idea of Pof8 and Bmc1 scaffolded on TER1 is reminiscent of LARP7 and MePCE in the 7SK snRNP, with Pof8/LARP7 recruiting Bmc1/MePCE to the RNA substrate. Similar to our data showing Pof8 recruiting Bmc1 to TER1 and the telomerase holoenzyme, LARP7 has also been demonstrated to recruit MePCE to the 7SK snRNP in human cells (152). Thus, the protein-protein interaction and subsequent recruitment to RNA substrates by LARP7 appears evolutionarily conserved in fission yeast and higher eukaryotes. We also present data demonstrating that the presence of Pof8-like proteins is nearly universally correlated with the presence of Bin3-like proteins in fungi, suggesting that the Bmc1-Pof8 interaction is highly conserved and more prevalent than previously anticipated. Since Pof8 is required to load Bmc1 onto the telomerase RNA and U6 snRNA in fission yeast, this phylogenetic distribution raises the question of whether Bin3/Bmc1 homologs in fungi lacking a LARP7 homolog have evolved a mechanism to bind RNA targets in a Pof8/LARP7 independent fashion.

Since TER1 undergoes several processing steps before assembly into the telomerase holoenzyme, we were able to assess TER1 processing state to determine when Bmc1 interacts with TER1 with respect to the timing of TER1 maturation. We show that Bmc1-associated TER1 has a mature 3′ end, indicative of spliceosome-catalyzed end processing, and a 5′ TMG cap. This is consistent with previously reported data on the timing of Pof8 binding; since our data indicates that the interaction between Bmc1 and TER1 is dependent on Pof8, the most parsimonious explanation is that Pof8, and thus Bmc1, bind TER1 following 3′ maturation and TMG capping, preceding the binding of the Lsm2-8 complex (11). We show that the interaction between Bmc1 and TER1 is dependent on Pof8, leading to the conclusion that Bmc1 interacts with TER1 at the same stage as Pof8, resulting in the hierarchical assembly of the active telomerase holoenzyme.

The finding that Bmc1-associated TER1 is immunoprecipitated by a TMG antibody argues against a catalytic role for Bmc1 in TER1 processing. Our data, coupled with previous work characterizing the cap structure on the mature TER1 bound to Trt1 (92, 93), supports the idea that Bmc1 has a capping-independent function in the telomerase holoenzyme. LARP7 binding to MePCE in the 7SK snRNP inhibits its capping activity; MePCE, in turn, promotes the interaction between 7SK and LARP7, thereby stabilizing the complex (160). In the *S. pombe* telomerase holoenzyme and U6 snRNP, we can hypothesize that Pof8 may also inhibit the methyltransferase activity of Bmc1 by binding to and occluding the active site. This is consistent with our results suggesting a transient interaction between Pof8 and U6 that may function to load Bmc1 on U6. In such a model, an interaction between Bmc1 and Pof8 is necessary to recruit Bmc1 to U6 and following dissociation of Pof8, the catalytic site of Bmc1 would become available to cap U6. It is curious to note that *bmc1* deletion has no effect on U6 levels (Figure 5A), although such a finding is consistent with what has been observed for human U6 upon

MePCE depletion (64). Since the lack of an MePCE-catalyzed cap on human 7SK is associated with an increase in exoribonucleolytic degradation(64), this therefore raises the question as to the function of the γ-monomethyl phosphate cap on U6, if not to protect the 5′ end from exoribonucleolytic degradation.

Additionally, our work identifying Bmc1 as a telomerase-associated protein brings to mind work identifying a box H/ACA motif at the 3′ end of vertebrate telomerase RNA (174). Box H/ACA RNAs form an RNP complex with Dyskerin/Cbf5, Nop10, Nhp2, and Gar1 to guide noncoding RNA pseudouridylation (175, 176). Although Dyskerin is a pseudouridine synthase, to date no evidence has pointed to a modification function for Dyskerin in the context of telomerase RNA. Rather, the Dyskerin-containing H/ACA complex has a structural role in telomerase biogenesis, with binding of the H/ACA RNP to telomerase RNA leading to a conformational change in the RNA that promotes 3′ processing and maturation over exosome-mediated decay (100). This is reminiscent of the apparent catalytic independent role we observed for Bmc1 in fission yeast telomerase, although our data point towards Bmc1 having a role promoting Pof8 binding to TER1, perhaps also through Bmc1-mediated conformational changes in TER1. The decreased TER1 levels observed upon *bmc1* deletion (Figure 5A) can likely be attributed to the decreased interaction between Pof8 and TER1 in the absence of Bmc1. We therefore propose a model in which the direct interaction between Bmc1 and Pof8 both recruits Bmc1 to the telomerase holoenzyme, as well as promotes Pof8 binding to TER1. This in turn promotes Lsm2-8 binding to the exposed 3′ end of TER1, which protects TER1 from exosome-mediated degradation (11, 13, 14). The resulting TER1-containing RNP then recruits Trt1, forming a stable complex capable of extending telomeres.

Another facet of this work builds on the idea that components of the telomerase holoenzyme are more conserved than previously appreciated. In addition to the ubiquitous telomerase reverse transcriptase, previous work has identified LARP7 family proteins in both ciliates and yeast (11–13, 120), arguing a level of evolutionary conservation. We now also provide evidence indicating the presence of RNase P and RNase MRP subunits in fission yeast, much like the RNase P and RNase MRP subunits found in the budding yeast telomerase complex (163–165). The presence of RNase P and RNase MRP subunits in two divergent yeast species supports the importance of these factors in the function of a breadth of telomerase holoenzymes.

Our results indicating that Bmc1 is part of the telomerase holoenzyme were quite unexpected, as Bmc1 has been well-characterized in higher eukaryotes for its role in the processing, maturation, and protection of RNA Polymerase III transcripts (64, 160). An intriguing idea involves polymerase switching through telomerase RNA evolution. Ciliate telomerase RNA is transcribed by RNA Polymerase III and subsequently binds the LARP7 homolog p65 through the terminal polyuridylate stretch common to RNA Polymerase III transcripts (120, 122). Since MePCE and LARP7 also associate with RNA Polymerase III transcripts, it is possible that the Pof8-bound RNA Polymerase II transcribed TER1, and the *S. pombe* telomerase RNP as a whole, represent an intermediate step in the evolution of telomerase RNA between ciliates and the RNA Polymerase II transcribed telomerase RNA of higher eukaryotes. Future work should investigate the presence of Bmc1/MePCE homologs in the telomerase holoenzymes of other species, particularly in ciliates, which possess both an RNA Polymerase III transcribed telomerase RNA and a LARP7 homolog. Such findings will continue to develop emerging ideas regarding conservation in telomerase RNA processing and the composition of telomerase RNPs.

2.5 Methods

Strains, constructs, and growth media

Strains were grown in yeast extract with supplements (YES) or Edinburgh Minimal Media (EMM), as indicated. Tag integration and knockouts were generated with a previously described PCR-based strategy and verified by PCR and western blotting (177) (primer sequences in Supplementary Table 3). Protein A-tagged strains were generated according to (178). The *bmc1*Δ strain was constructed by replacing the *bmc1* open reading frame with the phleomycin resistance cassette and flanking primers containing 750 nucleotides of homology to the *bmc1* genomic locus. Correct genotypes were selected on YES plates with the corresponding antibiotic (200 μg/mL G418, Sigma; 100 μg/mL Nourseothricin, GoldBio; 100 μg/mL phleomycin, Invivogen). Other strains were created by mating and antibiotic selection. A list of strains is provided in Supplementary Table 4.

Native protein extract and immunoprecipitation

S. pombe cells were grown in YES at 32°C to mid-log phase, harvested, and subject to cryogenic disruption using a mortar and pestle. Cell powder was lysed in 50 mM NaCl, 20 mM Hepes pH 7.4, 55 mM KOAc, 0.5% Triton X, 0.1% Tween-20, 0.2 mM PMSF, 1:100 Protease Inhibitor Cocktail (Thermo, 78430), and 0.004 U/μL RNase inhibitor (Invitrogen, AM2694). For Protein A-tagged strains, immunoprecipitation was carried out with Rabbit IgG-conjugated (MP-Biomedicals, SKU 085594) Dynabeads (Invitrogen, 14301) as described (38). Myc-tagged proteins were immunoprecipitated with Protein G Dynabeads (Invitrogen, 10003D) coated with anti-myc antibody (Cell Signaling, 2276S). Beads were washed 4 times with 400 μL lysis buffer. For RNA immunoprecipitations, bound RNA was isolated by treatment of beads with 0.1% SDS

and 0.2 mg/mL Proteinase K (Sigma, P2308) at 37°C for 30 minutes, followed by extraction with phenol: chloroform:isoamyl alcohol (25:24:1) and ethanol precipitation.

RNA preparation and Northern blotting

Total RNA was isolated from 1% of native protein extracts by incubation with 0.5% SDS, 0.2 mg/mL proteinase K (Sigma, P2308), 20 mM Tris HCl pH 7.4, and 10 mM EDTA pH 8.0 for 15 minutes at 50°C, followed by phenol: chloroform extraction and ethanol precipitation. Northern blot analysis was performed as described using 8% TBE-urea polyacrylamide gels (179). Briefly, electrophoresed RNA was transferred to positively charged nylon membranes (Perkin Elmer, NEF988001) with the iBlot 2 system (Thermo, IB21001) and probed with ^{32}P γ-ATP-labeled DNA probes (probe sequences provided in Supplementary Table 5). For RNase H digestion, RNA was incubated with 25 pmol RNase H probe (provided in Supplementary Table 5) for 5 minutes at 65°C and slow cooled to 37°C, followed by digestion with 5 U RNase H (NEB, M02975) for 30 minutes at 37°C. The reaction was stopped with the addition of 25 μM EDTA pH 8.0 and phenol: chloroform extraction and ethanol precipitation. TMG-capped RNAs were isolated from RNase H-treated immunoprecipitates with Protein G Dynabeads coated with an α-TMG antibody (Sigma, MABE302), according to (180).

qRT-PCR and semi-quantitative RT-PCR

1 μg Turbo DNase-treated RNA was reverse transcribed with the iScript cDNA synthesis kit (BioRad, 1708890), treated with 0.5 μL RNase cocktail (Invitrogen, AM2286), and diluted 1:10. cDNA was quantified using the SensiFAST SYBR No-Rox kit (Bioline, BIO-98005) and 1 μM of each primer (primer sequences provided in Supplementary Table 5). qPCR settings were as follows: 95°C for 10 minutes and 40 cycles consisting of 10 seconds at 95°C, 20 seconds at 60°C, and 20 seconds at 72°C, followed by melting curve analysis. TER1 and U6 levels were

normalized to *act1* mRNA levels and the average wild type Ct value, and subsequently subject to unpaired two-tailed student's *t*-tests and, where applicable, one-way ANOVA followed by a Tukey posthoc test with α set to 0.05 (Supplementary Data 4).

For semi-quantitative RT-PCR, DNase-treated RNA, 10 nmol dNTP mix, and 10 pmol gene-specific reverse primers (Supplementary Table 5) were heated to 65°C and slow-cooled to 37°C before reverse transcription with 5 U AMV-RT (NEB, M0277L) at 42°C for 1 hour. cDNA was amplified with Taq Polymerase (NEB, MO273L) using standard protocols and the following cycling conditions: 5 minute initial denaturation at 94°C, 22 (TER1) or 17 (U6) cycles of 30 seconds at 94°C, 30 seconds at 57°C, and 1 minute at 72°C, and a final 10 minute extension at 72°C.

RIP Seq

Libraries were constructed from immunoprecipitated RNA samples by the RNomics Platform at the Université de Sherbrooke in Sherbrooke, Quebec. RNA quality was assessed with a Bioanalyzer small RNA chip (Agilent, 5067-1548). Libraries were constructed with the NEBNext Ultra II Directional Kit (NEB, E7760S) and amplified with 10 PCR cycles. cDNA libraries were sequenced on an Illumina NextSeq 500 with 2 runs per sample, each for 50-bp single-end reads. Following fastp processing (Version 0.20.1), reads from the first sequencing run were aligned to the fission yeast genome (ASM294v2) with Bowtie 2 (181, 182) and counted with featurecounts (183) using the EF2 build of the ENSEMBL fission yeast genome. Differential expression analysis was performed using edgeR, with reads filtered to include transcripts with at least 1 count per million (CPM) in each sample and libraries were normalized by Trimmed Mean of M-values (TMM)(184, 185).

Circularized Rapid Amplification of cDNA Ends (cRACE)

Immunoprecipitated RNA was treated with 2 U TURBO DNase (Invitrogen, AM2239) and dephosphorylated with 1 U calf intestinal alkaline phosphatase (NEB, M0290), followed by decapping and circularization with RNA 5′ Pyrophosphohydrolase (NEB, M0356S) and T4 RNA Ligase 1 (NEB, M0204S). TER1 was amplified from circularized RNA with the OneStep RT-PCR Kit (Qiagen, 210210) (primer sequences in Supplementary Table 5). cRACE products were cloned into the pGEM-T vector (Promega, A1360) and sequenced by the TCAG DNA Sequencing Facility at the Hospital for Sick Children in Toronto.

Mass spectrometry and GO analysis

Half of the native protein extract was pre-treated with 0.625 U/μL Benzonase (Millipore, E1014) at 37°C for 30 minutes. The reaction was stopped with 5 mM EDTA pH 8.0 and Protein A immunoprecipitation was performed in the same manner as for RNA immunoprecipitations. After washes with lysis buffer, beads were washed with 0.1 M NH_4OAc and 0.1 mM $MgCl_2$ and eluted with 0.5 M NH_4OH for 20 minutes at room temperature. Eluates were lyophilized and subject to in-solution tryptic digestion. LC-MS/MS analysis was performed by the IRCM Proteomics Discovery Platform on a Q Exactive HF.

Raw data was processed and analyzed using the MaxQuant software package 1.5.1.2 (186) and the fission yeast UP000002485 reference proteome (24/11/2019). Settings used for MaxQuant analysis were as reported (187). Proteins present in immunoprecipitations from both biological replicates and absent from control immunoprecipitations were considered genuine Bmc1 interacting partners and ranked by peak intensity. Proteins that showed a complete loss of spectral counts upon benzonase addition were considered nucleic acid-dependent interactions. PANTHER overrepresentation tests (GO Ontology database released 2019-12-09) were conducted on the top 50 Bmc1 interacting partners. Fisher's exact tests with False Discovery

Rate (FDR) correction were performed using the GO biological process complete and GO cellular component complete data sets.

Co-immunoprecipitation and western blotting

S. pombe cells were grown in YES at 32°C to mid-log phase, harvested, and subject to cryogenic disruption using a mortar and pestle. Cell power was lysed in Co-IP lysis buffer (10 mM Tris HCl pH 7.5, 150 mM NaCl, 0.5% NP40, 1:100 Protease Inhibitor Cocktail). Immunoprecipitations were carried out as described and proteins were eluted by resuspending beads in 2X SDS loading buffer (100 mM Tris HCl pH 6.8, 4% SDS, 20% glycerol, 0.2% bromophenol blue) and boiling at 95°C for 5 minutes. Western blot analyses were performed using monoclonal anti-myc (Cell Signaling, 2276S) at 1:5000 and monoclonal anti-beta actin (abcam, ab8226) at 1:2500 for primary antibodies and HRP-conjugated anti-mouse (Cell Signaling, 7076) at 1:5000 for secondary antibodies. Protein A-tagged proteins were detected with HRP-conjugated polyclonal anti-Protein A (Invitrogen, PA1-26853) at 1:5000.

Glycerol gradient sedimentation

Native protein extracts were separated on a 10 mL 20-50% glycerol gradient (20 mM HEPES pH 7.6, 1 mM MgOAc, 1 mM DTT, 300 mM KOAc) and spun in an SW41 rotor for 20 hours at 30,000 rpm according to (188). Individual fractions were divided in 2 for protein extraction by TCA precipitation and RNA extraction with phenol: chloroform.

Telomerase activity assay

The telomerase activity assay was performed as described (11). Briefly, bead slurries (see immunoprecipitation) were incubated at 30°C for 90 minutes in a 10 μL reaction containing 50 mM Tris HCl pH 8.0, 1 mM MgOAc, 5% glycerol, 1 mM spermidine, 1 mM DTT, 100 mM KOAc, 0.2 mM dATP, dCTP, and dTTP, 5 μM telomerase assay primer (Supplementary Table

5), and 0.3 μM 3000 Ci/mmol [α-^{32}P] dGTP (Perkin Elmer, BLU512H250UC). The reaction was stopped with the addition of 0.5% SDS, 10 mM EDTA pH 8.0, 20 mM Tris HCl pH 7.5, 2 μg/μL Proteinase K (Sigma), and 1000 cpm [γ-^{32}P] ATP-labeled 100-mer oligonucleotide and incubation at 42°C for 15 minutes, followed by phenol: chloroform extraction and ethanol precipitation. RNase A-treated samples were pre-incubated with 20 ng RNase A (Invitrogen, AM2271) at 30°C for 10 minutes. Extension products were separated on a 10% urea-TBE polyacrylamide sequencing gel at 60 W for 90 minutes, dried and exposed to a PhosphorScreen, and imaged with a Typhoon imager.

Genomic DNA extraction, southern blotting, and chromosome fusion PCR

Genomic DNA was extracted from logarithmically growing cells according to (12). For southern blotting, 15 μg genomic DNA was digested overnight with EcoRI or ApaI and separated on a 1% agarose gel, transferred to positively charged nylon membranes (Perkin Elmer, NEF988001) by capillary transfer in 10X SSC, and probed with a ^{32}P γ-ATP-labeled telomere probe (probe sequence provided in Supplementary Table 5). The chromosome fusion PCR was adapted from (11). Briefly, 50 μL PCR reactions contained 1 μL genomic DNA, 0.4 μM forward and reverse primers (sequences provided in Supplementary Table 5), 200 μM dNTPs, 1X Taq ThermoPol Buffer (NEB), and 1.25 U Taq Polymerase (NEB, M0273). The *Trt1* gene was amplified as a loading control in an identical PCR reaction containing the corresponding primers. The PCR reaction consisted of an initial denaturation at 95°C for 5 minutes, followed by 32 cycles of 95°C for 15 seconds, 55°C for 30 seconds, and 68°C for 3 minutes, with a final extension at 68°C for 10 minutes.

Structure prediction

The structure of *S. pombe* Bmc1 was predicted using Phyre2 (189) and aligned with the co-crystal structure of the *H. sapiens* MePCE methyltransferase domain bound to 7SK snRNA and SAH (6DCB (157)) in PyMol (190). Primary sequences were aligned with the Clustal Omega Multiple Sequence Alignment tool (191).

Phylogenetic tree construction and search for Bin3-like and Pof8-like sequences

Protein sequences (GeneCatalogs) of 472 fungal species were downloaded from the JGI website (https://mycocosm.jgi.doe.gov/) in fasta format. 5614520 proteins were downloaded and merged into a single multifasta file. A blast (Blastp) against all proteins was performed using diamond blastp (192) with a minimum e-value of 1e-5 and outfmt 6 (for tabular output). In order to identify homologous proteins, proteins were clustered together if they shared at least 50% similarity over 70% of coverage using SiLiX (193). When a cluster contained two or more paralogous genes derived from duplications, the species was removed from the cluster. Finally, only clusters with a minimum of 100 species were retained for further analysis. Following these cleaning steps, we obtained 5328 clusters containing one gene per species. Proteins sequences of each cluster were aligned using MAFFT (v7.271) with default parameters (https://mafft.cbrc.jp/alignment/server/). Multiple alignments were cleaned using trimA1 (v1.4.rev22 build [2015-05-21]) with -st 0.01 option. Fastree (version 2.1.10 SSE3) with default parameters were used to build phylogenetic trees (194). The consensus fungi tree was obtained using ASTRAL (astral.5.6.3) software with default parameters (195). To detect the presence of genes coding for Bin3-like and Pof8-like proteins, blast searches (blastp and tbalstn) were performed on each studied fungus genome, using initially either the full-length *S. pombe* Bin3/Bmc1 protein sequence or the *S. pombe* Pof8 xRRM conserved motif. This procedure was

repeated in each fungal clade using clade-specific Bin3-like and Pof8-like sequences detected by the initial search using *S. pombe* sequences. Finally, new blast searches were performed all over again, this time using Bin3-like or Pof8-like "probes" made of a collection of sequences representing the diversity of these two proteins in fungi.

Statistics and reproducibility

For qPCR analyses, two-tailed unpaired student's t-tests were performed and, where applicable, one-way ANOVA followed by a Tukey posthoc test with a set to 0.05. RIP-Seq, RNA IP coupled to qPCR, and total RNA qPCR experiments were performed in biological triplicate, IP mass spectrometry, IP western blots, RNA IP coupled to northern blots, glycerol gradient analysis, and telomere southern blots were repeated in biological duplicate, and telomerase assays were repeated in biological quadruplicate.

Data availability

The mass spectrometry proteomics data have been deposited to the ProteomeXchange Consortium via the PRIDE (196) partner repository with the dataset identifier PXD023356 and 10.6019/PXD023356. RNA Seq data have been deposited in NCBI's Sequence Read Archive (SRA) database under BioProject number PRJNA776661. Source data, supplementary datasets, and supplementary tables can be accessed online: https://www.nature.com/articles/s41467-022-28985-3.

2.6 Acknowledgements

We thank Toru Nakamura and Virginia Zakian for sharing published yeast strains and Marc Fabian and Raymund Wellinger for helpful comments on the manuscript. J.P. is supported by a Canada Graduate Scholarship (Doctoral) from the National Sciences and Engineering Research

Council of Canada. M.A.B. is supported by a Discovery Grant from NSERC ("Impact of chemical modification of noncoding RNAs on gene expression in *S. pombe*"). J.M.D. is supported by the Institut Universitaire de France (IUF), J.-M.D. and M.E.B. by the CNRS and the University of Perpignan (UPVD) and their study is set within the framework of the "Laboratoires d'Excellences (LABEX)" TULIP (ANR-10-LABX-41) and of the "École Universitaire de Recherche (EUR)" TULIP-GS (ANR-18-EURE-0019).

2.7 Supplementary information

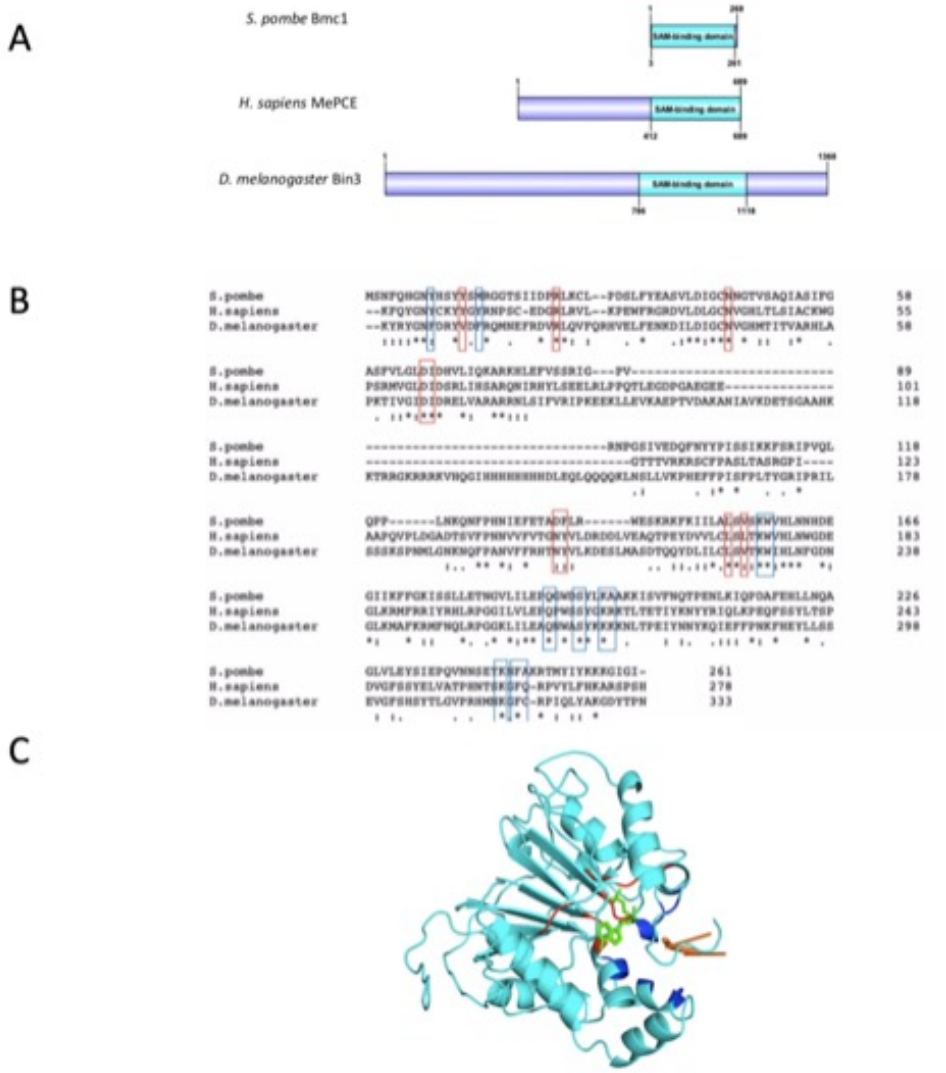

Figure S1: Bmc1 is the *S. pombe* methyl phosphate capping enzyme (MePCE) homolog
A) Schematic of the domain architecture of Bmc1 homologs from *S. pombe, H. sapiens,* and *D. melanogaster.*
B) Clustal alignment of the methyltransferase/SAM-binding domains of *S. pombe* Bmc1, *H. sapiens* MePCE, and *D. melanogaster* Bin3. Predicted SAM-binding residues are indicated in red and nucleotide-binding residues are in blue.
C) Phyre2 (189) structure prediction of *S. pombe* Bmc1 bound to a 5′ terminal guanosine (orange) and SAH (green). Predicted SAM-binding residues are in red and nucleotide-binding residues are in blue.

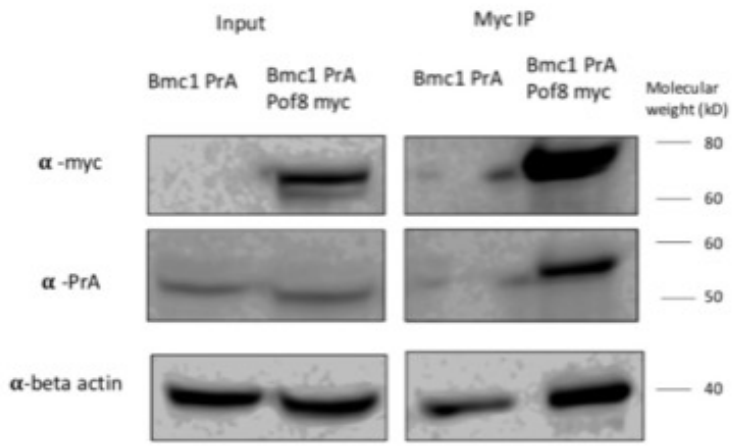

Figure S2: Reciprocal co-immunoprecipitations validate an interaction between Bmc1 and Pof8

The interaction between Bmc1 and Pof8 was confirmed by α-myc co-immunoprecipitation. Source data are provided as a Source Data file.

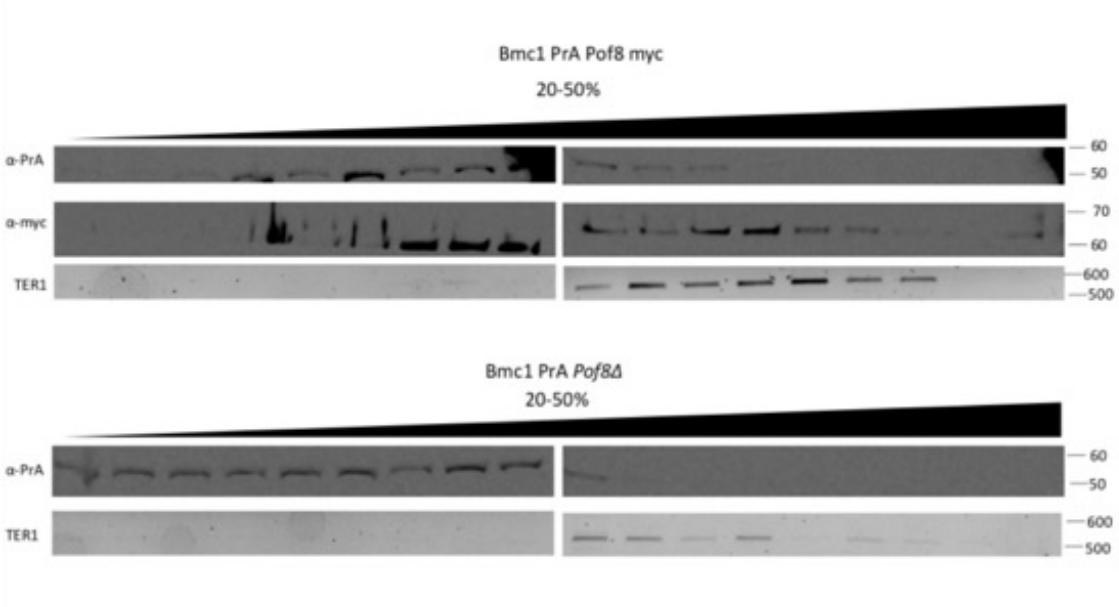

Figure S3: Glycerol gradient sedimentation of Bmc1, Pof8, and TER1 in a wild type and *pof8*Δ strain

Western blot and semi-quantitative RT-PCR of Bmc1 PrA, Pof8 myc, and TER1 in gradient fractions. Source data are provided as a Source Data file.

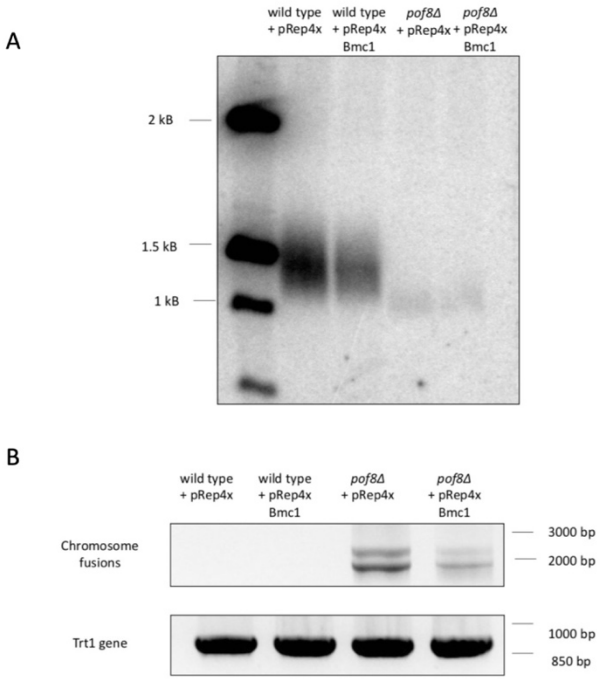

Figure S4: Bmc1 overexpression fails to rescue *pof8*Δ-dependent telomere defects
A) Southern blot comparing telomere length from wild type and *pof8*Δ strains following 2 re-streaks on minimal media (1 re-streak= 20-25 generations) overexpressing an empty vector (pRep4x) or Bmc1. Genomic DNA was digested with EcoRI.
B) Chromosome fusion PCR (top). The Trt1 gene was amplified from genomic DNA as a loading control (bottom). Template DNA from the same genomic DNA as (A). Source data are provided as a Source Data file.

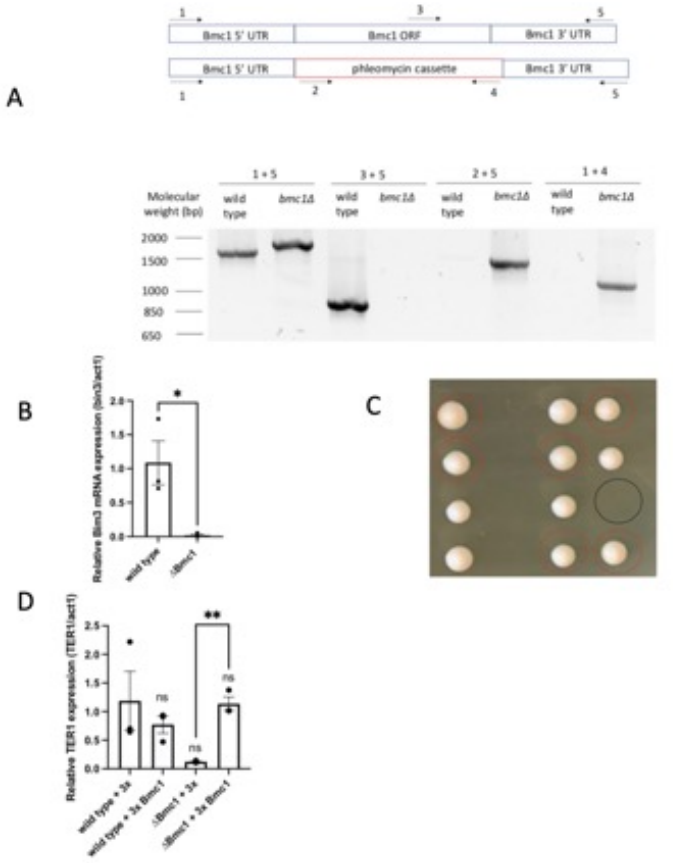

Figure S5: Validation of a Bmc1 knockout strain confirms its viability
A) Schematic of Bmc1 knockout (top) and PCR validation of the resultant strain using the indicated primers.
B) qRT-PCR of *bmc1* mRNA normalized to *act1* mRNA for wild type and *bmc1*Δ strains (mean± standard error, two-tailed unpaired t-test * at $p<0.05$) (n= 3 biological replicates). P-values over each bar represent results of a two-tailed unpaired t-test with a wild type strain.
C) Backcrossing of *bmc1*Δ and a wild type strain, followed by tetrad dissection, confirms viability of the *bmc1*Δ strain on rich media. Tetrads from the same spore are arranged in columns. Resulting haploid colonies possessing phleomycin resistance are circled in red and colonies that did not grow after tetrad dissection are circled in black.
D) qRT-PCR of TER1 normalized to *act1* mRNA for wild type and *bmc1*Δ strains transformed with an empty vector (pRep3x) or Bmc1 (mean± standard error, two-tailed unpaired t-test * at $p<0.05$, ** at $p<0.01$) (n= 3 biological replicates). P-values over each bar represent results of a two-tailed unpaired t-test with a wild type strain. Source data are provided as a Source Data file.

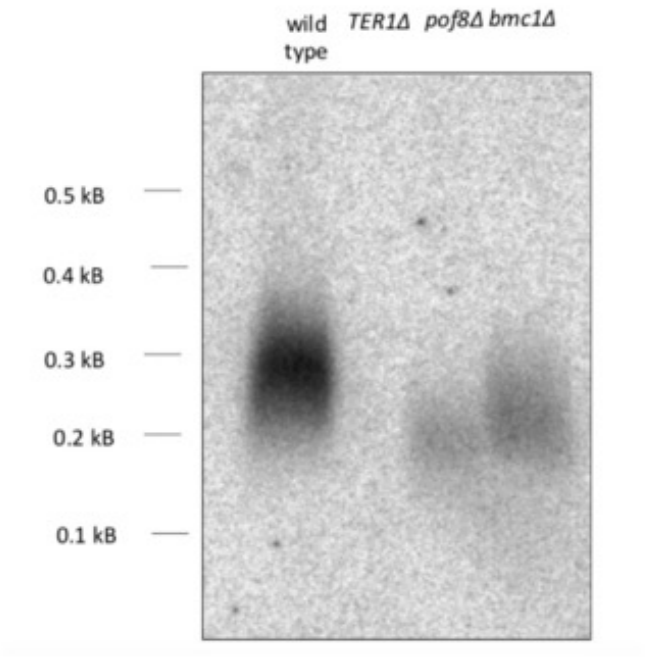

Figure S6: Bmc1 and Pof8 are not strictly required for telomere maintenance
Southern blot comparing ApaI-digested genomic DNA isolated after 5 re-streaks on rich media. A lack of signal with a telomeric probe represents survivors that have lost telomeric DNA and circularized their chromosomes (*TER1*Δ). Source data are provided as a Source Data file.

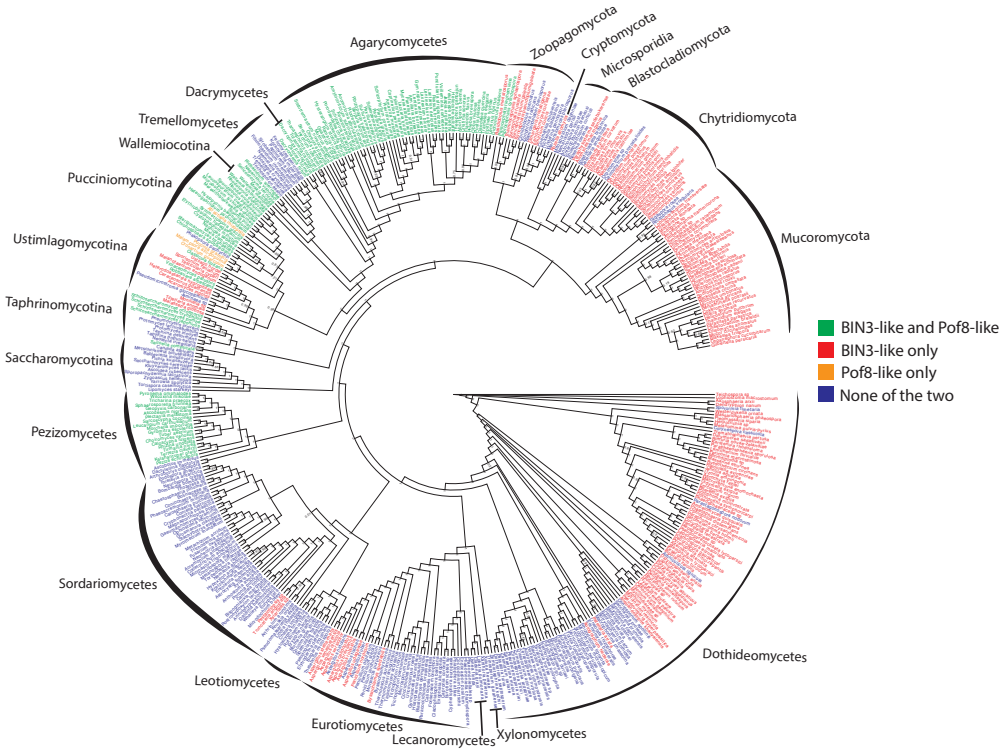

Figure S7: Phylogenic distribution of Bmc1/Bin3 and Pof8 in fungi
Complete consensus cladogram describing the phylogenic relationships of 472 species representative of fungi phylum and classes and highlighting (using a color code) the distribution of Bin3 and Pof8 in these species. Only posterior probabilities inferior to 1 are shown.

Chapter 3: The fission yeast methyl phosphate capping enzyme Bmc1 guides 2'-O-methylation of the U6 snRNA

Jennifer Porat[1], Viktor A. Slat[2], Stephen D. Rader[2,3], and Mark A. Bayfield[1*]
1. Department of Biology, York University, Toronto, Canada
2. Department of Biochemistry and Molecular Biology, University of British Columbia, Vancouver, Canada
3. Department of Chemistry and Biochemistry, University of Northern British Columbia, Prince George, Canada
*Correspondence: bayfield@yorku.ca (M.A.B.)

This chapter has been submitted for publication and a version has been published as a preprint as Porat J, Slat V.A., Rader S.D., and Bayfield M.A. The fission yeast methyl phosphate capping enzyme Bmc1 guides 2'-O-methylation of the U6 snRNA. *bioRxiv* 2023.01.27.525755; doi: https://doi.org/10.1101/2023.01.27.525755

Contributions: J.P. conceived of the study, designed, performed, and analyzed all experiments, and wrote the manuscript with input from all authors. V.A.S. analyzed RNA Seq data (Figure 5A, C, D, E, S5) under the supervision of S.D.R. M.A.B. conceived of the study, designed experiments, supervised the project, and edited the manuscript.

3.1 Abstract

Splicing requires the tight coordination of dynamic spliceosomal RNAs and proteins. U6 is the only spliceosomal RNA transcribed by RNA Polymerase III and undergoes an extensive maturation process. In humans and fission yeast, this includes addition of a 5' γ-monomethyl phosphate cap by members of the Bin3/MePCE family. Previously, we have shown that the Bin3/MePCE homolog Bmc1 is recruited to the *S. pombe* telomerase holoenzyme by the LARP7 family protein Pof8, where it acts in a catalytic-independent manner to protect the telomerase RNA and facilitate holoenzyme assembly. Here, we show that Bmc1 and Pof8 also interact in a U6-containing snRNP. We demonstrate that Bmc1 and Pof8 promote 2'-O-methylation of U6 and identify and characterize a non-canonical snoRNA that guides this methylation. Further, we show that fission yeast strains deleted of Bmc1 or Pof8 show altered U6 snRNP assembly patterns, supporting a more general role for these factors in guiding noncoding RNP assembly beyond the telomerase RNP. These results are thus consistent with a novel role for Bmc1/MePCE family members in stimulating U6 post-transcriptional modifications.

3.2 Introduction

Pre-mRNA splicing, comprised of intron excision and subsequent exon ligation, relies on dynamic RNA-RNA and RNA-protein interactions in the spliceosome (reviewed in (197)). The spliceosome contains upwards of 100 proteins (198) and 5 uridylate-rich small nuclear RNAs (snRNAs): U1, U2, U4, U5, and U6. The U6 snRNA, which forms part of the catalytic core of the spliceosome (70), undergoes several conformational changes during pre-spliceosome assembly and splicing catalysis, which enables its interaction with other spliceosomal RNAs and the switch between a catalytically active and inactive state (199). As such, U6 biogenesis and

maturation is complex and tightly regulated to ensure correct functioning in the spliceosome (reviewed in (200)).

In addition to being the most highly conserved of the snRNAs, U6 is also the only snRNA transcribed by RNA Polymerase III (RNAP III) (201). Transcription of U6 by RNAP III is associated with the addition of a 5' γ-monomethyl phosphate cap catalyzed by enzymes of the Bin3/MePCE (methyl phosphate capping enzyme) family (64, 67, 153) and a 3' uridylate tail. U6 contains a 5' stem loop critical for 5' capping (202), as well as an internal stem loop (ISL) that forms during splicing catalysis. The ISL is mutually exclusive with U4/U6 base pairing that occurs in pre-spliceosome snRNPs (203). U6 also contains 2'-O-methylated, pseudouridylated, and m6A-modified nucleotides, with pseudouridines largely present towards the 5' end and 2'-O-methylations tending to cluster in the ISL (65, 204). Moreover, U6 maturation in the fission yeast *Schizosaccharomyces pombe* involves the splicing of an mRNA-type intron, thought to arise from reverse splicing, as the intron is located near the catalytic nucleotides of U6 (158, 159, 205–207). Most information about the timing of U6 processing events has come from elegant studies in budding yeast (reviewed in (200)). However, since budding yeast U6 lacks 2'-O-methylations and a Bmc1 homolog (68, 123), several questions remain as to the timing and importance of post-transcriptional modifications with respect to other U6 processing steps in organisms like fission yeast and humans.

In addition to 5' γ-monomethyl phosphate capping enzymes, several other proteins have been linked to U6 processing. These include the La protein, which associates with nascent U6 transcripts through the 3' uridylate tail (56), and the Lsm2-8 complex, which binds end-matured U6 and remains stably associated through spliceosome assembly (60, 61, 208). Recent work revealed that mammalian LARP7, a La-Related Protein (LARP) previously linked to MePCE in

the context of the 7SK snRNP (124), is also involved in post-transcriptional processing of U6. LARP7 promotes 2'-O-methylation of U6 by the methyltransferase fibrillarin, which in turn contributes to splicing fidelity at elevated temperatures in humans and in male germ cells in mice (131, 132). Conversely, ciliate and fission yeast LARP7 homologs have been well studied for their roles in telomerase biogenesis (11–15, 120). We and others have reported that the *S. pombe* LARP7 protein Pof8 associates with the Bin3/MePCE homolog Bmc1 in the telomerase holoenzyme, that this interaction is important for optimal telomerase activity, and that the link between these proteins is evolutionarily conserved across diverse fungal species (68, 123, 209). Thus, while much has been learned about MePCE/Bmc1 function in the 7SK snRNP and telomerase, its precise role in U6 biogenesis and function remains unknown.

In this work, we set out to examine the role of Bmc1 in U6 biogenesis and spliceosome function. We have identified a new RNP containing the U6 snRNA and the telomerase components Bmc1, Pof8, and Thc1, and show that this complex is required for wild type levels of 2'-O-methylation in the U6 ISL and U6 snRNP assembly. We also show that while Bmc1's 5' capping catalytic activity is not required for its function in promoting 2'-O-methylation of U6, an intact Pof8-Lsm2-8 interaction is. Finally, we show that Bmc1 deletion influences the splicing of some introns under wild-type and heat-shock conditions, consistent with previous work linking human LARP7 to splicing robustness, and that efficient splicing upon heat shock is largely dictated by intronic features including 5' splice site sequences. Together, these data point towards an intricate network of post-transcriptional processing events that are critical for normal U6 maturation, and provide the first direct evidence for a function of the Bin3/MePCE family in promoting U6 snRNP assembly.

3.3 Results

3.3.1 Bmc1 forms a U6-containing complex with the telomerase proteins Pof8 and Thc1

Our previous work characterizing Bmc1 as a component of the telomerase holoenzyme also revealed interactions between Bmc1 and various other noncoding RNAs, including the U6 snRNA (Figure S1A) (68). We therefore tested whether Bmc1 has a role in the biogenesis, stability, or function of these transcripts, and if this function is linked to the Bmc1-interacting telomerase components Pof8 and Thc1. Having already demonstrated that Pof8 is required to recruit Bmc1 to the telomerase RNA TER1 (68), we determined the protein binding requirements for U6. In contrast to what has been reported for TER1, for which reduced binding to Pof8 persists in the absence of Bmc1 (68, 209), we found that all three proteins are necessary for an interaction with U6 (Figure 1A, S1B). Our results indicating an interaction between Pof8 and U6 are also consistent with previous work identifying mammalian LARP7 as a U6-interacting protein (131, 132), suggesting that LARP7 family members have conserved functions related to U6, in addition to the established evolutionary conservation of LARP7 in telomerase (11–13).

As an additional means to confirm U6 snRNP formation, we fractionated native cell extracts on glycerol gradients and compared protein and RNA sedimentation in wild type and knockout yeast strains (Figure 1B, S1C). A substantial fraction of Bmc1 and Pof8 co-migrated with U6, and importantly, co-migration of Pof8 with U6 was impaired upon deletion of Bmc1 (Figure 1B), as well as co-migration of Bmc1 with U6 upon deletion of Pof8 (Figure S1C). We propose that Bmc1, Pof8, and Thc1 associate with U6 simultaneously, with all three proteins required to be present to initiate formation of the Bmc1-containing U6 snRNP. Together, these data point towards the existence of a new U6-containing complex that also shares components

with the telomerase holoenzyme, providing a new and surprising link between two seemingly disparate fission yeast noncoding RNA pathways.

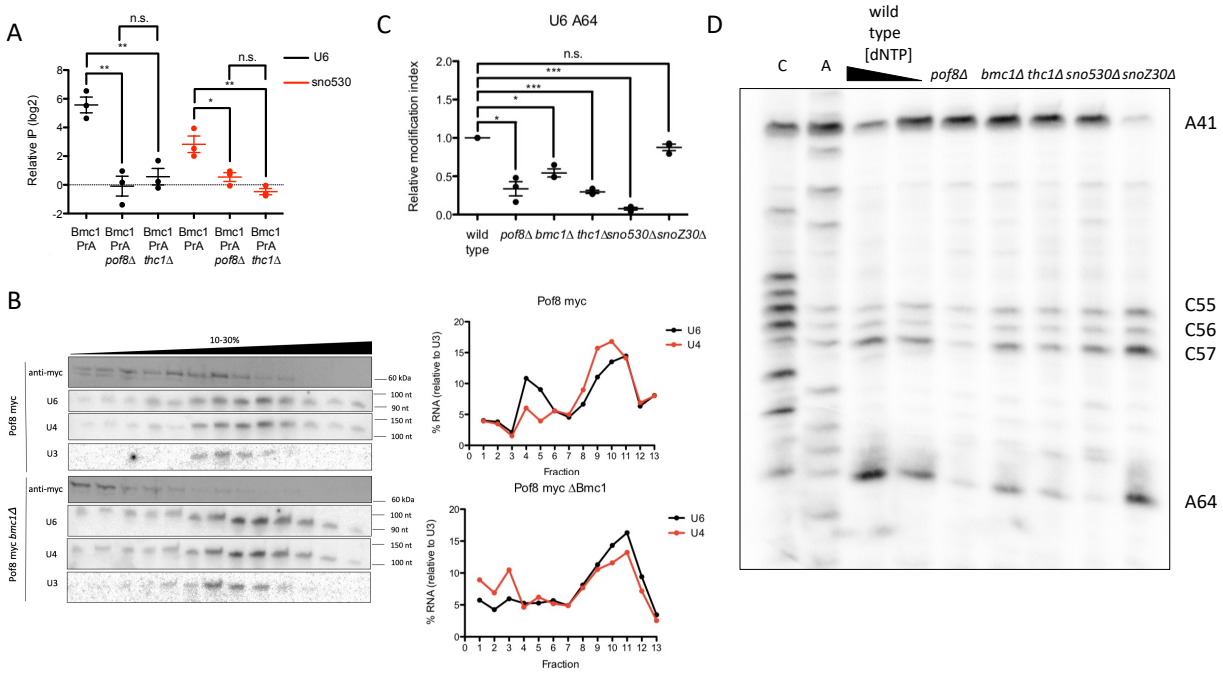

Figure 1: Bmc1, Pof8, and Thc1 promote 2′-O-methylation of U6
A) qRT-PCR of U6 and sno530 in Bmc1 PrA immunoprecipitates, normalized to immunoprecipitation from an untagged strain (mean± standard error, two-tailed unpaired *t* test, **p*<0.05, ***p*<0.01) (n= 3 biological replicates).
B) Glycerol gradient sedimentation of myc-tagged Pof8, U4, and U6, and U3 from wild type (Pof8 myc) and *bmc1*Δ strains. U4 and U6 signals were normalized to U3 for calculating relative migration in the gradient.
C) Quantification of relative 2′-O-methylation-induced reverse transcriptase stops at A64, compared to a wild type strain (mean± standard error, two-tailed paired *t* test, **p*<0.05, ***p*<0.01, *** *p*<0.001) (n= 3 biological replicates).
D) 2′-O-methylation primer extension of U6 at high (1.5 mM) and limiting (0.1 mM) dNTP concentrations. 2′-O-methylated sites are indicated.

3.3.2 Bmc1, Pof8, and Thc1 promote 2′-O-methylation of U6

To gain further insight into the role of the Bmc1-containing U6 snRNP, we examined our Bmc1 RIP-Seq dataset (68), which revealed an interaction between Bmc1 and snoZ30, which guides 2'-O-methylation of U6 at position 41 (80) (Figure S1A, S2A, B). Further supporting the idea that U6 complex formation is contingent on the presence of all three proteins, we observed a loss of snoZ30 binding to Bmc1 upon knockout of any member of the complex (Figure S2A). The observed interaction between Bmc1 and snoZ30, coupled with the well-characterized function of mammalian LARP7 in facilitating snoRNA-guided 2'-O-methylation of U6 by the methyltransferase fibrillarin (131, 132) provided initial clues as to the function of this new U6-containing snRNP. To determine if Bmc1, Pof8, and Thc1 influence 2'-O-methylation, we mapped U6 2'-O-methylation sites by performing primer extensions at low dNTP concentrations (80). Although snoZ30 is the sole annotated U6-modifying snoRNA in fission yeast (80), several other 2'-O-methylated sites have been identified in U6, including A64 (65). Deletion of Bmc1, Pof8, and Thc1 resulted in no observable changes in 2'-O-methylation at the snoZ30-modified A41, but we did detect a reproducible decrease in modification at several other sites, most notably A64 (Figure 1C, D, Figure S3).

Initial attempts at identification of the U6 A64-methylating snoRNA using box C/D snoRNA consensus sequences and base pairing rules (210) yielded no other obvious snoRNA candidates, so we instead turned to our Bmc1 RIP-Seq dataset in the hope we might identify novel snoRNAs (Figure S1A). The uncharacterized fission yeast noncoding RNA, SPNCRNA.530 (henceforth referred to as sno530), contains a D box, a putative C box one nucleotide different from the C box consensus motif, and a region with 12 nucleotides of complementarity with U6, with a single non-Watson Crick base pair (Figure S2C). It is also

noteworthy that the predicted secondary structure of sno530 does not position the C and D boxes flanking a hairpin, as is common for canonical box C/D snoRNAs (Figure S2C). We validated the interaction between Bmc1 and sno530 by RNP immunoprecipitation/qPCR and showed that much like snoZ30 and U6, this interaction is dependent on the presence of the assembled Bmc1-Pof8-Thc1 complex (Figure 1A). Deletion of snoZ30 and sno530 resulted in a loss of 2'-O-methylation at A41 and A64, respectively, suggesting that sno530 is indeed the A64 U6-modifying snoRNA (Figure 1C, D, Figure S3). We obtained similar results using a complementary method that exploits the tendency for 2'-O-methylations to block RNase H cleavage following the annealing of a chimeric DNA-2'-O-methylated RNA oligo targeting the suspected 2'-O-methylated site (211, 212) (Figure S4A). This also served to provide evidence for 2'-O-methylation at C57, suggesting that it, too, is another site in U6 whose modification is similarly guided by Bmc1 and Pof8 (Figure S4B). While our knockout studies unambiguously identify sno530 as the A64 U6-modifying snoRNA, the unusual sequence and architecture of sno530 relative to snoZ30 is more reminiscent of the divergent box C'/D' motifs that stimulate rRNA 2'-O-methylation by providing additional regions of complementarity surrounding the methylated site (213, 214).

3.3.3 Bmc1, Pof8, and Thc1 are involved in U6 snRNP assembly

We then wondered how disruption of the Bmc1-containing U6 snRNP might impact spliceosome assembly. We observed small differences in U6 sedimentation in glycerol gradients, with a less abundant, lighter sedimenting U6-containing fraction appearing in addition to co-sedimentation with U4 (compare U6 and U4 in lanes 3-6 in Figure 1B and S1C), suggesting a U6-containing complex without U4. Consistent with this, we note that the migration of Pof8,

Bmc1, and Thc1 does not fully overlap with U4/U6 in the gradient, but is rather shifted towards lighter fractions, arguing against the complete inclusion of the Bmc1-Pof8-Thc1 complex in the U4/U6 di-snRNP (Figure 1B, S1C). As the lighter sedimenting U6 species is not evident in Bmc1 and Pof8 KO strains (compare U6 and U4 in lanes 3-6 in Figure 1B and S1C relative to Bmc1 and Pof8 KO strains), we hypothesized that Bmc1, Pof8, and Thc1 interact with U6 before the U4/U6 di-snRNP.

To obtain clearer resolution of distinct U6-containing complexes, we ran cell extracts on native gels and analyzed spliceosomal RNAs by northern blotting. We observed a single, prominent band for all spliceosomal RNAs except U6, which migrated as 2 distinct complexes (Figure 2A). We could assign the higher molecular weight complex, which comigrates with U4 but not U2 or U5, as the U4/U6 di-snRNP. The U4/U6 di-snRNP, as well as other spliceosomal snRNPs and the non-spliceosomal U3 snRNP, showed no change in relative intensity or migration upon deletion of Bmc1, Pof8, Thc1, or sno530. However, we did observe a significant and reproducible decrease in the intensity of the lower molecular weight U6-containing snRNP upon deletion of Bmc1, Pof8, and Thc1 (Figure 2A, B), consistent with this band representing the Bmc1-containing U6 snRNP. The persistence of this complex upon loss of sno530 suggests that complex formation is not reliant on the ability to modify U6 at A64. Although U6 and sno530 are associated with Bmc1 (Figure 1A), sno530 is therefore not required for the stability of the U6 snRNP observed in native gels.

To understand when Bmc1 interacts with U6 with respect to spliceosome formation, we extracted Bmc1 immunoprecipitated RNPs under native conditions and ran total and Bmc1-associated RNA on native gels. Bmc1-bound U6 did not co-migrate with the U4/U6 di-snRNP (Figure 2C), suggesting that Bmc1 interacts with U6 outside of the U4/U6 di-snRNP, in line with

the Bmc1/Pof8/Thc1-associated mono U6 snRNP band (2A, B). Based on these results, we hypothesize that the Bmc1-containing U6 complex, which promotes 5' capping and 2'-O-methylation, forms upstream of the U4/U6 di-snRNP.

Native fission yeast cell extracts do not form detectable amounts of the U4/U6.U5 tri-snRNP (215, 216), so we focused our further efforts on examining U4/U6 base pairing by performing a solution hybridization assay on cold phenol-extracted total RNA to maintain U4/U6 base pairing (Figure 2D). This differs from native spliceosomal snRNP gels (Figure 2A) in that it only assesses RNA-RNA interactions, without changes in mobility due to protein binding. We detected minor defects in U4/U6 assembly upon Bmc1, Pof8, or Thc1 deletion, as measured by the increase in "free" U4 relative to U4 complexed in the di-snRNP, although the increase in the fraction of free U4 did not reach statistical significance (Figure 2D, E). Consistent with the increase in free U4 in the knockout strains, glycerol gradients revealed an increase in lighter sedimenting U4 in the knockout strains (Figure 1B, S1B, compare lanes 1-3 in wild type versus knockouts). Although U6 is in excess over U4, the increase of free U4 in the knockouts suggests that the absence of Bmc1, Pof8, and Thc1 may result in a non-functional, alternate pathway for U4 that does not involve U4/U6 di-snRNP formation. The lack of U4/U6 pairing defects upon the loss of sno530 further suggests that it is largely the Bmc1-Pof8-Thc1 protein complex dictating U4/U6 pairing, not the single A64 2'-O-methylation. Still, UV melt analysis of the U6-interacting region of U4 and the U6 internal stem loop (ISL), with or without 2'-O-methylation of A64, revealed a slight increase in U4-U6 duplex stability with 2'-O-methylation, consistent with previous findings reporting on the stabilizing properties of 2'-O-methylation on RNA duplex formation (217–219) (Figure 2F).

Subsequent steps in spliceosome formation involve unwinding of the U6 ISL and forming base pairing between U4 and U6, both of which are promoted by the U4/U6 di-snRNP assembly factor Prp24 (220, 221). We generated an endogenously tagged Prp24 strain and assessed the interaction between Prp24 and U4 and U6. Pof8 and Bmc1 deletion resulted in a decreased interaction between Prp24 and U4 and U6, suggesting that Bmc1 and Pof8 promote the association of U4 and U6 with Prp24, which in turn may promote the formation of the U4/U6 di-snRNP (Figure 2G, H). In sum, our results are consistent with the existence of a Bmc1/Pof8/Thc1-containing U6 snRNP, with Bmc1/Pof8/Thc1 dissociating from U6 during establishment of the U4/U6 di-snRNP.

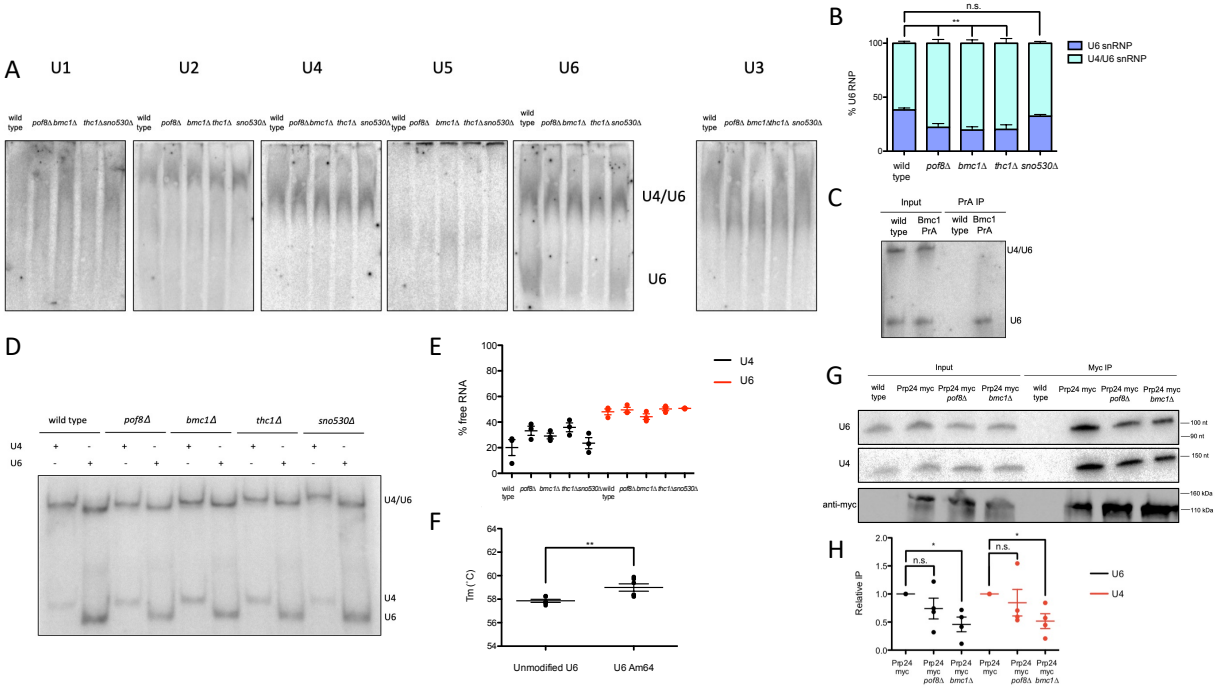

Figure 2: Bmc1, Pof8, and Thc1 promote U4/U6 di-snRNP assembly
A) Native northern blot analysis of spliceosomal and non-spliceosomal (U3) snRNPs from native yeast cell extracts.
B) Quantification of U6-containing snRNPs from wild type and knockout yeast cell extracts (mean± standard error, two-tailed unpaired *t* test, $^{**}p<0.01$) (n= 4 biological replicates).
C) Native northern blot analysis of total and Bmc1-immunoprecipitated U6.
D) Solution hybridization of U4/U6 pairing in wild type and knockout yeast strains using radiolabeled probes targeting the 5′ end of U4 and 3′ end of U6.

E) Quantification of U4/U6 pairing from solution hybridization assay, expressed as the fraction of non-duplexed U4 and U6 ("free RNA") (mean± standard error) (n= 3 biological replicates).
F) T_m values from UV melt curve analysis of U4/U6 pairing with unmodified and A64-2′-O-methylated U6 oligos (mean± standard error, two-tailed unpaired *t* test, $^{**}p<0.01$) (n= 6 technical replicates).
G) Northern and western blot analysis of U4, U6, and myc-tagged Prp24 from total cell extracts and myc-immunoprecipitates.
H) Quantification of Prp24-immunoprecipitated U4 and U6, relative to Prp24 myc (mean± standard error, two-tailed unpaired *t* test, $^{*}p<0.05$) (n= 4 biological replicates).

3.3.4 Bmc1 5′ capping catalytic activity is not required for promoting 2′-O-methylation of U6

With previous studies indicating that Bmc1 5′ γ-phosphate methyltransferase catalytic activity is dispensable for telomerase activity (209), we assayed a combination of previously described and newly constructed putative Bmc1 catalytic mutants for the ability to promote U6 2′-O-methylation. We mutated residues that are both highly conserved between Bmc1 and human MePCE, and well-positioned in structure predictions to interact with the methyltransferase byproduct SAH (Figure 3A). HA-tagged Bmc1 mutants were transformed into a Bmc1 knockout yeast strain and profiled for U6 2′-O-methylation as above (Figure 3B, C). While the Bmc1 mutants were more lowly expressed than wild type Bmc1, some mutants still promoted 2′-O-methylation to a greater extent than the empty vector (Figure 3C). Further, normalization of relative 2′-O-methylation levels to Bmc1 expression confirmed a statistically significant increase in 2′-O-methylation for all Bmc1 mutants compared to the empty vector (Figure 3D). This suggests that, as in telomerase, Bmc1 5′ γ-phosphate methyltransferase catalytic activity is not critical for its function in U6 2′-O-methylation.

For further characterization of Bmc1 catalytic mutants, we chose the Bmc1 L153A V155A mutant, which showed the highest expression across biological replicates. As measured

by co-immunoprecipitation, L153A V155A still interacted with Pof8, suggesting that catalytic activity is also not required for complex formation (Figure 3E). Further, L153A V155A interacted with U6, indicating that 5′ γ-phosphate methyltransferase catalytic activity is not required for U6 binding (Figure 3E).

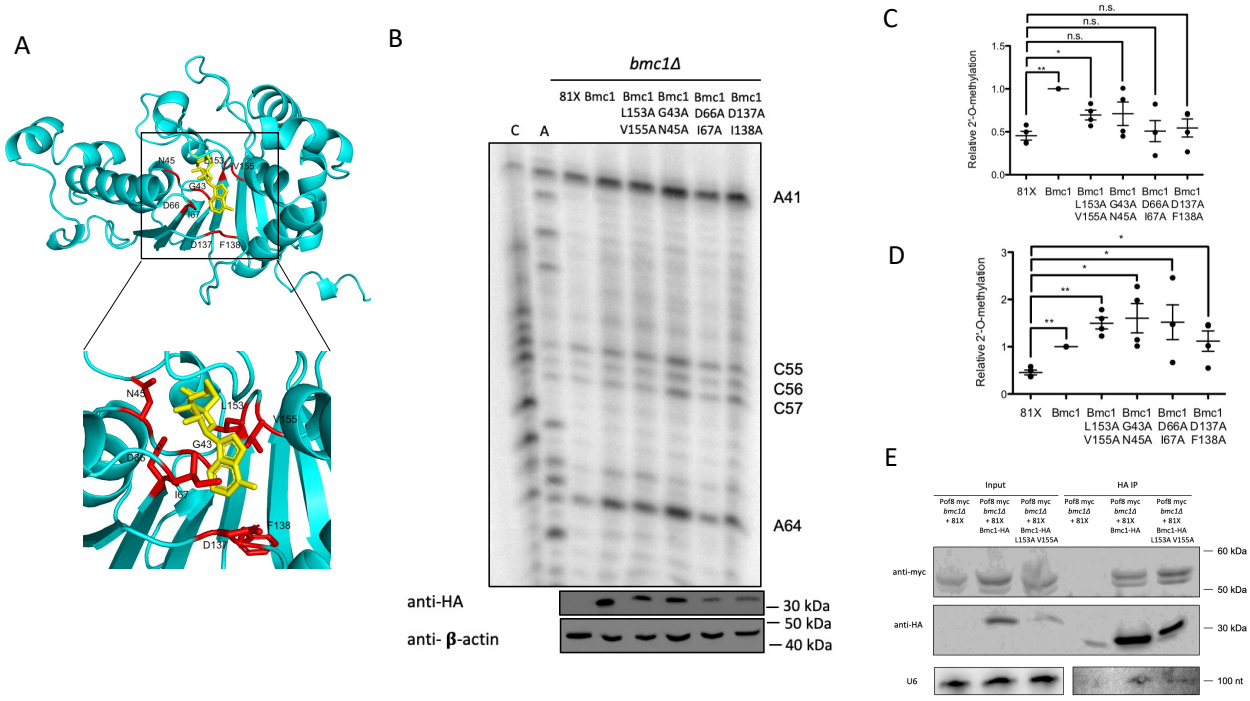

Figure 3: Bmc1 catalytic activity is not a requirement for 2′-O-methylation of U6
A) AlphaFold (222) structure prediction of Bmc1 aligned to the SAH-bound (yellow) catalytic domain of MePCE (PDB 6DCB) (157) with mutations indicated in red. Inset: side chain interactions with SAH.
B) U6 2′-O-methylation primer extension in *bmc1*Δ cells transformed with the indicated plasmid. 2′-O-methylated sites are indicated. Western blots for Bmc1-HA expression and b-actin are indicated below.
C) Quantification of relative 2′-O-methylation-induced reverse transcriptase stops at A64, compared to wild type Bmc1-HA (mean± standard error, two-tailed paired *t* test, **p*<0.05, ***p*<0.01) (n= 4 biological replicates).
D) Quantification of relative 2′-O-methylation-induced reverse transcriptase stops at A64, compared to wild type Bmc1-HA, normalized to average Bmc1-HA expression relative to b-actin (mean± standard error, two-tailed paired *t* test, **p*<0.05, ***p*<0.01) (n= 4 biological replicates).
E) Western blot and northern blot analysis of co-immunoprecipitation of HA-tagged Bmc1, myc-tagged Pof8 and U6.

3.3.5 The xRRM and Pof8-Lsm2-8 interaction are important determinants for U6 2′-O-methylation

As an established member of the LARP7 family of proteins, the protein-interacting and RNA binding domains of Pof8 have been well-characterized in the context of the telomerase RNP (11–15). Pof8 contains a divergent La motif that lacks the conserved uridylate-binding residues typically seen in LARP7 proteins (11), so its interaction with the telomerase RNA TER1 is mediated by the RRM1, xRRM, and the N-terminal region that makes direct protein-protein contacts to Lsm2-8, which in turn binds the uridylate-rich 3′ end of TER1 (11–14). As mutations to these regions have been shown to impair Pof8 binding to TER1 and telomere length homeostasis, we looked at the impact of these same mutations on U6 2′-O-methylation (Figure 4A). In contrast to what has been observed for TER1, where both RRMs are important for binding, only mutations to the xRRM and the Lsm2-8 binding region caused a significant reduction in 2′-O-methylation at A64 (Figure 4B, C).

To further understand the molecular basis for the drop in 2′-O-methylation, we immunoprecipitated Bmc1 in a Pof8 knockout strain re-expressing the Pof8 mutants (Figure 4D, E). Bmc1 co-immunoprecipitated all Pof8 mutants, suggesting that the 2′-O-methylation defect is not due to complete disruption of the Bmc1-Pof8 interaction (Figure 4D). The Bmc1-U6 interaction, which is dependent on the presence of Pof8 (Figure 1A), was almost completely lost in the Lsm2-8-binding mutant (Δ2-10), suggesting that its 2′-O-methylation defect may be due to a loss in U6 association with the Bmc1-Pof8-Thc1 complex (Figure 4D, E). Surprisingly, we detected no loss in U6 binding with the xRRM mutant, indicating that while U6 still interacts with the Bmc1-Pof8-Thc1 snRNP in the context of the xRRM mutant, the xRRM may have another function in facilitating U6 2′-O-methylation (Figure 4D, E), potentially through the

binding of the snoRNA, as has been suggested for human LARP7 (131). Alternatively, as the xRRM in the ciliate LARP7 protein p65 has been suggested to possess RNA chaperone activity to remodel the ciliate telomerase RNA (122, 151), it is tempting to speculate that similar xRRM-mediated RNA chaperone activity may play a role in correctly positioning U6 for 2′-O-methylation.

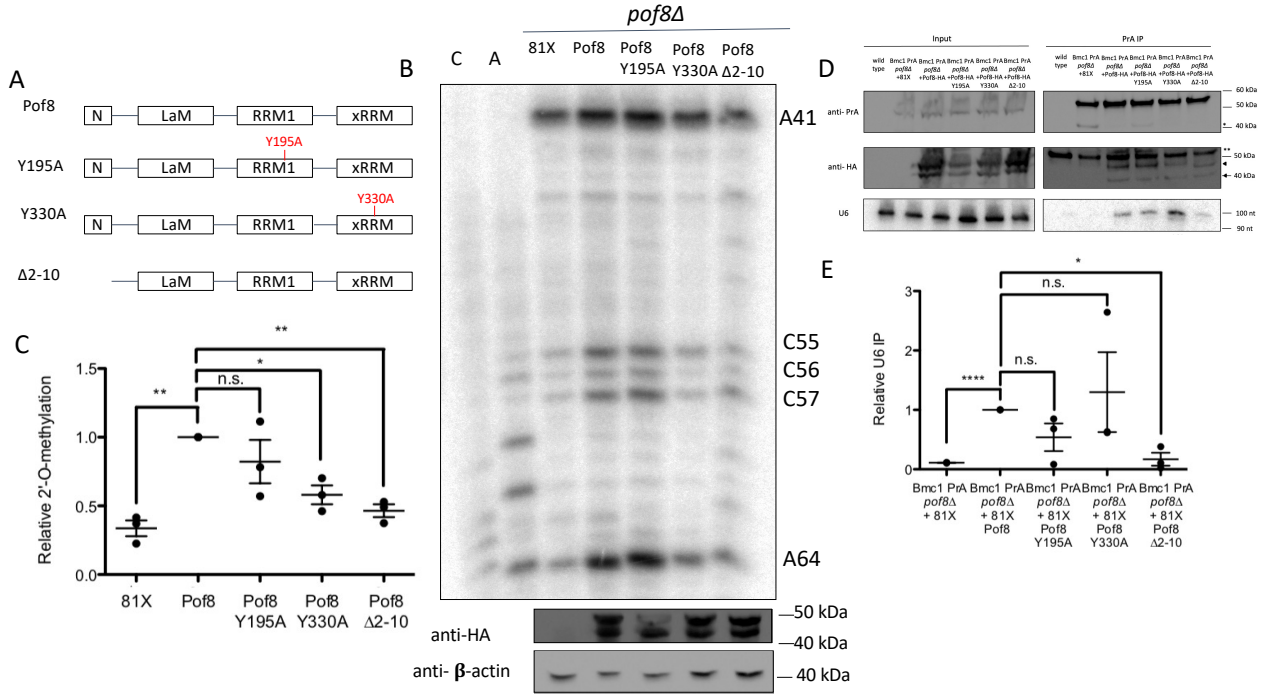

Figure 4: The xRRM and Lsm2-8-binding surface are important in Pof8-mediated 2′-O-methylation of U6

A) Schematic of Pof8 domains and mutants used in this study. N= N-terminal domain, LaM= La motif, RRM1= RNA Recognition Motif 1, xRRM= extended RNA Recognition Motif.

B) U6 2′-O-methylation primer extension in *pof8*Δ cells transformed with the indicated plasmid. 2′-O-methylated sites are indicated. Western blots for Pof8-HA expression and b-actin are indicated below.

C) Quantification of relative 2′-O-methylation-induced reverse transcriptase stops at A64, compared to wild type Pof8-HA (mean± standard error, two-tailed paired *t* test, *p<0.05, **p<0.01) (n= 3 biological replicates).

D) Northern and western blot analysis of U6, PrA-tagged Bmc1, and HA-tagged Pof8 from total cell extracts and PrA-immunoprecipitates. *Bmc1 PrA cleavage products, **An additional band cross-reacting with the antibody, arrows indicate Pof8 HA.

E) Quantification of Bmc1-immunoprecipitated U6, relative to the Pof8-HA-expressing strain (mean± standard error, two-tailed paired *t* test, *p<0.05, *p<0.01, ****p<0.0001) (n= 3 biological replicates).

3.3.6 Bmc1 deletion has a minor effect on intron retention

Having observed Bmc1-dependent defects in U6 2'-O-methylation and U6 snRNP assembly, we tested the effects of Bmc1 deletion on pre-mRNA splicing. To that end, we performed short-read, paired-end sequencing on RNA extracted from wild type and Bmc1 knockout yeast strains and quantified intron retention as a proxy for splicing (223, 224). We also measured intron retention in wild type and knockout cells heat shocked for 15 minutes at 42˚C, which has been shown to impact splicing in fission yeast (225). We observed significant increases in intron retention following heat shock, similar to what has been reported in mammalian cells (226) (Figure S5A, B). Although we observed slight increases in intron retention in Bmc1 knockout cells compared to wild type cells, very few of these splicing events at 32˚C passed our significance cut-off, and no splicing events at 42˚C were statistically significant (Figure S5C, D), although this may be due to greater sample to sample variability across our triplicate replicates for this data set (Figure S6). Still, as mean intron retention values indeed showed an increase upon Bmc1 deletion (Figure 5A), we chose several representative intron retention events to validate with semi-quantitative RT-PCR (one of which, intron 1 of pud1, displayed a statistically significant increase upon Bmc1 deletion at 32˚C in our RNA Seq dataset). We observed an increase in intron retention following heat shock, and confirmed their further impaired splicing in the context of the Bmc1 deletion (Figure 5B, S7). Conversely, a ribosomal protein gene, which have been reported to be efficiently spliced relative to non-ribosomal protein genes in budding yeast (227, 228), and did not show heat shock or Bmc1 associated changes in our RNA-Seq data set, was confirmed to have no changes in intron retention in response to heat shock or Bmc1 deletion (Figure 5B, S7). We note that these validated Bmc-1 affected introns have higher than average intron retention rates in normal cells

and as such, may not be representative of the average splicing event. Together, these data indicate that Bmc1 does not have a major effect on pre-mRNA splicing, but that Bmc1 likely contributes to splicing robustness, similar to what has been described for mammalian LARP7 deletion in human cells (131, 132).

We also examined other factors that could contribute to heat shock-sensitive splicing defects. We compared intronic features between heat shock-sensitive introns, classified as introns exhibiting a greater than 2-fold increase in intron retention upon heat shock and a false discovery rate less than 0.05, and remaining introns (heat shock insensitive) (Figure 5C-E, S5A, B). In line with previous data indicating that intron retention in fission yeast can arise from a weak 5' splice site (229), we noted that heat shock-sensitive introns have a weaker 5' splice site score in the context of a wild type and *bmc1*Δ strain, with no significant differences in 3' splice site scores (Figure 5C,D). Additionally, heat shock-sensitive introns displayed lower minimum free energy, indicative of a link between intron structure and splicing changes in response to heat shock (Figure 5E).

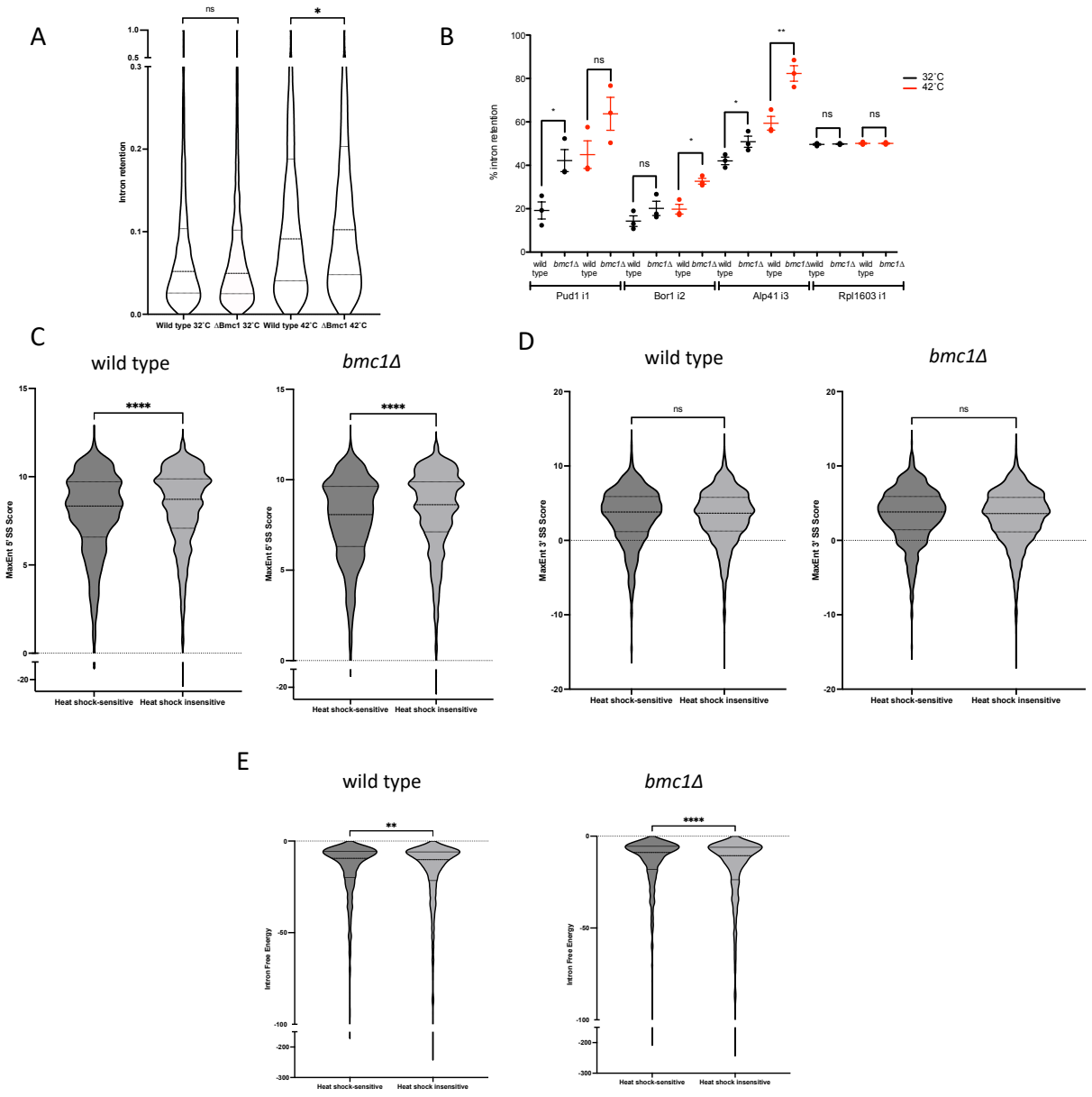

Figure 5: Bmc1 deletion leads to minor splicing defects

A) Average intron retention from 3 biological replicates for wild type and *bmc1*Δ strains grown at 32˚C or heat shocked at 42˚C (two-tailed unpaired t-test with Welch's correlation, * p<0.05). B) Semi-quantitative RT-PCR in wild type and *bmc1*Δ strains grown at 32˚C or heat shocked at 42˚C for intron 1 of *pud1*, intron 2 of *bor1*, intron 3 of *alp41*, and intron 1 of *rpl1603* (mean± standard error, two-tailed unpaired *t* test, *p<0.05, **p<0.01) (n= 3 biological replicates). C-E) Comparison of 5' splice site scores (C), 3' splice site scores (D), and intron minimum free energy (kcal/mol) (E) for heat shock-sensitive and insensitive introns in wild type and *bmc1*Δ cells. Heat shock-sensitive introns were classified as introns that exhibited a greater than 2-fold increase in intron retention following heat shock and a false discovery rate less than 0.05. Remaining introns are classified as heat shock insensitive. Only introns with greater than 4 reads

supporting splicing in all biological replicates were included (two-tailed unpaired t-test with Welch's correlation, **p<0.01, ****p<0.0001).

3.4 Discussion

Conserved functions for LARP7 family proteins in splicing and U6 2′-O-methylation

This work represents the first report of an MePCE homolog with a role in splicing and spliceosome assembly, beyond 5′ methyl phosphate cap addition of U6. In our efforts to investigate functions for Bmc1 beyond telomerase, we revealed an unanticipated overlap between components of the yeast telomerase holoenzyme and a U6-containing snRNP. While it is surprising that Bmc1, Pof8, Thc1, and Lsm2-8 interact with 2 very distinct non-coding RNAs produced by different polymerases, both RNAs possess uridylate-rich sequences recognized by Lsm2-8 and highly structured regions, including stem loops in U6 and pseudoknots in telomerase, that act as scaffolds to recruit other RNP components. These common features may provide an explanation as to why these divergent RNAs share a common set of protein binding partners. Such RNP plasticity is not unique to fission yeast telomerase and U6, but may represent a shared feature of LARP7 and MePCE family proteins. Mammalian LARP7 and MePCE are particularly well-studied for their roles in capping and stabilizing the 7SK snRNP (64, 124–126), transcriptional control through DDX21 (212), directing U6 modification (131, 132), and snRNP assembly through the SMN complex (230). Thus, continuing to study the RNA interactome of MePCE and LARP7 homologs across species will likely yield additional insight into how these proteins associate with and influence various classes of non-coding RNAs. It is also possible that Bmc1, Pof8, and Thc1 interactions with U6 are mediated entirely by direct interactions with Lsm2-8, which in turn directly contacts U6, much like Prp24 interacts with U6 by directly

binding Lsm2-8 (231). Future structural and biochemical studies will lend insight into the protein-protein and protein-RNA interactions that cooperate to form the U6 snRNP.

Several fungal species, including *S. cerevisiae*, lack both a LARP7 and MePCE homolog (68, 123). As deletion or depletion of LARP7/Pof8 or MePCE/Bmc1 does not influence U6 stability in species where this has been investigated (64, 68, 131, 132, 209), the function of LARP7 and MePCE family members in U6 biogenesis and function has remained unclear. This work expands our understanding of the evolutionary conservation of LARP7 family members, with shared or unique functions relating to the telomerase, U6, and 7SK RNAs, depending on the species under investigation (Figure 6A). Further links can be drawn between the functional consequences of LARP7- and Pof8-mediated promotion of U6 2′-O-methylation. LARP7 or Pof8 deletion and the subsequent decrease in 2′-O-methylation of U6 results in no functional consequences under standard physiological conditions, but becomes important for maintaining splicing fidelity under heat stress, in the case of human LARP7, and male germ cells in mice (131, 132). As the loss of A64 modification alone results in no changes to U6 snRNP assembly, compared to the changes observed upon Bmc1, Pof8, and Thc1 deletion, we anticipate that it is either a combination of the loss of several 2′-O-methylations or the loss of the Bmc1-Pof8-Thc1 U6 snRNP that leads to increased intron retention at elevated temperatures upon Bmc1 deletion (Figure 3). Future studies aimed at teasing apart this mechanism in mammalian and yeast cells will provide additional insight into the intertwining role of RNA modifications and RNP biogenesis complexes in spliceosome assembly.

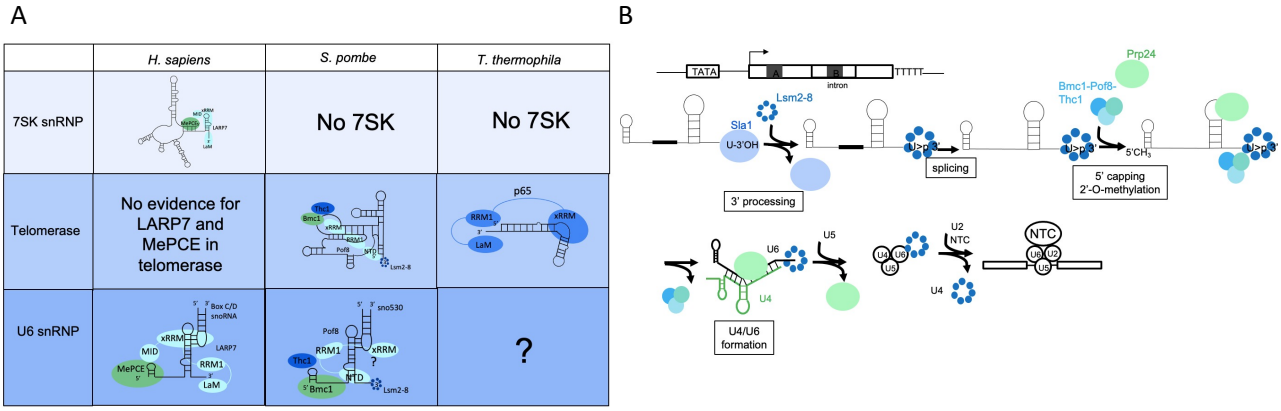

Figure 6: Evolutionary convergence and divergence of Bmc1/MePCE and Pof8/LARP7 in noncoding RNA processing
A) Summary of Bmc1/MePCE and Pof8/LARP7/p65 functions in the 7SK snRNP, telomerase holoenzyme, and U6 snRNP. LaM= La motif, RRM1= RNA Recognition Motif 1, xRRM= extended RNA Recognition Motif, NTD= N-terminal domain (Lsm2-8-interacting region), MID= MePCE-Interacting Domain. The existence and composition of a U6 snRNP in *T. thermophila* is currently unknown.
B) Schematic of the U6 biogenesis pathway in fission yeast. NTC= NineTeen Complex.

Another question that emerges from this study concerns the minor splicing defects observed in Bmc1 knockout cells at elevated temperatures. Previous studies on mammalian LARP7 proposed that LARP7-guided 2'-O-methylation of U6 is not an important factor for splicing as a whole, but rather contributes to splicing robustness (131, 132). Although recent reports indicate that alternative splicing in fission yeast may be more widespread than previously thought (225, 232, 233), splicing complexity in fission yeast is still less than that observed in mammalian cells, which may explain why we do not observe any drastic splicing changes upon Bmc1 deletion. It remains to be determined whether Bmc1 affects other aspects of splicing that have not been tested here, such as splicing efficiency and fidelity, or whether Bmc1-associated defects in splicing might be greater under different stresses. In addition, Bmc1 promotes 2'-O-methylation in the internal stem loop of U6, which does not base pair with the 5' or 3' splice site.

Thus, modulation of ISL modifications might not be expected to manifest as a robust splicing defect. This is in contrast to what has been reported for the loss of m^6A in *S. pombe* U6, where affected introns are enriched for an adenosine at the fourth position of the intron, which directly base pairs with the m^6A (74).

Emerging importance of the xRRM in RNA folding and function

Fission yeast, possessing a LARP7 homolog that functions in telomerase like its ciliate counterpart (11–15, 68, 209), and U6 2′-O-methylation in an analogous manner to its mammalian homologs, may represent an evolutionary intermediate bridging RNA binding proteins between ciliates and mammals. The 7SK snRNA, which has only been found in animals (156) likely arose independently from the more widely distributed LARP7 and MePCE, suggesting the need for continued studies into 7SK-independent functions for LARP7 and MePCE. Of note, the conservation of the xRRM between fungal, mammalian, and ciliate LARP7 proteins, rather than the La motif (11–13, 68, 123) may provide a reason explaining the diverse RNA substrates bound by LARP7 homologs, compared to the more well-conserved classes of RNA binding partners of other LARPs across species (123). xRRM-mediated binding to structured stem loops like the telomerase RNA pseudoknot (14), SL4 of 7SK (234), and U6-modifying snoRNAs (131) may be a better determinant than 3′ terminal uridylate stretches for predicting LARP7 binding. The importance of the xRRM in the biogenesis and stability of telomerase RNA, 7SK, and U6 may be linked to its RNA chaperone activity, which has been proposed to have a role in promoting RNA folding (122, 151). Our finding that mutation of the xRRM of Pof8 impairs 2′-O-methylation of U6 without disrupting U6 binding (Figure 5D) may provide further evidence that the xRRM has functions beyond U6 binding and raises additional

questions as to the mechanism by which RNA chaperones can coordinate snoRNA and target RNA binding to carry out efficient 2′-O-methylation. Importantly, xRRM chaperone activity is not limited to LARP7 family proteins, as the RRM2/xRRM of the human La protein has also been shown to promote RNA folding (104, 235, 236).

New insights into U6 biogenesis in fission yeast

This work also sheds light on the timing of U6 biogenesis steps in fission yeast (Figure 6B). We have previously shown that Lsm2-8 interacts with both mature and intron-containing U6, suggesting that intron removal occurs after 3′ end processing and the switch from La to Lsm2-8 (60, 68). Conversely, Bmc1 and Pof8 interact solely with the spliced form of U6 (68). This, coupled with our finding that the Lsm2-8-interacting region of Pof8 is required for the Bmc1-U6 interaction (Figure 5D, E), indicates that Lsm2-8 binding occurs prior to splicing and recruitment of the Bmc1-Pof8-Thc1 complex. Our data indicating that Bmc1 co-purifies with U6-modifying snoRNAs (Figure 1 and Figure S2) suggests that U6 then undergoes 5′ capping by Bmc1 and 2′-O-methylation, prior to Bmc1-Pof8-Thc1 dissociation from U6 and U4/U6 di-snRNP assembly mediated by Prp24. Since deletion of Bmc1 or Pof8 results in decreased association of Prp24 with U4 and U6 (Figure 2), the Bmc1-Pof8-Thc1 complex may play a role in the handoff to Prp24. This role may be mediated by xRRM-linked chaperone activity that remodels U6 to better position it to interact with Prp24 and U4. Our finding of a new U6 biogenesis complex thus adds another layer of regulation to spliceosome assembly. Still, it remains unknown whether Bmc1, Pof8, and Thc1 only interact with U6 during its biogenesis, or re-associate with U6 when it is reassembled into the U4/U6 di-snRNP for subsequent rounds of splicing catalysis. Notably, our finding of a mono-U6 snRNP containing Bmc1 and Pof8 that

promotes internal modifications of U6 is consistent with earlier reports of the human m^6A methyltransferase METTL16 present in a mono-U6 snRNP with MePCE and LARP7 (72). Since mammalian U6 also undergoes 5′ methyl phosphate capping by MePCE and LARP7-mediated 2′-O-methylation, it will be interesting to examine the interplay between MePCE, LARP7, and METTL16, and how these factors may function in promoting the formation of the U4/U6 di-snRNP in higher systems.

Taken together, this work adds to the growing body of literature on the catalytic-independent functions of RNA modification enzymes (reviewed in (41)). While this raises questions as to the precise function of Bmc1 catalytic activity on the 5′ end of U6, *in vitro* binding assays showed that catalytic activity of the human MePCE promotes 7SK retention following catalysis (157). It remains to be found if this extends to other MePCE/Bmc1 targets like U6, and how U6 snRNP assembly may be regulated in species lacking MePCE/Bmc1 and LARP7 homologs.

3.5 Materials and Methods

Yeast strains and growth

Strains were grown at 32˚C in yeast extract with supplements (YES) or Edinburgh Minimal Media (EMM), as indicated. Tag integration and knockouts were generated as described in (68) (primer sequences provided in supplementary table 1). A list of yeast strains is provided in supplementary table 2.

Native protein extracts and immunoprecipitation

Native protein extractions and immunoprecipitations were carried out as described in (68). Protein A-tagged strains were immunoprecipitated with Rabbit IgG-conjugated (MP-Biomedicals, SKU 085594) Dynabeads (Invitrogen, 14301) (38) and myc- and HA-tagged proteins were immunoprecipitated with Protein A/G beads (GeneBio, 22202B-1) coated with anti-myc antibody (Cell signaling, 2276S) at a dilution of 1:250 or anti-HA antibody (Cell signaling, 3724S) at a dilution of 1:50. Total RNA was isolated from cell extracts with 0.5% SDS, 0.2 mg/mL Proteinase K (Sigma, P2308), 20 mM Tris HCl pH 7.5, and 10 mM EDTA pH 8.0 for 15 minutes at 50˚C, followed by phenol: chloroform: isoamyl (25:24:1) extraction and ethanol precipitation. Immunoprecipitated RNA was isolated by incubating beads in 0.1% SDS and 0.2 mg/mL Proteinase K for 30 minutes at 37˚C, followed by phenol: chloroform: isoamyl alcohol extraction. For native northern blots, input RNA was extracted in the same manner as immunoprecipitated RNA. Relative immunoprecipitation efficiency was calculated by dividing the IP signal by the input signal. Western blots were performed using anti-myc (Cell signaling, 2276S) at 1:5000, anti-beta actin (Abcam, ab8226) at 1:1250, HRP-conjugated anti-mouse (Cell signaling, 7076) at 1:5000, anti-HA (Cell signaling, 3724S) at 1:1000, HRP-conjugated anti-rabbit (Cell signaling, 7074S) at 1:5000, or HRP-conjugated polyclonal anti-Protein A (Invitrogen, PA1-26853) at 1:5000.

RNA preparation, northern blotting, 2′-O-methylation detection, and solution hybridization

Total RNA was extracted with hot phenol, separated on 10% TBE-urea polyacrylamide gels, and transferred to positively charged nylon membranes (Perkin Elmer, NEF988001) as per (179). For native RNA extraction to detect U4/U6 duplexes, RNA was extracted with cold phenol, as per (237). Solution hybridization was performed as per (238) and resolved on 9% TBE gels. Probe

sequences for ^{32}P γ-ATP-labeled DNA probes for northern blotting are provided in supplementary table 3. Primer extensions to detect 2′-O-methylation were performed based on protocols from (80). Briefly, 5 μg RNA was incubated for 5 minutes at 85˚C in a 10 μL reaction containing ^{32}P γ-ATP-labeled probe, 50 mM Tris HCl pH 7.4, 60 mM NaCl, then transferred to 55˚C for 20 minutes to allow the probe to anneal. Reverse transcription was carried out with 1.5 mM (high concentration) or 0.1 mM (limiting concentration) dNTP mix and 2.5 U AMV-RT (NEB, M0277S) and 1 hour incubation at 42˚C. cDNA products were separated on 8% TBE-urea sequencing gels, dried, and exposed to Phosphor screens overnight. Relative 2′-O-methylation was calculated by determining the ratio of each RT stop relative to the total signal in each lane (all RT stops and full length U6). 2′-O-methylations were also detected by RNase H (NEB, M0297S) digestion of 2 μg with 25 pmol chimeric RNA-DNA probes, as per (211). Probe sequences targeting C57 and A64 2′-O-methylations are provided in supplementary table 3.

qRT-PCR and semi-quantitative RT-PCR

1 μg TURBO DNase-treated RNA was reverse transcribed with the iScript cDNA reverse transcription kit (Biorad, 1708890) or 5 U AMV-RT (NEB, M0277S) and gene-specific reverse primers. qRT-PCR was performed with the SensiFAST SYBR No-Rox kit (Bioline, BIO-98005) and 1 μM of each primer, with settings outlined in (68). For semi-quantitative RT-PCR, cDNA was amplified with Taq polymerase (NEB, MO273L) using the following cycling conditions: 5 min initial denaturation at 94˚C, 26 (pud1, alp41) or 27 (rpl1603, bor1) cycles of 30 s at 94˚C, 30 s at 50˚C, and 1 minute at 72˚C, and a final 5 minute extension at 72˚C. cDNA was resolved on 10% TBE gels.

Native yeast extract preparation, native snRNP gels, and glycerol gradient sedimentation

Pellets from 1 L yeast cultures were resuspended to 1 g/mL in AGK400 buffer (10 mM HEPES KOH pH 7.9, 400 mM KCl, 1.5 mM $MgCl_2$, 0.5 mM DTT, 1 mM PMSF, and protease inhibitor cocktail (Sigma, P8215)), frozen in liquid nitrogen, and ground to fine powder with a mortar and pestle. Powder was thawed on ice and spun in a JA 25.50 rotor (Beckman) for 16 minutes at 15,000 rpm and the supernatant was subsequently spun in a 70.1 Ti rotor (Beckman) for 45 minutes at 50,000 rpm to pellet ribosomes and heavy molecular weight complexes. Supernatants were flash frozen and stored at -80˚C. For native snRNP gels, glycerol with xylene cyanol and bromophenol blue was added to 30 µg cell extract (final glycerol concentration= 10%) and fractionated on 4% 19:1 acrylamide: bis-acrylamide native gels (15 cm x 18 cm) for 220 minutes at 240 V and 4 degrees, then transferred to nylon membranes for northern blotting. For glycerol gradients, cell extracts from 1.0 g frozen cell powder were layered on an 11 mL 10-30% glycerol gradient (50 mM Tris HCl pH 7.4, 25 mM NaCl, 5 mM $MgCl_2$) and spun in an SW41Ti rotor (Beckman) for 20 hours at 30,900 rpm. Fractions were collected starting from the top of the gradient and RNA and proteins were extracted with phenol: chloroform: isoamyl alcohol (25:24:1) and TCA precipitation, respectively.

UV melt curves

UV melt curves were recorded on a Cary BIO 100 spectrometer with a 6 x 6 temperature-controlled cell holder. 2 µL 10 mM U4 and modified or unmodified U6 RNA oligos in 96 µL buffer (10 mM KH_2PO_4 pH 7.0 and 200 mM KCl) was heated and cooled from 50˚C to 65˚C at a rate of 2˚C per minute without collecting data, then re-heated and cooled while monitoring absorbance at 260 nm at 1˚C intervals. Absorbance at 260 nm at each temperature point was

normalized to absorbance at 50˚C and absorbance curves were fitted with an equation for one site specific binding with a Hill slope to determine T_m values. RNA sequences are provided in supplementary table 3.

RNA Seq and intron retention analysis

DNase-treated RNA was rRNA-depleted (Qiagen, 334215) and stranded libraries were prepared by Genome Québec. cDNA libraries were sequenced on a NovaSeq6000 with 150 bp paired-end reads. Reads were aligned to the fission yeast genome (ASM294v2) with Bowtie2 (181). Intron retention was quantified using IRFinder (version 2.0.1), as per (223). Any introns flagged as having a low sequencing depth or fewer than 4 reads to support splicing were not considered for statistical analysis. Differential intron retention was calculated using DESeq2 (239). Sequence extraction for *S. pombe* introns was carried out using BEDTools v2.3.0 (240) and sequences are provided in dataset S1. 5′ splice sites (3 bases in the exon and 6 bases in the intron) and 3′ splice sites (20 bases in the intron and 3 bases in the exon) were scored with MaxEntScan using a maximum entropy model (241). Intron free energy of the thermodynamic ensemble (kcal/mol) was calculated using RNAfold v2.5.1 (242).

Data availability

The data supporting the findings of this study are available from the corresponding author upon reasonable request. RNA Seq data have been deposited in NCBI's Sequence Read Archive (SRA) database under BioProject number PRJNA918556. Supplementary tables are available at https://www.biorxiv.org/content/10.1101/2023.01.27.525755v2

3.6 Acknowledgments

We thank Dave Brow for comments on the manuscript. J.P. is supported by a Canada Graduate Scholarship (Doctoral) from the National Sciences and Engineering Research Council of Canada. M.A.B. is supported by a Discovery Grant from NSERC ("Impact of chemical modification of noncoding RNAs on gene expression in *S. pombe*"). S.D.R. is supported by a Discovery Grant from NSERC ("The molecular mechanism of U6 snRNA activation for pre-mRNA splicing") and a Sector Innovation Program Grant from GenomeBC (RC18-3517). This research was enabled in part by support provided by the BC DRI Group and the Digital Research Alliance of Canada (alliancecan.ca).

3.7 Supplementary information

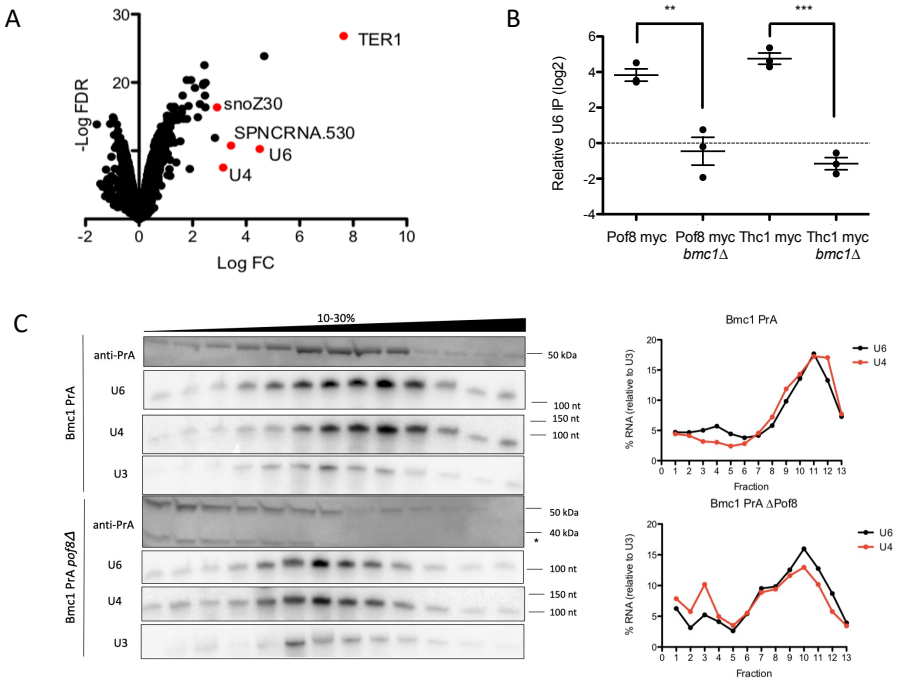

Figure S1: Bmc1, Pof8, and Thc1 cooperate to bind U6 and U6-associated noncoding RNAs
A) Enrichment of Bmc1 PrA-associated transcripts compared to an untagged control (n= 3 biological replicates). Axes represent log2 of fold change (FC) and negative log of false discovery rate (FD) (Benjamini-Hochberg adjusted P value ≤0.05). Data taken from (68).
B) qRT-PCR of U6 in Pof8 myc and Thc1 myc immunoprecipitates, normalized to immunoprecipitation from an untagged strain (mean± standard error, two-tailed unpaired t test, **p<0.01, ***p<0.001) (n= 3 biological replicates).
C) Glycerol gradient sedimentation of PrA-tagged Bmc1, U4, U6, and U3 from wild type (Bmc1 PrA) and pof8Δ strains. Cleavage products are indicated with an asterisk. U4 and U6 signals were normalized to U3 for calculating relative migration in the gradient.

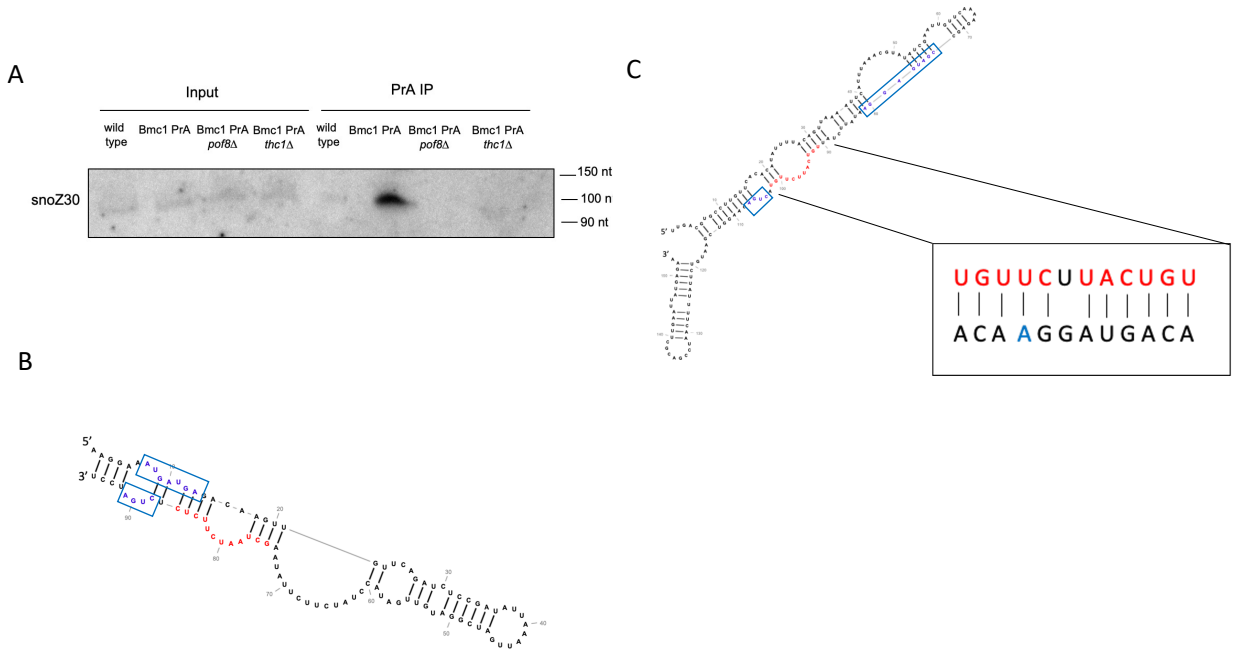

Figure S2: snoZ30 and sno530 are Bmc1-interacting, U6-modifying snoRNAs
A) Northern blot analysis of snoZ30 in total RNA and PrA immunoprecipitates from an untagged strain (wild type) and wild type and knockout PrA-tagged strains.
B) Secondary structure prediction (243) of snoZ30. C and D boxes are indicated in blue and U6-binding site is indicated in red.
C) Secondary structure prediction (243) of sno530. C and D boxes are indicated in blue and U6-binding site is indicated in red. Inset: U6-interacting region, highlighting Watson Crick and non-Watson Crick base pairs with U6 (black). A64 is indicated in blue.

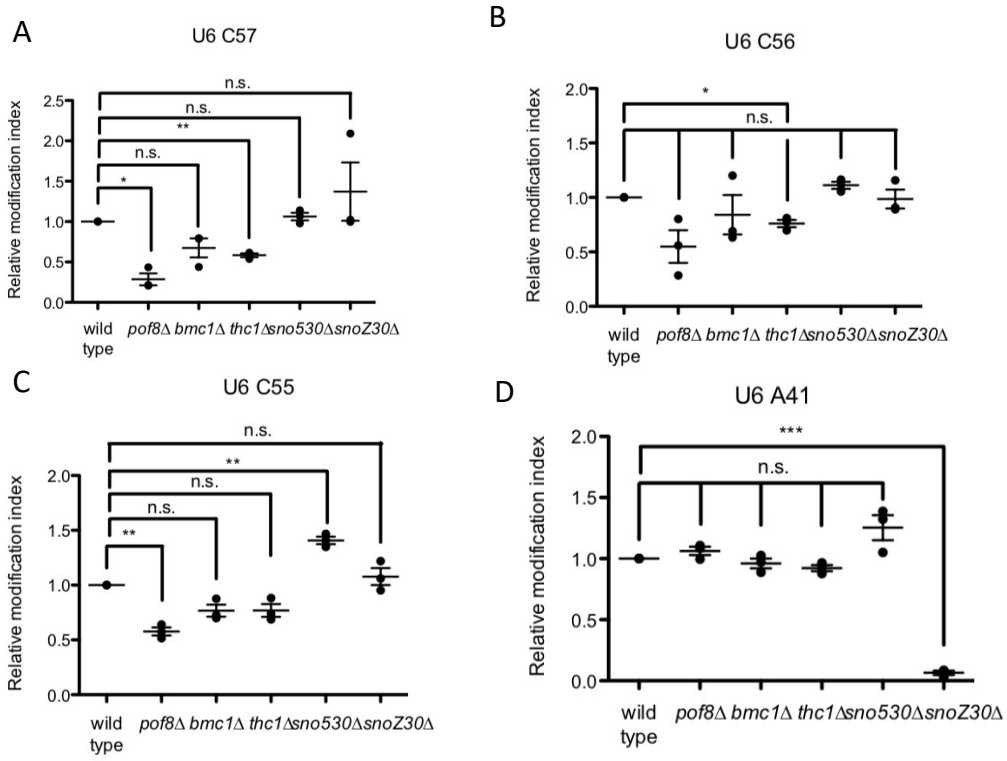

Figure S3: Bmc1, Pof8, and Thc1 influence 2′-O-methylation of U6
Quantification of relative 2′-O-methylation-induced reverse transcriptase stops, compared to a wild type strain, for C57 (A), C56 (B), C55 (C), and A41 (D) (mean± standard error, two-tailed paired t test, *p<0.05, **p<0.01, *** p<0.001) (n= 3 biological replicates).

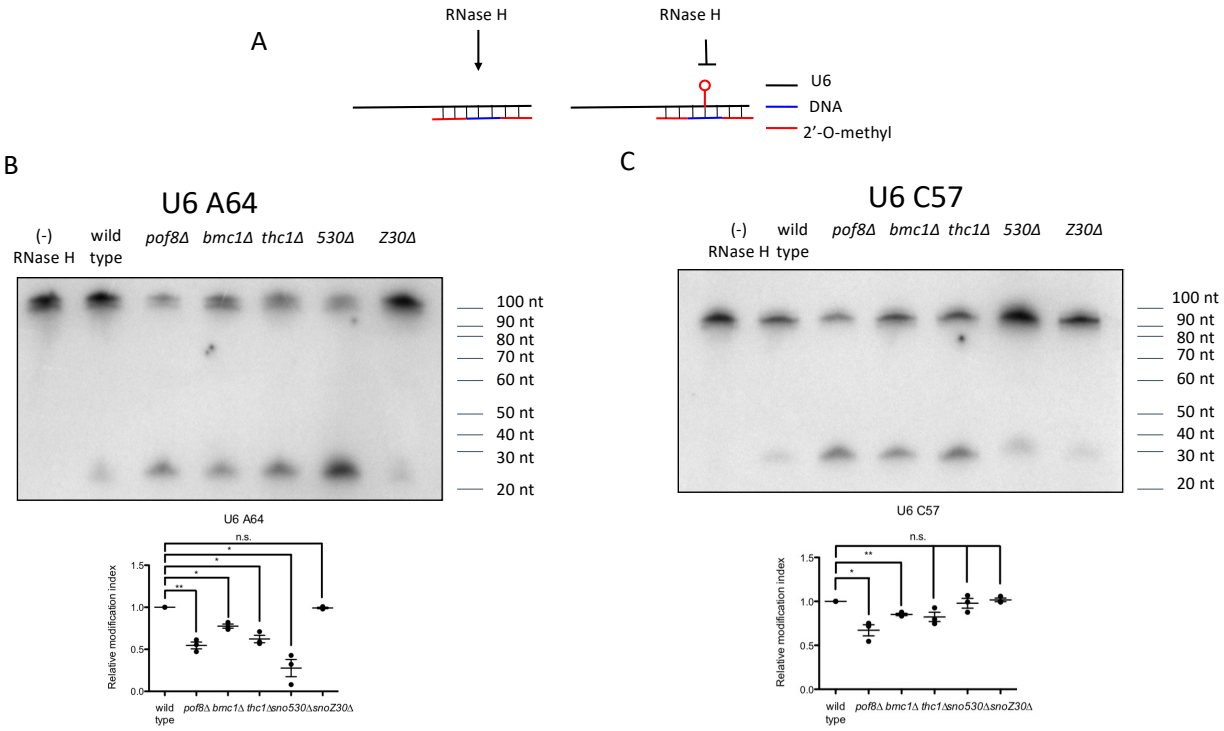

Figure S4: RNase H cleavage validates 2′-O-methylation of U6 at A64 and C57
A) Schematic of RNase H cleavage assay to detect 2′-O-methylations (211, 212).
B-C) Northern blot analysis and quantification of 2′-O-methylation at A64 (B) and C57 (C). Relative modification is expressed as a fraction of the cleaved band relative to total U6 (mean± standard error, two-tailed paired t test, *p<0.05, **p<0.01) (n= 3 biological replicates).

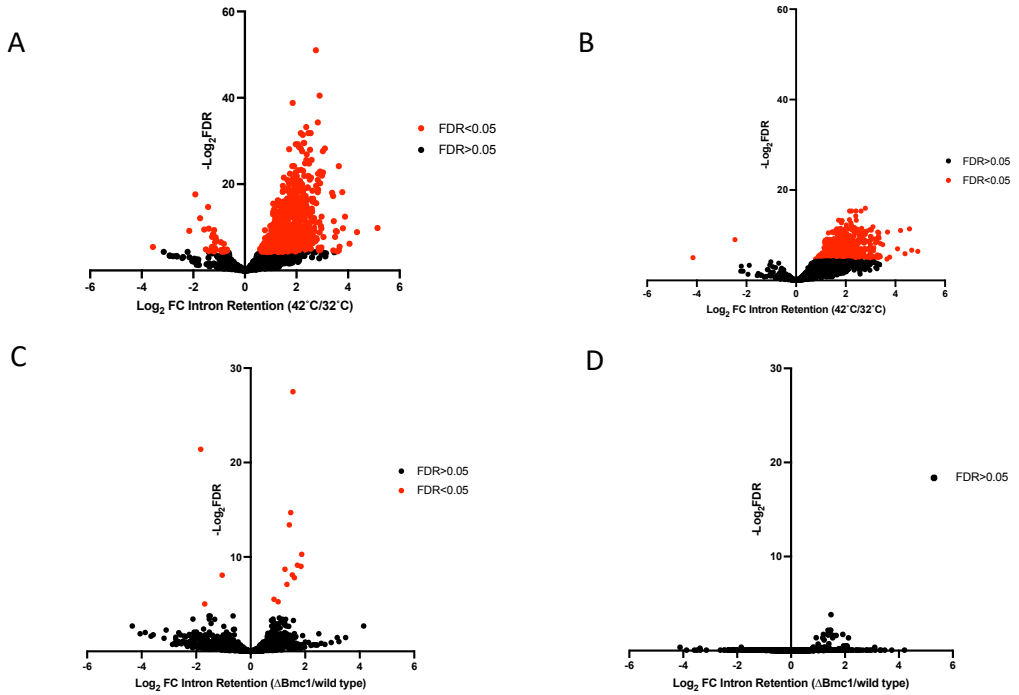

Figure S5: Heat shock and Bmc1 deletion lead to changes in intron retention.
A-B) Changes in intron retention in wild type (A) and *bmc1*Δ (B) strains grown at 32˚C or heat shocked for 15 minutes at 42˚C (n=3 biological replicates). Axes represent log2 of fold change (FC) and negative log2 of false discovery rate (FD) (Benjamini-Hochberg adjusted *P* value ≤0.05).
C-D) Changes in intron retention in wild type and *bmc1*Δ strains grown at 32˚C (A) or heat shocked for 15 minutes at 42˚C (B) (n=3 biological replicates). Axes represent log2 of fold change (FC) and negative log2 of false discovery rate (FDR) (Benjamini-Hochberg adjusted *P* value ≤0.05).

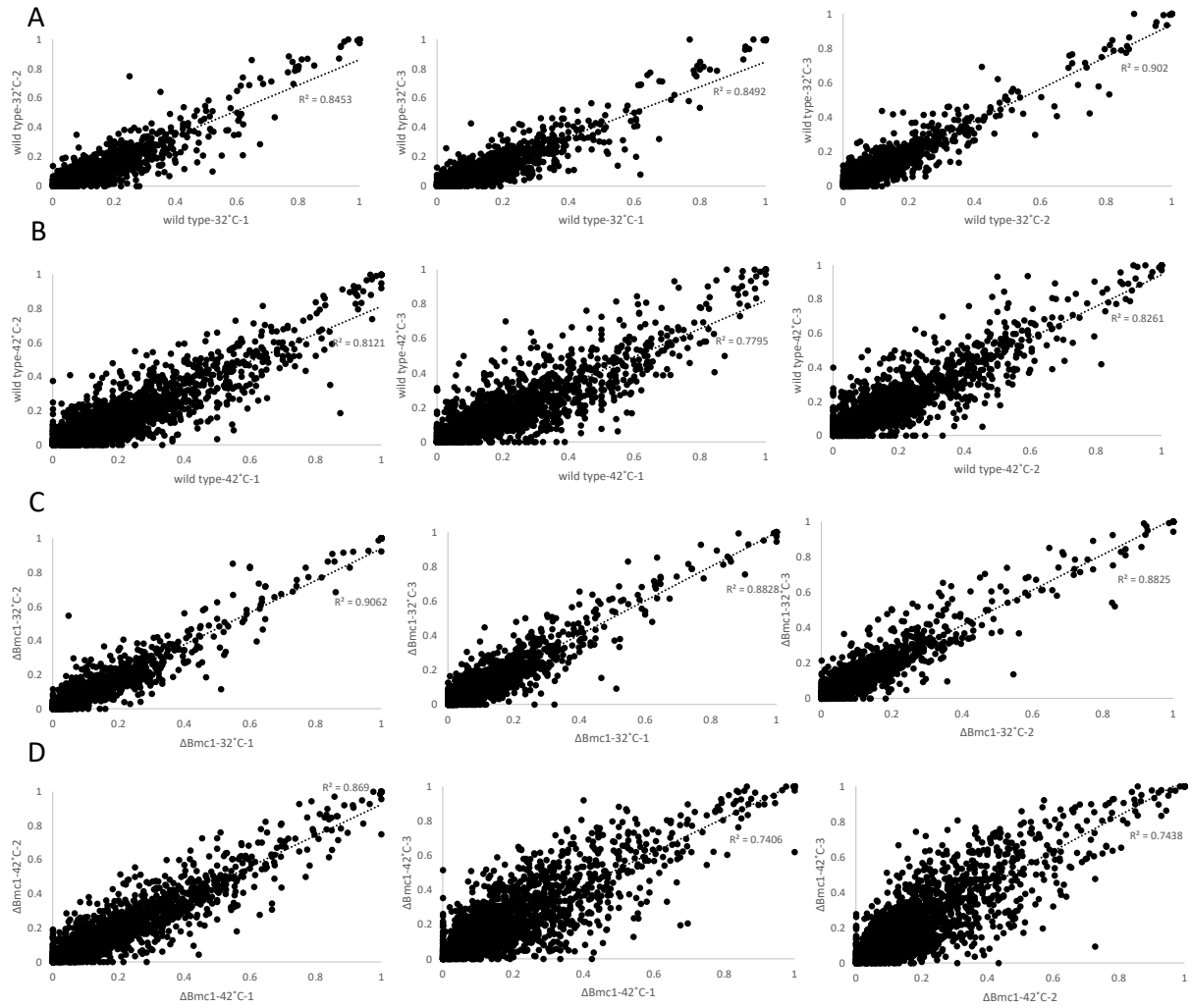

Figure S6: Correlations between replicates for RNA-Seq of wild-type and *bmc1*Δ strains with and without heat shock.
Intron retention values for wild type RNA Seq samples grown at 32˚C (A) and 42˚C (B) and ΔBmc1 cells grown at 32˚C (C) and 42˚C (D). R^2 values are displayed.

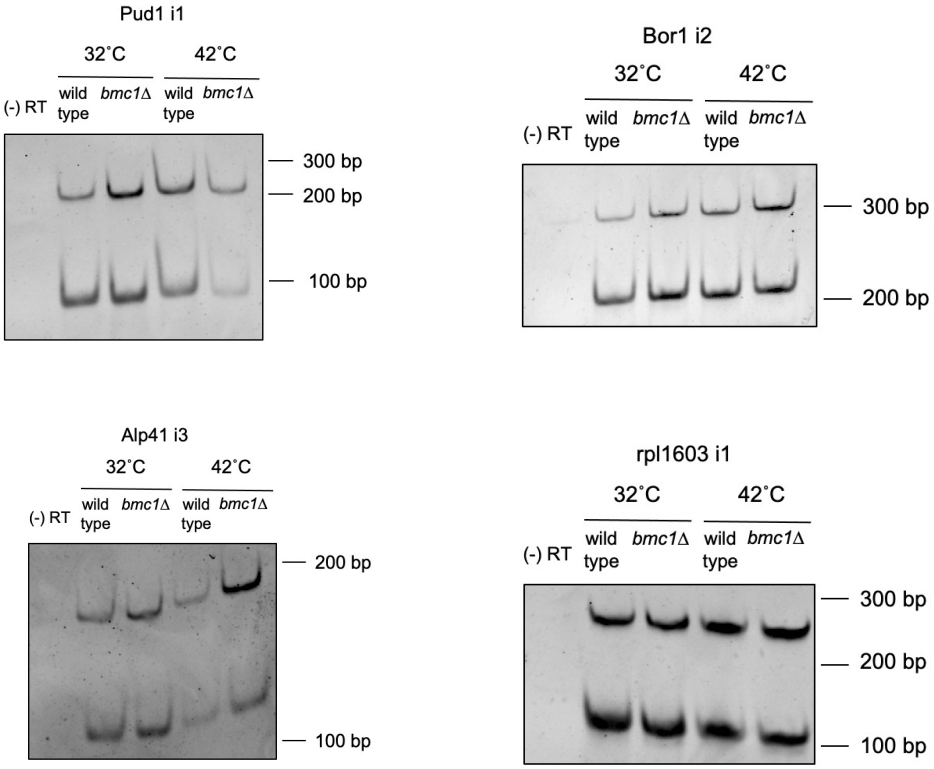

Figure S7: Semi-quantitative RT-PCR validation of heat shock- and Bmc1-sensitive intron retention events.
Representative gels contributing to quantifications in figure 5B.

Chapter 4: The tRNA methyltransferase Trm1 promotes eukaryotic pre-tRNA maturation through catalytic and non-catalytic activities

Jennifer Porat[1], Ana Vakiloroayaei[1], Taylor Cargill[1], and Mark A. Bayfield[1*]
1. Department of Biology, York University, Toronto, Canada
*Correspondence: bayfield@yorku.ca (M.A.B.)

This chapter has been submitted for publication and a preprint has been published as Porat J, Vakiloroayaei A, Cargill T, and Bayfield M.A. The tRNA methyltransferase Trm1 promotes eukaryotic pre-tRNA maturation through catalytic and non-catalytic activities. *bioRxiv.* 2023.04.12.536578; doi: https://doi.org/10.1101/2023.04.12.536578

Contributions: J.P. conceived of the study, designed, performed, and analyzed all experiments, and wrote the manuscript with input from all authors. A.V. carried out pulse-labeling of mitochondrial protein synthesis (Figure S1), performed initial investigation of Trm1 methylation activity in the nucleus and mitochondria, constructed the *trm1*Δ yeast strain, and initial versions of M1- and M24-expressing plasmids. T.C. assisted in protein purification for Figures 4D and 5. M.A.B. conceived of the study, designed experiments, supervised the project, and edited the manuscript.

4.1 Abstract

tRNAs undergo an extensive maturation process involving post-transcriptional modifications often associated with tRNA structural stability and promoting the native fold. Impaired post-transcriptional modification has been linked to human disease, likely through defects in translation, mitochondrial function, and increased susceptibility to degradation by various tRNA decay pathways. More recently, evidence has emerged that bacterial tRNA modification enzymes can act as tRNA chaperones to guide tRNA folding in a manner independent from catalytic activity. Here, we provide evidence that the fission yeast tRNA methyltransferase Trm1, which dimethylates nuclear- and mitochondrial-encoded tRNAs at G26, can also promote tRNA functionality in the absence of catalysis. We show that wild type and catalytic-dead Trm1 are active in an *in vivo* tRNA-mediated suppression assay and possess *in vitro* RNA folding activity, suggesting an alternate function as a tRNA chaperone. Further, we demonstrate crosstalk between Trm1 and the RNA chaperone La, with La binding to the 3′ end and body of nascent pre-tRNA inhibiting tRNA dimethylation *in vivo* and *in vitro*. Collectively, these results support the hypothesis for multi-functional tRNA modification enzymes that combine catalytic and non-catalytic activities to shape tRNA structure and function.

4.2 Introduction

Owing to their critical role in translation, tRNAs are subject to numerous processing and quality control steps to ensure their structural stability and functionality. In eukaryotes, this involves removal of a 5′ leader and 3′ trailer sequence; where applicable, removal of an intron; CCA addition and aminoacylation of the mature 3′ end; as well as the acquisition of post-transcriptional modifications (reviewed in (41, 244)). While most post-transcriptional

modifications are non-essential, especially in yeast, the combination of modifications on a given tRNA is an important determinant for structural stability and functionality. Modifications to the anticodon loop affect translational fidelity by maintaining the correct open reading frame and influencing codon-anticodon base-pairing, whereas modifications to the tRNA body primarily affect structure and folding (245). Importantly, studies have found that pre-tRNAs lacking certain post-transcriptional modifications are prone to misfolding and subsequently targeted for decay by the nuclear surveillance machinery (46, 47), while hypomodified mature tRNAs are degraded in the cytoplasm by the rapid tRNA decay pathway (49).

Links between pre-tRNA structure and escape from decay are especially relevant in the context of the function of the eukaryotic RNA chaperone La. The La protein interacts with the 3′ uridylate trailer of RNA Polymerase III transcripts, including nascent pre-tRNAs, through a binding pocket formed by the eponymous La motif and RNA recognition motif 1 (RRM1) (8, 109, 110, 112). As such, a major role of the La protein is to protect the 3′ end of pre-tRNAs from exoribonucleolytic degradation and direct the order of pre-tRNA end processing (reviewed in (106)). La binding to the 3′ trailer results in 5′ leader processing by RNase P followed by 3′ trailer cleavage, the latter of which enables La dissociation and recycling onto a new pre-tRNA substrate (113, 246). 3′ end binding by La is particularly important for structurally defective pre-tRNAs, which rely on La for protection from decay by the nuclear exosome (48). However, 3′ end protection alone is insufficient to rescue increasingly defective pre-tRNAs from nuclear surveillance, necessitating a second activity mapping to the canonical RNA binding surface of the RRM1 (48, 113). Further insight into this alternate activity revealed that the RRM1 interacts with the pre-tRNA body, where it can act as an RNA chaperone to assist pre-tRNA folding (38, 104, 113). Coupling of La's two distinct binding modes—3′ uridylate binding and contacts to the

tRNA body—enables high-affinity engagement of pre-tRNAs, resulting in their stabilization and proper folding (113).

As tRNAs can also achieve their native, functional conformation through post-transcriptional modifications, the La protein has been proposed to function redundantly with tRNA modification enzymes. In agreement with this, deletion of La is synthetically lethal with the deletion of several tRNA modification enzymes in budding and fission yeast grown at elevated temperatures, where tRNA misfolding can occur (38, 145). Rescue of synthetic lethality by wild type La, but not RRM1 mutants defective for RNA chaperone activity, further supports the idea that La and tRNA modification enzymes have roles in promoting correct tRNA folding (38). Among the modification enzymes that function redundantly with La, N2, N2-dimethylation at G26 by the tRNA methyltransferase Trm1 (247), has been demonstrated to stabilize pre-tRNA *in vitro* and *in vivo* (38, 39). G26 dimethylation has been linked to structural stability at the junction between the anticodon and variable arm, or hinge region; accordingly, the absence of Trm1 in fission yeast is associated with charging defects for certain tRNA species, implying a role in promoting correct folding (38). But while studies on the structure stabilizing effect of Trm1-catalyzed methylation have largely been limited to pre-tRNAs in the nucleus, a mitochondrial Trm1 isoform containing an N-terminal mitochondrial targeting sequence has also been described, leading to the modification of select G26-containing mitochondrial-encoded tRNAs (27, 248). The human mitochondrial isoform, which has been linked to promoting protein synthesis, cellular proliferation, and redox homeostasis through modification of mt-tRNA Ile^{UAU}, mt-tRNA Ala^{UGC}, and mt-tRNA Arg^{UCG}, arises from alternative splice isoforms that include or exclude the mitochondrial targeting sequence (27). In contrast, budding yeast Trm1 isoforms

arise from alternate transcription start sites that yield proteins differing in the presence of the mitochondrial targeting sequence (248).

The structural and functional importance of post-transcriptional modifications on both nuclear- and mitochondrial-encoded tRNAs has been well-established (reviewed in (249)), but recent evidence points to the idea that post-transcriptional modification enzymes may have alternate functions related to tRNA folding (41). Notably, the bacterial tRNA pseudouridine synthase TruB and methyltransferase TrmA promote tRNA folding even in the absence of catalysis, leading to their characterization as tRNA chaperones (117, 118). Although a catalytically inactive mutant of the eukaryotic TrmA homolog Trm2 can rescue a growth defect associated with a mutant allele of tRNA Ser^{CGA}, suggesting that the dual function of tRNA modification enzymes is evolutionarily conserved (135), to date there has been no mechanistic insight into how eukaryotic tRNA modification enzymes promote tRNA folding independent from catalytic activity.

Here, we use the tRNA methyltransferase Trm1 from *Schizosaccharomyces pombe* to examine how catalytic and catalytic-independent activities shape eukaryotic pre-tRNA maturation and processing. We demonstrate that mutation of a key catalytic residue results in a complete loss of dimethylation on nuclear- and mitochondrial-encoded tRNAs *in vitro* and *in vivo*, yet still promotes pre-tRNA maturation and function in a tRNA-mediated suppression assay. We also uncover the timing of Trm1-mediated dimethylation with respect to other pre-tRNA processing activities and unexpectedly show that the *S. pombe* La protein Sla1 opposes tRNA modification by Trm1. Finally, we provide evidence that both wild-type and catalytically inactive Trm1 are functional in an RNA folding assay *in vitro*, suggesting that it also acts as a tRNA chaperone. These data are thus consistent with the idea that tRNA modification enzymes

have retained modification and folding activities throughout evolution and use a combination of these activities to ensure proper tRNA structure and function.

4.3 Results

4.3.1 Alternate transcriptional start sites yield nuclear- and mitochondrially-targeted Trm1 in *S. pombe*

As in Trm1 from budding yeast, fission yeast Trm1 can exist as a nuclear- or mitochondrial-targeted isoform produced from alternate transcription start sites (Figure 1A). Two alternate transcription start sites have been mapped for fission yeast Trm1: one producing a ~250 nucleotide 5′ UTR ahead of the first ATG (this isoform will henceforth be referred to as M1, for beginning at the first methionine), and a second with a ~10 nucleotide 5′UTR ahead of a downstream ATG (M24, beginning at the 24th amino acid) (Figure 1A) (250). While both isoforms have been shown to target mitochondrially-encoded tRNAs in budding yeast, the N-terminal extension in the longer isoform enhances the efficiency of mitochondrial targeting, resulting in a predominantly mitochondrial-localized protein compared to the nuclear-localized shorter isoform (248). Quantification of the relative abundance of both transcripts in wild type cells grown in rich media revealed that the nuclear-targeted transcript is approximately four times as abundant as the mitochondrially-targeted transcript at steady state levels (Figure 1B). Consistent with the idea that modifications to the tRNA body do not dramatically alter bulk translation, pulse labeling revealed no defects in mitochondrial or cytoplasmic translation upon Trm1 deletion (Figure S1).

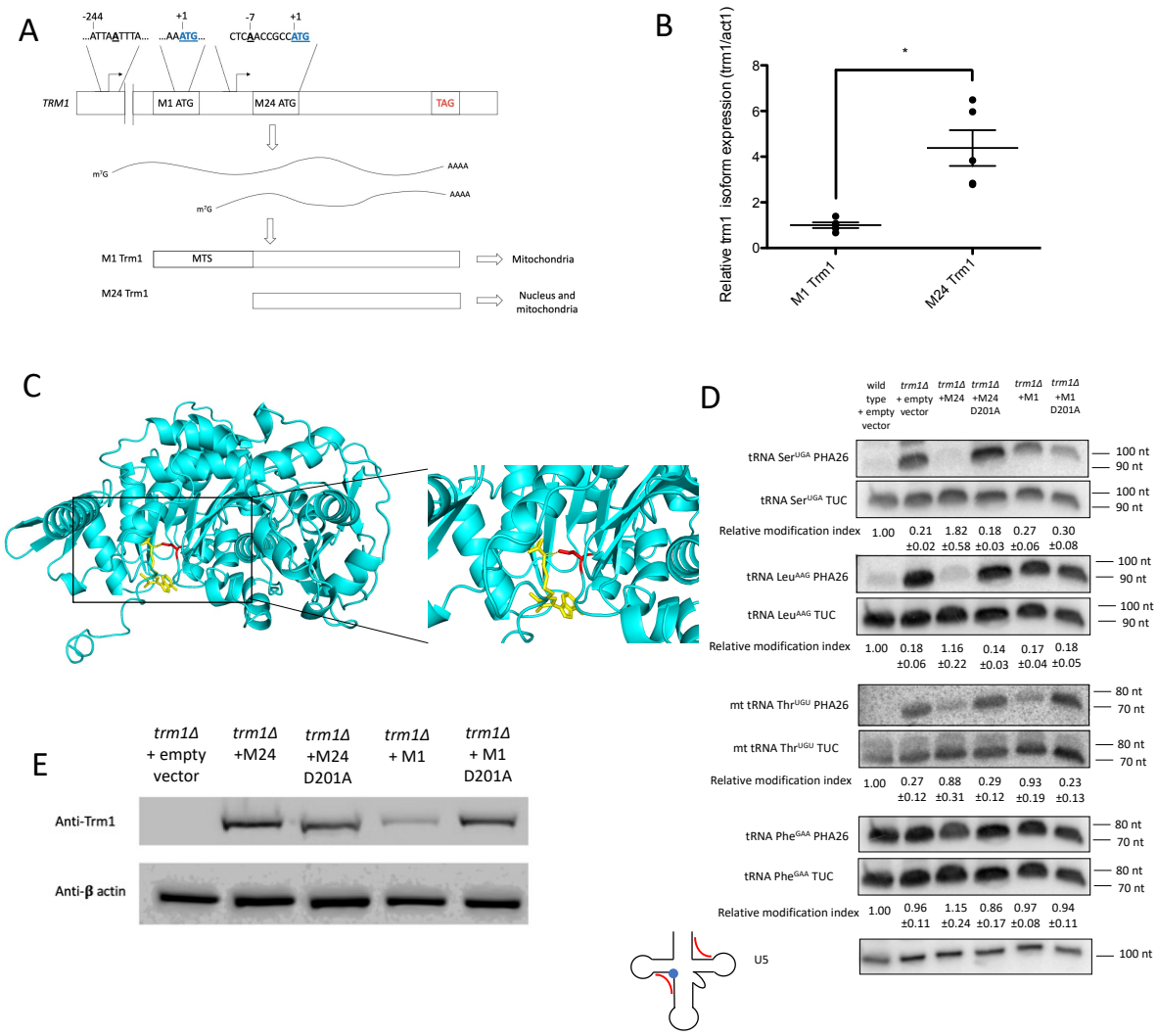

Figure 1: *S. pombe* Trm1 modifies nuclear- and mitochondrial-encoded tRNAs at G26
A) Schematic of alternate transcription start sites giving rise to nuclear- and mitochondrial-targeted Trm1 isoforms.
B) qRT-PCR of *trm1* mRNA isoforms normalized to *act1* mRNA (mean± standard error, two-tailed unpaired t-test * at $p<0.05$) (n= 5 biological replicates).
C) AlphaFold (222) structure prediction of Trm1 aligned to SAH-bound Trm1 from *Pyrococcus horikoshii* (PDB 2EJU) (251). Inset: Hydrogen bonding between SAH (yellow) and D201 (red).
D) PHA26 northern blot of nuclear- and mitochondrial-encoded tRNA. Northern blots were stripped and re-probed for U5 as a loading control. Relative modification index represents the TUC signal divided by the PHA26 signal and normalized to a wild type strain (mean±SEM, n= 3 biological replicates). Left: schematic depicting binding sites of the PHA26 and TUC probes (red). G26 is represented by a blue circle.
E) Western blot of Trm1 and β-actin in a *trm1*Δ strain transformed with the indicated plasmids.

4.3.2 D201 is a key catalytic residue for N2, N2-dimethylation of nuclear- and mitochondrially-encoded tRNAs

To investigate potential modification-independent functions of Trm1, we aligned an AlphaFold (222) prediction of *S. pombe* Trm1 to the structure of an archaeal Trm1 homolog bound to SAH (252), mutated an aspartic acid in the conserved catalytic site to alanine (D201A) (Figure 1C) and monitored Trm1-catalyzed modification of nuclear- and mitochondrially-encoded tRNAs with a northern blotting assay, positive hybridization in the absence of modification at G26 (PHA26) (39, 253). This assay uses a probe complementary to the region overlapping G26, such that dimethylation at G26 impairs probe hybridization, resulting in a decrease in signal intensity. An additional probe targeting the TUC loop, which is free of modifications that interfere with probe hybridization, serves as an internal normalization for tRNA abundance (Figure 1D). The D201A mutant showed a comparable decrease in modification as *trm1*Δ cells transformed with an empty vector, in the context of the nuclear- and mitochondrially-targeted isoforms, despite similar levels of protein accumulation as the wild type isoforms (Figure 1D, E). Moreover, these northern blots demonstrate subcellular targeting of the Trm1 isoforms: M24 Trm1 robustly modifies nuclear- and mitochondrial-encoded tRNAs, consistent with its proposed localization to the nucleus and mitochondria, while M1 Trm1 only modifies mitochondrially-encoded tRNAs, suggesting that it is solely present in the mitochondria (Figure 1D). These results also confirmed the previously demonstrated substrate specificity of Trm1, where G26-containing tRNAs exhibit different levels of Trm1-catalyzed modification (39). Certain nuclear-encoded tRNAs, including tRNA Ser^{UGA} and tRNA Leu^{AAG} are robustly modified by endogenous Trm1 (Figure 1D, “wild type”) and overexpressed M24 Trm1, while the

PHA26 probe anneals to the G26-containing tRNA Phe^{GAA} in a manner that remains unchanged based on the presence of Trm1, consistent with a lack of modification.

To rule out defects in tRNA binding contributing to a lack of modification by D201A, we purified recombinant wild type and D201A M24 Trm1 and measured *in vitro* binding affinity to pre-tRNA Ser^{UGA} using electrophoretic mobility shift assays (EMSA). Wild type and D201A exhibited comparable binding affinity, suggesting that disruption of the putative catalytic site does not impair tRNA binding (Figure 2A, B). We also set up *in vitro* methylation reactions with pre-tRNA Ser^{UGA}, recombinant Trm1, and SAM, and measured modification efficiency by primer extension, as dimethylation on the Watson-Crick face is sufficient to cause a reverse transcriptase (RT) stop (38, 254). The lack of modification by D201A *in vitro* (Figure 2C), evident by the lack of RT stop, and by PHA26 northern blotting *in vivo* (Figure 1D) confirm that D201A is indeed catalytically inactive, thus enabling further studies into potential catalytic-independent functions of Trm1.

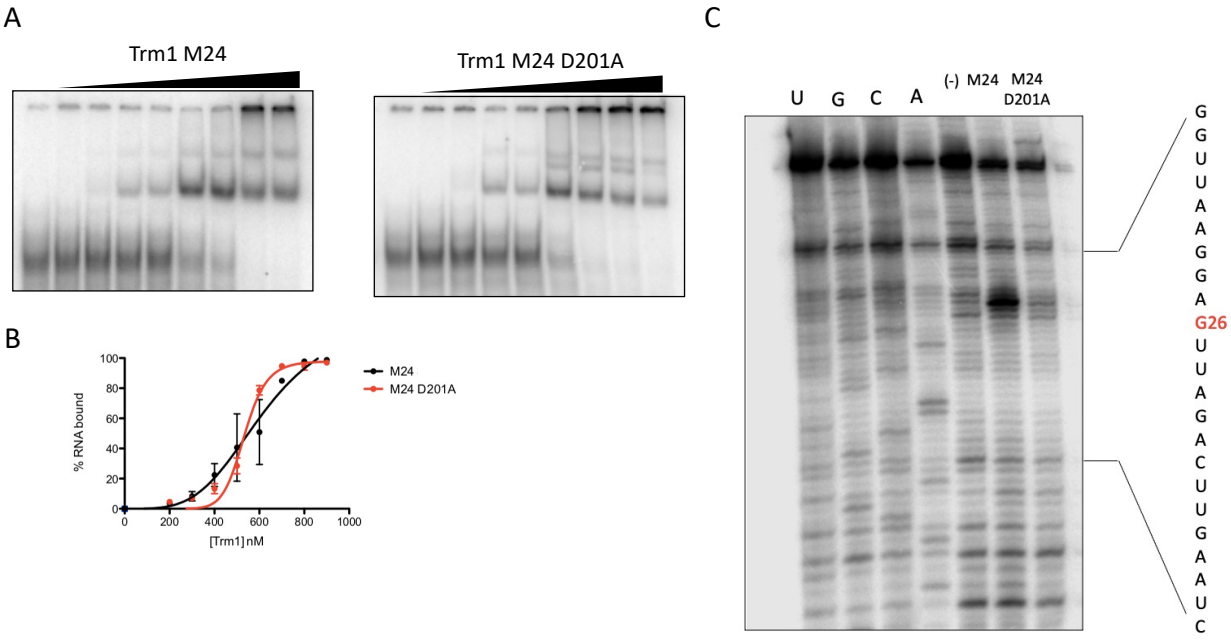

Figure 2: D201A supports *in vitro* tRNA binding, but not methylation
A) EMSAs of Trm1 M24 and M24 D201A with radiolabeled pre-tRNA Ser^{UGA}.
B) Binding curves of A) (mean±SEM, n= 3 technical replicates).
C) Primer extension of *in vitro* methylated tRNA Ser^{UGA}. The sequences flanking G26 are indicated.

4.3.3 Trm1 promotes tRNA-mediated suppression through catalytic and catalytic-independent activities

The tRNA-mediated suppression assay has been used to test various aspects of pre-tRNA processing including 3′ processing, pre-tRNA folding, and modification (reviewed in (179, 255)). The assay relies on a mutation to the anticodon of tRNA Ser^{UCA}, allowing stop codon readthrough of a nonsense mutation in the AIR carboxylase gene which, when fully functional, prevents the accumulation of a red metabolic intermediate (255, 256). The G35C mutation that enables nonsense decoding also impairs anticodon-intron base pairing in the suppressor pre-tRNA, resulting in a misfold that increases susceptibility of the pre-tRNA to exosome-mediated decay (48). Suppressor pre-tRNA misfolding can be rescued by overexpression of pre-tRNA

processing factors, thus enabling identification and insight into the mode of action of pre-tRNA binding proteins, including the RNA chaperone La (48, 113). We and others have previously demonstrated that Trm1 is active in promoting tRNA-mediated suppression (38, 39), although this could be due to a stabilizing effect from the modification, a separate pre-tRNA processing activity that functions independently from modification, or a combination of these.

Wild type and catalytically inactive nuclear-targeted Trm1 promote suppression of the tRNA Ser^{UCA} allele in a *sla1* null background, suggesting that modification is not strictly required for suppression activity (Figure 3A). Still, the addition of the U47:6C mutation to the suppressor tRNA, which is associated with further misfolding and a reliance on the RNA chaperone activity of La (104, 257), resulted in partial suppression by wild type Trm1 but not D201A (Figure S2A). This is suggestive of two distinct activities for Trm1: its established methyltransferase activity, which has been previously shown to stabilize tRNA structure (38), and a modification-independent activity that is dependent on tRNA binding. tRNA binding alone is sufficient for suppression activity in the context of the tRNA Ser^{UCA} allele, whereas binding and modification are required for the more defective suppressor tRNA allele.

It has also been reported that deletion of the RNA Polymerase III repressor Maf1 causes anti-suppression, which is counter-intuitive with the increase in tRNA transcription observed upon Maf1 deletion (39). However, the anti-suppression phenotype can be explained by hypomodification of the suppressor tRNA by Trm1, as Trm1—and presumably other pre-tRNA binding proteins— become limiting with the resultant increase in the pre-tRNA pool (39). Complete and near-complete suppression of tRNA Ser^{UCA} is achieved by wild type and catalytically inactive Trm1, respectively, in the *maf1*Δ strain (Figure 3A). In the model whereby Trm1 becomes limiting in the absence of Maf1, suppression by D201A suggests that it is not

only the Trm1-catalyzed modification that becomes limiting, but also tRNA binding by Trm1, further supporting the notion of a catalytic-independent function for Trm1.

To decipher the mechanism by which Trm1 promotes tRNA-mediated suppression, we quantified the abundance of the suppressor tRNA at the precursor and mature level (Figure 3B, S2B-D). Probes against the tRNA Ser^{UCA} intron were used to detect the precursor, which migrates as 2 distinct bands in the absence of the yeast La protein Sla1, representing the leader-containing, trailer-processed and leader- and trailer-processed species, while a probe overlapping the exon junctions was used to detect the mature suppressor tRNA. We did not observe an increase in mature suppressor tRNA levels upon expression of wild type or catalytically inactive Trm1, suggesting that suppression by Trm1 is not the result of increased suppressor tRNA levels, as has previously been reported for suppression observed upon suppressor tRNA gene duplication (Figure 3B, S2D) (257). Similarly, tRNA-mediated suppression of tRNA Ser^{UCA} by human or *S. pombe* La is largely due to 3′ trailer binding and protection of the suppressor pre-tRNA from exosome-mediated decay, which is characterized by the stabilization of a 3′ trailer-containing suppressor pre-tRNA species relative to an empty vector (48, 113). We can rule out suppression due to 3′ end protection by Trm1, as evident by the lack of stabilization of the 3′ trailer-containing species relative to the empty vector (Figure 3B, pre-tRNA Ser^{UCA} and endogenous pre-tRNA Lys^{CUU}, compare to intensity of the nascent pre-tRNA in Figure 4C with hLa). It is worth noting that stabilization of the 5′ and 3′ processed pre-tRNA species occurs upon overexpression of D201A, which supports the idea that in the absence of catalysis, Trm1 remains bound to and stabilizes the pre-tRNA (Figure 3B, top panel).

We also performed the PHA26 assay to investigate the role of Trm1 modification in tRNA-mediated suppression (Figure 3B, third panel) The suppressor tRNA-containing strain

possesses endogenous Trm1, so the lack of complete modification (represented by a decrease in signal intensity with the PHA26 probe) of the suppressor tRNA with an empty vector agrees with previous reports that Trm1 is normally the limiting factor in tRNA modification (39). The suppressor tRNA only becomes fully modified upon wild type Trm1 overexpression, with overexpression of D201A resulting in comparable modification levels to an empty vector (Figure 3B). The PHA26 assay also provides information on the timing of Trm1 modification with respect to pre-tRNA processing activities. We observed no change in PHA signal intensity upon Trm1 expression in the trailer-processed, leader-containing pre-tRNA (Figure 3B, top band in top panel), suggesting that it is not a substrate for modification, but noted a decrease in signal intensity for the leader- and trailer-processed pre-tRNA and mature tRNA, supporting a previously proposed model that Trm1 modification occurs after Sla1 binding and 3′ end processing (38) (Figure 3C-E).

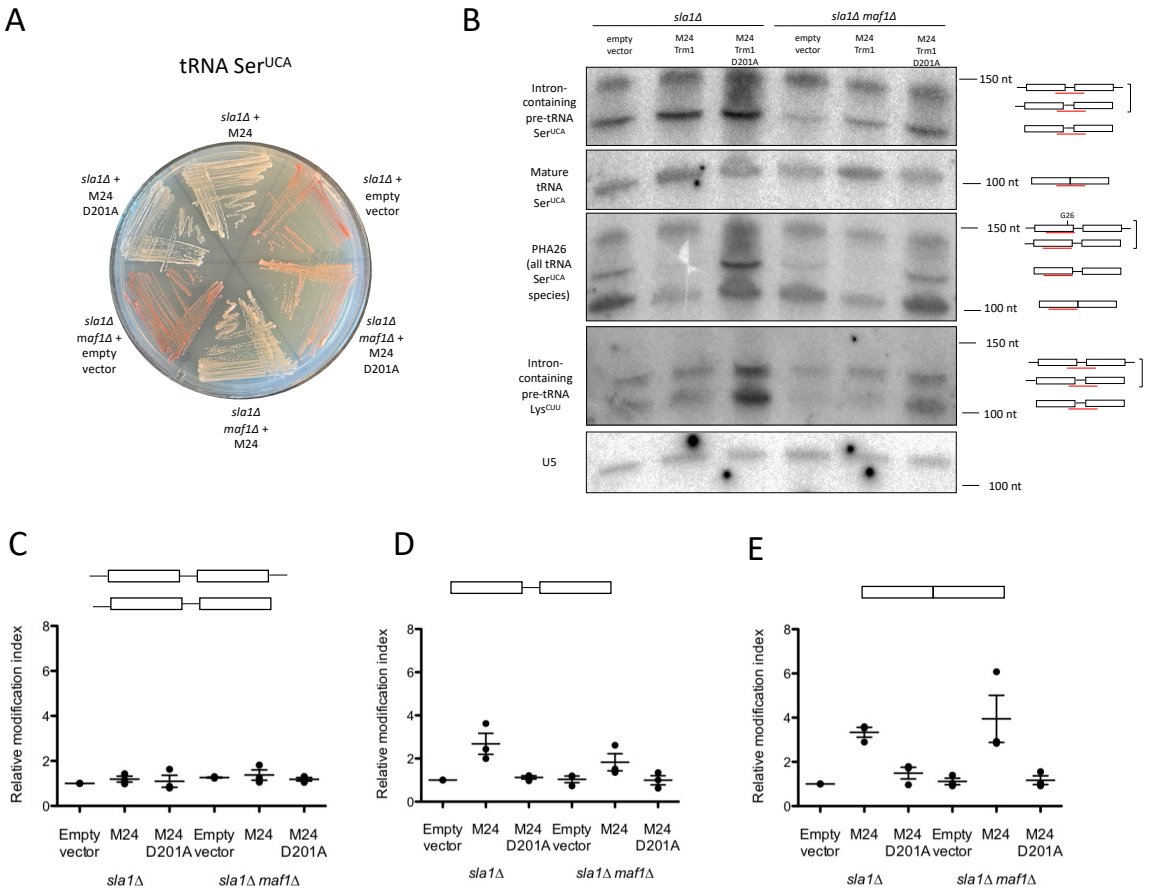

Figure 3: Trm1 promotes tRNA-mediated suppression independent of catalytic activity
A) tRNA-mediated suppression with wild type and catalytically inactive Trm1 in a *sla1*Δ and *sla1*Δ *maf1*Δ background.
B) Northern blot of tRNA Ser^{UCA} processing intermediates and G26 modification status and 3′ end protection of pre-tRNA Lys^{CUU}.
C-E) Quantification of relative modification at G26, relative to the *sla1*Δ strain expressing an empty vector. Relative modification was calculated by normalizing the PHA26 signal (overlapping G26) to probes targeting the intron-containing precursor (C and D) and mature suppressor (E).

4.3.4 Trm1 competes with the RNA chaperone La for pre-tRNA binding

While previous reports indicate that tRNAs become hypomodified at G26 upon Maf1 deletion (39), we did not observe any modification differences with and without endogenous Maf1 (Figure 3C-E). Since those previous measurements were performed in a *sla1*+ strain and

our data are from a *sla1*Δ strain, we examined the relationship between Sla1 and Trm1-dependent modification. Strikingly, we detected an increase in G26 modification upon Sla1 deletion for leucine and serine tRNAs, suggesting a possible competition between Sla1 and Trm1 for pre-tRNA binding (Figure 4A). As the La protein has been reported to make multiple contacts to pre-tRNAs—engagement of the uridylate trailer and pre-tRNA body (48, 113, 258)—we took advantage of previously characterized mutants of the human La protein (hLa) to map competition to La's various domains and RNA binding modes (Figure 4B). We measured tRNA-mediated suppression activity, steady-state precursor and mature tRNA levels, and G26 modification status for the suppressor tRNA Ser^{UCA} in a *sla1*Δ strain transformed with wild type or mutant hLa (Figure 4B, C). As has been previously reported, mutations to uridylate-binding residues in the La motif (Q20A Y24A D33I) led to decreased suppression activity. In contrast, mutations to the RRM1, which result in impaired RNA chaperone activity but unchanged uridylate binding (113), exhibited no defects in the tRNA-mediated suppression assay, in agreement with the idea that tRNA Ser^{UCA} predominantly requires 3′ end protection, but not RNA chaperone activity, for complete suppression (48) (Figure 4B). This is evident from stabilization of the top suppressor tRNA band on the northern blots, corresponding to the nascent, 5′ leader- and 3′ trailer-containing pre-tRNA species, for wild type and RRM1 hLa mutants (Figure 4C).

Like overexpressed Trm1 (Figure 3B), endogenous Trm1 displays the same modification preferences for modifying end-processed pre-tRNA (Figure 4C). Further, we observed a decrease in G26 modification of the suppressor tRNA in strains transformed with wild type hLa and the RRM1 mutant Y114A F155A, which displays decreased RNA chaperone activity but no pre-tRNA binding defects (48), a complete rescue of modification similar to the empty vector by the

uridylate-binding mutant, and partial rescue by the RRM1 loop-3 R142A R143A K148A K151A mutant, which is defective in both RNA chaperone activity and pre-tRNA binding (104, 113) (Figure 4C). These results suggest that competition between La and Trm1 is linked to La's pre-tRNA affinity, with mutations that disrupt uridylate or tRNA body binding, which contribute additively to pre-tRNA affinity (113), leading to increased modification at G26. Notably, these results also reveal that the apparent hLa-dependent increases in mature suppressor tRNA levels, which has been used as an indicator of the degree of tRNA-mediated suppression activity, can arise from a combination of changes in mature tRNA levels and differences in G26 modification. Changes in mature suppressor tRNA levels in the presence or absence of wild type or mutant hLa are less pronounced when using a probe that does not overlap with G26 (Figure 4C, compare relative mature tRNA Ser^{UCA} to apparent relative mature tRNA Ser^{UCA}). Thus, mature suppressor tRNA levels are not the sole determinant that can be used to predict or assign meaning to tRNA-mediated suppression activity, providing additional evidence for the hypothesis that an increase in specific tRNA activity due to modification or folding is linked to tRNA-mediated suppression activity.

To determine whether La binding to pre-tRNA acts as a shield to prevent Trm1 binding and modification of nuclear-encoded pre-tRNAs, we pre-incubated pre-tRNA with and without recombinant hLa and set up an *in vitro* methylation time course to examine changes in G26 dimethylation. We observed decreased methylation in the presence of hLa, particularly at earlier time points in the reaction (Figure 4D, E), consistent with our *in vivo* data demonstrating that La inhibits Trm1 modification. As the methylation reaction occurs in the absence of any cellular factors that promote tRNA processing, including other modification enzymes and end-processing endo and exoribonucleases, this is suggestive of La itself acting as a barrier to Trm1-mediated

methylation, rather than decreasing dimethylation indirectly, through its roles in facilitating pre-tRNA processing.

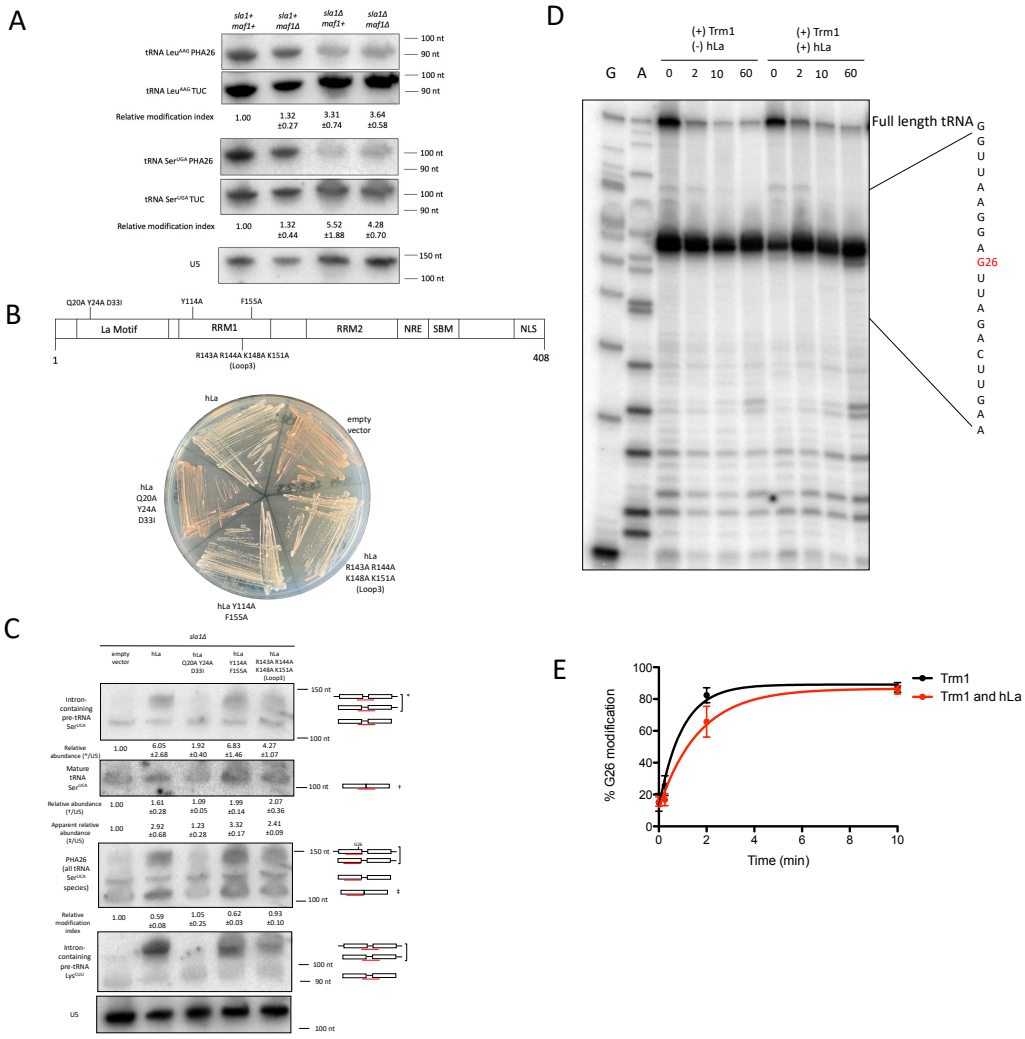

Figure 4: La and Trm1 influence pre-tRNA end-processing and G26 dimethylation
A) PHA26 northern blots of nuclear-encoded tRNA in wild type, *maf1*Δ, *sla1*Δ, and *sla1*Δ *maf1*Δ cells. Northern blots were stripped and reprobed for U5 as a loading control. Relative modification index represents the TUC signal divided by the PHA26 signal and normalized to a wild type strain (mean±SEM, n= 3 biological replicates)
B) Schematic of human La (hLa) domains with indicated mutations and tRNA-mediated suppression of wild type and mutant hLa constructs in a *sla1*Δ background
C) Northern blot of tRNA Ser^{UCA} processing intermediates, G26 modification status, and tRNA Lys^{CUU} end protection.
D) Primer extension of *in vitro* methylated tRNA Ser^{UGA} over time
E) Quantification of *in vitro* methylation of tRNA Ser^{UGA} over time, calculated as the ratio of the G26 RT stop to full length tRNA (mean±SEM, n= 4 independent replicates).

4.3.5 Trm1 folds tRNA *in vitro*

As our data point towards Trm1 possessing a catalytic-independent function that promotes tRNA functionality *in vivo*, we considered the possibility that Trm1 might function as a tRNA chaperone, much like the bacterial tRNA modifying enzymes TruB and TrmA (117, 118). We employed an *in vitro* FRET-based RNA annealing and dissociation assay that has been used to characterize RNA chaperone activity for La and La Related Proteins (104, 105). This assay uses complementary RNA oligos 5′ end labeled with Cy3 or Cy5, such that annealing of the oligos will result in FRET between the two fluorophores, from which we can calculate the rate of annealing (k_{ann}), followed by the addition of an unlabeled competitor to assess strand dissociation activity (k_{SD}), which is accompanied by a decrease in FRET between the two fluorophores (Figure 5A). In the absence of strand dissociation, as measured by an increase in FRET following competitor addition, the rate constant calculated in the second phase is considered k_{ann2}. Consistent with previous data (104, 105), strand annealing and strand dissociation were enhanced by the addition of recombinant human La (Figure 5B, C). We also observed strand annealing and dissociation for wild type and catalytically inactive Trm1, suggesting that they are capable of folding RNA *in vitro* (Figure 5B, C). Our *in vivo* data demonstrating that Trm1 is active in a tRNA-mediated suppression assay independent of catalysis, coupled with our *in vitro* data supporting an RNA chaperone-like activity, point towards Trm1 acting as a tRNA chaperone, similar to prokaryotic tRNA modification enzymes.

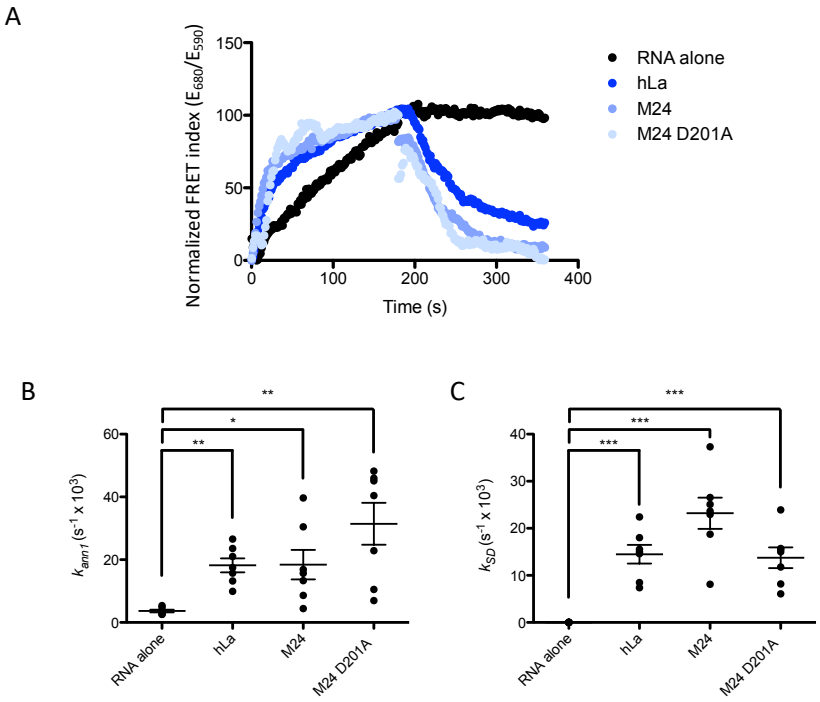

Figure 5: Trm1 folds RNA *in vitro*
A) RNA strand annealing (phase I) and dissociation (phase II), as indicated by changes in FRET index (emission at 680 nm/emission at 590 nm) between the Cy3- and Cy5-labeled substrates. Phase II was initiated with the addition of an unlabeled competitor RNA at t=180 seconds. Representative traces are shown.
B-C) Strand annealing (B) and dissociation (C) rate constants calculated with RNA alone, recombinant hLa, or wild type or catalytically inactive M24 Trm1 (mean± standard error, two-tailed paired t-test * at $p<0.05$, ** at $p<0.01$, *** at $p<0.001$) (n= 7 independent replicates).

4.4 Discussion

In this work, we provide evidence of both catalytic and catalytic-independent roles for the fission yeast tRNA methyltransferase Trm1. That these dual functions appear to be conserved across prokaryotes and eukaryotes speaks to both the propensity for RNA to adopt misfolded or alternate, non-functional conformations (107), and the importance of resolving tRNA misfolds to

ensure optimal function in translation. While we have shown that wild type and catalytically inactive Trm1 promotes the proper processing and folding of the Ser^{UCA} suppressor tRNA, it remains to be found how Trm1 chaperones endogenous misfolded pre-tRNAs. We anticipate that Trm1 uses its tRNA folding activity to guide pre-tRNA folding in the nucleus, while Trm1-catalyzed dimethylation is particularly important for additional stabilization to resolve more severe misfolds. This is especially evident when comparing tRNA-mediated suppression of various suppressor tRNA mutants. The G35C suppressor tRNA mutation (Ser^{UCA}) only results in a misfold at the pre-tRNA level, due to altered base-pairing with the intron which is later removed and thus the mature suppressor tRNA possesses the same fold as endogenous tRNA Ser^{UGA}. In contrast, adding the U47:6C mutation leads to a misfold that persists in the mature tRNA in the cytoplasm, compounded by the fact that the degree of misfold in U47:C is also greater than that of tRNA Ser^{UCA}. Therefore, while the catalytic-independent activity alone is sufficient for Trm1 associated tRNA Ser^{UCA} stabilization and folding in the nucleus, tRNA Ser^{UCA} U47:6C requires both Trm1-mediated pre-tRNA stabilization in the nucleus and the Trm1-catalyzed modification that remains on the mature tRNA in the cytoplasm for suppression activity (Figure 3, Figure S2).

The finding that the catalytically inactive D201A mutant promotes tRNA-mediated suppression in a *sla1*Δ strain, but only partial suppression in a *sla1*Δ *maf1*Δ strain provides additional evidence supporting the importance of both catalytic and non-catalytic functions to ensure proper tRNA structure and function (Figure 3). The increase in tRNA transcription resulting from the deletion of the RNA Polymerase III repressor Maf1 may in turn lead to an increase in the persistence of defective pre-tRNAs as tRNA processing factors, including Trm1, become limiting. Thus, the ability to benefit from Trm1's modification and folding activity could

be more effective at resolving misfolds. Alternately, since tRNA modification can lead to product release from the enzyme, as has been demonstrated for the tRNA pseudouridine synthase TruB (142, 259), the lack of catalysis observed with D201A might be expected to lead to pre-tRNA retention by Trm1, thus compounding the effect of Trm1 becoming limited if it is unable to effectively recycle onto new substrates. Another unexpected result concerns the nature of the correlation between mature suppressor tRNA levels and the degree of tRNA-mediated suppression activity, as has been posited to partially explain why the La protein promotes tRNA-mediated suppression (48). We found that the apparent increase in mature suppressor tRNA levels can at least partially be attributed to a decrease in modification at G26, supporting the idea of exercising caution when designing northern blotting probes to avoid sites of bulky modifications on the Watson-Crick face (253). Rather, our results point towards tRNA-mediated suppression activity as a function of the combination of suppressor tRNA levels and specific activity per suppressor tRNA molecule (Figure 3, Figure 4). For Trm1, which promotes tRNA-mediated suppression in the absence of increasing mature tRNA levels, this may be due in part to stabilization imparted by the modification, or Trm1-mediated tRNA folding leading to increased stability or accommodation by the ribosome. We can also infer differences in the mechanism of tRNA-mediated suppression for tRNA Ser^{UCA} by hLa and Trm1: hLa primarily acts by stabilizing the 3′ end of the nascent suppressor pre-tRNA to protect it from degradation by the nuclear surveillance pathway, while Trm1 appears to increase suppressor tRNA functionality without affecting tRNA levels. Moreover, La and Trm1 act on different pre-tRNA species—La targeting nascent, trailer-containing pre-tRNA and Trm1 modifying intron-containing, end-processed pre-tRNA—suggesting that pre-tRNAs have multiple chances to fold correctly at different stages in the pre-tRNA processing pathway.

Additionally, while this work serves to reinforce the importance of La-mediated 3′ end protection and tRNA chaperone activity for tRNA-mediated suppression, it also revealed a surprising link between the La protein and Trm1 modification (Figure 4). Previously, Trm1 and La were hypothesized to function redundantly in the tRNA biogenesis pathway (38, 145), with La-mediated pre-tRNA stabilization thought to increase the window in which Trm1 could modify pre-tRNAs in the nucleus (38). While it is indeed likely that Trm1 and La have redundant functions — both promote pre-tRNA stability and folding— it is interesting that they oppose each other with respect pre-tRNA occupancy, in that the interaction between La and pre-tRNA prevents Trm1 from accessing and modifying pre-tRNAs, presumably through a shielding effect (113, 258). It remains to be found whether a relationship between La and Trm1 exists in humans, where La proteins harbor an additional RNA recognition motif (RRM2 or xRRM) within a more divergent C-terminal domain that has been implicated in La's RNA chaperone activity (236, 260, 261). The extent to which the C-terminal domain influences tRNA binding *in vivo* remains unknown, although its propensity for sequence-independent binding to structured, hairpin-containing RNA (236, 262) may affect how La engages the pre-tRNA body. Further, exploring how La may influence the installation of other modifications occurring at the pre-tRNA stage will likely be an active area of future research.

Finally, our work identifying nuclear and mitochondrial functions for Trm1 in *S. pombe* adds to the growing body of literature proposing coordination of the nuclear and mitochondrial genomes through tRNA modifications (263). In budding and fission yeast, this may be achieved by altering the balance of transcription of the nuclear- and mitochondrially-targeted Trm1 isoforms, which will in turn influence the degree of G26 dimethylation of nuclear- and mitochondrially-encoded tRNAs. Still, how Trm1-catalyzed tRNA modifications may alter

cytoplasmic and mitochondrial translation remains unknown. Although we showed that there are no defects in bulk translation upon deletion of Trm1, we do not exclude the possibility that dimethylation at G26 alters the dynamics of codon recognition, as has been described for methylation of human mitochondrial Serine and Threonine tRNAs at position 32 by METTL8 (264). Additionally, studying the interplay between Trm1 and other nuclear-encoded enzymes that similarly modify mitochondrial tRNAs will continue to inform our understanding of the control and potential co-regulation of the nuclear and mitochondrial genomes.

Our work underscores the complexity of tRNA maturation in a model eukaryote by highlighting the multi-functional nature of a tRNA modification enzyme. The data presented here support the growing idea that tRNA modification enzymes can have roles beyond catalysis, and that this holds true in prokaryotes and eukaryotes. The extent to which this applies to other tRNA modification enzymes, and RNA modification enzymes more generally, will be an exciting area of future research that will continue to inform our understanding of the mechanisms underlying RNA fold and function.

4.5 Materials and Methods

Yeast strains and constructs

Standard laboratory techniques were used to culture *S. pombe* cells at 32°C. Tag integration and knockouts were generated with a previously described PCR-based strategy and verified by PCR and western blotting (177) (strains are provided in supplementary table 1). Plasmids were introduced with lithium acetate and selected on minimal media lacking supplements (EMM-ura) (265) (supplementary table 2). Mutations were introduced by site-directed mutagenesis and verified by sequencing. tRNA-mediated suppression growth assays were performed as described (179).

RNA and protein extractions and northern and western blotting

S. pombe cells were grown at 32°C and harvested at mid-log phase. Total RNA was isolated with hot acid phenol and northern analysis was performed as described using 15% TBE-urea polyacrylamide gels (179). Band intensities were quantified with ImageQuant TL software. For PHA26 northerns (39), relative modification index values represent the intensity of the TUC signal divided by the intensity of the PHA26 signal and normalized to a wild type strain or empty vector. For tRNA-mediated suppression northerns, blots were probed with the indicated ^{32}P-labeled probes and an equimolar amount of unlabeled competitor probe to prevent hybridization of the labeled probe with the endogenous tRNA Ser^{UGA} (probe sequences are provided in supplementary table 3). Total protein was extracted according to (179) and western blots were probed with a custom anti-Trm1 antibody (gift from Dr. Richard Maraia, NIH) at 1:2000 and for β-actin at 1:1250.

cDNA synthesis and qRT-PCR

1 µg Turbo DNase-treated RNA was reverse transcribed with the iScript cDNA synthesis kit (BioRad, 1708890), treated with 0.5 µL RNase cocktail (Invitrogen, AM2286), and diluted 1:10 before quantification using the SensiFAST SYBR No-Rox kit (Bioline, BIO-98005). qRT-PCR was performed with 1 µM of each primer (a common reverse primer for both Trm1 isoforms and isoform-specific forward primers, probes provided in supplementary table 3) with the following qRT-PCR settings: 95˚C for 10 minutes and 40 cycles consisting of 10 seconds at 95˚C, 20 seconds at 60˚C, and 20 seconds at 72˚C. Trm1 levels were normalized to *act1* mRNA and

normalized M1 Trm1 signal was subtracted from normalized M24 Trm1 signal to calculate relative M24 Trm1 levels.

Pulse labeling of mitochondrial protein synthesis

Pulse labeling was performed according to (266). Briefly, *S. pombe* cells were initially grown in EMM-ura + 2% glucose, then inoculated into fresh EMM-ura with 0.1% glucose and 2% galactose and grown at 32˚C for 6 generations to a final OD_{600} less than 1 x 10^7 cells/mL. Cell pellets corresponding to ~2.5 x 10^7 cells were washed with 500 µL reaction buffer (40 mM potassium phosphate pH 6.0, 2% galactose, 0.1% glucose), pelleted, resuspended in 500 µL reaction buffer with 10 mg/mL cycloheximide, and incubated at room temperature for 15 minutes. Cycloheximide was omitted to evaluate cytoplasmic translation. 5 µL [^{35}S]-methionine was directly added to the cell suspension, mixed thoroughly, and incubated for 30 minutes at room temperature. Cells were pelleted and the pellet was resuspended in 75 µL solubilization buffer (1.8 M NaOH, 1 M β-mercaptoethanol, 0.01 mM PMSF) and mixed. 500 µL water was added and proteins were TCA-precipitated, followed by separation on a 17.5% SDS gel, transfer to a nitrocellulose membrane, and exposed to a Phosphor screen overnight.

Recombinant protein purification and electrophoretic mobility shift assay (EMSA)

Recombinant His-tagged protein expression was induced in *Escherichia coli* with 1 mM IPTG at 16˚C for 18 hours and purified over a Ni^{2+} column (His-TRAP, GE-Amersham), followed by a second round of purification over a heparin column (Hi-TRAP, GE-Amersham). Proteins were concentrated into 1X EMSA buffer (20 mM Tris HCl pH 7.6, 100 mM KCl, 0.2 mM EDTA pH 8.0, 1 mM DTT) and quantified by SDS-PAGE. EMSAs were performed as described (38).

Briefly, 3000 cpm PAGE purified, T7-transcribed ^{32}P α-ATP-labeled pre-tRNAs (sequences provided in supplementary table 4) were heated to 95°C and slow-cooled to room temperature before addition to a 20 uL reaction containing 1X EMSA buffer. Increasing amounts of recombinant Trm1 were added to the reaction mix, followed by incubation at 32°C for 20 minutes. Reactions were cooled on ice for 2 minutes and complexes were resolved on 8% non-denaturing polyacrylamide gels run at 4°C and 100V. The proportion of bound tRNA was quantified with ImageQuant TL software and binding curves were fit to a non-linear specific binding curve (Hill slope) with GraphPad Prism 6.0.

In vitro methylation and primer extension

5 μM T7-transcribed pre-tRNA Ser^{UGA} was methylated for 3 hours at 32˚C in a 25 μL reaction containing 100 mM Tris HCl pH 7.5, 0.1 mM EDTA pH 8.0, 10 mM $MgCl_2$, 40 mM NH_4Cl_2, 1 mM DTT, 100 mM SAM (NEB, B9003S), and 5 μM recombinant Trm1. For competition between hLa and Trm1, 5 μM pre-tRNA Ser^{UGA} was pre-incubated alone or with 5 μM recombinant hLa in a 50 μL reaction for 20 minutes at 32˚C in methylation reaction buffer without $MgCl_2$ and SAM. Reactions were snap chilled on ice to preserve complexes, followed by the addition of recombinant Trm1, 2 mM $MgCl_2$, and 100 mM SAM. Reactions were incubated at 32˚C and samples were removed at indicated time points and immediately purified by phenol: chloroform: isoamyl alcohol (25:24:1) extraction. Primer extensions were performed with SuperScript III (Invitrogen, 18080093) following standard methods.

FRET assays

FRET assays were performed as described (104, 105). Briefly, unlabeled and Cy5- and Cy3-labeled RNA substrates were synthesized by IDT (sequences provided in supplementary table 4) and used at a final concentration of 25 nM. Where applicable, recombinant proteins were added to 400 µL reactions at a final concentration of 100 nM immediately prior to taking measurements. Fluorescence emission at 590 and 680 nm was recorded on a Cary Eclipse fluorimeter with readings taken in half-second time-points over a period of 180 seconds. Strand dissociation measurements were initiated immediately following strand annealing with the addition of 1 µM unlabeled competitor RNA. Strand annealing and dissociation rate constants were determined by calculating a FRET index (emission at 680 nm divided by emission at 590 nm) over time and normalizing values between 0 and 1. Curves were fitted to an equation for one-phase association (strand annealing) or one-phase decay (strand dissociation) in Graphpad Prism 6.0.

Data availability

Supplementary tables can be accessed at
https://www.biorxiv.org/content/10.1101/2023.04.12.536578v1

4.6 Acknowledgements

We thank Dr. Richard Maraia for the Trm1 antibody and *maf1*Δ yeast strain. J.P. is supported by a Canada Graduate Scholarship (Doctoral) from the National Sciences and Engineering Research Council of Canada. M.A.B. is supported by a Discovery Grant from NSERC ("Impact of chemical modification of noncoding RNAs on gene expression in *S. pombe*").

4.7 Supplementary information

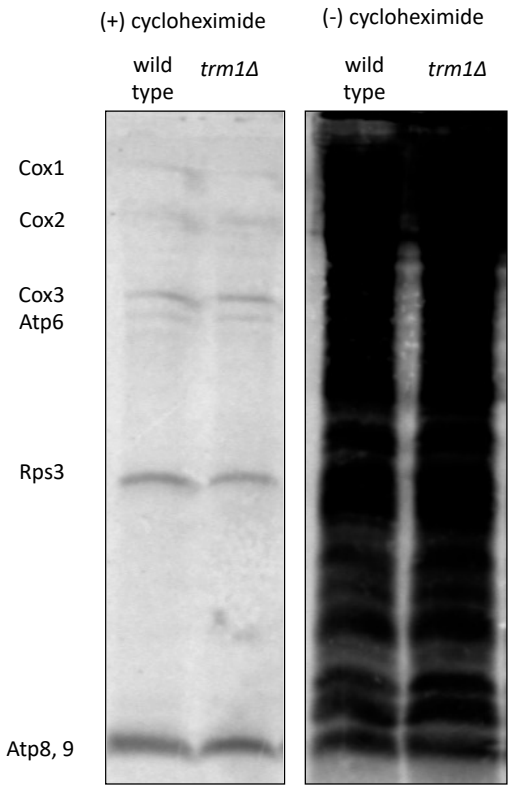

Figure S1: Bulk cytoplasmic and mitochondrial translation are unaffected by Trm1 deletion
30-minute pulse-labeling of newly synthesized mitochondrial (+ cycloheximide) and total (- cycloheximide) proteins in a wild type and *trm1*Δ strain. Mitochondrially synthesized proteins are indicated.

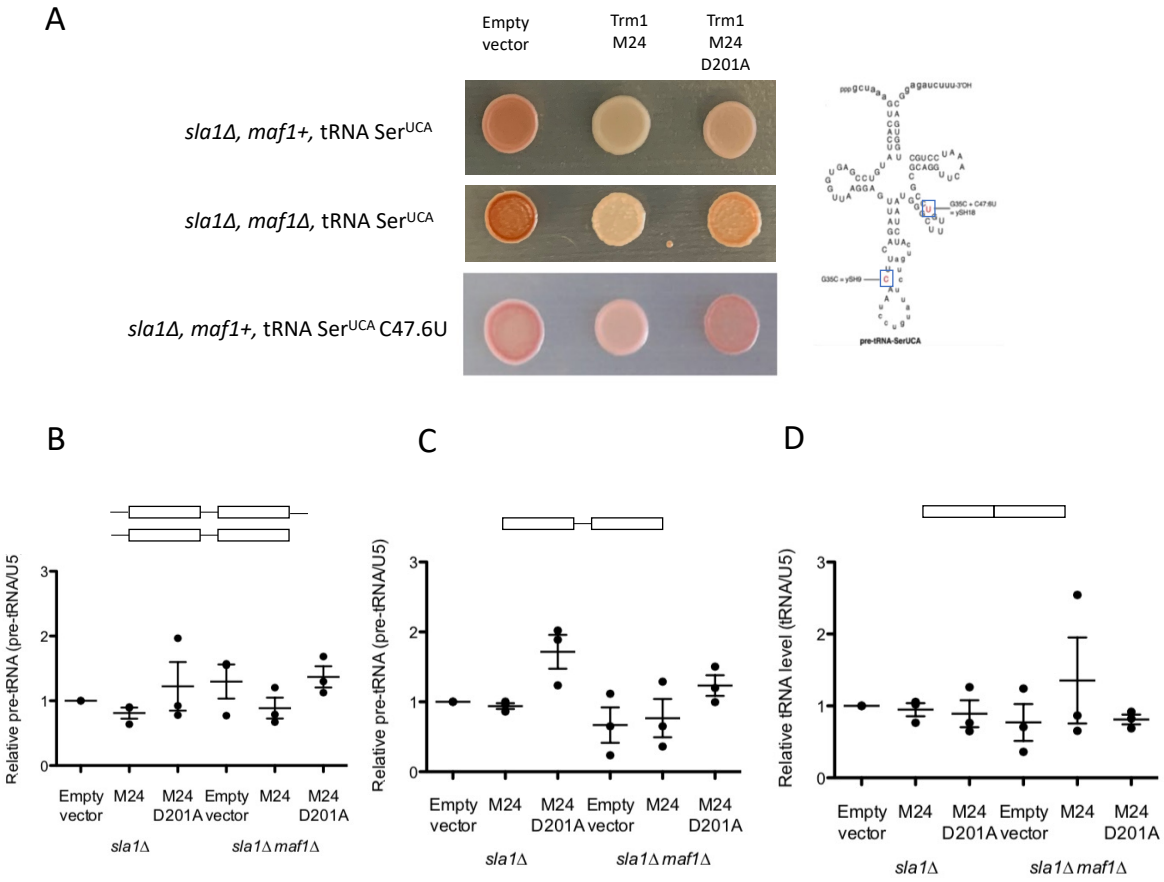

Figure S2: Trm1-dependent suppression activity is linked to the presence of Sla1 and Maf1 and the nature of the suppressor tRNA allele

A) tRNA-mediated suppression with wild type and catalytically inactive Trm1 in a *sla1*Δ and *sla1*Δ *maf1*Δ background with increasingly defective suppressor tRNA alleles.

B-D) Quantification of the abundance of suppressor tRNA processing intermediates relative to U5.

Chapter 5: New roles for RNA modification enzymes—exploring the transcriptome beyond modifications

Portions of section 5.3 were previously published (Porat J, Kothe U, and Bayfield M.A., Revisiting tRNA chaperones: New players in an ancient game, *RNA.* **27:** 543-559 (2021)).

5.1 RNA modification enzymes use catalytic-independent activities to influence noncoding RNA form and function

There exists an intricate network of RNA processing factors, including RNA binding proteins and modification enzymes, that coordinate and compete to ultimately influence the fate of diverse classes of noncoding RNAs. While the contribution of post-transcriptional modifications to RNA structure and function has been explored in great detail (reviewed in (1)), the idea of catalytic-independent functions for RNA modification enzymes has only very recently begun to be investigated in mechanistic detail. Catalytic-independent activities can be identified using catalytic-dead mutants that are still functional in another biological context or uncovering new functions that do not rely on catalytic activity. A caveat to this is that it can be difficult to completely uncouple catalysis from catalytic-independent functions, especially in cases when it is the catalytic function that is required for viability, as is the case for many rRNA-modifying enzymes (267). Nevertheless, the work presented in this dissertation aims to expand upon the idea that catalysis is not the only important function of eukaryotic RNA modification enzymes, much like what has been described for prokaryotic tRNA modification enzymes (117, 118) (Figure 1, Figure 2).

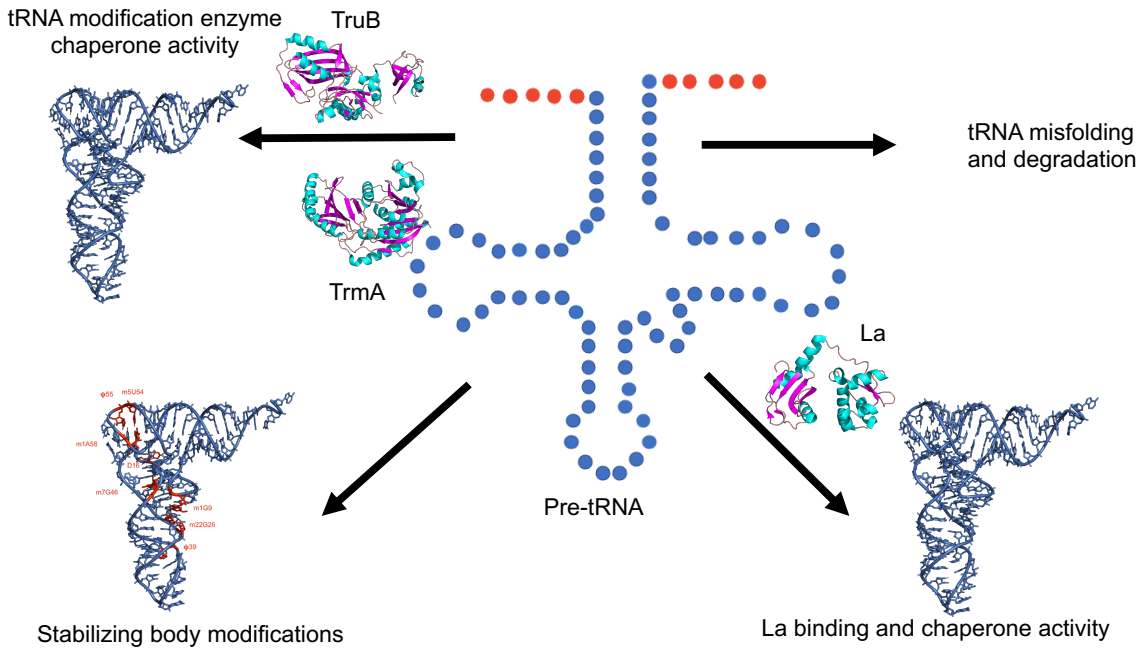

Figure 1: pre-tRNAs benefit from post-transcriptional modifications and RNA chaperone activity

Schematic of the various pathways a pre-tRNA can take during biogenesis. Pre-tRNAs can misfold, leading to degradation or non-functionality; acquire stabilizing modifications throughout the tRNA body; refold with the help of an RNA chaperone; or benefit from a combination of modification and RNA chaperone activity through dual function modification enzymes.

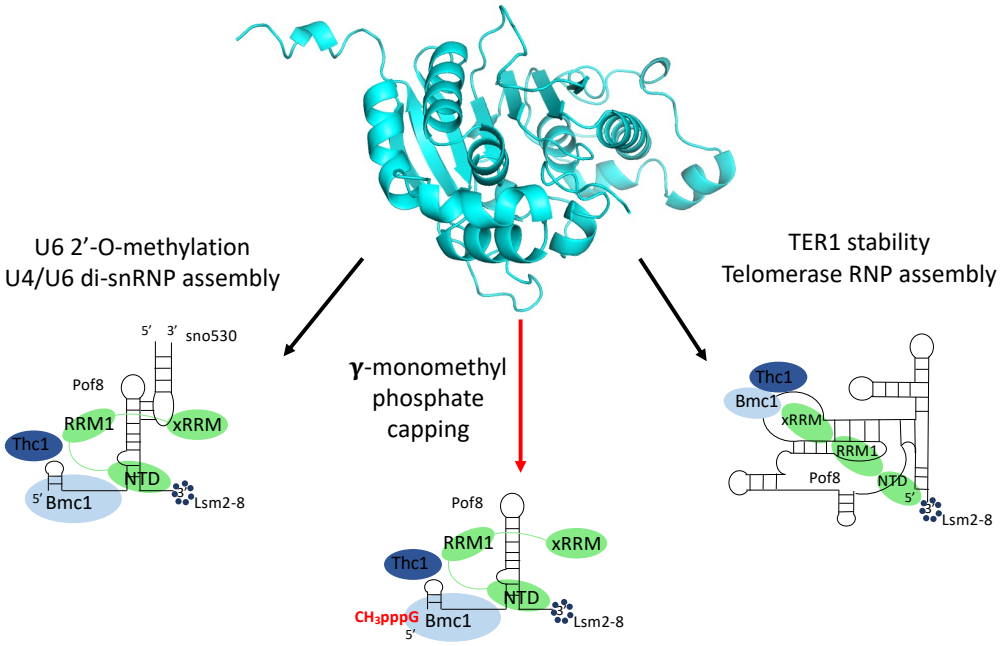

Figure 2: The methyltransferase Bmc1 possesses catalytic (red arrow) and catalytic-independent functions that influence noncoding RNA biogenesis in *S. pombe*
Alphafold (222) structure prediction of Bmc1 and schematics of its roles in 5′ capping the U6 snRNA, promoting U6 2′-O-methylation, and U6 snRNP and telomerase holoenzyme assembly.

In this work, we demonstrated that the *S. pombe* RNA methyltransferases Bmc1 and Trm1 possess catalytic-independent functions distinct from their well-characterized methyltransferase activity. In addition to catalyzing the addition of a 5′ γ-monomethyl phosphate cap on the U6 snRNA (65), **Bmc1 also interacts with the telomerase RNA TER1**, an RNAP II transcript possessing a 5′ TMG cap installed independently of Bmc1, to **protect it from exoribonucleolytic degradation** and **promote its association with the telomerase holoenzyme** (Chapter 2, Figure 2 and Figure 5). In this situation, we can characterize Bmc1's functions in telomerase holoenzyme assembly and TER1 protection—both activities that do not require synthesis of a 5′ γ-monomethyl phosphate cap— as catalytic-independent functions.

We also used a predicted catalytic-dead mutant to show that **2′-O-methylation of U6 and the interaction between Bmc1 and U6 do not require catalysis** (Chapter 3, Figure 4).

Importantly, the human methyl phosphate capping enzyme becomes catalytically inactive when bound to LARP7 in the 7SK snRNP, resulting in a functional switch from 7SK 5′ capping to 7SK snRNP assembly and stability (129, 160). The conservation of both catalytic and catalytic-independent activities for MePCE homologs across evolution hints at the importance of both functions, despite occurring in the context of divergent RNPs. It becomes tempting to speculate that catalytic-independent functions, which drive RNP formation and stability to an arguably greater degree than a single cap methylation (160), may be the more critical function for MePCE homologs functioning in the telomerase, U6, or 7SK RNP. In agreement with this, the disruption of Bmc1 5′ capping activity had no effects on telomerase biogenesis or U6 2′-O-methylation (209) (Chapter 3), and the presence of the methyl donor SAM does not affect the ability of human MePCE to promote 7SK snRNP assembly (160).

We also examined the catalytic and non-catalytic functions of the tRNA methyltransferase Trm1, providing evidence that a eukaryotic tRNA modification enzyme behaves similarly to its bacterial counterparts in moonlighting as a tRNA chaperone (Chapter 4). This study, which used the tRNA-mediated suppression assay to monitor tRNA folding and processing *in vivo*, revealed that **a catalytic-dead Trm1 mutant supports proper pre-tRNA processing and function** (Chapter 4, Figure 3). We also uncovered an unexpected crosstalk between Trm1 and the well-studied RNA chaperone La, with La binding to pre-tRNAs resulting in decreased Trm1-catalyzed tRNA methylation (Chapter 4, Figure 4). While previous models of pre-tRNA maturation proposed that La and Trm1 cooperate to ensure proper pre-tRNA processing (38, 145), we instead suggest that their redundant functions in promoting pre-tRNA folding may serve to increase the pool of pre-tRNAs that benefit from chaperone-induced refolding. The La protein and the tRNA chaperone/modification enzyme TruB do not

discriminate between folded and misfolded substrates, which limits the efficiency of resolving misfolds (38, 117). In a situation where La becomes limiting with respect to the pre-tRNA pool, the presence of another tRNA chaperone like Trm1 increases the chance that more pre-tRNAs will assume a native, functional fold.

In sum, the data described here support an emerging model in which RNA modification enzymes can possess alternate, non-catalytic functions. In line with this idea, evidence suggests that snoRNAs, which base-pair with target RNA to guide pseudouridylation or 2′-O-methylation (see Chapter 3 for an example), do not always have a role in carrying out post-transcriptional modifications. Notably, the U3 snoRNA pairs with the 5′ external transcribed spacer (5′ETS) of the 35S pre-rRNA and nucleates snoRNP assembly to result in cleavage of the 5′ETS without catalyzing any modification (268, 269). Upstream of U3 binding, the human m^5C methyltransferase NOP2/NSUN1 interacts with box C/D snoRNAs to recruit U3 and U8 to the 5′ETS, with catalytic activity similarly dispensable for NOP2/NSUN1 function in ribosome biogenesis (270). snoRNAs have also been demonstrated to harbor catalytic-independent functions in modulating alternative splicing, with base-pairing between the snoRNA and pre-mRNA predicted to mask splice sites or recruit snoRNPs that compete with the U1 snRNP for pre-mRNA binding (271–273). Further investigation into potential catalytic-independent functions of other RNA modification enzymes will continue to inform our ideas on the mechanisms and rules governing RNA structure, stability, and function.

5.1.1 Are RNA modifications always functional?

A major question that has emerged over the course of this dissertation concerns whether RNA modifications themselves are functional, or simply a by-product allowing for modification

enzyme dissociation. There are numerous examples where modifications have a clear impact on RNA structure and function—within this work alone, we have demonstrated that 2′-O-methylation of U6 influences U4/U6 duplex formation and G26 dimethylation of tRNAs becomes especially important for increasingly defective suppressor tRNA alleles—but it becomes more uncertain in the case of Bmc1/MePCE. Injection of *in vitro* γ-monomethyl phosphate-capped 7SK and U6 into *Xenopus* oocytes increased transcript stability relative to a 5′ triphosphate (274), although depletion of MePCE or deletion of Bmc1 had no effects on U6 stability in human and yeast cells, respectively (64, 68). To further complicate matters, a 5′ γ-monomethyl phosphate increases the affinity of the methyltransferase domain of human MePCE for the 5′ end of the 7SK snRNA (157), suggesting a mechanism by which MePCE remains bound to 7SK in the 7SK snRNP following catalysis. As it is unclear whether it is the cap structure itself, or MePCE binding the 5′ end of 7SK, that lends 7SK protection from exoribonucleolytic digestion, further work must be conducted before a conclusion can be reached as to the importance of the modification. Examining rescue of 7SK stability with catalytically active and inactive MePCE in an MePCE knockdown should provide initial evidence on the importance of the 5′ methyl phosphate capping activity of MePCE, which will complement our work demonstrating that catalysis is not required for U6 stability in yeast (Chapter 3).

MePCE is in atypical enzyme, in the sense that it has a higher affinity for its product than its substrate (157). Most enzymes release the product following modification, as has been demonstrated for tRNA modification enzymes including the dual pseudouridine synthase/tRNA chaperone TruB (142, 259). In agreement with this, it has been hypothesized that the slow catalytic rate of TruB may have evolved as a way of prolonging the window in which TruB can interact with the tRNA to assist its folding prior to modification and subsequent product release

(117, 142). Still, a complete lack of catalytic activity resulting in TruB remaining bound to the tRNA would be detrimental to tRNA processing, both because bound TruB could prevent interactions with other tRNA processing factors to cause a stall in processing and because this would limit the amount of tRNAs that can benefit from TruB-mediated chaperone activity. La displays similar binding preferences for substrates over products, as it displays high affinity binding for pre-tRNAs due to additive effects from interactions with the 3′ uridylate-containing trailer and the pre-tRNA body, but dissociates once the 3′ trailer is cleaved, leading to efficient recycling onto new pre-tRNA substrates (113). One might then imagine a situation in which modulating the kinetics of RNA modification or processing acts as a mechanism to regulate the amount of time an RNA chaperone can associate with its substrates and the rate at which it can be recycled onto new substrates.

5.2 Conserved RNA binding proteins assemble into diverse complexes across evolution

A major theme of this work is that evolutionarily conserved RNA binding proteins use common domains and protein interaction partners to engage a wide range of substrates across different species. Most notable are Bmc1/Bin3/MePCE and Pof8/LARP7, which are physically associated with each other—and indeed appear to have co-evolved (Chapter 2)—and tend to bind structured, uridylate-containing RNAs, although the identity of the RNA and RNP in which it is found is variable among different organisms. While previous research suggested the importance of the La motif as a conserved RNA binding domain shared by LARP7 homologs (reviewed in (261)), a broader, more comprehensive examination of LARP7 homologs across eukaryotes revealed that the C-terminal xRRM is more highly conserved than the La motif (123). In agreement with this, while only some LARP7 homologs use the La motif to bind their targets

(human LARP7 and *T. thermophila* p65 use the La motif and RRM1 to bind the 3′ uridylate trailer of RNAP III transcripts (120, 124, 131, 132)), to date all examined LARP7 homologs use the xRRM (9, 14, 122, 131, 132, 234). The ability of the xRRM to engage both single and double-stranded RNA, with no reported sequence specificity, may provide an explanation as to the diverse array of substrates reported for LARP7 homologs, from the RNAP III-transcribed 7SK and U6 snRNA to the RNAP II-transcribed fission yeast telomerase RNA (5).

While it is likely that Bmc1 interacts with both U6 and the telomerase RNA through its interaction with Pof8—or through Lsm2-8, which directly binds the 3′ ends of U6 and telomerase (60, 94) and interacts with Bmc1 (Chapter 2)— another possibility linking these two very different RNA substrates is that both possess unexpected or non-canonical introns. The 3′ end of telomerase RNA is produced through an incomplete splicing reaction, whereby the 3′ end of the 5′ exon becomes the mature 3′ end of the transcript (101). Conversely, U6 undergoes a standard splicing reaction to excise the intron, although this is unusual in that RNAP III transcripts do not usually contain introns (158, 159, 205, 207). Other than Bmc1 influencing pre-mRNA splicing by promoting 2′-O-methylation of U6 and U4/U6 di-snRNP assembly (Chapter 3), to date there are no known links between Bmc1/MePCE and introns. Still, it is curious that there are only two known atypically spliced transcripts in *S. pombe* and Bmc1 interacts with both. Whether there is some kind of crosstalk or interaction between Bmc1 and the spliceosome remains unknown, but may represent an intriguing area of future research.

Such substrate diversity is not limited to LARP7 and MePCE family proteins, as several recent studies revealed that tRNA- and rRNA-modifying enzymes also modify mRNA. The exact function of various mRNA modifications is still under debate, but mRNA pseudouridylation has been demonstrated to impact pre-mRNA splicing (275), stop codon

readthrough (276), and mRNA decoding by the ribosome (277). While these findings were initially surprising, considering the different structures, processing pathways, and subcellular localization that can exist for tRNA, rRNA, and mRNA, additional work revealed that these RNA modification enzymes do, in fact, recognize small structural motifs common to more than one class of RNA. The human pseudouridine synthase Pus4 (the homolog of the bacterial tRNA modification enzyme and tRNA chaperone TruB), initially characterized for tRNA modification at position 55, also modifies mRNA through recognition of a hairpin structure consisting of a 5 base pair stem and 7 base pair loop that resembles the pseudouridine-containing TUC loop in tRNA (18). Similarly, the yeast pseudouridine synthase Pus1, which also modifies tRNA and the spliceosomal U2 and U6 snRNA (278–280), targets mRNA for pseudouridylation through a bulged stem-loop structure similar to the stem-loop structures found in Pus1's ncRNA targets (19). The conservation of multi-substrate pseudouridine synthases across species, coupled with their established tRNA chaperone activity and the propensity to target structured regions in mRNA, leads to the exciting hypothesis that RNA modification enzymes may also act as mRNA chaperones to influence their splicing or translation by refolding the structured regions situated around modification sites. As we work to establish the idea that RNA modification enzymes have alternate functions as RNA chaperones, it is hoped that additional research will be conducted to extend this emerging phenomenon to mRNA-modifying enzymes.

5.3 Modifications upon modifications: the regulation of post-transcriptional modifications through circuits

As RNA modifications rarely occur in isolation—which is particularly true for tRNAs—there has been an increase in interest in modification circuits, i.e. the preferential introduction of

modifications in a certain order, and how modification circuits impact tRNA structural stability (anticodon modification circuits reviewed in (281)). Yeast and bacterial tRNA body modifications, particularly in the elbow region, are installed in a preferential order. Pseudouridylation of nucleotide 55 typically occurs on nascent, unmodified tRNA and once tRNA is modified, Ψ55 promotes subsequent modifications, including methylation at nucleotide 54 (119, 282). Modification circuits have also been demonstrated for vertebrate tRNAs, with TUC loop modifications installed early in tRNA biogenesis, followed by leader and trailer processing, additional body and anticodon modifications, and intron removal (283, 284). Such findings may reflect the structural changes arising from modification or potential tRNA chaperone activity, with certain later-acting modification enzymes requiring specific conformations that may be facilitated by earlier-acting modification enzymes at different points in the tRNA maturation pathway. Sure enough, Ψ55 modification by TruB on the bacterial tRNA Phe^{GAA} was found to stabilize base-stacking interactions in the elbow region, thereby increasing the affinity of tRNA for the methyltransferase TrmA, which modifies nucleotide 54 (119, 144). While it is likely the modification is directly influencing tRNA structure to promote subsequent modifications, it is also possible that TruB binding to the tRNA may be sufficient to induce structural changes in the elbow region. It is therefore worth noting that the role of post-transcriptional modifications in promoting the installation of other modifications may confound the hypothesized non-catalytic functions of RNA modification enzymes.

Interestingly, the strength and dependence on modification circuits varies depending on the tRNA, with yeast tRNA Phe^{GAA} showing greater perturbations in modification in Pus4 and Trm2 knockout strains than total cellular tRNA, suggesting its increased sensitivity to modification circuits (282). The order of installation of tRNA modifications also likely relies on

subcellular localization of tRNA modification enzymes. Understanding how tRNA modification enzymes act as tRNA chaperones may offer further insight into the mechanisms by which specific tRNA conformations shape body modification circuits. As other classes of ncRNA, including snRNA and rRNA, also possess multiple modifications on the same transcript, it remains to be found whether the modifications are installed in a specified order. Further, as more high-throughput modification mapping techniques continue to reveal the landscape of mRNA modifications, mRNAs may yet emerge as another multi-modified RNA species with the potential for regulation of modification installation.

5.4 Final thoughts (for now)

The work undertaken in this dissertation aims to provide a new framework in which to view RNA modifications and the enzymes that catalyze them. While RNA modifications have traditionally been studied for their role in modulating RNA structure and stability, we propose that certain modifications may also have additional roles in regulating the interaction between RNA modification enzymes and their substrates through differences in affinity for the modified versus unmodified or processed versus unprocessed RNA. Still, this work is only in its infancy and although we provide evidence for catalytic-independent functions for Bmc1 and Trm1 in fission yeast, it remains to be found how widespread a phenomenon it is to have dual-function RNA modification enzymes. This work is therefore intended as a guide to inform (and hopefully inspire) future work exploring the complex natures of RNA modification enzymes and the numerous ways they promote and influence RNA biogenesis, structure, and function.

Appendix A: Use of tRNA-mediated suppression to assess RNA chaperone function

Jennifer Porat[1] and Mark A. Bayfield[1*]
1. Department of Biology, York University, Toronto, Canada
*Correspondence: bayfield@yorku.ca (M.A.B.)

This appendix was previously published as Porat J. and Bayfield M.A. Use of tRNA-mediated suppression to assess RNA chaperone function. *Methods Mol Biol.* **2106:** 107-120 (2020). https://doi.org/10.1007/978-1-0716-0231-7_6

Contributions: J.P. helped develop the method, designed, performed, and analyzed all experiments, and wrote the manuscript. M.A.B. helped develop the method, designed experiments, supervised the project, and edited the manuscript.

Abstract

La proteins have well-established roles in the maturation of RNA polymerase III transcripts, including pre-tRNAs. In addition to protecting the 3′ end of pre-tRNAs from exoribonuclease digestion, La proteins also promote the native fold of the pre-tRNA using RNA chaperone activity. tRNA-mediated suppression in the fission yeast *S. pombe* has been an invaluable tool in determining the mechanistic basis by which La proteins promote the maturation of defective pre-tRNAs that benefit from RNA chaperone activity. More recently, tRNA-mediated suppression has been adapted to test for RNA chaperone function in the La-related proteins and in the promoting of tRNA function by tRNA modification enzymes. Thus tRNA-mediated suppression can be a useful assay for the investigation of various proteins hypothesized to promote tRNA folding through RNA chaperone related activities.

Introduction

The investigation of RNA chaperone activity is often performed *in vitro*, using methods that rely on strand annealing, strand displacement or the promotion of folding of ribozymes (285). *In vivo* methods to study RNA chaperone activity are less common, and moreover, the availability of *in vivo* assays has been largely limited to prokaryotic systems (286, 287). In order to expand the versatility of assays to better suit the study of RNA chaperones in eukaryotic systems, a cell-based assay designed to test the ability of an RNA chaperone to remodel a misfolded tRNA into a functional structure has been developed. tRNA-mediated suppression has been used to characterize the chaperone activity of a number of eukaryotic proteins, including the La protein.

The La protein is a highly abundant eukaryotic RNA binding protein with functions in RNA metabolism and gene expression. The La protein's propensity to bind the 3′ polyuridylate stretch of nascent RNA polymerase III transcripts has been extensively studied, most notably for its role in protecting pre-tRNAs from exoribonucleolytic degradation (246). Further studies have revealed that the La protein also harbors strand annealing and displacement activities mapping to regions distinct from its polyuridylate binding sites, suggesting an additional function as an RNA chaperone (48, 104, 235, 260). This RNA chaperone activity is hypothesized to aid IRES- and uORF-mediated translation, as well as promote pre-tRNA processing and maturation by resolving misfolds (38, 288). Accordingly, we have developed the tRNA-mediated suppression assay to test tRNA-specific RNA chaperone activity. Using the fission yeast *Schizosaccharomyces pombe* as a model eukaryotic system to evaluate tRNA maturation, this assay is capable of measuring, in living cells, the ability of a suspected RNA chaperone to remodel a misfolded suppressor tRNA and rescue it from degradation.

Suppressor tRNAs arise from mutations to the anticodon loop, enabling read-through of stop codons and the subsequent incorporation of the newly cognate amino acid into the growing polypeptide chain (255, 289). Originally characterized in bacteria and yeast, suppressor tRNAs have recently been developed in mammalian cells (290). Like their wild type counterparts, suppressor tRNAs rely on correct processing for functionality, and can benefit from RNA chaperone activity to attain their native fold. We have made use of *ade6-704,* an *S. pombe* allele with a nonsense mutation in the *ade6* gene, to monitor processing and chaperone activities relating to a suppressor tRNA. The *ade6-704* allele encodes a truncated form of AIR carboxylase, an enzyme that is part of the fission yeast adenine biosynthetic pathway. During growth under limiting adenine conditions, yeast cells carrying the *ade6-704* allele accumulate a

red metabolic intermediate in the adenine biosynthetic pathway that oxidizes to form a red pigment and pink/red colonies, however pigment accumulation can be suppressed with a functional suppressor tRNA that allows for synthesis of the full length AIR carboxylase protein and a consequent release of the block in the adenine biosynthetic pathway, resulting in the growth of white yeast colonies (255, 291). A detailed summary of tRNA-mediated suppression in *S. pombe*, including important considerations with respect to experimental interpretations and how this method has been used to study a number of aspects of tRNA biogenesis has recently been reviewed in (255).

We have designed various serine based UGA-suppressor tRNA alleles with base substitutions that make the tRNA reliant on chaperone activity for functionality (48, 105, 292, 293). Of the 2 alleles, MSer G37:10, C47.6U (Figure 1A; integrated into the *leu1* locus in the La null (*sla1*-) fission yeast strain ySH18) requires more extensive chaperone activity to suppress pigment accumulation, while MSer G37:10 (found in the *sla1*- yeast strain ySH9) is also capable of moderate activity in the presence of a protein that binds to and protects the 3′ end of the tRNA from exoribonucleolytic degradation (255). To inform differences in 3′ end protection and RNA chaperone activity, we use a northern blotting assay that detects various pre-tRNA processing intermediates. In *S. pombe*, polyuridylate binding proteins such as the La protein protect pre-tRNAs from 3′ exoribonucleolytic nibbling (246). In the presence of a protein that binds to and stabilizes the 3′ end, a northern blot detecting intron-containing pre-tRNA species shows 3 sharp, well-defined bands corresponding to the nascent pre-tRNA, the leader-processed, and leader- and trailer-processed species (294). Proteins that display RNA chaperone activity but not stable 3′ binding may suppress pigment accumulation, but the nascent tRNA and leader-processed tRNA bands still run as a smear, similar to La null cells. We have previously used this system to

demonstrate that the human La-related proteins 4, 6 and 7 promote tRNA-mediated suppression in the absence of 3′ end protection, despite these proteins having no characterized role in the expression of pre-tRNAs (105). Notably, these proteins also displayed activity in RNA chaperone assays *in vitro*. Mutations to candidate RNA chaperones that test for loss of tRNA-mediated suppression should be accompanied by Western blots (using an antibody for a common protein tag engineered into all mutants) to ensure that loss of function is not due simply to loss of candidate RNA chaperone protein expression. Recently, we have shown that this system can also be used to test for the activity of a tRNA modification enzyme in *S. pombe* (38, 39).

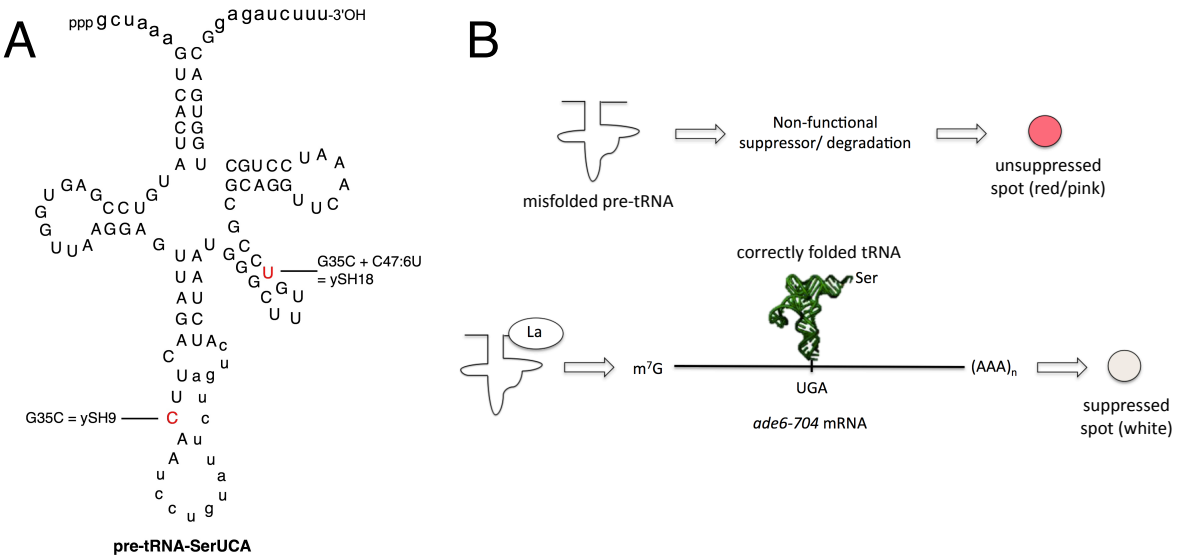

Figure 1: Schematic of the tRNA-mediated suppression assay
A) Suppressor alleles used for tRNA-mediated suppression. Lower case letters correspond to nucleotides removed during processing. Red nucleotides are mutated relative to the parent tRNA Ser^{UGA}. The anticodon mutation in the strain ySH9 results in a mismatch between the anticodon and intron position G37:10 relative to the parent tRNA Ser^{UGA} that promotes its degradation and inhibits tRNA-mediated suppression; ySH18 combined this mutation with C47:6U.
B) Schematic representation for tRNA-mediated suppression. Base substitutions in the mutated suppressor pre-tRNA make it prone to misfold, resulting in a non-functional tRNA that is often targeted for degradation. Without a suppressor tRNA, full-length AIR carboxylase is not synthesized and *S. pombe* cells accumulate a red metabolic intermediate (top panel). RNA chaperones, such as the La protein, can remodel the misfolded suppressor pre-tRNA and help it attain its native fold, permitting correct charging. The mature suppressor tRNA is capable of reading through the stop codon in the *ade6-704* mRNA, resulting in synthesis of full-length AIR carboxylase and suppression of pigment accumulation (bottom panel).

tRNA-mediated suppression presents a supplemental or alternative method to conventional *in vitro* RNA chaperone assays, as well as well-established *in vivo* assays using prokaryotic systems. Here we present a detailed protocol describing the colorimetric *in vivo* assay to measure chaperone activity, a northern blotting assay to distinguish RNA chaperone function from other pre-tRNA stabilizing activities, and a western blot procedure to assess RNA chaperone levels. Strategies for how other suppressor tRNAs could be adapted to this system in *S. pombe* are also discussed.

2. Materials

2.1 tRNA-mediated suppression

1. Edinburgh minimal media lacking uracil (EMM-ura): 11.77 g/L EMM-dextrose base, 0.225 g/L each of adenine, histidine, leucine, and lysine. Autoclave the media (20 min sterilization) and add sterile dextrose to a final concentration of 20 g/L.
2. EMM-ura plates with low adenine: EMM-ura media with 0.003 g/L adenine (for ade3 plates) or 0.01 g/L adenine (for ade10 plates) with 20 g/L yeast-grade agar. Autoclave the media (20 min sterilization) and add sterile dextrose post-autoclaving to a final concentration of 20 g/L.
3. YES media (yeast extract with supplements): 5g/L yeast extract, 0.225 g/L each of the following: adenine, leucine, histidine, uracil and lysine. Fill to 850 ml with ddH20, autoclave, then add 150 ml filter sterilized 20% dextrose (final concentration dextrose 30g/L).
4. 10 mg/ml Salmon Sperm DNA.
5. 10X LiOAc (1M Lithium Acetate, autoclaved).
6. 10X TE (100 mM Tris-HCl pH 8.0/ 10 mM EDTA pH 8.0, autoclaved).
7. 50% PEG 3350 (autoclaved).

8. TE-LiOAc (enough for 10 transformations): 100 µl 10X LiOAc, 100 µl 10X TE, 800 µl sterile ddH20, on ice.

9. Polyethylene glycol (PEG)-LiOAC (enough for 10 transformations): 1 ml 10X LiOAc, 1 ml 10X TE, 8 ml sterile 50% PEG, on ice.

10. pRep4 vector.

2.2 Northern blot

All solutions used for RNA work should be prepared with nuclease-free water.

1. EMM-ura media (see item 1 section 2.1).

2. Acid-saturated phenol, pH 4.3 – 4.5.

3. RNA extraction buffer A: 50 mM sodium acetate, pH 5.2, 10 mM EDTA, pH 8.0.

4. Buffer A-saturated acid phenol: Mix acid-saturated phenol and RNA extraction buffer A in a 1:1 ratio and nutate at room temperature for 20 min. Remove the aqueous layer and add 1 volume of RNA extraction buffer A to the phenol layer, followed by another 20 min nutation at room temperature. Remove the aqueous layer and warm at 37°C.

5. Complete RNA extraction buffer A: RNA extraction buffer A with 1% SDS.

6. Phenol: chloroform: isoamyl alcohol (25:24:1 v/v/v).

7. 3 M Sodium acetate, pH 5.2.

8. 20 mg/ml Glycogen.

9. 100% ethanol.

10. 70% ethanol.

11. 5X TBE: 54 g Tris base, 27.5 g boric acid and 20 ml 0.5 M EDTA (pH 8.0) in 1 L.

12. Mini (i.e. mini-Novex or similar) 15% TBE Urea gels (1X TBE, 7 M urea, 15% acrylamide)

13. 2X Formamide loading dye: 80% deionized formamide, 10 mM EDTA, 0.06% bromophenol blue, 0.06% xylene cyanol.

14. iBlot 2 Dry Blotting System.

15. iBlot 2 nitrocellulose transfer stacks**.**

16. GeneScreen Plus Hybridization Transfer Membrane.

17. DNA Transfer Lamp.

18. T4 PNK and 10X T4 PNK buffer.

19. Northern probes:

Lys CUU pre-tRNA (hybridizes to intron): 5′CTTCTGATACCATTCGTAAGAGTC3′

Lys CUU 3′ Trailer: 5′AAATTAACCTCCCAAG3′

U5: 5′CTGGTAAAAGGCAAGAAACAGATACG3′

20. [γ-^{32}P] ATP (3000 Ci/mmol EasyTide)

21. Hybridization oven

22. 20X SSC: 3M sodium chloride, 300 mM trisodium citrate.

23. Northern blot hybridization buffer: 6X SSC, 1% SDS, 2X Denhardt's solution, 0.1 mg/ml yeast RNA.

24. Northern blot wash buffer: 2X SSC, 0.1% SDS.

25. Northern blot stripping buffer: 0.1X SSC, 0.1% SDS.

26. Storage Phosphor Screen.

27. Typhoon Imaging System

28. ImageQuant TL.

2.3 Western blot

1. NET-2 buffer (approximately 500 µl per sample): 50 mM Tris-HCl pH 7.5, 150 mM NaCl, 0.05% NP-40., 1 mM PMSF. Make fresh and keep on ice.

2. EMM-ura liquid media (see item 1, section 2.1).

3. Primary antibodies: Anti-6XHis, Anti-Rps6.

4. 100 mM PMSF (phenylmethylsulfonyl fluoride) in EtOH.

5. Acid washed glass beads 400-600 µm, water rinsed and sterilized.

6. 2 ml screw cap tubes, VWR 16466-060 or similar.

7. Mini-Beadbeater-16, BioSpec or other glass bead-based homogenizer.

3. Methods:

Following transformation of candidate RNA chaperones into a strain containing a defective suppressor tRNA (see Note 1), candidate colonies are grown on low-adenine media and monitored for color change indicative of tRNA mediated suppression (Fig. 2A and B) (see Note 1). Different chaperone activities can then be confirmed through northern blotting-based assays designed to test pre-tRNA 3′ end protection and monitor mature levels of suppressor tRNA (Fig. 2C).

3.1 tRNA-mediated suppression

Candidate RNA chaperones are cloned into pRep4 (295) or other *ura+ S. pombe* expression vectors (see Notes 2, 3, and 4) and transformed into *S. pombe* as described below.

1. In order to transform pRep4-based candidate RNA chaperone plasmids into *S. pombe*, a pRep4 empty vector (negative control) and pRep4-hLa or pRep4-Sla1 (positive control) should be included.

2. Streak ySH9, ySH18, or other suppressor-tRNA/*ade6-704*-containing strains on YES plates and grow at 32°C until single colonies appear.

3. Pick a single colony with a sterile pipette tip and grow a 50 ml culture overnight in sterile YES media at 32°C with shaking (see Note 5).

4. The next morning, dilute the overnight culture into (10 ml x the number of transformations to be performed, i.e. 30 ml for three transformations) fresh YES media to a final $OD_{600\ nm}$ of 0.2 and let the culture grow to mid-log phase ($OD_{600\ nm}$ 0.6-1.0).

5. Pellet cells (3000 x g) for 2 minutes, wash with 10 ml of sterile water, and pellet cells again. 6. Keep cells on ice from now on.

7. Resuspend the cell pellet in (100 µl x number of transformations. i.e. 300 µl for three transformations) TE-LiOAC solution containing 0.5 mg/ml salmon sperm DNA.

8. To the cell suspension add 1 µg of plasmid and 700 µl ice cold, sterile PEG-LiOAc solution.

9. Vortex to mix and heat shock for 15 minutes at 42°C.

10. Pellet cells at 8000 x g for 1 minute at room temperature, aspirate the supernatant.

11. Resuspend the cell pellet in 200 µl sterile water.

12. Plate all cells on EMM-ura and grow at 32°C until colonies appear.

13. Pick single colonies from the transformation plate and grow the transformed suppressor tRNA-containing strain to mid-log phase in EMM-ura at 32°C.

14. Using a micropipettor and sterile plastic tips, spot 3-4 lL yeast culture on EMM-ura plates with low adenine and leave plates on bench until spots dry (see Note 6).

15. Invert and incubate plates at 32°C until spots come up (approximately four days).

16. Incubate plates on bench for a few days at room temperature to enhance color change (see Note 7).

3.2 Northern Blot to assess pre-tRNA stabilization

Northern blotting of pre-tRNA Lys CUU is performed to assess tRNA-mediated suppression associated with 3′ end protection (48, 105). We have adapted the use of the iBlot semi-dry transfer apparatus (Invitrogen) for transfers to positively charged nylon membranes as the very rapid transfer generates very sharp bands for pre-tRNA species that differ in length by only a few nucleotides.

1. To extract total RNA from the transformed suppressor tRNA-containing strain (see Note 8), grow a culture to mid-log phase in 50 ml EMM-ura at 32°C.

2. Pellet cells, wash with an equal volume of sterile water, and pellet cells again.

3. Resuspend the cell pellet in 250 µl complete RNA extraction buffer A.

4.Add 750 µl warm buffer A-saturated acid phenol.

5. Vortex to mix and incubate at 65°C for 4 minutes, vortexing occasionally.

6. Centrifuge at maximum speed for 3 minutes and remove the aqueous layer to a new tube.

7. Add 250 µl complete RNA extraction buffer A to the phenol layer, vortex to mix.

8. Incubate at 65°C for 4 minutes, vortexing occasionally.

9. Centrifuge at maximum speed for 3 minutes.

10. Add the aqueous layer to the tube (see item 6, section 3.2).

11. Add an equal volume of phenol: chloroform: isoamyl alcohol and vortex to mix

12. Centrifuge at maximum speed for 3 minutes and remove the aqueous layer to a new tube.

13. Add 2 µl 20 mg/ml glycogen, 1/10th volume 3M sodium acetate, pH 5.2, and 1 ml 100% ethanol.

14. Incubate at -80°C for 1 hour.

15. Remove 100 µl of ethanol slurry and centrifuge at 4°C for 10 minutes at maximum speed.

16. Without disrupting the pellet, remove the ethanol and wash with 500 µl 70% ethanol.

17. Centrifuge at maximum speed for 5 minutes and remove the ethanol.

18. Air-dry the pellet for 10 minutes and resuspend in 10 µl nuclease-free water.

19. Quantitate RNA by spectrophotometer (1 µl).

20. Check for RNA integrity by adding 2X formamide loading dye to remaining 9 µl and running RNA on a mini TBE-urea gel followed by ethidium bromide staining.

21. Using data from item 19, remove sufficient ethanol slurry so as to precipitate at least 10 µg total RNA (see Note 9).

22. Wash pellet in 500 µl 70% ethanol and air dry pellet.

23. Pre-run a mini 15% TBE urea gel at 120 V and 4°C for 20 minutes.

24. While gel is running, resuspend RNA pellet from item 22 in 10 µl 2X formamide loading dye.

25. Heat at 95°C for 10 minutes, followed by snap chilling for 2 minutes on ice.

26. Load the RNA on the pre-run 15% urea TBE gel and run at 120 V and 4°C until xylene cyanol dye has run off the gel (see Note 10).

27. Transfer RNA to a Genescreen Plus nylon membrane using the P0 program on the iBlot 2 Dry Blotting System (20 V for 1 min, 23 V for 4 min, 25 V for 2 min). To do this, open an iBlot2

nitrocellulose transfer stack and replace the nitrocellulose membrane with a Genescreen Plus membrane cut to the same size.

28. Once the transfer is complete, UV crosslink RNA to the membrane for 90 seconds on high power with a DNA Transfer Lamp (see Note 11).

29. Incubate the membrane in roller bottle in the hybridization oven at 40°C with 20 ml Northern blot hybridization buffer for 2 hours.

30. Label 50 pmol oligonucleotide probe in a 20 µl reaction containing 2 µl 10X T4 PNK buffer, 1 µl T4 PNK, and 2 µl [γ-^{32}P] ATP.

31. Incubate the reaction at 37°C for 45 minutes, followed by 65°C for 20 minutes.

32. Heat 10 µl labeled Lys CUU pre-tRNA probe to 95°C for 10 minutes and add to the 20 ml Northern blot hybridization buffer.

33. Incubate the membrane with constant rolling in the hybridization oven at 40°C overnight.

34. Wash the membrane with 30 mL Northern blot wash buffer at 50°C for 20 minutes.

35. Repeat washes twice more, for a total of 3 washes, with the final wash at room temperature.

36. Wrap the membrane with plastic wrap and expose to a Phosphorimager screen overnight.

37. Image with a Typhoon or similar imaging system and quantify band intensity with ImageQuant software.

38. To strip the labeled probe from the membrane, wash with 30 ml Northern blot stripping buffer at 70°C for 20 minutes. Repeat washes twice more, for a total of 3 washes (see Note 12).

3.3 Western blot testing for RNA chaperone abundance

1. Grow a 10 ml overnight culture of a single colony from the pRep4-based transformation (see section 3.1) in 10 ml EMM-ura at 32°C.

2. Dilute cells to an $OD_{600\ nm}$ of 0.2 in 50 ml fresh EMM-ura media in a sterile 250 ml Erlenmeyer flask and grow at 32°C to mid-log phase (OD_{600} nm of 0.6-1.0).

3. Pellet cells at 3000 x g and discard supernatant.

4. Resuspend cells in 1 ml sterile water and transfer to 2 ml screw cap tube.

5. Spin cells at 4°C at 3000 x g for 5 minutes and discard supernatant.

6. Resuspend cells in 100 µl cold NET-2 buffer and keep on ice. All steps should now be done on ice or in a cold room.

7. Add approximately 100 µl glass beads to the cell suspension.

8. Lyse cells using bead-beater in cold room. Set to "homogenize" for 1 minute (See Note 13).

9. Add another 100 µl cold NET-2 buffer and sediment at full speed at 4°C in microfuge for 5 minutes.

10. Remove supernatant to fresh tube.

11. Add another 100 µl cold NET-2 buffer to beads/pellet and flick tube to mix beads with minimal disruption to cell membrane pellet.

12. Allow beads to settle and combine supernatant with supernatant (see item 10, section 3.2).

13. Spin combined supernatants and spin at 4°C at full speed in microfuge for 15 minutes.

14. Remove supernatant to fresh tube.

15. Add glycerol to a final concentration of 10% and freeze in dry ice/ethanol bath.

16. Store lysates at -80°C.

17. Estimate lysate total protein concentration using SDS-PAGE/Coomassie staining or colormetric assay (Bradford or BCA).

18. Load equal amounts of lysate on SDS-PAGE and perform western blot for tagged RNA chaperone candidate (anti His6X) and endogenous loading control (Rps6p) according to manufacturer's instructions.

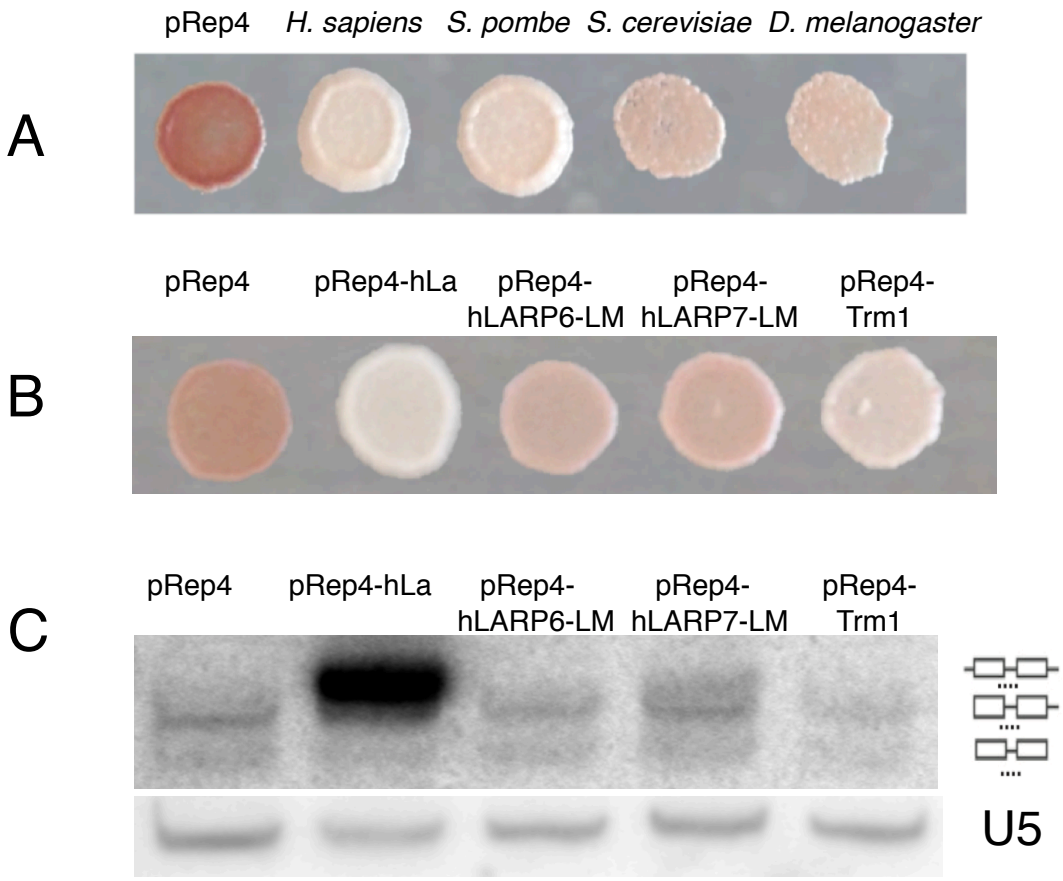

Figure 2: Typical results for tRNA-mediated suppression
tRNA-mediated suppression is compatible with La proteins from different species cloned into pRep4 (A), as well as non-La proteins, including the La modules of the human La-related proteins 6 and 7 (105) and the *S. pombe* tRNA methyltransferase Trm1 (38) (B).
C) Northern blotting with an intron-detecting probe for tRNA Lys^{CUU} helps differentiate and correlate tRNA-mediated suppression with 3′ end protection as is demonstrated with human La. Stripping and reprobing for the U5 snRNA can be done as a loading control.

Notes:

1. The assay described in this method uses tRNA-Ser^{UCA} suppressor tRNA alleles with a UCA anticodon to decode the ade6-704 allele, but other suppressor tRNAs could also be used, for example to test tRNA-mediated suppression associated with tRNA modification enzymes that do not modify suppressor- tRNA-Ser^{UCA} or its parent allele tRNA-Ser^{UGA}. Briefly, genes for suppressor-tRNAs of interest can be cloned into the multi-cloning site of pJK148 ((296) and available at ATCC). This can then be used as a template for site-directed mutagenesis of mutant tRNA alleles predicted to cause tRNA misfolding and thus rescue by candidate RNA chaperones. Suppressor tRNA alleles cloned into pJK148 can then be integrated into the *S. pombe* chromosome by linearizing the plasmid with NdeI, which cuts in the middle of the *leu1+* marker, and transformation of this linearized plasmid into a *leu-* strain of *S. pombe*. Other suppressor tRNAs that have been previously characterized in fission yeast include the leucine *sup8e* allele (297) which is also capable of decoding the stop codon in the *ade6-704* allele, and the serine *sup3i* allele (298), which must be used in conjunction with the *ade7-413* allele (299).
2. pRep4 is advisable as expression of the RNA chaperone in the multi-cloning site is repressible upon addition of thiamine to the growth media, and this can also take advantage of the use of pRep4-hLa or pRep4-Sla1 as positive controls in the assay. The pRep4, pRep4-hLa, and pRep4-Sla1 plasmids, as well as the suppressor tRNA and *ade6-704* containing *S. pombe* strains ySH9 and ySH18, can be ordered from the Yeast Genetic Resource Center (Japan). tRNA-mediated suppression as described herein will only work when using *S. pombe* with the *ade6-704* allele. *S. pombe* strains with the *ade6-704* allele will appear dark red when grown with limited adenine.
3. It is advisable to include a tag in the cloning of the candidate RNA chaperone to check for expression levels in *S. pombe* cells, especially when candidate RNA chaperone mutants will be

tested for loss of tRNA-mediated suppression so as to confirm that a loss of activity is not simply due to a loss of protein expression. We typically clone a 6XHis tag at the C-terminus (105).

4. When testing RNA chaperone activity of an *S. pombe* protein, it may be necessary to knock out the endogenous copy to see differences in suppression activity between a strain transformed with an empty vector and a strain transformed with the suspected RNA chaperone.

5. Use sterile technique and reagents when working with *S. pombe*. When dealing with liquid cultures, don't fill conicals or flasks more than halfway to allow for sufficient aeration during growth. Overnight cultures may take up to three nights to grow.

6. Incubate plates overnight at 32 °C before spotting to keep plates free from moisture.

7. Growing yeast on plates containing 0.003 g/L adenine results in darker red or pink colonies, compared to growth on plates containing 0.01 g/L adenine. Proteins with weaker chaperone activity tend to display more noticeable color change on plates with 0.01 g/L adenine.

8. Any RNA extraction method can be used, however the hot phenol method typically gives the best yield when working with *S. pombe*. For highly sensitive downstream applications (ex. monitoring tRNA acylation), follow the phenol: chloroform: isoamyl alcohol step with a chloroform/isoamyl alcohol wash.

9. 20 µg RNA may be required, especially when detecting pre-tRNA species.

10. We have had success differentiating pre-tRNA processing intermediates using either 8% or 15% TBE-urea polyacrylamide gels. Some optimization here may be required. For an 8% gel, run the gel until the xylene cyanol has run approximately three-quarters the length of the gel.

11. Baking the blot dry in a vacuum oven at 80°C can increase the number of times the blot can be reprobed.

12. Reprobe the membrane with the Lys CUU 3′ trailer probe (incubate at 32°C) to confirm 3′ end binding activity, and the U5 probe (incubate at 46°C) as an internal control to verify even loading.

13. Alternatively a vortex can be used, but typically gives lower yield.

Acknowledgements

We thank R. Maraia, R. Intine, Y. Huang, A. Sakulich, S. Koduru, S. Hasson, A. Mozlin, J. Mazeika, R. Hussain, A. Vakiloroayaei and A. Naeeni for their assistance in the development of tRNA-mediated suppression and its use in assessment of RNA chaperone function. We also thank R. Maraia for critical reading of the manuscript. This work is supported by a Discovery Grant from the Natural Science and Engineering Research Council (NSERC) of Canada to MA Bayfield.

Appendix B: Copyright permissions

ELSEVIER LICENSE
TERMS AND CONDITIONS

Mar 03, 2023

This Agreement between Jennifer Porat ("You") and Elsevier ("Elsevier") consists of your license details and the terms and conditions provided by Elsevier and Copyright Clearance Center.

License Number	5501580872405
License date	Mar 03, 2023
Licensed Content Publisher	Elsevier
Licensed Content Publication	Molecular Cell
Licensed Content Title	Transcriptional Networking Cap-tures the 7SK RNA 5′-γ-Methyltransferase
Licensed Content Author	Stewart Shuman
Licensed Content Date	Aug 17, 2007
Licensed Content Volume	27
Licensed Content Issue	4
Licensed Content Pages	3
Start Page	517
End Page	519
Type of Use	reuse in a thesis/dissertation
Portion	figures/tables/illustrations
Number of figures/tables/illustrations	1
Format	electronic
Are you the author of this Elsevier article?	No
Will you be translating?	No
Title	RNA methyltransferases
Institution name	York University
Expected presentation date	May 2023
Portions	Figure 1
Requestor Location	Jennifer Porat 4700 Keele Street Toronto, ON M3J 1P3 Canada Attn: York University
Publisher Tax ID	GB 494 6272 12
Total	0.00 CAD
Terms and Conditions	

Chapter 1, figure 3

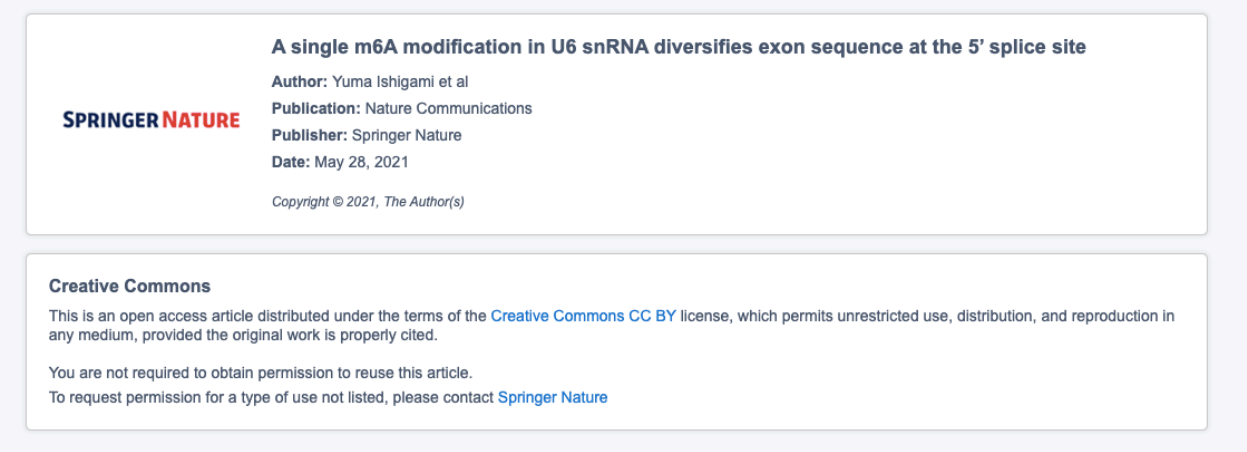

A single m6A modification in U6 snRNA diversifies exon sequence at the 5' splice site

Author: Yuma Ishigami et al

Publication: Nature Communications

Publisher: Springer Nature

Date: May 28, 2021

Chapter 1, figure 4

References

1. D. Wiener, S. Schwartz, The epitranscriptome beyond m6A. *Nat. Rev. Genet. 2020 222* **22**, 119–131 (2020).
2. S. Gerstberger, M. Hafner, T. Tuschl, A census of human RNA-binding proteins. *Nat. Rev. Genet.* **15**, 829–845 (2014).
3. M. W. Hentze, A. Castello, T. Schwarzl, T. Preiss, A brave new world of RNA-binding proteins. *Nat. Rev. Mol. Cell Biol.* **19**, 327–341 (2018).
4. A. Cléry, M. Blatter, F. H. T. Allain, RNA recognition motifs: boring? Not quite. *Curr. Opin. Struct. Biol.* **18**, 290–298 (2008).
5. M. Singh, C. P. Choi, J. Feigon, xRRM. *RNA Biol.* **10**, 353–359 (2013).
6. C. Alfano, *et al.*, Structural analysis of cooperative RNA binding by the La motif and central RRM domain of human La protein. *Nat. Struct. Mol. Biol.* **1**, 323–329 (2004).
7. M. Wegener, K. J. Dietz, The mutual interaction of glycolytic enzymes and RNA in post-transcriptional regulation. *RNA* **28**, 1446–1468 (2022).
8. O. Kotik-Kogan, E. R. Valentine, D. Sanfelice, M. R. Conte, S. Curry, Structural Analysis Reveals Conformational Plasticity in the Recognition of RNA 3′ Ends by the Human La Protein. *Structure* **16**, 852–862 (2008).
9. C. D. Eichhorn, R. Chug, J. Feigon, hLARP7 C-terminal domain contains an xRRM that binds the 3′ hairpin of 7SK RNA. *Nucleic Acids Res.* **44**, 9977–9989 (2016).
10. B. M. Lunde, C. Moore, G. Varani, RNA-binding proteins: Modular design for efficient function. *Nat. Rev. Mol. Cell Biol.* **8**, 479–490 (2007).
11. D. J. Páez-Moscoso, *et al.*, Pof8 is a La-related protein and a constitutive component of telomerase in fission yeast. *Nat. Commun.* **9**, 587 (2018).
12. A. K. Mennie, B. A. Moser, T. M. Nakamura, LARP7-like protein Pof8 regulates telomerase assembly and poly(A)+TERRA expression in fission yeast. *Nat. Commun.* (2018) https:/doi.org/10.1038/s41467-018-02874-0.
13. L. C. Collopy, *et al.*, LARP7 family proteins have conserved function in telomerase assembly. *Nat. Commun.* **9**, 557 (2018).
14. X. Hu, *et al.*, Quality-Control Mechanism for Telomerase RNA Folding in the Cell. *Cell Rep.* **33** (2020).
15. R. Basu, C. D. Eichhorn, R. Cheng, R. D. Peterson, J. Feigon, Structure of S. pombe telomerase protein Pof8 C-terminal domain is an xRRM conserved among LARP7 proteins. *RNA Biol.* **18**, 1181–1192 (2020).
16. M. A. Machnicka, *et al.*, MODOMICS: A database of RNA modification pathways - 2013 update. *Nucleic Acids Res.* **41**, D262–D267 (2013).
17. M. Helm, J. D. Alfonzo, Posttranscriptional RNA modifications: Playing metabolic games in a cell's chemical legoland. *Chem. Biol.* **21**, 174–185 (2014).
18. M. Safra, R. Nir, D. Farouq, I. V. Slutzkin, S. Schwartz, TRUB1 is the predominant pseudouridine synthase acting on mammalian mRNA via a predictable and conserved code. *Genome Res.* **27**, 393–406 (2017).
19. T. M. Carlile, *et al.*, mRNA structure determines modification by pseudouridine synthase 1. *Nat. Chem. Biol.* **15**, 966–974 (2019).
20. S. Sharma, *et al.*, Yeast Kre33 and human NAT10 are conserved 18S rRNA cytosine acetyltransferases that modify tRNAs assisted by the adaptor Tan1/THUMPD1. *Nucleic Acids Res.* **43**, 2242–2258 (2015).
21. J. Li, *et al.*, Structural basis of regulated m7G tRNA modification by METTL1–WDR4.

Nature **613**, 391–397 (2023).
22. T. Pan, Modifications and functional genomics of human transfer RNA. *Cell Res.* (2018) https:/doi.org/10.1038/s41422-018-0013-y.
23. F. Tuorto, F. Lyko, Genome recoding by tRNA modifications. *Open Biol.* (2016) https:/doi.org/10.1098/rsob.160287.
24. M. Pereira, *et al.*, Impact of tRNA modifications and tRNA-modifying enzymes on proteostasis and human disease. *Int. J. Mol. Sci.* (2018) https:/doi.org/10.3390/ijms19123738.
25. S. Sekar, *et al.*, Alzheimer's disease is associated with altered expression of genes involved in immune response and mitochondrial processes in astrocytes. *Neurobiol. Aging* **36**, 583–591 (2015).
26. R. Shaheen, *et al.*, A homozygous truncating mutation in PUS3 expands the role of tRNA modification in normal cognition. *Hum. Genet.* (2016) https:/doi.org/10.1007/s00439-016-1665-7.
27. J. M. Dewe, B. L. Fuller, J. M. Lentini, S. M. Kellner, D. Fu, TRMT1-catalyzed tRNA modifications are required for redox homeostasis to ensure proper cellular proliferation and oxidative stress survival. *Mol. Cell. Biol.* **37**, MCB.00214-17 (2017).
28. K. Zhang, *et al.*, An intellectual disability-associated missense variant in TRMT1 impairs tRNA modification and reconstitution of enzymatic activity. *Hum. Mutat.* (2020) https:/doi.org/10.1002/humu.23976.
29. N. Dyubankova, *et al.*, Contribution of dihydrouridine in folding of the D-arm in tRNA. *Org. Biomol. Chem.* (2015) https:/doi.org/10.1039/c5ob00164a.
30. D. R. Davis, Stabilization of RNA stacking by pseudouridine. *Nucleic Acids Res.* (1995) https:/doi.org/10.1093/nar/23.24.5020.
31. P. C. Durant, D. R. Davis, Stabilization of the anticodon stem-loop of tRNA(Lys,3) by an A+-C base-pair and by pseudouridine. *J. Mol. Biol.* **285**, 115–131 (1999).
32. M. I. Newby, N. L. Greenbaum, A conserved pseudouridine modification in eukaryotic U2 snRNA induces a change in branch-site architecture. *RNA* **7**, 833–845 (2001).
33. M. I. Newby, N. L. Greenbaum, Investigation of Overhauser effects between pseudouridine and water protons in RNA helices. *Proc. Natl. Acad. Sci. U. S. A.* **99**, 12697–12702 (2002).
34. Y. Xu, K. Vanommeslaeghe, A. Aleksandrov, A. D. MacKerell, L. Nilsson, Additive CHARMM force field for naturally occurring modified ribonucleotides. *J. Comput. Chem.* (2016) https:/doi.org/10.1002/jcc.24307.
35. J. Anderson, *et al.*, The essential Gcd10p-Gcd14p nuclear complex 15 required for 1-methyladenosine modification and maturation of initiator methionyl-tRNA. *Genes Dev.* **12**, 3650–3662 (1998).
36. J. Edqvist, K. B. Ståby, H. Grosjean, Enzymatic formation of N2,N2-dimethylguanosine in eukaryotic tRNA: Importance of the tRNA architecture. *Biochimie* (1995) https:/doi.org/10.1016/0300-9084(96)88104-1.
37. K. D. Sonawane, R. S. Bavi, S. B. Sambhare, P. M. Fandilolu, Comparative Structural Dynamics of tRNAPhe with Respect to Hinge Region Methylated Guanosine: A Computational Approach. *Cell Biochem. Biophys.* (2016) https:/doi.org/10.1007/s12013-016-0731-z.
38. A. Vakiloroayaei, N. S. Shah, M. Oeffinger, M. A. Bayfield, The RNA chaperone La promotes pre-tRNA maturation via indiscriminate binding of both native and misfolded

targets. *Nucleic Acids Res.* **45**, 11341–11355 (2017).
39. A. G. Arimbasseri, *et al.*, RNA Polymerase III Output Is Functionally Linked to tRNA Dimethyl-G26 Modification. *PLoS Genet.* **11**, e1005671 (2015).
40. E. Westhof, P. Dumas, D. Moras, Restrained refinement of two crystalline forms of yeast aspartic acid and phenylalanine transfer RNA crystals. *Acta Crystallogr. Sect. A* **44**, 112–123 (1988).
41. J. Porat, U. Kothe, M. A. Bayfield, Revisiting tRNA chaperones: New players in an ancient game. *RNA* **27**, 543–559 (2021).
42. P. Mitchell, E. Petfalski, A. Shevchenko, M. Mann, D. Tollervey, The exosome: A conserved eukaryotic RNA processing complex containing multiple 3'→5' exoribonucleases. *Cell* (1997) https:/doi.org/10.1016/S0092-8674(00)80432-8.
43. J. LaCava, *et al.*, RNA degradation by the exosome is promoted by a nuclear polyadenylation complex. *Cell* (2005) https:/doi.org/10.1016/j.cell.2005.04.029.
44. F. Wyers, *et al.*, Cryptic Pol II transcripts are degraded by a nuclear quality control pathway involving a new poly(A) polymerase. *Cell* (2005) https:/doi.org/10.1016/j.cell.2005.04.030.
45. S. Hamill, S. L. Wolin, K. M. Reinisch, Structure and function of the polymerase core of TRAMP, a RNA surveillance complex. *Proc. Natl. Acad. Sci. U. S. A.* (2010) https:/doi.org/10.1073/pnas.1003505107.
46. S. Kadaba, *et al.*, Nuclear surveillance and degradation of hypomodified initiator tRNA Met in S. cerevisiae. *Genes Dev.* **18**, 1227–1240 (2004).
47. S. Kadaba, X. Wang, J. T. Anderson, Nuclear RNA surveillance in Saccharomyces cerevisiae: Trf4p-dependent polyadenylation of nascent hypomethylated tRNA and an aberrant form of 5S rRNA. *RNA* (2006) https:/doi.org/10.1261/rna.2305406.
48. Y. Huang, M. A. Bayfield, R. V. Intine, R. J. Maraia, Separate RNA-binding surfaces on the multifunctional la protein mediate distinguishable activities in tRNA maturation. *Nat. Struct. Mol. Biol.* **13**, 611–618 (2006).
49. A. Alexandrov, *et al.*, Rapid tRNA decay can result from lack of nonessential modifications. *Mol. Cell* (2006) https:/doi.org/10.1016/j.molcel.2005.10.036.
50. I. Chernyakov, J. M. Whipple, L. Kotelawala, E. J. Grayhack, E. M. Phizicky, Degradation of several hypomodified mature tRNA species in Saccharomyces cerevisiae is mediated by Met22 and the 5′-3′ exonucleases Rat1 and Xrn1. *Genes Dev.* (2008) https:/doi.org/10.1101/gad.1654308.
51. J. M. Whipple, E. A. Lane, I. Chernyakov, S. D'Silva, E. M. Phizicky, The yeast rapid tRNA decay pathway primarily monitors the structural integrity of the acceptor and T-stems of mature tRNA. *Genes Dev.* (2011) https:/doi.org/10.1101/gad.2050711.
52. Z. Li, S. Reimers, S. Pandit, M. P. Deutscher, RNA quality control: Degradation of defective transfer RNA. *EMBO J.* (2002) https:/doi.org/10.1093/emboj/21.5.1132.
53. J. Houseley, J. LaCava, D. Tollervey, RNA-quality control by the exosome. *Nat. Rev. Mol. Cell Biol.* (2006) https:/doi.org/10.1038/nrm1964.
54. K. M. Reinisch, S. L. Wolin, Emerging themes in non-coding RNA quality control. *Curr. Opin. Struct. Biol.* (2007) https:/doi.org/10.1016/j.sbi.2007.03.012.
55. J. Urbonavičius, J. M. B. Durand, G. R. Björk, Three modifications in the D and T arms of tRNA influence translation in Escherichia coli and expression of virulence genes in Shigella flexneri. *J. Bacteriol.* (2002) https:/doi.org/10.1128/JB.184.19.5348-5357.2002.
56. J. Rinke, J. A. Steitz, Association of the lupus antigen La with a subset of U6 snRNA

molecules. *Nucleic Acids Res.* **13**, 2617–2629 (1985).
57. V. Shchepachev, H. Wischnewski, E. Missiaglia, C. Soneson, C. M. Azzalin, Mpn1, Mutated in Poikiloderma with Neutropenia Protein 1, Is a Conserved 3'-to-5' RNA Exonuclease Processing U6 Small Nuclear RNA. *Cell Rep.* **2**, 855–865 (2012).
58. V. Shchepachev, H. Wischnewski, C. Soneson, A. W. Arnold, C. M. Azzalin, Human Mpn1 promotes post-transcriptional processing and stability of U6atac. *FEBS Lett.* **589**, 2417–2423 (2015).
59. A. L. Didychuk, *et al.*, Usb1 controls U6 snRNP assembly through evolutionarily divergent cyclic phosphodiesterase activities. *Nat. Commun.* **8**, 497 (2017).
60. E. J. Montemayor, *et al.*, Molecular basis for the distinct cellular functions of the Lsm1-7 and Lsm2-8 complexes. *RNA* **26**, 1400–1413 (2020).
61. E. J. Montemayor, *et al.*, Architecture of the U6 snRNP reveals specific recognition of 3′-end processed U6 snRNA. *Nat. Commun.* **9** (2018).
62. J. Mouaikel, C. Verheggen, E. Bertrand, J. Tazi, R. Bordonné, Hypermethylation of the cap structure of both yeast snRNAs and snoRNAs requires a conserved methyltransferase that is localized to the nucleolus. *Mol. Cell* **9**, 891–901 (2002).
63. Y. T. Yu, M. Di Shu, J. A. Steitz, Modifications of U2 snRNA are required for snRNP assembly and pre-mRNA splicing. *EMBO J.* **19**, 5783–5795 (1998).
64. C. Jeronimo, *et al.*, Systematic Analysis of the Protein Interaction Network for the Human Transcription Machinery Reveals the Identity of the 7SK Capping Enzyme. *Mol. Cell* **27**, 262–274 (2007).
65. J. Gu, J. R. Patton, S. Shimba, R. Reddy, Localization of modified nucleotides in Schizosaccharomyces pombe spliceosomal small nuclear RNAs: Modified nucleotides are clustered in functionally important regions. *RNA* **2**, 909–918 (1996).
66. S. Shimba, R. Reddy, Purification of human U6 small nuclear RNA capping enzyme. Evidence for a common capping enzyme for γ-monomethyl-capped small RNAs. *J. Biol. Chem.* (1994).
67. R. Singh, R. Reddy, y-Monomethyl phosphate: A cap structure in spliceosomal U6 small nuclear RNA (mRNA splicing/RNA processing/RNA modification). *Proc. Nadl. Acad. Sci. USA* **86**, 8280–8283 (1989).
68. J. Porat, M. El Baidouri, J. Grigull, J.-M. Deragon, M. A. Bayfield, The methyl phosphate capping enzyme Bmc1/Bin3 is a stable component of the fission yeast telomerase holoenzyme. *Nat. Commun.* **13**, 1277 (2022).
69. S. Shuman, Transcriptional Networking Cap-tures the 7SK RNA 5′-γ-Methyltransferase. *Mol. Cell* **4**, 517–519 (2007).
70. S. M. Fica, *et al.*, RNA catalyzes nuclear pre-mRNA splicing. *Nature* **503**, 229 (2013).
71. S. Shimba, J. A. Bokar, F. Rottman, R. Reddy, Accurate and efficient N-6-adenosine methylation in spliceosomal U6 small nucelar RNA by HeLa cell extract in vitro. *Nucleic Acids Res.* **23**, 2421–2426 (1995).
72. A. S. Warda, *et al.*, Human METTL16 is a N 6 -methyladenosine (m 6 A) methyltransferase that targets pre-mRNAs and various non-coding RNAs. *EMBO Rep.* **18**, 2004–2014 (2017).
73. K. E. Pendleton, *et al.*, The U6 snRNA m6A Methyltransferase METTL16 Regulates SAM Synthetase Intron Retention. *Cell* (2017) https:/doi.org/10.1016/j.cell.2017.05.003.
74. Y. Ishigami, T. Ohira, Y. Isokawa, Y. Suzuki, T. Suzuki, A single m6A modification in U6 snRNA diversifies exon sequence at the 5' splice site. *Nat. Commun.* **12**, 3244 (2021).

75. M. T. Parker, *et al.*, m{6}A modification of U6 snRNA modulates usage of two major classes of pre-mRNA 5' splice site. *Elife* **11**, e78808 (2022).
76. J. Liang, *et al.*, Small Nucleolar RNAs: Insight Into Their Function in Cancer. *Front. Oncol.* **9**, 587 (2019).
77. T. Kiss, E. Fayet-Lebaron, B. E. Jády, Box H/ACA Small Ribonucleoproteins. *Mol. Cell* **37**, 597–606 (2010).
78. P. Ganot, B. E. Jády, M.-L. Bortolin, X. Darzacq, T. Kiss, Nucleolar Factors Direct the 2′-O-Ribose Methylation and Pseudouridylation of U6 Spliceosomal RNA. *Mol. Cell. Biol.* **19**, 6906–6917 (1999).
79. K. T. Tycowski, Z. H. You, P. J. Graham, J. A. Steitz, Modification of U6 spliceosomal RNA is guided by other small RNAs. *Mol. Cell* **2**, 629–638 (1998).
80. H. Zhou, Y. Q. Chen, Y. P. Du, L. H. Qu, The Schizosaccharomyces pombe mgU6-47 gene is required for 2′-O-methylation of U6 snRNA at A41. *Nucleic Acids Res.* **30**, 894–902 (2002).
81. G. Wu, *et al.*, Pseudouridines in U2 snRNA stimulate the ATPase activity of Prp5 during spliceosome assembly. *EMBO J.* **35**, 654–667 (2016).
82. D. Gilley, E. H. Blackburn, The telomerase RNA pseudoknot is critical for the stable assembly of a catalytically active ribonucleoprotein. *Proc. Natl. Acad. Sci. U. S. A.* **96**, 6621–6625 (1999).
83. C. W. Greider, E. H. Blackburn, Identification of a specific telomere terminal transferase activity in tetrahymena extracts. *Cell* **43**, 405–413 (1985).
84. C. W. Greider, E. H. Blackburn, A telomeric sequence in the RNA of Tetrahymena telomerase required for telomere repeat synthesis. *Nature* **337**, 331–337 (1989).
85. J. Lingner, L. L. Hendrick, T. R. Cech, Telomerase RNAs of different ciliates have a common secondary structure and a permuted template. *Genes Dev.* **8**, 1984–1998 (1994).
86. J. Wu, *et al.*, A novel hypoxic stress-responsive long non-coding RNA transcribed by RNA polymerase III in Arabidopsis. *RNA Biol.* **9**, 302–313 (2012).
87. J. Song, *et al.*, The conserved structure of plant telomerase RNA provides the missing link for an evolutionary pathway from ciliates to humans. *Proc. Natl. Acad. Sci. U. S. A.* **116**, 24542–24550 (2019).
88. P. Fajkus, *et al.*, Telomerase RNA in Hymenoptera (Insecta) switched to plant/ciliate-like biogenesis. *Nucleic Acids Res.* **51**, 420–433 (2023).
89. J. Feng, *et al.*, The RNA component of human telomerase. *Science (80-.).* **269**, 1236–1241 (1995).
90. D. Fu, K. Collins, Human telomerase and Cajal body ribonucleoproteins share a unique specificity of Sm protein association. *Genes Dev.* **20**, 531–536 (2006).
91. A. G. Seto, A. J. Zaug, S. G. Sobel, S. L. Wolin, T. R. Cech, Saccharomyces cerevisiae telomerase is an Sm small nuclear ribonucleoprotein particle. *Nature* **401**, 177–180 (1999).
92. J. Leonardi, J. A. Box, J. T. Bunch, P. Baumann, TER1, the RNA subunit of fission yeast telomerase. *Nat. Struct. Mol. Biol.* **15**, 26–33 (2008).
93. C. J. Webb, V. A. Zakian, Identification and characterization of the Schizosaccharomyces pombe TER1 telomerase RNA. *Nat. Struct. Mol. Biol.* **15**, 34–42 (2008).
94. W. Tang, R. Kannan, M. Blanchette, P. Baumann, Telomerase RNA biogenesis involves sequential binding by Sm and Lsm complexes. *Nature* **484**, 260–264 (2012).
95. S. K. Gupta, *et al.*, The Trypanosoma brucei telomerase RNA (TER) homologue binds

core proteins of the C/D snoRNA family. *FEBS Lett.* **587**, 1399–1404 (2013).
96. J. D. Podlevsky, Y. Li, J. J. L. Chen, The functional requirement of two structural domains within telomerase RNA emerged early in eukaryotes. *Nucleic Acids Res.* **44**, 9891–9901 (2016).
97. D. Logeswaran, *et al.*, Biogenesis of telomerase RNA from a protein-coding mRNA precursor. *Proc. Natl. Acad. Sci. U. S. A.* **119**, e2204636119 (2022).
98. D. Nguyen, *et al.*, A Polyadenylation-Dependent 3′ End Maturation Pathway Is Required for the Synthesis of the Human Telomerase RNA. *Cell Rep.* **13**, 2244–2257 (2015).
99. C. K. Tseng, *et al.*, Human Telomerase RNA Processing and Quality Control. *Cell Rep.* **13**, 2232–2243 (2015).
100. C. K. Tseng, H. F. Wang, M. R. Schroeder, P. Baumann, The H/ACA complex disrupts triplex in hTR precursor to permit processing by RRP6 and PARN. *Nat. Commun.* **9**, 5430 (2018).
101. J. A. Box, J. T. Bunch, W. Tang, P. Baumann, Spliceosomal cleavage generates the 3′ end of telomerase RNA. *Nature* **456**, 910–914 (2008).
102. R. Kannan, *et al.*, Intronic sequence elements impede exon ligation and trigger a discard pathway that yields functional telomerase RNA in fission yeast. *Genes Dev.* **27**, 627–638 (2013).
103. H. Hermann, *et al.*, snRNP Sm proteins share two evolutionarily conserved sequence motifs which are involved in Sm protein-protein interactions. *EMBO J.* **14**, 2076–2088 (1995).
104. A. R. Naeeni, M. R. Conte, M. A. Bayfield, RNA chaperone activity of human La protein is mediated by variant RNA recognition motif. *J. Biol. Chem.* **287**, 5472–5482 (2012).
105. R. H. Hussain, M. Zawawi, M. A. Bayfield, Conservation of RNA chaperone activity of the human La-related proteins 4, 6 and 7. *Nucleic Acids Res.* (2013) https:/doi.org/10.1093/nar/gkt649.
106. M. A. Bayfield, J. Vinayak, K. Kerkhofs, F. Mansouri-Noori, La proteins couple use of sequence-specific and non-specific binding modes to engage RNA substrates. *RNA Biol.* **18**, 168–177 (2019).
107. D. Herschlag, RNA chaperones and the RNA folding problem. *J. Biol. Chem.* **270**, 20871–20874 (1995).
108. L. Rajkowitsch, *et al.*, RNA chaperones, RNA annealers and RNA helicases. *RNA Biol.* **4**, 118–130 (2007).
109. J. Rinke, J. A. Steitz, Precursor molecules of both human 5S ribosomal RNA and transfer RNAs are bound by a cellular protein reactive with anti-La Lupus antibodies. *Cell* (1982) https:/doi.org/10.1016/0092-8674(82)90099-X.
110. J. E. Stefano, Purified lupus antigen la recognizes an oligouridylate stretch common to the 3′ termini of RNA polymerase III transcripts. *Cell* **36**, 145–154 (1984).
111. M. B. Mathews, A. M. Francoeur, La antigen recognizes and binds to the 3'-oligouridylate tail of a small RNA. *Mol. Cell. Biol.* **4**, 1134–1140 (1984).
112. M. Teplova, *et al.*, Structural basis for recognition and sequestration of UUUOH 3′ temini of nascent RNA polymerase III transcripts by La, a rheumatic disease autoantigen. *Mol. Cell* **21**, 75–85 (2006).
113. M. A. Bayfield, R. J. Maraia, Precursor-product discrimination by la protein during tRNA metabolism. *Nat. Struct. Mol. Biol.* **16**, 430–437 (2009).
114. S. Horke, K. Reumann, C. Schulze, F. Grosse, T. Heise, The La motif and the RNA

recognition motifs of human La Autoantigen contribute individually to RNA recognition and subcellular localization. *J. Biol. Chem.* **279**, 50302–50309 (2004).
115. S. Horke, K. Reumann, M. Schweizer, H. Will, T. Heise, Nuclear trafficking of la protein depends on a newly identified nucleolar localization signal and the ability to bind RNA. *J. Biol. Chem.* **279**, 26563–26570 (2004).
116. A. Belisova, *et al.*, RNA chaperone activity of protein components of human Ro RNPs. *RNA* **11**, 1084–1094 (2005).
117. L. C. Keffer-Wilkes, G. R. Veerareddygari, U. Kothe, RNA modification enzyme TruB is a tRNA chaperone. *Proc. Natl. Acad. Sci. U. S. A.* **113**, 14306–14311 (2016).
118. L. C. Keffer-Wilkes, E. F. Soon, U. Kothe, The methyltransferase TrmA facilitates tRNA folding through interaction with its RNA-binding domain. *Nucleic Acids Res.* **48**, 7981–7990 (2020).
119. S. K.-L. Schultz, U. Kothe, tRNA elbow modifications affect the tRNA pseudouridine synthase TruB and the methyltransferase TrmA. *RNA* **26**, 1131–1142 (2020).
120. K. L. Witkin, K. Collins, Holoenzyme proteins required for the physiological assembly and activity of telomerase. *Genes Dev.* **18**, 1107–1118 (2004).
121. R. Prathapam, K. L. Witkin, C. M. O'Connor, K. Collins, A telomerase holoenzyme protein enhances telomerase RNA assembly with telomerase reverse transcriptase. *Nat. Struct. Mol. Biol.* **12**, 252–257 (2005).
122. M. Singh, *et al.*, Structural Basis for Telomerase RNA Recognition and RNP Assembly by the Holoenzyme La Family Protein p65. *Mol. Cell* **47**, 16–26 (2012).
123. J.-M. M. Deragon, Distribution, organization an evolutionary history of La and LARPs in eukaryotes. *RNA Biol.* **18**, 1–9 (2020).
124. N. He, *et al.*, A La-Related Protein Modulates 7SK snRNP Integrity to Suppress P-TEFb-Dependent Transcriptional Elongation and Tumorigenesis. *Mol. Cell* **29**, 588–599 (2008).
125. B. J. Krueger, *et al.*, LARP7 is a stable component of the 7SK snRNP while P-TEFb, HEXIM1 and hnRNP A1 are reversibly associated. *Nucleic Acids Res.* **36**, 2219–2229 (2008).
126. A. Markert, *et al.*, The La-related protein LARP7 is a component of the 7SK ribonucleoprotein and affects transcription of cellular and viral polymerase II genes. *EMBO Rep.* **9**, 569–575 (2008).
127. V. T. Nguyen, T. Kiss, A. A. Michels, O. Bensaude, 7SK small nuclear RNA binds to and inhibits the activity of CDK9/cyclin T complexes. *Nature* **414**, 322–325 (2001).
128. Z. Yang, Q. Zhu, K. Luo, Q. Zhou, The 7SK small nuclear RNA inhibits the CDK9/cyclin T1 kinase to control transcription. *Nature* **414**, 317–322 (2001).
129. Y. Yang, *et al.*, Structural basis of RNA conformational switching in the transcriptional regulator 7SK RNP. *Mol. Cell* **82**, 1724-1736.e7 (2022).
130. S. W. Olson, *et al.*, Discovery of a large-scale, cell-state-responsive allosteric switch in the 7SK RNA using DANCE-MaP. *Mol. Cell* **82**, 1708-1723.e10 (2022).
131. D. Hasler, *et al.*, The Alazami Syndrome-Associated Protein LARP7 Guides U6 Small Nuclear RNA Modification and Contributes to Splicing Robustness. *Mol. Cell* **77**, 1014-1031.e13 (2020).
132. X. Wang, *et al.*, LARP7-Mediated U6 snRNA Modification Ensures Splicing Fidelity and Spermatogenesis in Mice. *Mol. Cell* **77**, 999-1013.e6 (2020).
133. B. C. Persson, C. Gustafsson, D. E. Berg, G. R. Björk, The gene for a tRNA modifying enzyme, m5U54-methyltransferase, is essential for viability in Escherichia coli. *Proc.*

Natl. Acad. Sci. U. S. A. **89**, 3995–3998 (1992).
134. N. Gutgsell, *et al.*, Deletion of the Escherichia coli pseudouridine synthase gene truB blocks formation of pseudouridine 55 in tRNA in vivo, does not affect exponential growth, but confers a strong selective disadvantage in competition with wild-type cells. *RNA* **6**, 1870–1881 (2000).
135. M. J. O. Johansson, A. S. Byström, Dual function of the tRNA(m5U54)methyltransferase in tRNA maturation. *RNA* **8**, 324–335 (2002).
136. H. Grosjean, Fine-tuning of RNA functions by modification and editing. *Top. Curr. Genet.*, 442 (2005).
137. D. L. J. Lafontaine, D. Tollervey, "Regulatory Aspects of rRNA Modification and Pre-rRNA Processing" in *Modification and Editing of RNA*, (American Society of Microbiology, 2014), pp. 281–288.
138. D. Lafontaine, J. Vandenhaute, D. Tollervey, The 18S rRNA dimethylase Dim1p is required for pre-ribosomal RNA processing in yeast. *Genes Dev.* **9**, 2470–2481 (1995).
139. N. S. Gutgsell, M. Del Campo, S. Raychaudhuri, J. Ofengand, A second function for pseudouridine synthases: A point mutant of RluD unable to form pseudouridines 1911, 1915, and 1917 in Escherichia coli 23S ribosomal RNA restores normal growth to an RluD-minus strain. *RNA* **7**, 990–998 (2001).
140. M. O'Connor, S. T. Gregory, Inactivation of the RluD pseudouridine synthase has minimal effects on growth and ribosome function in wild-type Escherichia coli and Salmonella enterica. *J. Bacteriol.* **193**, 154–162 (2011).
141. C. Hoang, A. R. Ferré-D'Amaré, Cocrystal structure of a tRNA Ψ55 pseudouridine synthase: Nucleotide flipping by an RNA-modifying enzyme. *Cell* **107**, 929–939 (2001).
142. J. R. Wright, L. C. Keffer-Wilkes, S. R. Dobing, U. Kothe, Pre-steady-state kinetic analysis of the three Escherichia coli pseudouridine synthases TruB, TruA, and RluA reveals uniformly slow catalysis. *RNA* (2011) https:/doi.org/10.1261/rna.2905811.
143. C. Hoang, *et al.*, Crystal structure of pseudouridine synthase RluA: Indirect sequence readout through protein-induced RNA structure. *Mol. Cell* **24**, 535–545 (2006).
144. A. Alian, T. T. Lee, S. L. Griner, R. M. Stroud, J. Finer-Moore, Structure of a TrmA-RNA complex: A consensus RNA fold contributes to substrate selectivity and catalysis in m5U methyltransferases. *Proc. Natl. Acad. Sci. U. S. A.* **105**, 6876–6881 (2008).
145. L. A. Copela, G. Chakshusmathi, R. L. Sherrer, S. L. Wolin, The La protein functions redundantly with tRNA modification enzymes to ensure tRNA structural stability. *RNA* **12**, 644–654 (2006).
146. E. H. Blackburn, K. Collins, Telomerase: An RNP enzyme synthesizes DNA. *Cold Spring Harb. Perspect. Biol.* (2011) https:/doi.org/10.1101/cshperspect.a003558.
147. K. Collins, The biogenesis and regulation of telomerase holoenzymes. *Nat. Rev. Mol. Cell Biol.* (2006) https:/doi.org/10.1038/nrm1961.
148. T. M. Nakamura, *et al.*, Telomerase catalytic subunit homologs from fission yeast and human. *Science (80-.).* (1997) https:/doi.org/10.1126/science.277.5328.955.
149. C. Chapon, T. R. Cech, A. J. Zaug, Polyadenylation of telomerase RNA in budding yeast. *RNA* (1997).
150. C. M. O'Connor, K. Collins, A Novel RNA Binding Domain in Tetrahymena Telomerase p65 Initiates Hierarchical Assembly of Telomerase Holoenzyme. *Mol. Cell. Biol.* (2006) https:/doi.org/10.1128/mcb.26.6.2029-2036.2006.
151. M. Singh, C. P. Choi, J. Feigon, xRRM: A new class of RRM found in the telomerase La

family protein p65. *RNA Biol.* **10**, 353–359 (2013).
152. L. Muniz, S. Egloff, T. Kiss, RNA elements directing in vivo assembly of the 7SK/MePCE/Larp7 transcriptional regulatory snRNP. *Nucleic Acids Res.* (2013) https:/doi.org/10.1093/nar/gkt159.
153. M. S. Cosgrove, Y. Ding, W. A. Rennie, M. J. Lane, S. D. Hanes, The bin3 RNA methyltransferase targets 7SK RNA to control transcription and translation. *Wiley Interdiscip. Rev. RNA* (2012) https:/doi.org/10.1080/09540121.2017.1344767.
154. B. Xhemalce, S. C. Robson, T. Kouzarides, Human RNA methyltransferase BCDIN3D regulates MicroRNA processing. *Cell* (2012) https:/doi.org/10.1016/j.cell.2012.08.041.
155. A. Martinez, *et al.*, Human BCDIN3D monomethylates cytoplasmic histidine transfer RNA. *Nucleic Acids Res.* (2017) https:/doi.org/10.1093/nar/gkx051.
156. M. Marz, *et al.*, Evolution of 7SK RNA and its protein partners in metazoa. *Mol. Biol. Evol.* **26**, 2821–2830 (2009).
157. Y. Yang, C. D. Eichhorn, Y. Wang, D. Cascio, J. Feigon, Structural basis of 7SK RNA 5′-γ-phosphate methylation and retention by MePCE. *Nat. Chem. Biol.* **15**, 132–140 (2019).
158. T. Tani, Y. Ohshima, The gene for the U6 small nuclear RNA in fission yeast has an intron. *Nature* **337**, 87–90 (1989).
159. T. Tani, Y. Ohshima, mRNA-type introns in U6 small nuclear RNA genes: Implications for the catalysis in pre-mRNA splicing. *Genes Dev.* **5**, 1022–1031 (1991).
160. Y. Xue, Z. Yang, R. Chen, Q. Zhou, A capping-independent function of MePCE in stabilizing 7SK snRNA and facilitating the assembly of 7SK snRNP. *Nucleic Acids Res.* (2009) https:/doi.org/10.1093/nar/gkp977.
161. H. T. H. Beernink, K. Miller, A. Deshpande, P. Bucher, J. P. Cooper, Telomere maintenance in fission yeast requires an est1 ortholog. *Curr. Biol.* (2003) https:/doi.org/10.1016/S0960-9822(03)00169-6.
162. C. J. Webb, V. A. Zakian, Schizosaccharomyces pombe Ccq1 and TER1 bind the 14-3-3-like domain of Est1, which promotes and stabilizes telomerase-telomere association. *Genes Dev.* (2012) https:/doi.org/10.1101/gad.181826.111.
163. B. Lemieux, *et al.*, Active Yeast Telomerase Shares Subunits with Ribonucleoproteins RNase P and RNase MRP. *Cell* (2016) https:/doi.org/10.1016/j.cell.2016.04.018.
164. P. D. Garcia, *et al.*, Stability and nuclear localization of yeast telomerase depend on protein components of RNase P/MRP. *Nat. Commun.* (2020) https:/doi.org/10.1038/s41467-020-15875-9.
165. N. Laterreur, *et al.*, The yeast telomerase module for telomere recruitment requires a specific RNA architecture. *RNA* **24** (2018).
166. D. J. Paez-Moscoso, *et al.*, A putative cap binding protein and the methyl phosphate capping enzyme Bin3/MePCE function in telomerase biogenesis. *bioRxiv*, 2021.12.15.472819 (2021).
167. D. C. Zappulla, T. R. Cech, Yeast telomerase RNA: A flexible scaffold for protein subunits. *Proc. Natl. Acad. Sci. U. S. A.* (2004) https:/doi.org/10.1073/pnas.0403641101.
168. M. Barboric, *et al.*, 7SK snRNP/P-TEFb couples transcription elongation with alternative splicing and is essential for vertebrate development. *Proc. Natl. Acad. Sci. U. S. A.* (2009) https:/doi.org/10.1073/pnas.0903188106.
169. J. Hayles, *et al.*, A genome-wide resource of cell cycle and cell shape genes of fission yeast. *Open Biol.* (2013) https:/doi.org/10.1098/rsob.130053.
170. D. U. Kim, *et al.*, Analysis of a genome-wide set of gene deletions in the fission yeast

Schizosaccharomyces pombe. *Nat. Biotechnol.* (2010) https:/doi.org/10.1038/nbt.1628.
171. N. N. Lee, *et al.*, XMtr4-like protein coordinates nuclear RNA processing for heterochromatin assembly and for telomere maintenance. *Cell* **155** (2013).
172. S. Coy, A. Volanakis, S. Shah, L. Vasiljeva, The Sm Complex Is Required for the Processing of Non-Coding RNAs by the Exosome. *PLoS One* **8** (2013).
173. T. M. Nakamura, J. P. Cooper, T. R. Cech, Two modes of survival of fission yeast without telomerase. *Science (80-.).* **282** (1998).
174. J. R. Mitchell, J. Cheng, K. Collins, A Box H/ACA Small Nucleolar RNA-Like Domain at the Human Telomerase RNA 3′ End. *Mol. Cell. Biol.* (1999) https:/doi.org/10.1128/mcb.19.1.567.
175. A. G. Matera, R. M. Terns, M. P. Terns, Non-coding RNAs: Lessons from the small nuclear and small nucleolar RNAs. *Nat. Rev. Mol. Cell Biol.* (2007) https:/doi.org/10.1038/nrm2124.
176. D. L. J. Lafontaine, C. Bousquet-Antonelli, Y. Henry, M. Caizergues-Ferrer, D. Tollervey, The box H + ACA snoRNAs carry Cbf5p, the putative rRNA pseudouridine synthase. *Genes Dev.* (1998) https:/doi.org/10.1101/gad.12.4.527.
177. J. Bähler, *et al.*, Heterologous modules for efficient and versatile PCR-based gene targeting in Schizosaccharomyces pombe. *Yeast* (1998) https:/doi.org/10.1002/(SICI)1097-0061(199807)14:10<943::AID-YEA292>3.0.CO;2-Y.
178. M. Oeffinger, *et al.*, Comprehensive analysis of diverse ribonucleoprotein complexes. *Nat. Methods* (2007) https:/doi.org/10.1038/nmeth1101.
179. J. Porat, M. A. Bayfield, "Use of tRNA-Mediated Suppression to Assess RNA Chaperone Function" in *RNA Chaperones: Methods and Protocols*, T. Heise, Ed. (Springer US, 2020), pp. 107–120.
180. K. E. Hayes, J. A. Barr, M. Xie, J. A. Steitz, I. Martinez, Immunoprecipitation of Tri-methylated Capped RNA. *Bio-protocol* **8**, e2717 (2018).
181. B. Langmead, S. L. Salzberg, Fast gapped-read alignment with Bowtie 2. *Nat. Methods* **9** (2012).
182. B. Langmead, C. Trapnell, M. Pop, S. L. Salzberg, Ultrafast and memory-efficient alignment of short DNA sequences to the human genome. *Genome Biol.* **10** (2009).
183. Y. Liao, G. K. Smyth, W. Shi, FeatureCounts: An efficient general purpose program for assigning sequence reads to genomic features. *Bioinformatics* **30** (2014).
184. R. Liu, *et al.*, Why weight? Modelling sample and observational level variability improves power in RNA-seq analyses. *Nucleic Acids Res.* **43** (2015).
185. M. D. Robinson, D. J. McCarthy, G. K. Smyth, edgeR: A Bioconductor package for differential expression analysis of digital gene expression data. *Bioinformatics* **26** (2009).
186. J. Cox, M. Mann, MaxQuant enables high peptide identification rates, individualized p.p.b.-range mass accuracies and proteome-wide protein quantification. *Nat. Biotechnol.* (2008) https:/doi.org/10.1038/nbt.1511.
187. R. Drissi, M. L. Dubois, M. Douziech, F. M. Boisvert, Quantitative proteomics reveals dynamic interactions of the minichromosome maintenance complex (MCM) in the cellular response to etoposide induced DNA damage. *Mol. Cell. Proteomics* (2015) https:/doi.org/10.1074/mcp.M115.048991.
188. N. F. Lue, Y. Peng, Identification and characterization of a telomerase activity from Schizosaccharomyces pombe. *Nucleic Acids Res.* **25**, 4331–4337 (1997).
189. L. A. Kelley, S. Mezulis, C. M. Yates, M. N. Wass, M. J. E. Sternberg, The Phyre2 web

portal for protein modeling, prediction and analysis. *Nat. Protoc.* (2015) https:/doi.org/10.1038/nprot.2015.053.
190. W. L. DeLano, The PyMOL Molecular Graphics System, Version 1.8. *Schrödinger LLC* (2014) https:/doi.org/10.1038/hr.2014.17.
191. F. Sievers, D. G. Higgins, Clustal Omega. *Curr. Protoc. Bioinforma.* (2014) https:/doi.org/10.1002/0471250953.bi0313s48.
192. B. Buchfink, C. Xie, D. H. Huson, Fast and sensitive protein alignment using DIAMOND. *Nat. Methods* (2014) https:/doi.org/10.1038/nmeth.3176.
193. V. Miele, S. Penel, L. Duret, Ultra-fast sequence clustering from similarity networks with SiLiX. *BMC Bioinformatics* (2011) https:/doi.org/10.1186/1471-2105-12-116.
194. M. N. Price, P. S. Dehal, A. P. Arkin, FastTree 2 - Approximately maximum-likelihood trees for large alignments. *PLoS One* (2010) https:/doi.org/10.1371/journal.pone.0009490.
195. S. Mirarab, *et al.*, ASTRAL: Genome-scale coalescent-based species tree estimation in *Bioinformatics*, (2014) https:/doi.org/10.1093/bioinformatics/btu462.
196. Y. Perez-Riverol, *et al.*, The PRIDE database and related tools and resources in 2019: Improving support for quantification data. *Nucleic Acids Res.* (2019) https:/doi.org/10.1093/nar/gky1106.
197. M. E. Wilkinson, C. Charenton, K. Nagai, RNA Splicing by the Spliceosome. *Annu. Rev. Biochem.* **89**, 359–388 (2020).
198. I. Cvitkovic, M. S. Jurica, Spliceosome database: a tool for tracking components of the spliceosome. *Nucleic Acids Res.* **41** (2013).
199. K. Eysmont, *et al.*, Rearrangements within the U6 snRNA Core during the Transition between the Two Catalytic Steps of Splicing. *Mol. Cell* **75**, 538-548.e3 (2019).
200. A. L. Didychuk, S. E. Butcher, D. A. Brow, The life of U6 small nuclear RNA, from cradle to grave. *RNA* **24**, 437–460 (2018).
201. D. A. Brow, C. Guthrie, Spliceosomal RNA U6 is remarkably conserved from yeast to mammals. *Nature* **334**, 213–218 (1988).
202. R. Singh, R., Gupta, S., and Reddy, Capping of mammalian U6 small nuclear RNA in vitro is directed by a conserved stem-loop and AUAUAC sequence: conversion of a noncapped RNA into a capped RNA. *Mol. Cell. Biol.* **10**, 939–946 (1990).
203. A. Huppler, L. J. Nikstad, A. M. Allmann, D. A. Brow, S. E. Butcher, Metal binding and base ionization in the u6 rna intramolecular stem-loop structure. *Nat. Struct. Biol.* **9**, 431–435 (2002).
204. R. Reddy, H. Busch, "Small Nuclear RNAs: RNA Sequences, Structure, and Modifications" in *Structure and Function of Major and Minor Small Nuclear Ribonucleoprotein Particles*, (1988) https:/doi.org/10.1007/978-3-642-73020-7_1.
205. J. Potashkin, D. Frendewey, Splicing of the U6 RNA precursor is impaired in fission yeast pre-mRNA splicing mutants. *Nucleic Acids Res.* **17**, 7821–7831 (1989).
206. D. Frendewey, I. Barta, M. Gillespie, J. Potashkin, Schizosaccharomyces U6 genes have a sequence within their introns that matches the B box consensus of tRNA internal promoters. *Nucleic Acids Res.* **18**, 2025–2032 (1990).
207. D. A. Brow, C. Guthrie, Splicing a spliceosomal RNA. *Nature* **337**, 14–15 (1989).
208. X. Fu, *et al.*, Identification of transient intermediates during spliceosome activation by single molecule fluorescence microscopy. *Proc. Natl. Acad. Sci. U. S. A.* **119**, e2206815119 (2022).
209. D. J. Páez-Moscoso, *et al.*, A putative cap binding protein and the methyl phosphate

capping enzyme Bin3/MePCE function in telomerase biogenesis. *Nat. Commun.* **13**, 1067 (2022).
210. T. M. Lowe, S. R. Eddy, A computational screen for methylation guide snoRNAs in yeast. *Science (80-.).* **283**, 1168–1171 (1999).
211. Y. T. Yu, M. Di Shu, J. A. Steitz, A new method for detecting sites of 2′-O-methylation in RNA molecules. *RNA* **3**, 324–331 (1997).
212. E. Calo, *et al.*, RNA helicase DDX21 coordinates transcription and ribosomal RNA processing. *Nature* **518**, 249–253 (2015).
213. R. W. Van Nues, *et al.*, Box C/D snoRNP catalysed methylation is aided by additional pre-rRNA base-pairing. *EMBO J.* **30**, 2420 (2011).
214. R. W. van Nues, N. J. Watkins, Unusual C′/D′ motifs enable box C/D snoRNPs to modify multiple sites in the same rRNA target region. *Nucleic Acids Res.* **45**, 2016–2028 (2017).
215. T. Huang, J. Vilardell, C. C. Query, Pre-spliceosome formation in S.pombe requires a stable complex of SF1-U2AF59-U2AF23. *EMBO J.* **21**, 5516–5526 (2002).
216. W. Chen, *et al.*, Endogenous U2•U5•U6 snRNA complexes in S. pombe are intron lariat spliceosomes. *RNA* **20**, 308–320 (2014).
217. P. Prusiner, N. Yathindra, M. Sundaralingam, Effect of ribose O(2′)-methylation on the conformation of nucleosides and nucleotides. *BBA Sect. Nucleic Acids Protein Synth.* **366**, 115–123 (1974).
218. G. Kawai, *et al.*, Conformational Rigidity of Specific Pyrimidine Residues in tRNA Arises from Posttranscriptional Modifications That Enhance Steric Interaction between the Base and the 2′-Hydroxyl Group. *Biochemistry* **31**, 1040–1046 (1992).
219. H. Abou Assi, *et al.*, 2′-O-Methylation can increase the abundance and lifetime of alternative RNA conformational states. *Nucleic Acids Res.* **48**, 12365–12379 (2021).
220. A. Ghetti, M. Company, J. Abelson, Specificity of Prp24 binding to RNA: A role for Prp24 in the dynamic interaction of U4 and U6 snRNAs. *RNA* **1**, 132–145 (1995).
221. S. Martin-Tumasz, A. C. Richie, L. J. Clos, D. A. Brow, S. E. Butcher, A novel occluded RNA recognition motif in Prp24 unwinds the U6 RNA internal stem loop. *Nucleic Acids Res.* **39**, 7837–7847 (2011).
222. J. Jumper, *et al.*, Highly accurate protein structure prediction with AlphaFold. *Nature* **596**, 583–589 (2021).
223. C. Lorenzi, *et al.*, IRFinder-S: a comprehensive suite to discover and explore intron retention. *Genome Biol.* **22**, 307 (2021).
224. L. Schärfen, *et al.*, Identification of Alternative Polyadenylation in Cyanidioschyzon merolae Through Long-Read Sequencing of mRNA. *Front. Genet.* **12**, 818697 (2022).
225. A. R. Awan, A. Manfredo, J. A. Pleiss, Lariat sequencing in a unicellular yeast identifies regulated alternative splicing of exons that are evolutionarily conserved with humans. *Proc. Natl. Acad. Sci. U. S. A.* **110**, 12762–12767 (2013).
226. R. Shalgi, J. A. Hurt, S. Lindquist, C. B. Burge, Widespread Inhibition of Posttranscriptional Splicing Shapes the Cellular Transcriptome following Heat Shock. *Cell Rep.* **7**, 1362–1370 (2014).
227. M. A. Gildea, Z. W. Dwyer, J. A. Pleiss, Transcript-specific determinants of pre-mRNA splicing revealed through in vivo kinetic analyses of the 1st and 2nd chemical steps. *Mol. Cell* **82**, 2967-2981.e6 (2022).
228. J. D. Barrass, *et al.*, Transcriptome-wide RNA processing kinetics revealed using extremely short 4tU labeling. *Genome Biol.* **16**, 282 (2015).

229. G. Melangath, *et al.*, Functions for fission yeast splicing factors SpSlu7 and SpPrp18 in alternative splice-site choice and stress-specific regulated splicing. *PLoS One* **12**, e0188159 (2017).
230. C. Ji, *et al.*, Interaction of 7SK with the Smn complex modulates snRNP production. *Nat. Commun.* **12**, 1278 (2021).
231. S. D. Rader, C. Guthrie, A conserved Lsm-interaction motif in Prp24 required for efficient U4/U6 di-snRNP formation. *RNA* **8**, 1378–1392 (2002).
232. Z. Kuang, J. Boeke, S. Canzar, The dynamic landscape of fission yeast meiosis alternative-splice isoforms. *Genome Res.* **27**, 145–156 (2017).
233. J. Montañés, *et al.*, Native RNA sequencing in fission yeast reveals frequent alternative splicing isoforms. *Genome Res.* **32**, 1215–1227 (2022).
234. C. D. Eichhorn, Y. Yang, L. Repeta, J. Feigon, Structural basis for recognition of human 7SK long noncoding RNA by the La-related protein Larp7. *Proc. Natl. Acad. Sci. U. S. A.* **115**, E6457–E6466 (2018).
235. N. J. Kucera, M. E. Hodsdon, S. L. Wolin, An intrinsically disordered C terminus allows the la protein to assist the biogenesis of diverse noncoding RNA precursors. *Proc. Natl. Acad. Sci. U. S. A.* **108**, 1308–1313 (2011).
236. K. A. Brown, *et al.*, Distinct Dynamic Modes Enable the Engagement of Dissimilar Ligands in a Promiscuous Atypical RNA Recognition Motif. *Biochemistry* **55**, 7141–7150 (2016).
237. J. E. Burke, S. E. Butcher, D. A. Brow, Spliceosome assembly in the absence of stable U4/U6 RNA pairing. *RNA* **21**, 923–934 (2015).
238. M. L. Rodgers, A. L. Didychuk, S. E. Butcher, D. A. Brow, A. A. Hoskins, A multi-step model for facilitated unwinding of the yeast U4/U6 RNA duplex. *Nucleic Acids Res.* **44**, 10912–10928 (2016).
239. M. I. Love, W. Huber, S. Anders, Moderated estimation of fold change and dispersion for RNA-seq data with DESeq2. *Genome Biol.* **15**, 550 (2014).
240. A. R. Quinlan, I. M. Hall, BEDTools: A flexible suite of utilities for comparing genomic features. *Bioinformatics* **26**, 841–842 (2010).
241. G. Yeo, C. B. Burge, Maximum entropy modeling of short sequence motifs with applications to RNA splicing signals. *J. Comput. Biol.* **11**, 377–394 (2004).
242. R. Lorenz, *et al.*, ViennaRNA Package 2.0. *Algorithms Mol. Biol.* **6**, 26 (2011).
243. A. R. Gruber, R. Lorenz, S. H. Bernhart, R. Neuböck, I. L. Hofacker, The Vienna RNA Websuite. *Nucleic Acids Res.* **36**, W70–W74 (2008).
244. E. M. Phizicky, A. K. Hopper, tRNA biology charges to the front. *Genes Dev.* **24**, 1832–1860 (2010).
245. A. K. Hopper, Transfer RNA post-transcriptional processing, turnover, and subcellular dynamics in the yeast Saccharomyces cerevisiae. *Genetics* (2013) https:/doi.org/10.1534/genetics.112.147470.
246. C. J. Yoo, S. L. Wolin, The yeast La protein is required for the 3' endonucleolytic cleavage that matures tRNA precursors. *Cell* (1997) https:/doi.org/10.1016/S0092-8674(00)80220-2.
247. S. R. Ellis, M. J. Morales, J. M. Li, A. K. Hopper, N. C. Martin, Isolation and characterization of the TRM1 locus, a gene essential for the N2,N2-dimethylguanosine modification of both mitochondrial and cytoplasmic tRNA in Saccharomyces cerevisiae. *J. Biol. Chem.* **261**, 9703–9709 (1986).

248. S. R. Ellis, A. K. Hopper, N. C. Martin, Amino-terminal extension generated from an upstream AUG codon is not required for mitochondrial import of yeast N2,N2-dimethylguanosine-specific tRNA methyltransferase. *Proc. Natl. Acad. Sci. U. S. A.* **84**, 5172–5176 (1987).
249. T. Suzuki, The expanding world of tRNA modifications and their disease relevance. *Nat. Rev. Mol. Cell Biol.* **22**, 375–392 (2021).
250. M. Thodberg, *et al.*, Comprehensive profiling of the fission yeast transcription start site activity during stress and media response. *Nucleic Acids Res.* **47**, 1671–1691 (2019).
251. Ihsanawati, *et al.*, Crystal Structure of tRNA N-2, N-2-Guanosine Dimethyltransferase Trm1 from Pyrococcus horikoshii. *J. Mol. Biol.* **383**, 871–884 (2008).
252. T. Awai, *et al.*, Substrate tRNA recognition mechanism of a multisite-specific tRNA methyltransferase, Aquifex aeolicus Trm1, based on the X-ray crystal structure. *J. Biol. Chem.* **286**, 35236–35246 (2011).
253. A. Khalique, S. Mattijssen, R. J. Maraia, A versatile tRNA modification-sensitive northern blot method with enhanced performance. *RNA* **28**, 418–432 (2022).
254. Y. Motorin, S. Muller, I. Behm-Ansmant, C. Branlant, Identification of modified residues in RNAs by reverse transcription-based methods. *Methods Enzymol.* **425**, 21–53.
255. K. Rijal, R. J. Maraia, A. G. Arimbasseri, A methods review on use of nonsense suppression to study 3' end formation and other aspects of tRNA biogenesis. *Gene* **556**, 35–50 (2015).
256. Y. Huang, R. V. Intine, A. Mozlin, S. Hasson, R. J. Maraia, Mutations in the RNA Polymerase III Subunit Rpc11p That Decrease RNA 3′ Cleavage Activity Increase 3′-Terminal Oligo(U) Length and La-Dependent tRNA Processing. *Mol. Cell. Biol.* **25**, 621–636 (2005).
257. J. R. Iben, *et al.*, Comparative whole genome sequencing reveals phenotypic tRNA gene duplication in spontaneous Schizosaccharomyces pombe la mutants. *Nucleic Acids Res.* **39**, 4728–4742 (2011).
258. T. Gogakos, *et al.*, Characterizing Expression and Processing of Precursor and Mature Human tRNAs by Hydro-tRNAseq and PAR-CLIP. *Cell Rep.* **20**, 1463–1475 (2017).
259. V. Ramamurthy, S. L. Swann, J. L. Paulson, C. J. Spedaliere, E. G. Mueller, Critical aspartic acid residues in pseudouridine synthases. *J. Biol. Chem.* **274**, 22225–22230 (1999).
260. J. Kuehnert, *et al.*, Novel RNA chaperone domain of RNA-binding protein la is regulated by AKT phosphorylation. *Nucleic Acids Res.* (2015) https:/doi.org/10.1093/nar/gku1309.
261. M. A. Bayfield, R. Yang, R. J. Maraia, Conserved and divergent features of the structure and function of La and La-related proteins (LARPs). *Biochim. Biophys. Acta - Gene Regul. Mech.* **1799**, 365–378 (2010).
262. L. Martino, *et al.*, Analysis of the interaction with the hepatitis C virus mRNA reveals an alternative mode of RNA recognition by the human la protein. *Nucleic Acids Res.* **40**, 1381–1394 (2012).
263. M. T. Bohnsack, K. E. Sloan, The mitochondrial epitranscriptome: the roles of RNA modifications in mitochondrial translation and human disease. *Cell. Mol. Life Sci.* **75**, 241–260 (2018).
264. E. Schöller, *et al.*, Balancing of mitochondrial translation through METTL8-mediated m3C modification of mitochondrial tRNAs. *Mol. Cell* **81**, 4810-4825.E12 (2021).
265. G. Kanter-Smoler, A. Dahlkvist, P. Sunnerhagen, Improved method for rapid

transformation of intact Schizosaccharomyces pombe cells. *Biotechniques* (1994).
266. K. Gouget, F. Verde, A. Barrientos, In vivo labeling and analysis of mitochondrial translation products in budding and in fission yeasts. *Methods Mol. Biol.* **457**, 113–124 (2008).
267. S. Ito, *et al.*, A single acetylation of 18 S rRNA is essential for biogenesis of the small ribosomal subunit in saccharomyces cerevisiae. *J. Biol. Chem.* **289**, 26201–26212 (2014).
268. S. Kass, K. Tyc, J. A. Steitz, B. Sollner-Webb, The U3 small nucleolar ribonucleoprotein functions in the first step of preribosomal RNA processing. *Cell* **60**, 897–908 (1990).
269. J. M. X. Hughes, M. Ares, Depletion of U3 small nucleolar RNA inhibits cleavage in the 5' external transcribed spacer of yeast pre-ribosomal RNA and impairs formation of 18S ribosomal RNA. *EMBO J.* **10**, 4231–4239 (1991).
270. H. Liao, *et al.*, Human NOP2/NSUN1 regulates ribosome biogenesis through non-catalytic complex formation with box C/D snoRNPs. *Nucleic Acids Res.* **50**, 10695–10716 (2022).
271. M. Falaleeva, *et al.*, Dual function of C/D box small nucleolar RNAs in rRNA modification and alternative pre-mRNA splicing. *Proc. Natl. Acad. Sci. U. S. A.* **113**, E1625–E1634 (2016).
272. M. S. Scott, *et al.*, Human box C/D snoRNA processing conservation across multiple cell types. *Nucleic Acids Res.* **40**, 3676–3688 (2012).
273. S. Kishore, S. Stamm, The snoRNA HBII-52 regulates alternative splicing of the serotonin receptor 2C. *Science (80-.).* **311**, 230–232 (2006).
274. G. Shumyatsky, D. Wright, R. Reddy, Methylphosphate cap structure increases the stability of 7SK, B2 and U6 small RNAs in Xenopus oocytes. *Nucleic Acids Res.* **21**, 4756–4761 (1993).
275. N. M. Martinez, *et al.*, Pseudouridine synthases modify human pre-mRNA co-transcriptionally and affect pre-mRNA processing. *Mol. Cell* **82**, 645-659.e9 (2022).
276. H. Adachi, *et al.*, Targeted pseudouridylation: An approach for suppressing nonsense mutations in disease genes. *Mol. Cell* **83**, 637-651.e9 (2023).
277. D. E. Eyler, *et al.*, Pseudouridinylation of mRNA coding sequences alters translation. *Proc. Natl. Acad. Sci. U. S. A.* **116**, 23068–23074 (2019).
278. Y. Motorin, *et al.*, The yeast tRNA:pseudouridine synthase Pus1p displays a multisite substrate specificity. *RNA* **4**, 856–869 (1998).
279. S. Massenet, *et al.*, Pseudouridine Mapping in the Saccharomyces cerevisiae Spliceosomal U Small Nuclear RNAs (snRNAs) Reveals that Pseudouridine Synthase Pus1p Exhibits a Dual Substrate Specificity for U2 snRNA and tRNA. *Mol. Cell. Biol.* **19**, 2142–2154 (1999).
280. A. Basak, C. C. Query, A pseudouridine residue in the spliceosome core is part of the filamentous growth program in yeast. *Cell Rep.* **8**, 966–973 (2014).
281. L. Han, E. M. Phizicky, A rationale for tRNA modification circuits in the anticodon loop. *RNA* (2018) https:/doi.org/10.1261/rna.067736.118.
282. P. Barraud, *et al.*, Time-resolved NMR monitoring of tRNA maturation. *Nat. Commun.* **10**, 3373 (2019).
283. D. A. Melton, E. M. De Robertis, R. Cortese, Order and intracellular location of the events involved in the maturation of a spliced tRNA. *Nature* **284**, 143–148 (1980).
284. K. Nishikura, E. M. De Robertis, RNA processing in microinjected Xenopus oocytes. Sequential addition of base modifications in a spliced transfer RNA. *J. Mol. Biol.* **145**,

405–420 (1981).
285. L. Rajkowitsch, K. Semrad, O. Mayer, R. Schroeder, Assays for the RNA chaperone activity of proteins. *Biochem. Soc. Trans.* (2005) https:/doi.org/10.1042/BST0330450.
286. E. Clodi, K. Semrad, R. Schroeder, Assaying RNA chaperone activity in vivo using a novel RNA folding trap. *Embo J* (1999) https:/doi.org/10.1093/emboj/18.13.3776.
287. S. Phadtare, K. Severinov, M. Inouye, Assay of Transcription Antitermination by Proteins of the CspA Family. *Methods Enzymol.* (2003) https:/doi.org/10.1016/S0076-6879(03)71034-9.
288. M. Costa-Mattioli, Y. Svitkin, N. Sonenberg, La autoantigen is necessary for optimal function of the poliovirus and hepatitis C virus internal ribosome entry site in vivo and in vitro. *Mol. Cell. Biol.* (2004) https:/doi.org/10.1128/MCB.24.15.6861-6870.2004.
289. J. Kohli, T. Kwong, F. Altruda, D. Söll, G. Wahl, Characterization of a UGA-suppressing serine tRNA from Schizosaccharomyces pombe with the help of a new in vitro assay system for eukaryotic suppressor tRNAs. *J. Biol. Chem.* (1979).
290. R. Koukuntla, W. J. Ramsey, W. Bin Young, C. J. Link, U6 promoter-enhanced GlnUAG suppressor tRNA has higher suppression efficacy and can be stably expressed in 293 cells. *J. Gene Med.* (2013) https:/doi.org/10.1002/jgm.2696.
291. P. Szankasi, W. D. Heyer, P. Schuchert, J. Kohli, DNA sequence analysis of the ade6 gene of Schizosaccharomyces pombe. Wild-type and mutant alleles including the recombination hot spot allele ade6-M26. *J. Mol. Biol.* (1988) https:/doi.org/10.1016/0022-2836(88)90051-4.
292. R. V. A. Intine, *et al.*, Control of transfer RNA maturation by phosphorylation of the human La antigen on serine 366. *Mol. Cell* (2000) https:/doi.org/10.1016/S1097-2765(00)00034-4.
293. M. Hamada, A. L. Sakulich, S. B. Koduru, R. J. Maraia, Transcription termination by RNA polymerase III in fission yeast. A genetic and biochemically tractable model system. *J. Biol. Chem.* **275**, 29076–29081 (2000).
294. D. J. Van Horn, C. J. Yoo, D. Xue, H. Shi, S. L. Wolin, The La protein in Schizosaccharomyces pombe: a conserved yet dispensable phosphoprotein that functions in tRNA maturation. *RNA* (1997) https:/doi.org/10.1101/gad.241422.114.
295. K. Maundrell, Thiamine-repressible expression vectors pREP and pRIP for fission yeast. *Gene* **123**, 127–130 (1993).
296. J. B. Keeney, J. D. Boeke, Efficient targeted integration at leu1-32 and ura4-294 in Schizosaccharomyces pombe. *Genetics* **136**, 849–856 (1994).
297. R. Wetzel, J. Kohli, F. Altruda, D. Söll, Identification and nucleotide sequence of the sup8-e UGA-suppressor leucine tRNA from Schizosaccharomyces pombe. *MGG Mol. Gen. Genet.* **172**, 221–228 (1979).
298. H. Hottinger, *et al.*, The Schizosaccharomyces pombe sup3-i suppressor recognizes ochre, but not amber codons in vitro and in vivo. *EMBO J.* **3**, 423–428 (1984).
299. C. Niederberger, R. Gräub, A. Costa, J. Desgrès, M. E. Schweingruber, The tRNA N2,N2-dimethylguanosine-26 methyltransferase encoded by gene trm1 increases efficiency of suppression of an ochre codon in Schizosaccharomyces pombe. *FEBS Lett.* **464**, 67–70 (1999).